PETROGRAPHY, GEOCHEMISTRY AND EVOLUTION OF ROCK UNITS IN SHEET 241, OYO S.E., SOUTHWESTERN NIGERIA

ROFIAT RONKE ISIAQ

B.Sc. (Hons), (UNAD)

M.Sc. (Ibadan)

Matric. No.: 146566

A thesis in the Department of GEOLOGY

Submitted to the Faculty of Science in partial fulfilment of the requirement for the Degree of

DOCTOR OF PHILOSOPHY

of the

UNIVERSITY OF IBADAN.

June, 2021

ABSTRACT

The Basement Complex rocks of Southwestern Nigeria have been mapped regionally on a scale of 1:250,000. On this scale, many rock units are grouped together with very limited information on component members. However, such details are necessary for the understanding of the mineral potentials. Thus, the production of maps on larger scales, with more geologic information are very important. Sheet 241 Oyo SE falls within the Iseyin-Oyan Schist belt whose detailed geology and mineral potentials are yet to be fully understood. Therefore, this study was aimed at detailed mapping and assessment of mineralisation potentials of rock units of Sheet 241 Oyo SE, Southwestern Nigeria.

A geological field mapping exercise was undertaken by compass-traversing using a topographical map Sheet 241 (Oyo SE) (1:50 000) as base map. This involved detailed observation of outcrops for structural features, field relationship, measurements of trends and orientation of the rock units. The obtained rock samples were prepared into thin sections. Fifty-four rock samples were purposively analysed using inductively coupled plasma-mass spectrometry and X-ray fluorescence. Selected polished samples were analysed for specific minerals using SEM-EDX, while others were analysed for mineralogical content using X-ray Diffractometer. The rock units were characterised petrologically, while the geochemical data were interpreted using various geochemical binary and discriminatory diagrams.

Quartzite; quartz-schist and muscovite-garnetiferous schist; biotite hornblende gneiss; granodiorite gneiss; and biotite granite gneisses as well as leucogranite, variably intruded by pegmatite, quartz veins and dolerite dykes of varying thickness and lengths were identified. Texturally, the rocks exhibited granoblastic, porphyroblastic and augen textures. Folds, joint, shear zones, and foliation trending in NW-SE directions were observed. The compositional range of plagioclase feldspars in the granodiorite gneiss were oligoclase ($An_{10\text{-}43\text{-}27.82}$) to low andesine ($An_{31.42\text{-}31.81}$), while low oligoclase ($An_{11.15\text{-}11.75}$and$An_{11.46\text{-}27.82}$) were observed in the biotite hornblende and biotite granite gneisses. Biotite in granodiorite and biotite granite gneisses was phlogopitic, and siderophyllitic in biotite hornblende gneiss. Amphibole in the granodiorite gneiss was ferro-hornblende in

character. Garnet, chlorite, apatite, zircon, rutile and magnetite occurred as accessory minerals in the gneisses. The schists were of sedimentary protolith emplaced in the passive margin field and had undergone low to moderate degree of chemical weathering. The gneisses were dominantly derived from igneous origin of calc-alkaline magma type, which were peraluminous and emplaced in pre-plate to syn-collision granite field. Leucogranite rock was of I-type, emplaced in orogenic unfractionated granite field. All the rocks displayed enrichment in large ion lithophile elements and light rare earth elements, while they were depleted in the high strength field elements and heavy rare earth elements, with distinctive negative Eu anomalies, strongly indicating continental sources for all the rock units. Anomalous concentrations were observed for Au (<0.5-30.8ppb), Cu (0.7-64.2ppm), Pb (2.9-41.8ppm), Zn (18.6-136ppm) and Ni (1.8-13.4ppm) in the quartz schists, gneisses and pegmatite.

Ten rock units were delineated on Sheet 241, Oyo SE on a scale of 1:50,000 with the schist, gneisses and pegmatite found to be mineralised with anomalous gold concentrations.

Keywords: Mineralisation potential, Muscovite-garnetiferous schist, Continental protoliths, Calc-alkaline magma, Syn-collision granite

Word count: 486

CERTIFICATION

I certify that this work was carried out by ROFIAT RONKE ISIAQ in the Department of Geology, University of Ibadan.

.....

Supervisor

DrA.S. Olatunji
B.Sc (Hons) (Ilorin), M.Sc., Ph.D. (Ibadan)
Department of Geology,
University of Ibadan, Nigeria.

DEDICATION

This research work is dedicated to the Almighty God.

ACKNOWLEDGEMENTS

All praises be to Almighty Allah, the gracious, the merciful. May the peace and blessing of Allah be upon the noble prophet Muhammad (S.A.W), his household and the muslim generality.

My heartfelt gratitude goes to my supervisor Dr A. S. Olatunji for his understanding, advice, effective supervision and encouragement. There is no quantification of the things I have learnt from you. Your love for the profession and the advancement of others is contagious. I will also like to thank all the lecturers in the Department: Prof. O.A. Okunlola (HOD), Prof. A.I. Olayinka, Prof. M.N. Tijani and Prof. G.O. Adeyemi and Prof. O.A. Ehinola; Prof. M.E. Nton, Drs A.T. Bolarinwa, A.A. Omitogun,O.A. Boboye, O.C. Adeigbe, M.A. Oladunjoye, I.A. Oyediran, O.O. Osinowo, M.A. Adeleye, Aromolaran and Felicia F. Ajayi; A. Jayeoba and J.A. Aladejana and Miss Oluwatoyin Ajilore. The contributions of the late Prof. A.A. Elueze and late Dr I.M Akaegbobi are gratefully acknowledged. To the non-administrative staff and technicians, thank you for your contributions towards the successful completion of my postgraduate studies.

My appreciation goes to my Mineral Exploration (Geochemistry option) colleagues; thank you all for the forward push every time and for the tremendous help during the field mapping exercise, geochemical and mineral analyses as well as in data interpretations.

I am forever grateful to my parents, brothers and my other family members for their encouragement, moral and financial support always. The prayers and support of my loving husband, my beloved son and daughters are gratefully acknowledged.

To all who stood by me but not mentioned, I say thank you for making this research work another worthwhile experience!

TABLE OF CONTENTS

ABSTRACT	ii
CERTIFICATION	iv
DEDICATION	v
ACKNOWLEDGEMENTS	vi
LIST OF FIGURES	x
LIST OF TABLES	xviii
CHAPTER ONE: INTRODUCTION	1
1.1 General Statement	1
1.2 Justification of Research study	2
1.2 Aim	3
1.3 Objectives of study	3
1.4 Location of the Study Area	3
1.5 Scope of Work	4
1.6 Climate and Vegetation	6
1.7 Drainage and Topography	6
CHAPTER TWO: LITERATURE REVIEW	8
2.1 Review of the Geology of Nigeria	8
2.2 Geology of the Basement Complex of South Western Nigeria	12
2.3 Metamorphism in the South Western Nigeria Basement rocks	16
CHAPTER THREE: RESEARCH METHODOLOGY	18
3.1 Field Activities	18
3.2 Laboratory Analyses	18
3.2.1 Petrographic Analysis	18
3.2.2 Whole Rock Geochemistry Analyses	20
3.2.3 Scanning Electron Microscopy- Energy Dispersive X-Ray Fluorescence	21
3.2.4 X-Ray Diffraction (XRD)	23
3.3 Data Analysis	23
CHAPTER FOUR: RESULTS AND DISCUSSION	24
4.1 Field Relationship and Lithology	24
4.1.1 Quartzite	24

4.1.2 Schistose Rock 30
4.1.2.1 Quartz Schist 30
4.1.2.2 Muscovite Garnet Schist 39
4.1.2.3 Geochemistry of the Schistose Rock (Quartz and Muscovite Garnet Schists) 47
4.1.2.3.1 Major Oxides 47
4.1.2.3.2 Trace Element 56
4.1.2.3.3 Rare Earth Elements 62
4.1.3 Gneissose Rocks 65
4.1.3.1 Biotite Hornblende Gneiss (bHG) 65
4.1.3.2 Geochemistry of the Biotite-Hornblende Gneiss 75
4.1.3.2.1 Major Oxide 75
4.1.3.2.2 Trace Elements 83
4.1.3.2.3 Rare Earth Elements 90
4.1.3.3 Granodioritic Gneiss 93
4.1.3.4 Geochemistry of the Granodioritic Gneiss 105
4.1.3.4.1 Major Oxide 105
4.1.3.4.2 Trace Elements 113
4.1.3.4.3 Rare Earth Elements 117
4.1.3.5 Biotite Granite Gneiss 120
4.1.3.6 Geochemistry of the Biotite Granite Gneiss 139
4.1.3.6.1 Major Oxides 139
4.1.3.6.2 Trace Elements 152
4.1.3.6.3 Rare Earth Elements 158
4.1.4 Leucogranite 161
4.1.5 Minor Rocks 166
4.1.5.1 Pegmatite 166
4.1.5.2 Geochemistry of the Pegmatitic Rocks 172
4.1.5.2.1 Major Oxides 172
4.1.5.2.2 Trace Elements 176
4.1.5.2.3 Rare Earth Elements 180
4.1.5.3 Quartz Veins 183

4.1.5.4 Dolerite Dykes 183
4.2 Stuctural Elements 187
4.2.1 Regional Structural Orientation 187
4.2.2 Structures Observed on the Field 187
4.3 Geological Setting of the Study Area 202
4.3.1 Metamorphism 206
4.4 Mineral Chemistry 207
4.4.1 Feldspars 207
4.4.2 Biotite 241
4.4.3 Amphiboles 256
4.4.4 Accessory Minerals 261
4.5 Metallic Mineralisation Potentials of Sheet 241, Oyo SE 282
CHAPTER FIVE: SUMMARY AND CONCLUSION 290
5.1 Summary 290
5.2 Conclusion 292
5.3 Contribution to knowledge 292
References 293
Appendix 302

LIST OF FIGURES

Figure	Title	Page
Fig.1.1.	Location Map of Sheet 241 Oyo SE.	5
Fig.1.2.	Vegetation on the Study Area	7
Fig.3.1.	JEOL JXA-8100 Electron Microprobe Analyser Used for Mineral Chemistry of Gneissic Rocks at University of Cape Town, South Africa.	22
Fig.4.1.	(a) An overview of hog-back ridge of quartzite at Ikereku (b) Boulders of quartzite at the foot of Ikereku ridge.	25
Fig.4.2.	Typical photomicrograph of Quartz schist in transmitted Light.	28
Fig.4.3	Typical photomicrograph of Quartz schist in transmitted light.	29
Fig.4.4	Low lying quartz schist outcrop showing the development of quartz ribbons	31
Fig.4.5	(a) Low lying quartz schist outcrop (b) Hand specimen displaying well defined schistose plane.	32
Fig.4.6	Typical Photomicrograph of Quartz schist in Transmitted Light.	34
Fig.4.7	Typical Photomicrograph of Quartz schist in Transmitted Light.	35
Fig.4.8	Typical Photomicrograph of Quartz schist in Transmitted Light.	36
Fig.4.9	Typical Photomicrograph of Quartz schist in Transmitted Light	37
Fig.4.10	Typical Photomicrograph of Quartz Schist in Transmitted Light	38
Fig.4.11	Field Expression of Muscovite garnet Schist.	40
Fig.4.12	Hand Specimen of Muscovite garnet Schist.	41
Fig.4.13	Hand Specimen of Muscovite garnet Schist Showing Muscovite Flakes.	42
Fig.4.14	Typical Photomicrograph of Muscovite garnet Schist in Transmitted Light	44

Fig.4.15	Typical Photomicrograph of Muscovite garnet Schist in Transmitted Light	45
Fig.4.16	Typical Photomicrograph of Muscovite garnet Schist in Transmitted Light	46
Fig.4.17	Na_2O/Al_2O_3 versus K_2O/Al_2O_3 Variation Diagram of Quartz and Muscovite garnet schist	51
Fig.4.18	Plot of log (Fe_2O_3/K_2O) versus log (SiO_2/Al_2O_3) Diagram for Quartz and Muscovite garnet Schist Samples	52
Fig.4.19	Plot of K_2O/Na_2O versus SiO_2 Tectonic Discrimination Plot for the Analysed Quartz and Muscovite garnet Schist Samples	53
Fig.4.20	AKF Diagram for the Silica-saturated Low Pressure Pelitic Schist	55
Fig.4.21	Chondrite Normalized Plots of the Trace Elements in the Pelitic Schist	59
Fig.4.22	Plot of Th/Sc against Zr/Sc for the Pelitic Schist	61
Fig.4.23	REE Chondrite Normalized Plots for the Pelitic Schist rock	64
Fig.4.24	Outcrop of Biotite Hornblende Gneiss Showing: (a) Compositional Parallel Bands (b) Mafic Xenolith within Outcrop	66
Fig.4.25	Outcrop of Biotite Hornblende Gneiss Displaying Irregular Felsic bands at Alapata Village, Arulogun	67
Fig 4.26	Outcrop of Biotite Hornblende Gneiss Sample Showing Felsic Accumulation in Dilatant Shear Surface	68
Fig 4.27	Typical Photomicrograph of Biotite Hornblende Gneiss in Transmitted Light	71
Fig 4.28	Typical Photomicrograph of Biotite Hornblende Gneiss in Transmitted Light	72
Fig 4.29	Typical Photomicrograph of Biotite Hornblende Gneiss in Transmitted Light	73
Fig 4.30	Typical Photomicrograph of Biotite Hornblende Gneiss in Transmitted Light	74
Fig.4.31	Na_2O/Al_2O_3 versus K_2O/Al_2O_3 Variation Diagram of Biotite Hornblende Gneiss	79
Fig.4.32	R1-R2 Plot of Biotite Hornblende Gneiss indicating granitic origin	80
Fig.4.33	Classification Diagram of Biotite Hornblende Gneiss base on Na_2O+K_2O versus SiO_2	81
Fig.4.34	$Al_2O_3/ (CaO+Na_2O+K_2O)$ versus SiO_2 Binary Diagram of the Biotite Hornblende Gneiss	82

Fig.4. 35	Binary Diagram of Log(Zr/Y) vs Log(Zr) for the Biotite Hornblende Gneiss	86
Fig.4.36	Discriminate Binary Diagram of Log(Nb) versus Log(Y).	87
Fig.4.37	Discriminate Binary Diagram of R1 versus R2.	88
Fig.4.38	Chondrite Normalized Plot of the Trace Elements in the Biotite Hornblende Gneiss	89
Fig.4.39	Chondrite Normalized Plot of Rare Earth Elements (REE) in the Biotite Hornblende Gneiss	92
Fig.4.40	Over-View of Elongated Outcrop of Granodioritic Gneiss Rock.	94
Fig.4.41	Outcrop of Granodioritic Gneiss Displays the Compositional Banding	94
Fig.4.42	Exposure of Granodioritic Gneiss Showing Level of Overburden in an Active Quarry Site.	95
Fig. 4.43	Outcrop of Buried Granodioritic Gneiss Rock in an Abandon RCC Quarry Site, Moniya Area.	95
Fig.4.44	Hand Specimen of Granodioritic Gneiss Rock	96
Fig.4.45	Hand Specimen of Granodioritic Gneiss Rock	96
Fig 4.46	Typical Photomicrograph of Granodioritic Gneiss in Transmitted Light	98
Fig 4.47	Typical Photomicrograph of Granodioritic Gneiss in Transmitted Light	99
Fig 4.48	Typical Photomicrograph of Granodioritic Gneiss in Transmitted Light	100
Fig 4.49	Typical Photomicrograph of Granodioritic Gneiss in Transmitted Light	101
Fig.4.50	Diffractogram of Granodioritic Gneiss Depicting Predominant Quartz, Anorthite, Albite, Epidote and Microcline Peaks	103
Fig.4.51	Diffractogram of Granodioritic Gneiss Depicting Predominant Quartz, Albite and Biotite Peaks	105
Fig.4.52	Binary Plot of Na_2O/Al_2O_3 versus K_2O/Al_2O_3 for Granodioritic Gneiss Samples	107
Fig.4.53	Plot of (Na_2O+K_2O) versus SiO_2 for Granodioritic Gneiss on Classification Diagram	108

Figure	Title	Page
Fig.4.54	Ternary Diagram Based on Combination of Ab (Albite), An (Anothite) and Or (Orthoclase feldspar) for Granodioritic Gneiss. CIPW normative data as proposed by O'Connor (1965).	109
Fig.4.55	Plot of A.F.M. Ternary Diagram for Granodioritic Gneiss	110
Fig.4.56	A/NK versus A/CNK plot of Shand (1943) Discriminating Metaluminous, Peraluminous and Peralkaline Composition for the Granodioritic Gneiss.	111
Fig.4.57	Plot of R1-R2 Diagram for Granodioritic Gneiss	112
Fig.4.58	Discriminate Diagram of Nb versus Y for the Granodioritic Gneiss samples	115
Fig4.59	Spider Diagrams for Selected Trace Elements for the Granodioritic Gneiss	116
Fig.4.60	Chondrite Normalized Plot of Rare Earth Elements (REE) in the Granodioritic Gneiss	119
Fig.4.61	(a) Over-View of an Elongated Biotite Granite Gneiss Rock Along Idiroko-Imini Road. (b) Hand Specimen	121
Fig.4.62a	Overview of Biotite Granite Gneiss Outcrop at Adubiare, in Ilora Village.	122
Fig.4.62b	Overview of Low-lying Biotite Granite Gneiss Outcrop at Adubiare, in Ilora village.	122
Fig.4.63	Coarse Grained Sample of Biotite Granite Gneiss at Adejumo Village, off Iseyin-Ibadan Road.	123
Fig.4.64	Coarse Grained Sample of Biotite Granite Gneiss Along Ijaye- Iseyin Road.	124
Fig. 4.65	Coarse Grained Sample of Garnetiferous Gneiss Associated with the Biotite Granite Gneiss at Ori-Oke Muyideen Kasali Church.	125
Fig.4.66	Typical Photomicrograph of Biotite Granite Gneiss in Transmitted Light	129
Fig.4.67	Typical Photomicrograph of Biotite Granite Gneiss in Transmitted Light	130
Fig.4.68	Typical Photomicrograph of Biotite Granite Gneiss in Transmitted Light	131
Fig.4.69	Typical Photomicrograph of Biotite Granite Gneiss in Transmitted Light	132

Figure	Title	Page
Fig.4.70	Typical Photomicrograph of Biotite Granite Gneiss in Transmitted Light	133
Fig.4.71	Typical Photomicrograph of Biotite Granite Gneiss in Transmitted Light	134
Fig.4.72	Typical Photomicrograph of Biotite Granite Gneiss in Transmitted Light	135
Fig.4.73	Typical Photomicrograph of Biotite Granite Gneiss in Transmitted Light	136
Fig.4.74	Typical Photomicrograph of Biotite Granite Gneiss in Transmitted Light	137
Fig.4.75	Diffractogram of Biotite Granite Gneiss Sample Depicting Predominant Quartz, Albite and Biotite and Actinolite Peaks	138
Fig.4.76	Na_2O/Al_2O_3 versus K_2O/Al_2O_3 Variation Diagram of Biotite Granite Gneiss	142
Fig.4.77	Classification Diagram of Biotite Granite Gneiss Samples Base on Na_2O+K_2O versus SiO_2	144
Fig.4.78	R1-R2 Plot of Biotite Granite Gneiss Samples	145
Fig.4.79	Binary Plot of Na_2O against K_2O Showed I-type Granitoid for the Biotite Granite Gneiss	146
Fig.4.80	A/NK versus A/CNK Plot Discriminating Metaluminous, Peraluminous and Peralkaline Composition for the Biotite Granite Gneiss	147
Fig.4.81	$Al_2O_3/ (CaO+Na_2O+K_2O)$ versus SiO_2 Binary Diagram of the Biotite Gneiss	148
Fig.4.82	R1 versus R2 Discriminate Diagram for Biotite Granite Gneiss	149
Fig.4.83	Plot of Normalized Mean Concentration of Trace Elements with Chondrite in Biotite Granite Gneiss	155
Fig.4.84	Nb versus Y Discriminate Diagram for Biotite Granite Gneiss	156
Fig.4.85	Biotite granite gneiss in the Rb against Sr crustal thickness grid.	159
Fig.4.86	REE Chondrite Normalized Plots for the Biotite Granite Gneiss	160
Fig.4.87	Hand Sample Displaying Whitish Grey Leucocratic Granite	162
Fig 4.88	Typical Photomicrograph of Leucocratic Granite in	164

	Transmitted Light	
Fig 4.89	Typical Photomicrograph of Leucocratic Granite in Transmitted Light	165
Fig.4.90	Concordant Pegmatite Vein Intruded the Granodioritic Gneiss	167
Fig.4.91	Discordant Pegmatite Vein Intruded the Biotite Granite Gneiss	167
Fig.4.92	Typical Photomicrograph of Pegmatite in Transmitted Light	169
Fig.4.93	Typical Photomicrograph of Pegmatite in Transmitted Light	170
Fig.4.94	Diffractogram of Pegmatite Sample Depicting Predominant Quartz, Microcline, Anorthite and Potassic Pargasite Peaks	171
Fig.4.95	A/NK versus A/CNK Diagram Discriminating Metaluminous, Peraluminous and Peralkaline Composition for the Pegmatitic Samples	174
Fig.4.96	Plot of A.F.M. Ternary Diagram for Pegmatitic Samples	175
Fig.4.97	Binary Diagram Showing the Mineralization Potentials and Classification of the Pegmatite Samples	178
Fig.4.98	Plot of Normalized Mean Concentration of Trace Elements with Chondrite (Thompson, 1982) in Pegmatite Samples.	179
Fig.4.99	REE Chondrite Normalization of Pegmatite Sample	182
Fig.4.100	Irregular Exposure of Quartz Veins on the Granodioritic Gneiss Rock.	184
Fig.4.101	Quartz Phenocryst on the Granodioritic Gneiss Rock	184
Fig.4.102	Concordant Quartz Vein on the Biotite Hornlende Gneiss Rock.	185
Fig.4.103	Dolerite Dyke Intruded Biotite Hornblende Gneiss Rock at Ositedo Village.	186
Fig.4.104a	Lineaments Map of Sheet 241, Oyo SE from Aeromagnetic Map.	187
Fig.4.104b	Rose Diagram for the Lineaments Map of Sheet 241, Oyo SE	188
Fig.4.105	Regional Analytical Signal Map of Sheet 241, Oyo SE.	190
Fig.4.106a	Biotite Hornblende Gneiss Outcrop Displaying Foliation Band Forming Symmetrical Fold	191
Fig.4.106b	Rose Diagram of Foliation Trends in the Quartz Schist and Gneissous Rocks (n=70).	192
Fig.4.107	Biotite Hornblende Gneiss Outcrop Showing Crenulation Cleavage.	193
Fig.4.108	Shear Zone Trace Where Blocks of Rocks have been Displaced in a Fault like Manner, but without Prominent Development of Visible Faults in Biotite Hornblende Gneiss.	195

Fig.4.109	Convolute Fold Trace in Quartz Schist.	196
Fig.4.110	Symmetrical Fold in Biotite Hornblende Gneiss	197
Fig.4.111	Parallel Fold in Biotite Hornblende Gneiss Outcrop.	198
Fig.4.112	Ptygmatic Folds caused by Ductile Deformation of Biotite Hornblende Gneiss	199
Fig.4.113	Joint on Migmatitic Biotite Hornblende Gneiss.	200
Fig.4.114	Rose Diagram of Joint Trends in the Quartz Schist and Gneissous Rocks (n=58)	201
Fig. 4.115	Strike-slip Fault as Observed on Biotite Granite Gneiss.	203
Fig.4.116	Map of Ternary Image Map (K+Th+U) (a) On Scale of 1:100 000 (b) Study Area on Scale of 1:50 000.	204
Fig.4.117	Geological map of the study area.	205
Fig.4.118	Micro-Probe Image of Plagioclase Feldspars of Oligoclase Composition ($An_{23.81}Ab_{71.21}Or_{4.98}$) and Orthoclase ($Or_{84.08}Ab_{15.02}$) in the Granodioritic Gneiss	208
Fig.4.119	Micro-Probe Image of Plagioclase Feldspars of Oligoclase Composition ($An_{9.19}Ab_{73.90}Or_{16.90}$) and Orthoclase ($Or_{92.13}Ab_{7.87}$) in the Biotite Granite Gneiss	209
Fig.4.120	Plot of Ab-An-Or for Feldspars in the Granodioritic Gneiss	219
Fig.4.121	Plot of Ab-An-Or for Feldspars in the Biotite Granite Gneiss	235
Fig.4.122	Plot of Ab-An-Or for Feldspars in the Biotite Hornblende Gneiss	240
Fig.4.123	Micro-Probe Image of Biotite Flakes in the Biotite Granite Gneiss	243
Fig.4.124	(FeO(t)+MnO)-10*TiO_2-MgO Plot for Biotites in Rock	252
Fig.4.125	Plot of Al (iv) (apfu) vs Fe/(Fe+Mg) for Biotites in the Rock.	253
Fig.4.126	Plot of $FeO_{(t)}$-MgO-Al_2O_3 Showing the Peraluminous Nature of the Primary to Re-Equilibrated Biotites of Granodioritic and Biotite Granite Gneiss, while Biotite Hornblende Gneiss Shows Alkaline Nature.	254
Fig.4.127	Plot of MgO against FeO(t) Showing the Peraluminous Nature of the Primary to Re-Equilibrated Primary Biotites of Granodioritic and Biotite Granite Gneiss while Biotite Hornblende Gneiss Shows Alkaline Nature.	255

Fig.4.128	Micro-Probe Image of Hornblende Minerals in the Granodioritic Gneiss	257
Fig.4.129	Binary Plot of $Mg/(Mg+Fe^{2+})$ against Si (apfu) of Amphiboles in Granodioritic and Biotite Granite Gneiss	260
Fig4.130	Micro-Probe Image of Porphyroblastic Garnet in the Biotite Granite Gneiss	262
Fig.4.131	Plot of Alm-Gro-Pyr showing Almandine, Grossular and Pyrope Composition of Garnets in Biotite Granite Gneiss.	265
Fig.4.132	Plot of Alm-Sps-Pyr showing Almandine, Spessartine and Pyrope Composition of Garnets in Biotite Granite Gneiss.	266
Fig.4.133	Ternary Plot of $MgO-Fe_2O_3+FeO-Al_2O_3$ Showing Compositional Variations in Chlorite from Granodioritic Gneiss.	269
Fig.4.134	Ternary Plot of $SiO_2-MgO-Fe_2O_3+FeO$ Showing Compositional Variation in Chlorite from Granodioritic Gneiss.	270
Fig.4.135	Compositional Variations of Chlorites in Terms of Fe/(Fe+Mg) versus Si in the Granodioritic Gneiss.	271
Fig.4.136	Micro-Probe Image of Apatite in the Biotite Granite Gneiss.	272
Fig.4.137	Micro-Probe Image of Titanite and Zircon Inclusion in Quartz in the Biotite Granite Gneiss.	277
Fig.4.138.	Micro-Probe Image of Magnetite and Inclusion of Rutile Needle in Microcline in the Biotite Granite Gneiss	279
Fig.4.139	Copper (Cu) Metal Mineralisation in the Lithologic Units.	284
Fig.4.140	Lead (Pb) Metal Mineralisation in the Lithologic Units.	285
Fig.4.141	Zinc (Zn) Metal Mineralisation in the Lithologic Units.	286
Fig.4.142	Nickle (Ni) Metal Mineralisation in the Lithologic Units.	287
Fig.4.143	Gold (Au) Metal Mineralisation in the Lithologic Units.	288
Fig.4.144	Minimum and Maximum Concentrations of the Metallic Minerals in the different Lithologic Units	289

LIST OF TABLES

Table	Title	Page
Table 4.1.	Modal Composition of Minerals in Quartzite in the Study Area	27
Table 4.2	Modal Composition of Minerals in Quartz Schist in the Study Area	33
Table 4.3	Modal Composition of Minerals in Muscovite garnet Schist in the Study Area	43
Table 4.4	Result of Major Oxide Analyses of Pelitic Schist Unit.	48
Table 4.5	Comparison of Major Oxide of the Quartz Schist in the Study Area with Other Area within the Basement Complex of Nigeria.	49
Table 4.6	Results of Trace Element Analyses of Pelitic Schist Unit.	57
Table 4.7	Results of Rare Earth Element Analyses of Pelitic Schist Unit.	63
Table 4.8	Modal Composition of Minerals in Biotiite Hornblende Gneiss (BHG) in the Study Area	70
Table 4.9a	Results of Whole-Rock Oxide Analyses of the Biotite Hornblende Gneiss.	76
Table 4.9b	Results of Major Oxide Analyses of the Mafic and Felsic Portion of Biotite Hornblende Gneiss.	77
Table 4.10	Comparison of Major Oxide Geochemistry of this Study with Other Areas within the Basement Complex of Nigeria.	78
Table 4.11	Results of Trace Element Analyses of Biotite Hornblende Gneiss.	84
Table 4.12	Results of Rare Earth Element Analyses of Biotite Hornblende Gneiss Unit.	91
Table 4.13	Modal Composition of Minerals in Granodioritic Gneiss in the Study Area	97
Table 4.14	Modal Composition of X-Ray Diffractograms of Representative Samples of Granodioritic Gneiss in the Study Area.	104
Table 4.15	Results of Whole-Rock Analyses of Granodioritic Gneiss Rock Unit.	106

Table	Title	Page
Table 4.16	Results of Trace Elements Analyses of Granodioritic Gneiss Unit.	114
Table 4.17	Results of Rare Earth Element Analyses of Granodioritic Gneiss Unit.	118
Table 4.18	Modal Composition of Minerals in Biotite Granite Gneiss (bGG) in the Study Area	128
Table 4.19	Results of Whole-Rock Major Oxide Analyses of Biotite Granite Gneiss Unit.	141
Table 4.20	Ratio Calculations and Differentiation Indice from Major Oxides of the Biotite Granite Gneiss Unit.	150
Table 4.21	Comparison of the Average Major Oxides of the Biotite Granite Gneiss in the Study Area with Other Area.	151
Table 4.22	Results of Trace Element Analyses of Biotite Granite Gneiss Unit	152
Table 4.23	Results of Rare Earth Element Analyses of Biotite Granite Gneiss Unit	159
Table 4.24	Modal Composition of Minerals in Leucogranite in the Study Area.	163
Table 4.25	Modal Composition of Minerals in Pegmatite in the Study Area	168
Table 4.26	Results of Whole-Rock Major Oxide Analyses of Pegmatite Unit.	173
Table 4.27	Results of Trace Element Analyses of Pegmatite Samples.	177
Table 4.28	Result of Rare Earth Element Analyses of Pegmatite Sample	181
Table 4.29	Representative Mineral Chemistry of Plagioclase Feldspars in Granodioritic Gneiss.	210
Table 4.30	Structural Formulae of Plagioclase Feldspar in Granodioritic Gneiss.	211
Table 4.31	End Member Composition of Plagioclase Feldspars in Granodioritic Gneiss	212
Table 4.32	Representative Electron Microprobe Analyses of Plagioclase Feldspar in Granodioritic Gneiss.	213
Table 4.33	Structural Formulae of Plagioclase Feldspar in Granodioritic Gneiss.	214
Table 4.34	End Member Composition of Plagioclase Feldspars in Granodioritic Gneiss.	215
Table 4.35	Representative Electron Microprobe Analyses of Alkali Feldspar in Granodioritic Gneiss.	216

Table	Title	Page
Table 4.36	Structural Formulae of Alkali Feldspar in Granodioritic Gneiss.	217
Table 4.37	End Member Composition of Alkali Feldspars in Granodioritic Gneiss.	218
Table 4.38	Representative Electron Microprobe Analyses of Plagioclase Feldspar in Biotite Granite Gneiss.	221
Table 4.39	Structural Formulae of Plagioclase Feldspar in Biotite Granite Gneiss.	222
Table 4.40	End Member of Plagioclase Feldspar in Biotite Granite Gneiss.	223
Table 4.41	Representative Electron Microprobe Analyses of Plagioclase Feldspar in Biotite Granite Gneiss.	224
Table 4.42	Structural Formulae of Plagioclase Feldspar in Biotite Granite Gneiss.	225
Table 4.43	End member of Plagioclase Feldspar in Biotite Granite Gneiss.	226
Table 4.44	Representative Electron Microprobe Analyses of Alkali Feldspar in Biotite Granite Gneiss.	227
Table 4.45	Structural Formulae of Alkali Feldspar in Biotite Granite Gneiss.	228
Table 4.46	End Member Composition of Alkali Feldspars in Biotite Granite Gneiss	229
Table 4.47	Representative Electron Microprobe Analyses of Alkali Feldspar in Biotite Granite Gneiss.	230
Table 4.48	Structural Formulae of Alkali Feldspar in Biotite Granite Gneiss.	231
Table 4.49	End Member Composition of Alkali Feldspars in Biotite Granite Gneiss	232
Table 4.50	Representative Electron Microprobe Analyses of Alkali Feldspar in Biotite Granite Gneiss.	233
Table 4.51	Structural Formulae of Alkali Feldspar in Biotite Granite Gneiss.	234
Table 4.52	End Member Composition of Alkali Feldspars in Biotite Granite Gneiss	235
Table 4.53	Representative Electron Microprobe Analyses of Feldspar in Biotite Hornblende Gneiss.	237

Table	Title	Page
Table 4.54	Structural Formulae of Feldspar in Biotite Hornblende Gneiss based on 32 O_2	238
Table 4.55	End Member Composition of Feldspars in Biotite Hornblende Gneiss	239
Table 4.56	Representative Elemental Composition (wt %) of Biotite in Granodioritic Gneiss.	244
Table 4.57	Structural Formulae of Biotite in the Granodioritic Gneiss based on 24 O_2 atoms	245
Table 4.58	Representative Elemental Composition (wt %) of Biotite in Biotite Granite Gneiss.	246
Table 4.59	Structural Formulae of Biotite in the Biotite Granite Gneiss based on 24 O_2 atoms	247
Table 4.60	Elemental Composition (wt %) of Biotite in Biotite Granite Granite Gneiss.	248
Table 4.61	Structural Formulae of Biotite in the Biotite Granite Gneiss based on 24 O_2 atoms	249
Table 4.62	Elemental Composition (wt %) of Biotite in Biotite Hornblende Gneiss.	250
Table 4.63	Structural Formulae of Biotite in the Biotite Hornblende Gneiss based on 24 O_2 atoms	251
Table 4.64	Reformatted Oxide Percentages of Amphiboles in the Granodioritic and Biotite Granite Gneiss	258
Table 4.65	Structural Formulae and Classification of Amphibole based on 23 O_2.	259
Table 4.66	Microprobe Analyses and Structural Formulae of Garnets in the Biotite Granite Gneiss.	263
Table 4.67	Reformatted Oxide Percentages of Chlorites in Granodioritic Gneiss in the study area.	267
Table 4.68	Microprobe Analyses of Apatite on the Basis of $26O_2$ in the Granodioritic and Biotite Granite Gneiss.	273
Table 4.69	Microprobe Analyses of Titanite (sphene) on the Basis of 1Si in the Granodioritic and Biotite Granite Gneiss.	275
Table 4.70	Microprobe Analyses of Accessory Zircon on the Basis $16O_2$ in the Biotite Granite Gneiss.	276
Table 4.71	Microprobe Analyses of Accessory Rutile on the Basis $2O_2$ in the Biotite Granite Gneiss.	278
Table 4.72	Microprobe Analyses of Magnetite on the Basis $4O_2$ in the Granodioritic and Biotite Granite Gneiss.	280

Table 4.73 Summary of Selected Metallic Mineralisation Potentials in Lithologic Units. 283

CHAPTER ONE

INTRODUCTION

1.1 General Statement

The Precambrian rocks of Nigeria are still not very well understood because they are deep-seated and tend to be poorly exposed especially in typical rain forest environment. The evolution of the Nigerian basement lies within the Precambrian - Pan African mobile belt, to the east of the West African craton and to the west the Congo craton. The Nigerian shield is a southern continuation of the Touareg shield of central Sahara (Black *et al.*, 1994. and Caby, 1989).

The Geology of Nigeria is dominated by crystalline and sedimentary rocks both occupying approximately equal proportion. (Woakes, *et.al.* 1987). The crystalline rocks are made up of Precambrian Basement Complex and Phanerozoic rocks, outcrops largely in the north-central, south west and in the three smaller regions from north to south along the country's eastern boundary with Cameroun. The basement rocks of Nigeria are covered by the Mesozoic and Cenozoic sediments of the Dahomey and Niger Coastal Basin and intruded by Jurassic peralkaline granites toward the east and southern part (Breemen, *et. al*., 1975).

The pioneer geological studies of the Basement Complex of Nigeria started in the early 1900s with the first important published work was by Falconer (1911). The Precambrian Basement rock of the country consists mainly of three major rock assembleges which include: the ancient gneiss-migmatite complex (Rahaman.1988). Others are the low-medium grade metasediments or schist belts occupying relatively narrow troughs within the gneiss-migmatites complex referred to as the 'older metasediments' by McCurry,

(1976) and the intrusive suite of the Pan-African and (600Ma) granites and related rocks (Tubosun, *et al*. 1984). Minor units of the ancient complex include refolded quartzite and quartz schist and concordant bands, lenses and sheets of mafic bodies and calc-silicate rocks.

The Migmatite Gneiss Complex (MGC) is the most widespread and the region has been metamorphosed under medium- high amphibolites facies condition. Its composition ranges from granitic to granodioritic, has a regional vertical NE-SW and NNE-SSW trending foliations. The MGC exhibit open and asymmetrical folding with mainly N-S fold axis (Wright, 1971).

The Nigerian basement is better known as part of the Pan-African mobile belt as most of the crystalline shield area had been reworked 600Ma ago (Kennedy, 1964). Field and geochronological evidences have confirmed the polycyclic nature of the Nigerian Basement rocks (Emofurieta and Ekuajemi, 1995). Most of the crystalline Pre-Pan-African rocks in Nigeria basement bear Pan-African tectonic and mineralogical imprints thereby displaying chemical variations indicating that they originated from heterogeneous progenitors (Elueze, 1981). The Nigerian basement rock of Archaean age (>3.5 Ga) has been reported in the North central (Bruguier *et al*. 1994), while 2.4-2.5Ga ages have also been reported from gneisses in South western and in North Eastern part of the country with U-Pb Zircon dating (Dada*, et. al*. 1993).

1.2 Justification of Research study

The Basement Complex rocks of southwestern Nigeria have been mapped regionally with minimal geochemical data available for isolated regions. Some part of the south western Basement Complex terrain - the schist belts- such as Ilesha, Egbe-Isanlu areas have also been well studied because of their mineral potentials.

Limited study has been made in unravelling the complex geological history of some isolated areas which is almost entirely of highly deformed and metamorphosed igneous and sedimentary rocks. The needs to map on a larger scale in order to understand the petrographic and geochemical composition of the rocks is therefore necessary as this will

allow for a better understanding of the evolution and petrogenetic tendencies of the various rock units.

The study area lies within the Precambrian of southwestern Nigeria Basement Complex. The dominant rock types in the area include banded gneiss, quartzite and granite-gneiss (Rahaman, 1988). Little records of detail geological mapping of Sheet 241 (Oyo SE) have been recorded and the area had also not been subjected to any intense mineral search. This research work is intended to fill some of these gaps.

1.2 Aim

This research is aimed at conducting detailed geological mapping of lithologic units of Sheet 241, Oyo SE.

1.3 Objectives of study

The objectives of this study are to:

(i) Undertake detailed geological mapping of the study area with a view of producing the geological map on a scale of 1:50,000

(ii) Characterise the different lithological units of the study area.

(iii) Unravel their origin and evolution on the bases of field observations, whole rock geochemical data and mineral chemistry analyses.

(iv) Relate the geochemical variation/pattern results to possible mineral(s) occurrence(s).

1.4 Location of the Study Area

The study area falls in the topographic Sheet 241 (1:50 000) Oyo SE. The area lies within latitude $3^0$45'E and $4^0$00'E and longitude $7^0$30'N and $7^0$45'N with an area coverage of 1,595sq. Km (Fig.1.1).

1.5 Scope of Work

The work involves conducting detailed geological field mapping and laboratory analyses.The field mapping exercise involved systematic observation of outcrops for structural features and the determination of field relationship of the rocks. Identification and measurements of trends and orientation of the various rock units were conducted.

The laboratory works involved thin section preparation, whole-rock and trace elemental analysis for some of the representative rock samples using Inductively Couple Plasma Mass Spectrometry (ICP-MS), Inductively Couple Plasma Optical Emission Spectroscopy (ICP-OES) and X-Ray Fluorescence (XRF). Electron Microprobe and X-Ray diffraction (XRD) analyses were carried out on selected samples to determine their mineral chemistry.

The results of the chemical analyses were subjected to statistical analyses using Excel. Arc GIS and ArcView was used to produce both geologic and geochemical maps of the area while Geochemical Data Toolkit (GCDkit) software was used to interpret the data.

Conclusions and inferences were drawn from the lithological, structural, geochemical and mineral chemistry results with the aim of establishing the petrogenesis and geotectonic evolution of the rocks in the study area.

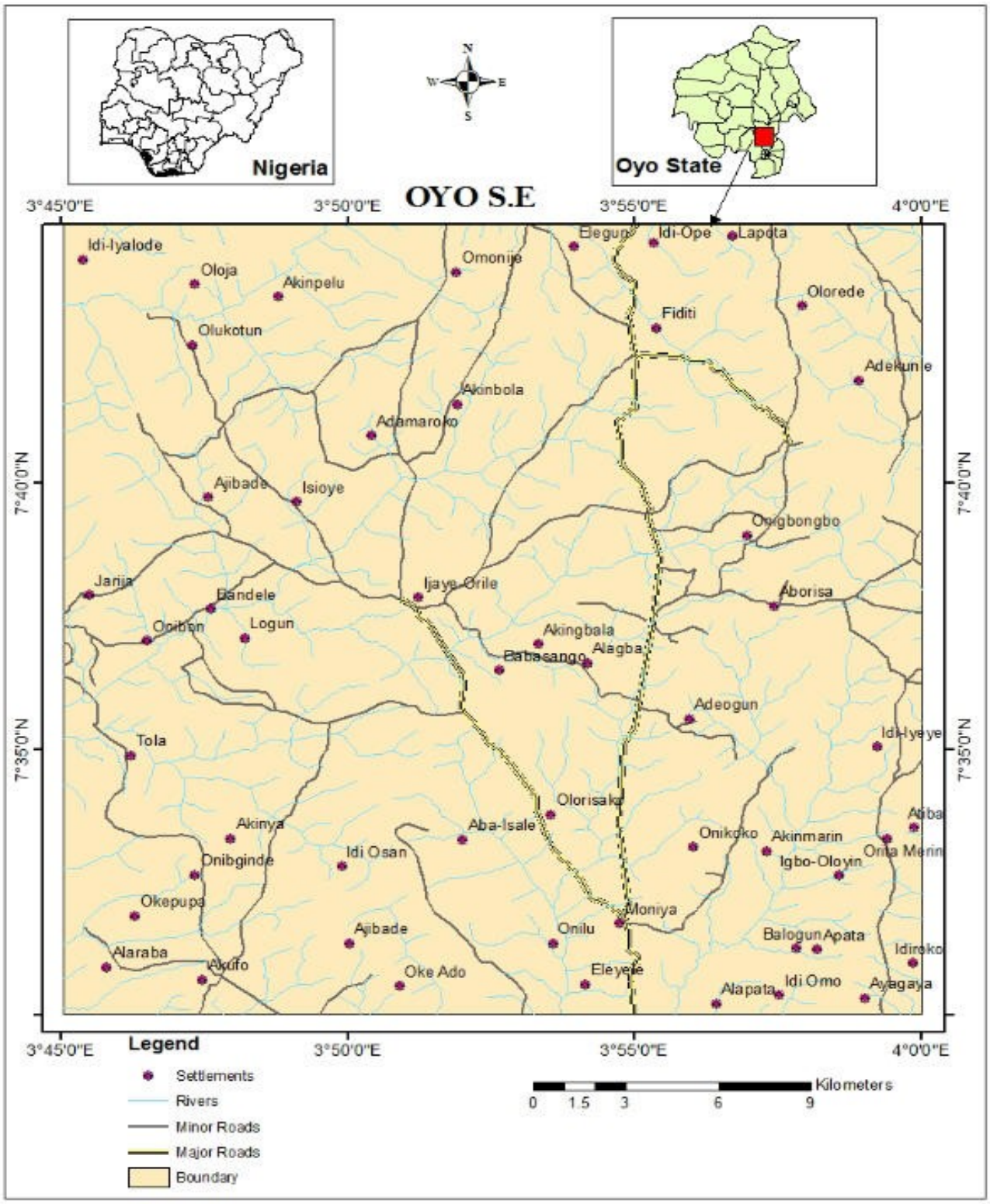

Fig.1.1 Location Map of Sheet 241 Oyo SE (After Federal Survey of Nigeria, 1964).

1.6 Climate and Vegetation

The study area falls within the high temperature and heavy rainfall region of south-western Nigeria. It experiences two major seasons: rainy/wet season and dry season. The rainy season is usually between March and October, reaching its peak in June with a break in August. The dry season is between November and March. The vegetation found is typical of a tropical rainforest. This comprises multitude of evergreen trees ranging from tropical hardwood, palm trees to green grasses (Fig 1.2).

1.7 Drainage and Topography

The study area is well drained with a dendritic drainage pattern. The rivers are made up of interconnecting rivulets and streams draining into the main rivers. The rivers and streams originate from the roots of the ridges and hills scattered over the areas.

Maximum elevations in the study area do not exceed 500 meter above the sea level, average elevation ranges from 200 to 300 meter. The relief is gentle in several places and steep in others.

Fig.1.2 Vegetation on the Study Area ***(coordinate: N07^{o} 30.793', E 03^{o} 55.134').***

CHAPTER TWO

LITERATURE REVIEW

2.1 Review of the Geology of Nigeria

The first recorded attempt at studying the geology of Nigeria was by Falconer (1911), during reconnaissance survey by the Federal Mineral Survey of Nigeria. He characterised the various schist belt of Nigeria when he concluded that most of the metals were of schist in origin.

Elueze (1982) conducted petrochemical study of the Precambrian gneisses and migmatite in the Western part of Nigeria. He revealed that the polycyclic Basement Complex which was evidently during the Pan-Afrícan tectogenesis, is composed dominantly of a wide range of textural and/or mineralogical types of gneisses and migmatites. The results of the chemical data showed that majority of the rocks are of supercrustal composition and are characterised by relative high contents of SiO_2, K_2O and related trace elements, while the melanocratic varieties have lower values of these elements but are comparatively enhanced in Fe, Ti, Cr and Ni concentration. He concluded that the rocks were derived from parents of varying compositions.

Kolawole, *et.al*. (2017) conducted field and structural mapping on a scale of 1:50 000 in the Kabba-Banu area of the Kabba-Lokoja-Igarra schist belt in order to determine the lithologic and structural features. The results revealed that the area is predominantly underlain by migmatite-schist suite which comprises migmatite-gneiss, migmatised schist and quartz-mica schist-quartzite complex which were intruded by N-S trending granite plutons and were closely associated with dolerite, pegmatite and aplitic veins. They concluded that the quartzite band suffered at least two thermotectonic orogenic events- E-W fold axis produced by N-S compressional force which was assumed to be

Eburnian age and N-S fold axis produced by E-W compressional stress assumed to be Pan-African events. Also, foliation and lineation trending E-W to NE-SW was interpreted to be ductile and earlier major structure, while minor brittle shear structure in the NW-SE to N-S directions were filled by quartz vein, dolerite, pegmatite dyke which served as conduits and pathways of the gold bearing fluids

Okunlola (2006) carried out petrographic and geochemical evaluation of pegmatite bodies around Aramoko, Ara and Ijero in SW Nigeria with a view to determining compositional trends that may be related to Ta-Nb mineralisation. Thin sections showed that quartz, microcline, albite and muscovite were the main mineral constituents while the geochemical result showed lower contents of SiO_2, Al_2O_3, K_2O, and CaO in sample from Aramoko than those of Ara and Ijero. However, Ta, Cs, Rb, Sn and Nb contents of samples were higher for those of Ijero compared to Aramoko occurrence. This was also similar to the work conducted on the schistose rocks around the Okemesi fold belt, IfeIlesha schist belt by Okunlola, *et al*. (2009). Quartzite, quartz schist and biotite muscovite schist were revealed from their systematic mapping and petrographic examinations, while the whole rock analytical results show that the rock units are comparable to those of post Archean pelitic-supracrustal rocks. The study further elucidates the possibility of the rocks evolving in a rifted environment of rapid subsidence, followed by closure which led to contemporaneous deformation of the sediments.

Elueze *et al*., (2004) determined the petrochemistry and petrogenesis of granite gneiss from Abeokuta area, southwestern Nigeria and concluded that the abundance and variation of major and minor trace elements suggest that the protoliths of the gneisses are mainly of igneous affinity, though with probable crustal contamination.

Elueze (1981) concluded that major and trace element abundances, ratios, and variation trends indicate that the bulk of the Ilesha metasediment reached a degree of chemical maturity similar to those of greywackes and sub-greywackes. He considered them to have been derived from clasticgranitoids deposited in a basin associated with rifting and relatively rapid subsidence.

Okonkwo, *et. al* (2004) conducted geochemical study of granitic rocks in Jebba area, southwestern Nigeria. They recognized two main groups of granitic rocks namely: variably foliated granitic gneiss which forms an elongated body concordant with the host rocks, and late, largely un-deformed, discordant bodies comprising both coarse-grained and fine-grained varieties of granite. Their geochemical data indicate that the granitic rocks are Fe-rich, while the granite gneiss contained significant higher concentration of Zr, Y, Nb and LREE. Also the potassic granite and the granitic gneiss are more siliceous than the un-deformed granites.

Elueze, *et.al*. (2008) studied the geochemical and petrogenetic trends of syenite and charnockitic rock of Oke-Iho and Osuntedo areas, south west of Ofiki in the Iseyin-Oyan schist belt. They found out that geochemical trends derived from major and trace elements and also elemental ratios of the two rock types indicated that Osuntedo charnockitic rock is richer in SiO_2, Al_2O_3 and K_2O with lower values of TiO_2, Fe_2O_3, MnO and MgO. Similarly, Na_2O and P_2O_5 values were lower than those obtained for the Oke-Iho syenite.

Oyinloye, (2011) examined the geology and geotectonic setting of the Basement Complex rocks (Amphibolite, hornblende gneiss and biotite granite gneiss) in Southwestern Nigeria with implication on provenance and evolution. He noted that geochemical, geology and petrological studies revealed that all these crystalline rocks were genetically related and had evolved by progressive differentiation of a parent basaltic magma to give rise to the protoliths. He further stated that chemical studies revealed that the magma of the protoliths were from a metasomatised mantle.

Dada, (1999) investigated the Archaean Migmatite-Gneiss Complex of Kaduna area for their major and trace elements geochemistry with a view to understanding its petrogenesis and evolution. His result revealed that the gneisses contained high Rb, Sr, K/Rb, K/Sr, low Ca and chondtite normalised negative anomalies in Nb, P, Ti with net improverishment in the HREE, while the amphibolites have low Mg-tholeiites and poor in LILE but enriched in P and HREE. He concluded that with high Al_2O_3/TiO_2, CaO/TiO_2, (La/Sm)n, (La/Yb)>30 and low Ti/Zn indicated amphibolites facies gneisses in high grade terrains and subduction related magma generation on volcanic arc setting. The two contrasting

amphibolites – the low Titanium Tudun Wada and high Titanium Kabala- both occurred as dismembered enclaves within the gneisses.

Olobaniyi, *et. al*. (2011) worked on chemical composition of chromite and intergrown chlorite in metamorphosed ultramafic rocks (serpentinite and talc schist) of the Egbe-Isanlu schist-belt, Southwestern Nigeria. They found out that chlorite was formed or re-equilibrated within the green schist metamorphic spectrum, and that chromite, originally contained in ultramafic rocks (peridotite), inferred to be similar in composition to chromite of stratiform deposits, suffered chemical alterations during metamorphism. The original peridotite was transformed into serpentinite and talc schist, while the altered chromite suffered a near complete loss of Al and Mg with enrichment of Cr, Ti Zn and Fe concentration.

Bafor (1981) reported that minor amounts of sulphide mineralisation occur in metagabbroic rocks exposed in Egbe area. He concluded that the ore minerals consist of pyrrhotite, ilmenite, pentlandite, chalcopyrite and pyrite occurring as fine dissemination in the metagabbroic rocks and appear to have been deposited from igneous hydrothermal fluid saturated in sulphur.

The Sarkin Pawa migmatite gneiss, North central Nigeria was investigated by Dada, (1999) for its geochemistry, U-Pb, Rb-Sr and accessory mineralogical characteristics. The results revealed that the migmatite gneisshas well develop foliation in form of lineated biotite and elongated megacrysts of microcline, while the SEM studies on the mineral grains confirmed abundant allanite, garnet, apatite, Zircon as well as their enrichment in REE. U-Pb dating on Zircon indicated a metamorphic age of 624 ±33Ma which is in agreement with the peak of the syn-tecto-metamorphic Pan-African event and its associated remobilisationin form of migmatisation of the original granodioritic rock with complete resetting of the emplacement age of the progenitor.

Microprobe analyses were carried out on the amphiboles, pyroxenes and epidote minerals in the amphibolites rock from Ife-Ilesha schist belt (Olanrewaju, *et. al*. 1993). The results showed that the clinopyroxene present in the foliated leucocratic amphibolites was CaO and Fe_2O_3 rich (ferrosalite) with low Al_2O_3 and Na_2O contents, while the amphibole

present was hornblende and epidote was compositionally similar to Fe-rich Al-poor epidote (clinozoisite). He concluded that the overall chemical features of the ferro magnesian mineral suggest that variable metamorphic load pressure prevailed in this area during regional metamorphism,

Ajayi, *et. al* (1999) used the technique of partial extraction method for regional lithogeochemical survey of Ife- Ilesha area. His objectives were to determine the level of metal abundance in the amphibolite as well as to assess the suitability of the surveying method used in exploration. His results revealed general normal background populations except for Cr, Ni and Cu which show the presence of anomalous populations. Moreso, multi-element geochemical anomalies occur in Ifewara, Itagunmodi, Araromi and Mokuro areas which correlated spatially with places where alluvial gold has been worked and exploited.

The vertical distribution of 17elements and 12 minerals along a 5.6m thick residual soil profile derived from banded biotite gneiss at Ile-Ife, was investigated by Emofurieta, *et. al.* (1995) using Atomic Absorption Spectrophometeric and X-ray diffractometric method and they concluded that given the average high alumina (25-55%) and Fe- oxide (6.71%) contents as well as the clayey nature, the lateritic mantle constituting the B-horizon is a potential raw material for burnt bricks, which was therefore considered economic assets if properly harnessed.

2.2 Geology of the Basement Complex of South Western Nigeria

The Basement Complex of South Western Nigeria lies to the East of the West African Craton in the region of late Precambrian to early Paleozoic. The Nigeria Basement complex extends westwards and is continuous with the Dahomeyan of the Dahomey-Togo-Ghana region. To the East and the South, the Mesozoic – Recent sediments of the Dahomey and Niger Delta cover the basement complex. The rocks have been classified into five major groups (Rahaman 1971, 1973).

- The Migmatite Gneiss Complex
- The Meta- sedimentary and Meta- volcanic rocks (Schist belts).

- The Pan African Granitoids (Older Granites)
- The Charnockitic, Gabbroic and Diorite rocks.
- The unmetamorphosed dolerite dykes.

The Migmatite Gneiss Complex

The migmatite Gneiss complex is the most widespread in the Basement complex of southwestern Nigeria. It comprises gneisses, quartzites, (typified by Ibadan and Iseyin type quartzites) Calc silicate rocks, biotite-hornblende Schist and amphibolites. The migmatite gneisses are composed of three main petrological units, which may not be observed on a single outcrop Rahaman, (1971).

I. The early Gneiss is a grey foliated biotite and or hornblende quartzo-feldspathic rock of granodiorite to quartz dioritic composition. Alternating mafic and quartzo-feldspathic material sometimes define a fine banding. More commonly, the quartzo-feldspathic material form impersistent streaks a few millimetres thick, which are invariably, aligned parallel to the foliation as defined by the mafic. The contact between the mafic and felsic materials is gradational. The early gneiss is best seen in the migmatites around Ibadan, Iseyin and Ikare (Rahaman, 1971).

II. Mafic to Ultramafic Bands: These are usually amphibolite, biotite and biotite hornblende schist or rarely meta-gabbros. They are usually strongly foliated with the foliation being parallel to that of the enclosing rocks, they may be completely absent in some outcrops (Rahaman, 1981).

III. Granitic or Felsic component: This is usually of granitic composition and varies in texture from aplitic to granitic to pegmatite.

It has largely modified pre-existing structure in the other two components. It occurs as (i)concordant to discordant veins and dykes of pegmatite.

(ii) Swarms of augen shaped Porphyroblast of white or pink microcline aligned along the pre-existing foliation in the host rock.

(iii) Indefinite impregnations commonly resulting in destruction of the structure of the host rock.

Depending on the relationship between these three components. Various types of gneisses can be distinguished.

The banded gneiss which is the most abundant type consisting of alternating parallel light and dark coloured bands. The dark bands may be an early gneiss and /or mafic-ultramafic rock and light bands are granitic. Individual bands vary in thickness from a few millimeters to tens of centimeters or even meters. The dark bands rarely exceed a meter in thickness.

Where the granitic material takes the form of indefinite impregnations more uniform gneiss commonly described as granite gneiss is produced.

Semi-banded gneisses form the transition between these two cases and have been described as transition gneisses.

The Meta-sedimentary and Meta-volcanic Rocks (Schist Belt)

These are composed of Meta sedimentary and Meta volcanic rocks that occupy the N-S trending synformal troughs in folded into the Achaean Migmatite Gneiss Complex. They are largely sediment dominated by pelites, semi-pelites and quartzite. In the Iseyin area, Rahaman (1973) had described biotite schist, biotite-garnet schist and biotite garnet-staurolite schist, together with amphibolite and talc-tremolite chlorite rocks. In some belts, chemical sediments are now present as marbles and Banded Iron Formation (BIF). Mafic to ultramafic rocks are present as amphibolites and ultramafitites. Minor felsic to intermediate meta-volcanic rocks and greywacke has also been described. The schist belts were about the best studied group of rocks in Nigeria (Russ, 1957; Truswell and Cope, 1963) because of the known mineralization such as gold, BIF, marble, and so on are associated with them.

Grant (1978), Holt (1982), and Turners (1983) based on structural and lithological associations suggested that some of the schist belts are of Kibaran (1110+200 Ma) and older age, whilst others are of Pan-African age (600Ma). Ajibade *et al.,* (1979) disagreed with the structural evidence and proposed a Pan-African age for the schist belts. Thus, the

age of the schist belts remains largely unknown as date varied from the Achaean to late Proterozoic have been proposed.

Pan African Granitoids (Older Granites)

The Older Granites were first distinguished from the Younger or Plateau tin-bearing alkali Granite (Falconer, 1911). They range in size from plutons to batholiths. The form of the bodies appears to be related to the environment in which the granite is emplaced. Circular to elliptical bodies occur in schist environment and more elongate bodies in Migmatite Gneiss terrains. The older granites are the most obvious manifestation of the Pan African Orogeny and constitute about 40-50% of the basement complex outcrop. They include rocks of a wide range of composition including tonalities, granites, granodiorites, adamellites, quartz monzonites, syenites, and pegmatite. Granitic-granodioritic compositions are the most common. Textually, they vary from strongly foliated gneiss varieties to un-deformed rocks. Available geochronological data show that most bodies were emplaced between 700-500Ma.

Under the Granitic-granodioritic rocks, Jones and Hockey (1964) recognized three main groups of granites, an early phase comprising granodiorites and quartz diorites; a main phase comprising coarse porphyritic biotite granite and a late phase comprising homogeneous granites, dykes, pegmatites, and aplites.

The Charnockitic and Dioritic Rocks

These are rocks emplaced during the Pan African Orogeny. Diorites rocks are more widely distributed and appear as small bodies and stocks. The Charnockites generally outcrops as smooth, widely distributed rounded boulders although in places like Oke-Patara and Osuntedo, they form isolated hills. They occur along the gneiss complex such as the occurrences at Lagun, Awo, and east of the Igarra formation (Rahaman, 1971).

The Un-metamorphosed Dolerite Dykes

Dolerite dykes are widespread on the Basement Complex and have been described in association with the gneisses and Older Granites. They occur as tabular, un-metamorphosed bodies crosscutting the foliation in the host rocks, and are regarded by most authors as the youngest member of the Basement Complex. They range in thickness from about a few millimeters to half a meter. The general trend of the dykes observed is between NE-SW and ENE-WSW(Jones and Hockey, 1964).

In some cases, closely spaced joints parallel to the trend of these dykes is observed in the host rocks in the immediate vicinity of the dykes. Dolerite dykes are generally fine-grained and black, but in some cases, pale green spots of olivine may be observed in the hand specimen. The texture is typically diabasic. The rock is composed largely of augite and plagioclase of andesine-labradorite composition. The contact between the dolerite dykes and the country rocks is always sharp and chilled. Grant (1970) obtained a whole-rock K-Ar age which is 478 ± 19Ma on an un-metamorphosed dolerite dyke from Ibadan. They therefore represent the latest Pan-African intrusions in the basement complex.

2.3 Metamorphism in the South Western Nigeria Basement rocks

On the basis of petrology, a medium pressure Barrovian and Low-medium pressure types of metamorphism had been suggested for the Precambrian basement rocks in south western Nigeria (Rahaman 1988). These metamorphic types are based on the occurrence of index minerals like chlorite, biotite and sillimanite in the basement rocks of southwestern Nigeria.

Rahaman (1988) therefore concluded that metamorphism in all Nigerian Precambriancomplex rocks especially that of Ife-Ilesha ranges from green schist to lower amphibolite metamorphic facies.

However, Oyinloye (1992) on the basis of petrology, field mapping and structural analyses reported that the prominent gneissicfoliations observed on some of the gneisses suggest that metamorphism actually reached anupper amphibolite facies in the rocks of the basement complex in Southwestern Nigeria.

Egbuniwe (1982) suggested a three phase of metamorphism (M_1, M_2 and M_3) associated with three phases of deformation (D_1, D_2, and D3) within the crystalline rocks of the basement complex inNorthern Nigeria. According to this author M_1 represents a period of progressive metamorphism to lower amphibolite facies. M_2 is described as retrogressive and reached only green schist grade as did M_3. In the southwest Boesse and Ocan (1988) recognized three phases of metamorphism but only two phases of deformation:

- M_1 is considered to be a syn-tectonic progressive phase of metamorphism to amphibolite facies with isoclinal folding, mineralogical banding and development of staurolite, sillimanite and garnet.
- M_2 is described as syn-tectonic and associated with shear deformation and
- M_3 being static retrogressing the earlier formed garnet and biotite to chlorite.

Oyinloye (1992) however suggested that;

- M_1 is syn-tectonic and perhaps synchronous with the formation of the large scale major fault zone indicated by formation of mylonite outcrops at Iwaraja.
- M_2 is also syn-tectonic and contemporaneous with D_2 as indicated by the development of micro faulting folding, fracturing, shearing, formation of phyllonite and mylonite with distorted garnet crystals surrounded by sillimanite crystals and mylonitised granite gneisses.

CHAPTER THREE

RESEARCH METHODOLOGY

3.1 Field Activities

The field mapping exercise was undertaken between September and October, 2014, December 2015 and February 2016 using a topographic map of sheet 241 Oyo SE (1:50,000) as the base map (Federal Mineral Survey of Nigeria, 1964). The location map was divided into grids for the comprehensive field exercise. Method employed for this study was geological traversing.

The geological field mapping exercise conducted by traversing the area involved detailed observation of outcrops, structural features (such as foliations, lineation, folds), field relationship of the rocks, measurements of trends and orientations of rock units were undertaken and fresh representative samples were obtained.

3.2 Laboratory Analyses

3.2.1 Petrographic Analysis

Thin section preparations were prepared on one-hundred representative rock samples collected from the study area for petrographic study at the thin-section laboratory at Department of Geology, University of Ibadan. The following procedures were undertaken on each rock sample.

Carefully selected rock sample was marked for cutting into flat rock slab in order to get the best information. The big diamond saw blade machine was used for the cutting.

The flat rock slabs were trimmed with a small diamond saw machine to make a thin section chip, which left it surface smooth.

The chip surface was then ground with coarse grit slurry of silicon carbide on a sheet of glass plate to removed pits and saw marks while a fine grit of silicon carbide was used to make a smoother finished. The chip was later put on a hot plate to warm up and dry.

A high strength epoxy was then mixed and smeared on the ground chip surface and the glass slide was put onto the chip. The bubbles produced were worked out with pencil eraser. The chip was left for some minute on the hot plate to glue to the epoxy and set hard.

A special small diamond saw was used to cut most of the excess chip from the glass slide leaving only 0.5mm of rock left on the slide. The chip was hand ground to final thickness of 30μm using a slurry of grit and water.
Precautions that were taken during the preparation of the thin sections include:

I. Pressing the glass slide on the thick part of the thin section was avoided in order to prevent grinding only one part.
II. Periodically checking of the thin section thickness was conducted with a polarizing microscope in order to avoid rock slice be too thin or even grind it completely off the slide.
III. The thickness was determined by looking at the interference colours of known minerals such as quartz and feldspars.

After hand grounding, the thin section was then put back on the hot plate to warm up. Canada balsam was smeared on the section surface and cover-slip was put onto it, the bubbles were worked out with a pencil eraser. The Canada balsam fills in the microscopically rough surface on the top of the thin section, making it appeared clear and transparent.

The prepared thin sections were studied under the petrographic microscope using transmitted light at the Petrography Laboratory in the Department of Geology, University of Ibadan, Nigeria.

3.2.2 Whole Rock Geochemistry Analyses

Thirty-six rock samples were pulverised prior to Whole-Rock geochemical analysis conducted at Bureau Veritas Minerals (BVM) Pty Ltd, Canada using Inductively Coupled-Mass Spectrometer method. Lithium Metaborate Fusion digestion technique was used to break down the samples. The fusion technique decomposes the most refractory matrices to provide total elemental compositions and can account for structural water while providing quantitative results for silicon. A 60-element analytical suite was selected comprising major, trace and rare elements including Total Carbon and Sulphur.

Quantitative analyses of eighteen representative rock samples were pulverised at the Department of Geology, University of Leicester using RETSCH PM400 Ball Mill. Samples were determined for the major and some trace elements by X-ray Fluorescence Spectroscopy using Empsilon XRF spectrometer by PANanalytical. Pellet discs were prepared for the X-Ray Fluorescence analysis. To prepare the pellet disc, 8.50g of the sample powder was weighed accurate to two decimal places to which was added 1.50g of Licowax C Micropowder PM Herzog organic binder. The mixture was then shaken to make the final powder homogenous and was made into discs using a pressure of 12 tonnes.This was done to ensure sample integrity under the vacuum and a consistent surface to receive the X-rays. The disc was then removed from the ram, bagged and labelled appropriately. The steel parts were again cleaned thoroughly with ethanol between each press to avoid cross- contamination.

The base metals and rare earth elements for the eighteen rock samples was performed by Inductively Couple Plasma - Optical Emission Spectroscopy method (ICP-OES). 0.50 gram of sample was digested in 100ml aqua regia and diluted by volume to 250ml with 18megaohm water. A further 0.25 g sub-sample refluxed with orthophosphoric acid for total rare earth element determination

To ensure the reliability, accuracy and reproducibility of the data generated, reference materials, blanks and duplicates were analysed with the samples.

3.2.3 Scanning Electron Microscopy- Energy Dispersive X-Ray Fluorescence

A total of seven representative polished sections were investigated with a Scanning Electron Microscopy attached with Energy Dispersive X-Ray Fluorescence Spectrometer (SEM-EDXRF). Four of the samples were analysed using the JEOL JXA-8100 Microprobe Analyzer at the University of Cape Town, South Africa (Fig.3.1), while the other three samples were analysed using a Zeiss EVO 50 (Zeiss, UK) with an INCA 350 software (Oxford Instruments, Incax-sight, UK) at the University of Wolverhampton (Fig.3.2) in-order to study the chemistry of the minerals.

The operating conditions of the instrument were 20- 25 kV accelerating voltage, 15–20nA beam current and peak and background counting times of 20 - 35s per element. Analytical standards were high purity metals, well-characterised synthetic oxides and natural minerals including MAD-10 Feldspar (K); Al_2O_3 (Al); SiO_2 (Si), Wollastonite (Ca);MgF_2 (F); GaP (P); MgO (Mg); albite (Na); Fe (Fe); and Ti (Ti) etc

Mineral phases were assessed from atomic proportions of constituent elements, obtained by semi-quantitative EDS X-ray microanalysis. X-ray spectra were optimised for quantification using cobalt optimisation standard and the correction of EDS data was performed on basis of the standard ZAF-correction procedure included in the INCA Energy Software

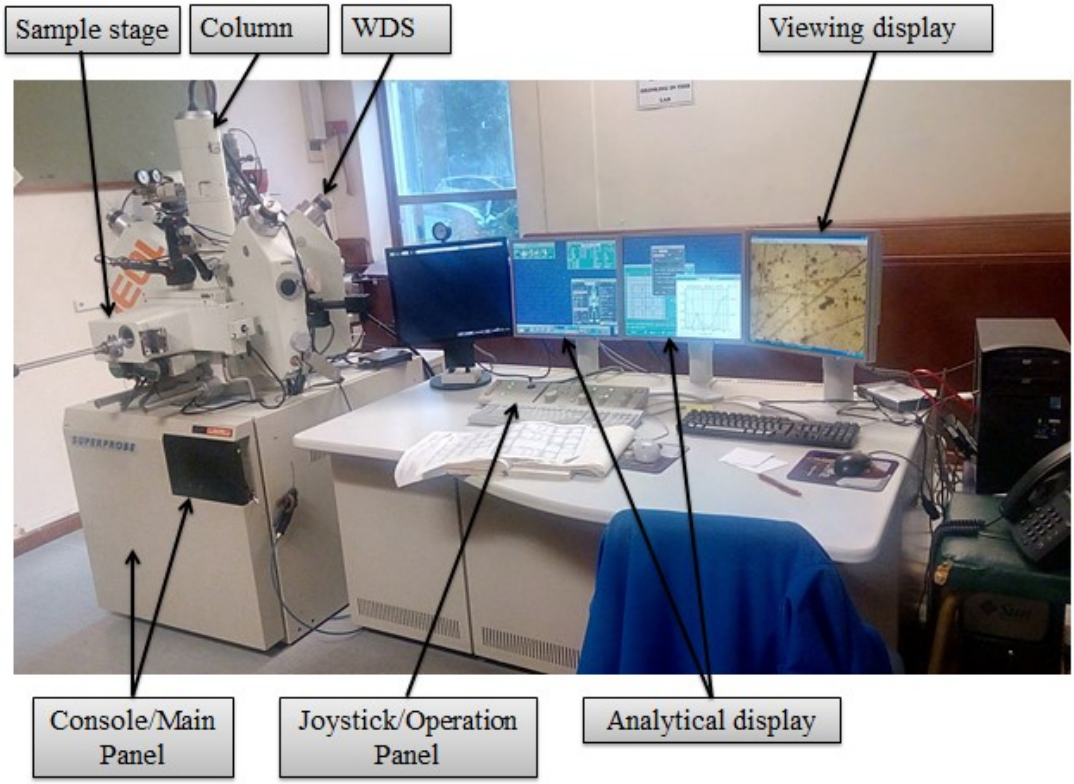

Fig.3.1. JEOL JXA-8100 Electron Microprobe Analyser Used for Mineral Chemistry of Gneissic Rocks at University of Cape Town, South Africa.

3.2.4 X-Ray Diffraction (XRD)

Three rock samples were pulverised to fine powder and analysed for mineralogical composition using PANalytical Empyrean X-Ray Diffractometer. Portions of the pulverised rock samples were placed on the flat auto-plate and pressed down to fill the entire perimeter of the plate using a glass plate. After obtaining a smooth and level sample powder surface, the plates were stacked on an auto-stand. A proportion of the X-rays were diffracted by the regular crystal structure of the samples.

XRD pattern of these samples were recorded over 2θ range of 5^0 to 70^0. The diffractometer was equipped with a graphite monochromated Cu Kα radiation source (8987 eV; ƛ = 1.5418Å). Mineral phase identification was made by searching the ICDD powder diffraction file database, with the help of Joint Committee on Powder Diffraction Standards (JCPDS) files while Data processing was carried out using Xpert High Score Plus software with a search/match facility and an ICDD database on a DEC Microvax Minicomputer interfaced to the diffractometer.

Two representative samples of granodioritic gneiss (G8 and G5) and one sample each of biotite granite gneiss (b15) and pegmatite (P3) were analysed using XRD methods.

3.3 Data Analysis

Microsoft Excel was used for the presentation and analysis of the geochemical results. Geochemical Data ToolKit (GCDkit) version 2.3 software was used to calculate CIPW norms, plot spider, multiple, ternary and binary, several geotectonic and discrimination diagrams.

The updated geological, topographical maps and images were digitised with the aid of Arcview GIS 3.2a and Global mapper geographical information system (GIS) software.

CHAPTER FOUR

RESULTS AND DISCUSSION

4.1 Field Relationship and Lithology.

Geological mapping of sheet 241 (Oyo SE) showed that the study area is underlain by Quartzite, Schistose rocks, Gneissose rocks, Leucogranite, pegmatite, dolerite and quartz veins. These are in conformity with many areas of the Basement Complex of Nigeria as recognised by Rahaman, (1976).The schistose rocks can be further divided into quartz schist and muscovite garnet schist, while the gneissose rocks are divided into three according to the lithological features of the rocks that were observed on the field:

Biotite Hornblende Gneiss (bHG)
Granodioritic Gneiss (GG)
Biotite Granite Gneiss (bGG)

4.1.1 Quartzite

The quartzite outcrops as good topographic features which rise up to about >200 meter in elevation, while some occur as small to big boulders on hills. Massive exposures were mapped in the eastern part (Coordinate: N07^{o} 37.189′, E 03^{o} 58.761') of the area. There is no quartzite in the western part but few pockets of foliated quartzite ridges outcrop in the central margin of the area. The quartzites were inter-banded with the biotite-hornblende gneiss and are closely associated with the quartz-schist.

Pocket of banded quartzite striking NE-SW and steeply dipping outcropping at the southern edge of the area exhibit distinct cleavage plane, highly jointed and fractured. The ridge is presently mined for quartz stones by artisanal (Coordinate-N07 31.063, E003 51.837). The quartzite is generally snow white, but some are brownish in colour and they are coarse grained in size (Fig.4.1).

a

b

Fig.4.1. (a) An Overview of Hog-back Ridge Quartzite at Ikereku. (b) Boulders of Quartzite at the Foot of Ikereku Ridge. ***(Coordinate: N07^{o} 37.189', E 03^{o} 58.761')***

Modal composition reveals quartz (87-88%), plagioclase feldspar (5-8%), biotite (2-3%) and opaque mineral (2%) were observed (Table 4.1).

The quartzites were granoblastic in texture with quartz minerals having very high percentage of the mineral composition. Anhedral quartz displayed irregular grain boundaries, grain fractures as well as undulose extinctions in response to recrystallization (Fig.4.2). Recrystallized sub-grains of quartz were also observed in Figure 4.3. Subhedral to anhedral plagioclase feldspar shows polysynthetic twinning and sphene occurred as accessory mineral.

Table 4.1. Modal Composition of Minerals in Quartzite in the Study Area

Sample No → **Mineral ↓**	Q1	Q2
Quartz	88	84
Plagioclase	5	8
Biotite	2	3
Sphene	-	3
Opaque	3	2
Total	100	100

a

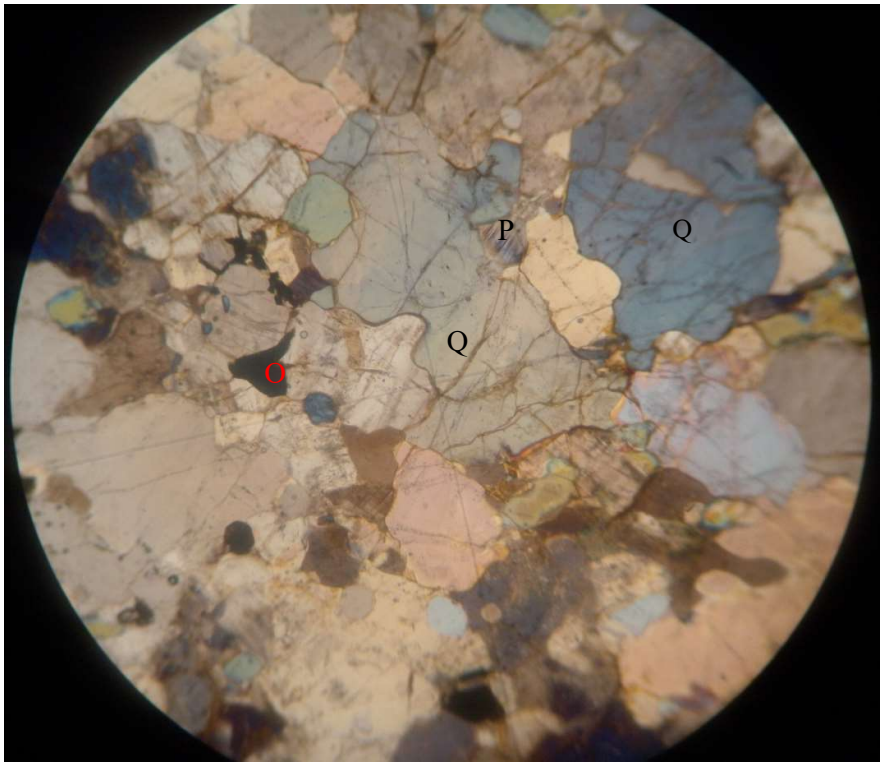

b

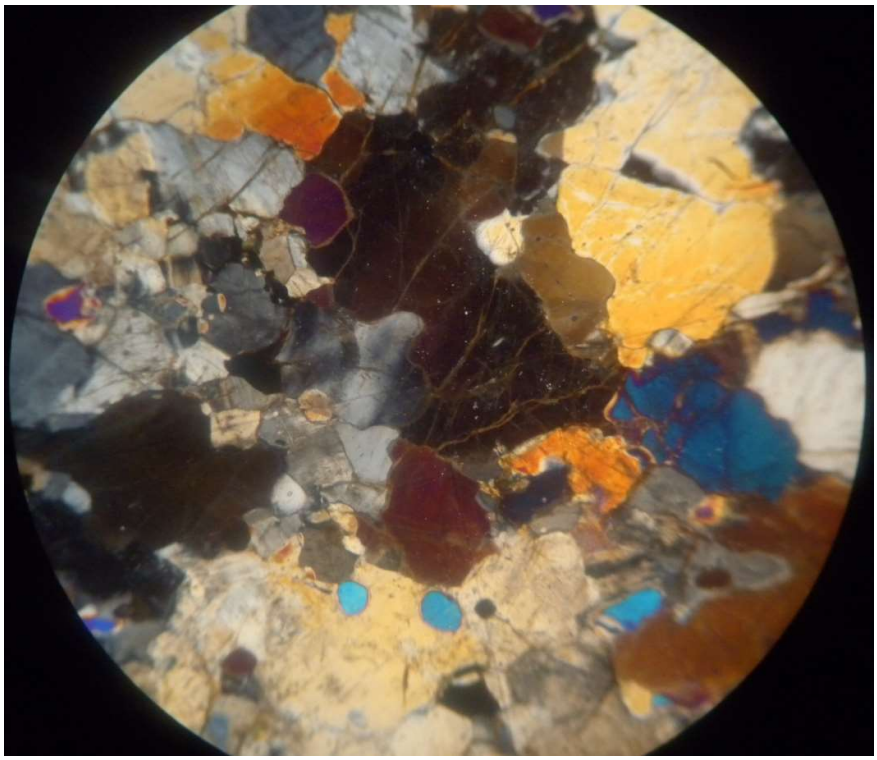

Fig. 4.2 Typical Photomicrograph of Quartz schist in Transmitted Light. *(a) plane polarised (b) cross polarised light (x40): indicating granoblastic anhedral quartz grains(Q) with irregular grain boundaries, plagioclase feldspar (P), and Opaque mineral (O).(Coordinate: N07^{o} 31.063', E 03^{o} 51.837').*

a

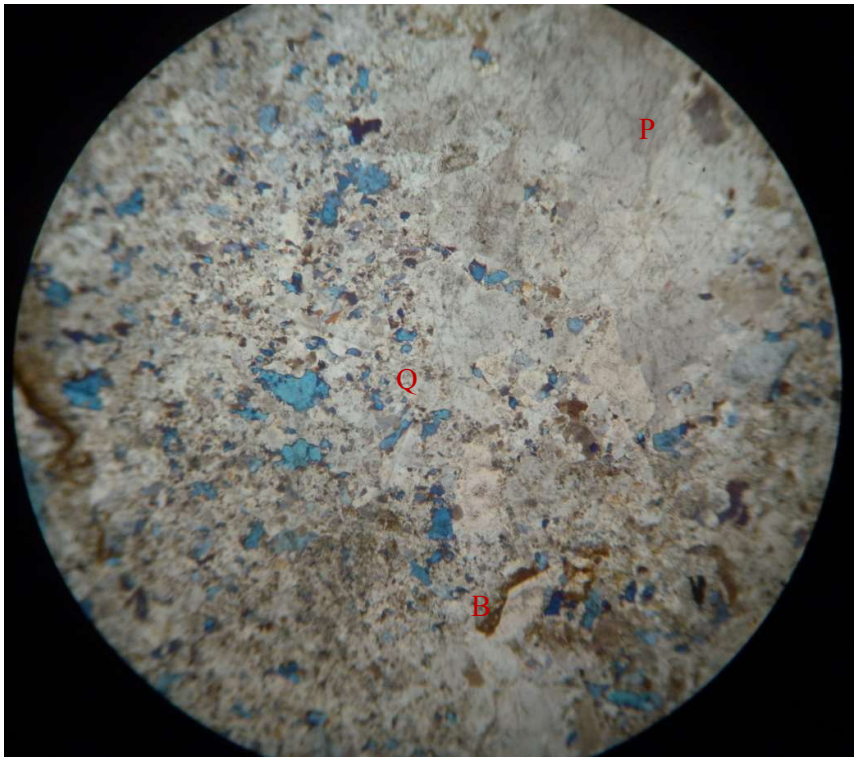

b

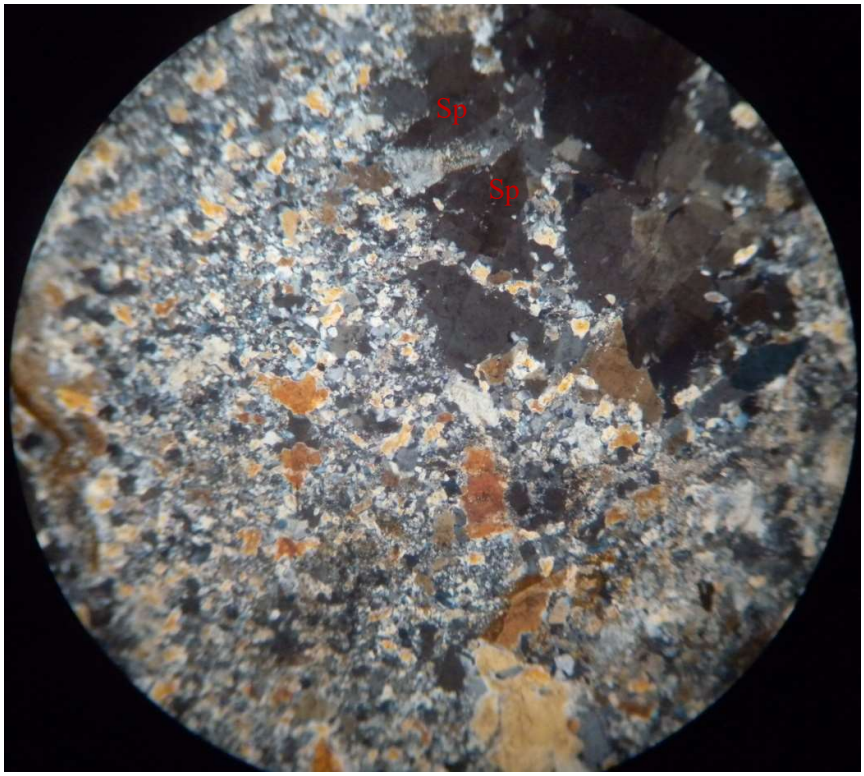

Fig. 4.3 Typical Photomicrograph of Quartz schist in Transmitted Light. *(a) plane polarised (b) cross polarised light (x40): showing recrystallized quartz grains(Q), plagioclase feldspar (P), biotite mineral (B) and sphene (Sp) (Coordinate: N07^o 37.189', E 03^o 58.761')*

4.1.2 Schistose Rock

4.1.2.1 Quartz Schist

The quartz schist was found in close association with the muscovite garnet schist in the south eastern part and inter-banded with the gneisses in the north-east and south-western part of the study area. They occur as low-lying rocks trending N-S with moderately dipping schistose planes. The quartz schist is fine to medium grained and dark in colour. There are dominant amount of quartz lens phenocryst showing development of quartz ribbons on some of the outcrops (Fig. 4.4). Micro folds as well as concordant quartzo -feldspathic veins were observed on some of the quartz schist (Fig. 4.5).

In transmitted light, the quartz schist contained quartz (35-55%), albite plagioclase feldspar (10-25%), microcline (2-15%), muscovite (2-25%), biotite (8-20%), hornblende (2-8%), chlorite (2-5%), orthoclase feldspars (2-8%), opaque mineral (2-4%) and accessory apatite (Table 4.2).

The grain sizes indicate in-equant texture with numerous platy muscovite and biotite minerals, which strongly defines preferred orientation of the rock (Fig. 4.6). Muscovite flakes occur as elongated plate intergrowth with brown biotite and chlorite forming spaced crenulation cleavages (S_2) on earlier fabrics in the matrix of quartz and plagioclase feldspars (Fig. 4.7). At the boundary of quartz-schist with other lithological unit, the mica minerals occurred as sparsely aligned grains within the quartzo-feldspartic minerals (Fig.4.8 and Fig.4.9). Quartz grains are subhedral, exhibit granulitic texture and sometimes show undulose extinctions (Fig.4.10). Microcline exhibit cross-hatched twinning and orthoclase feldspars occur in small percentage in the schist (Fig.4.8). Plagioclase (albite) occurs as euhedral porphyroblastic crystal displaying polysynthetic twinning and sometime sericitized having patchly pale brown appearance (Fig.4.8). Hornblende shows pleochroism from light green to brown and occur in the quartz schist bounded to the hornblende-biotite gneiss but absent in the schist bounded with the biotite granite gneiss (Fig.4.10).

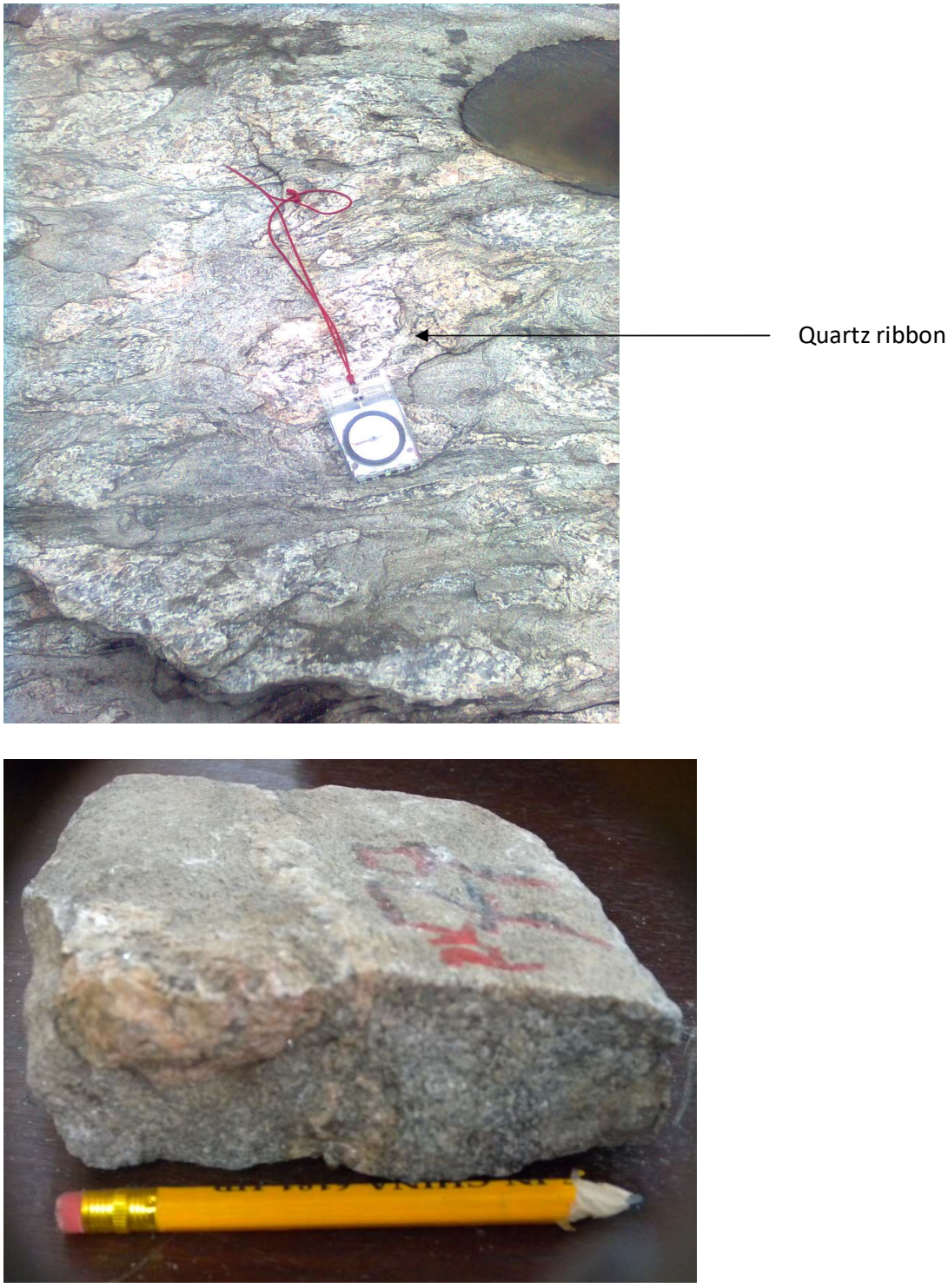

Fig. 4.4 (a) Low Lying Quartz Schist Outcrop Showing the Development of Quartz Ribbons (b) Hand specimen. *(coordinate: N07^{o} 33.260', E 03^{o} 58.821')*

(a)

(b)

Fig. 4.5 (a) Low Lying Quartz Schist Outcrop (b) Hand Specimen Displaying Well Defined Schistose Plane.*(Coordinate: N07^{o} 31.910', E 03^{o} 58.875')*

Table 4.2 Modal Composition of Minerals in Quartz Schist in the Study Area

Sample No → / Mineral ↓	QS1	QS2	QS3	QS4	QS5	QS6	QS7	QS8	Range
Quartz	38	45	45	45	55	40	40	43	38-55
Albite Plagioclase	20	18	10	10	15	15	25	20	10-25
Microcline	-	-	-	15	2	-	2	4	2-15
Chlorite	5	3	2	3	5	5	4	3	2-5
Muscovite	5	10	25	8	2	10	7	6	2-25
Biotite	18	12	11	10	15	20	8	10	8-20
Orthoclase Feldspar	8	5	3	2	4	8	5	4	2-8
Hornblende	3	3	-	-	2	2	7	8	2-8
Apatite	-	-	-	3	-	-	-	-	3
Opaque	3	4	4	4	-	-	2	2	2-4

(a)

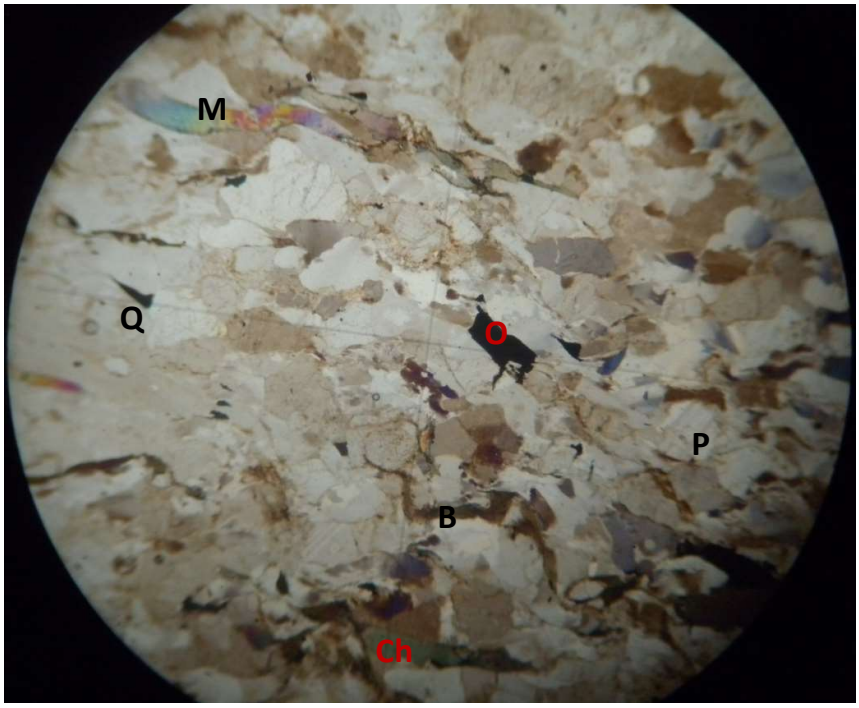

(b)

Fig. 4.6 Typical Photomicrograph of Quartz Schist in Transmitted Light. *(a) plane polarised (b) cross polarised light (x40): indicating preferred orientation of subhedral platy biotite (B) and muscovite (M) defining schistosity plane (S_2),anhedral quartz (Q), plagioclase feldspar (P), chlorite (Ch) and Opaque mineral (O).(Coordinate: N07^o 33.260', E 03^o 58.821')*

(a)

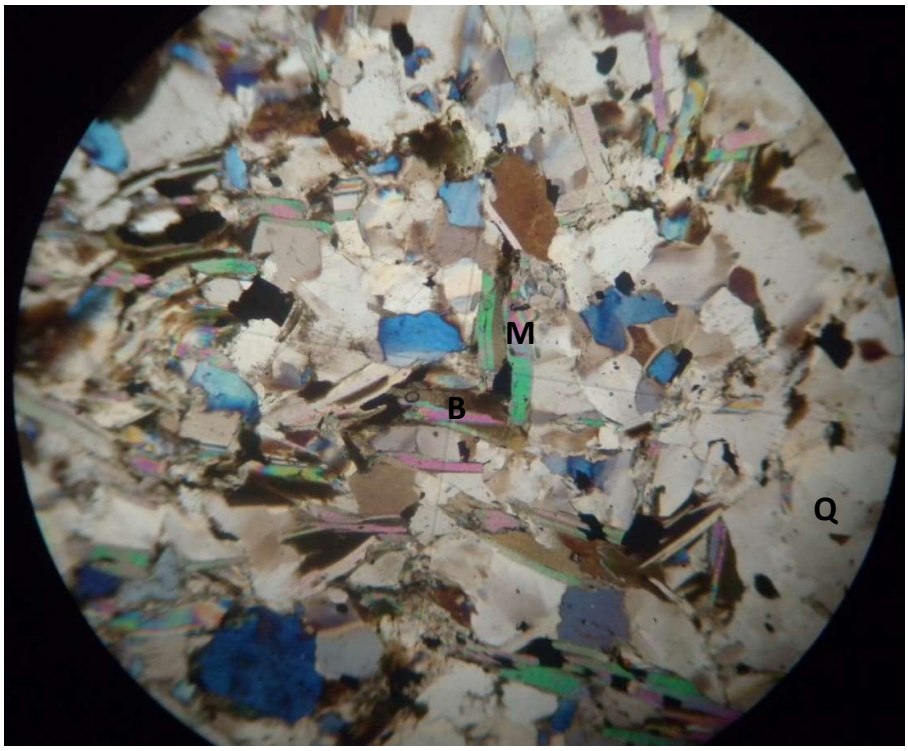

(b)

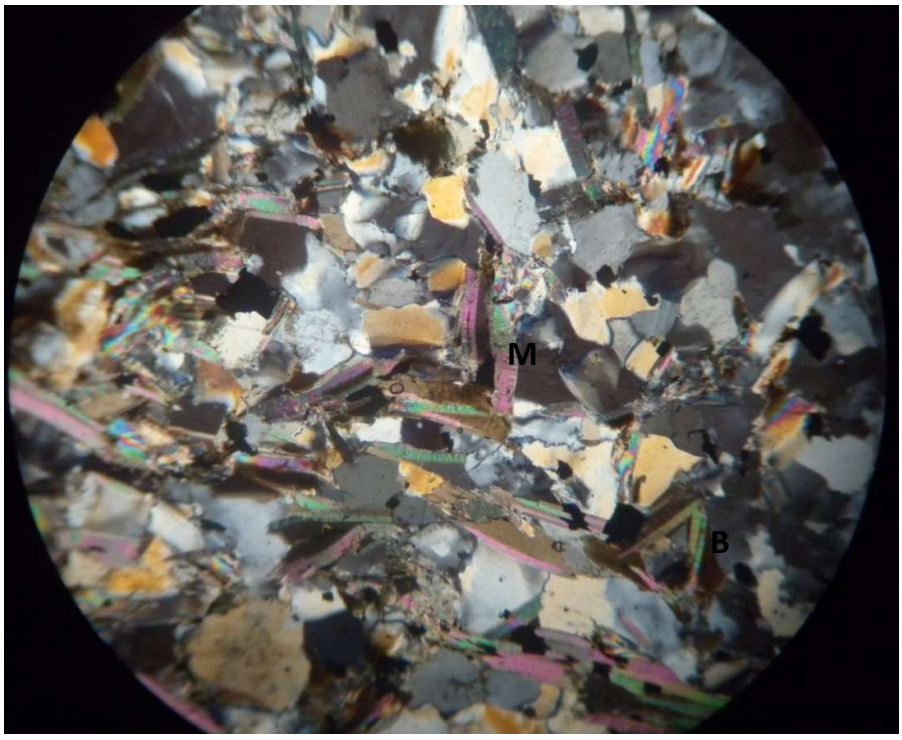

Fig 4.7 Typical Photomicrograph of Quartz Schist in Transmitted Light. *(a) plane polarised (b) cross polarised light (x40): indicating numerous platy biotite (B) and muscovite (M) displaying crenulations cleavage fabric (S_2) in a matrix of anhedral quartz (Q).(Coordinate: N07^o 31.910', E 03^o 58.875')*

a

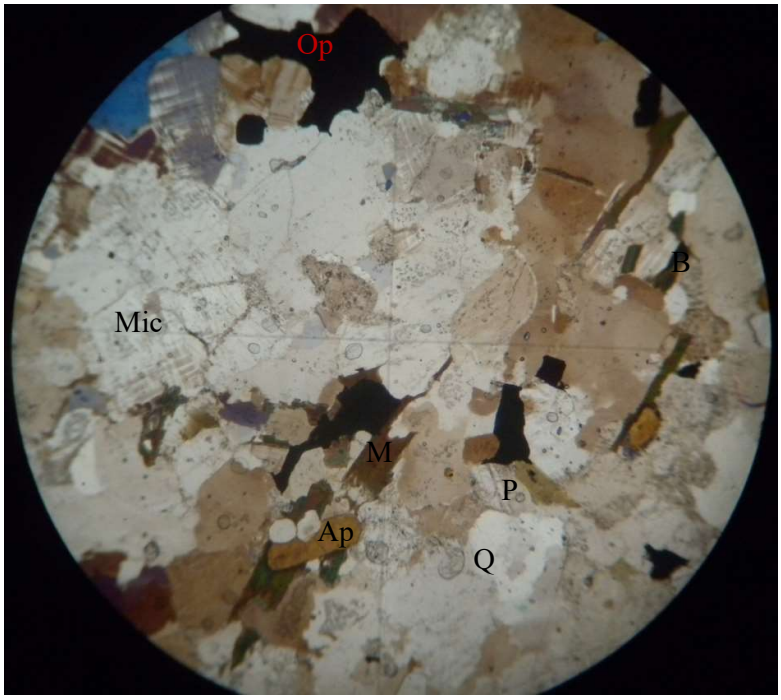

b

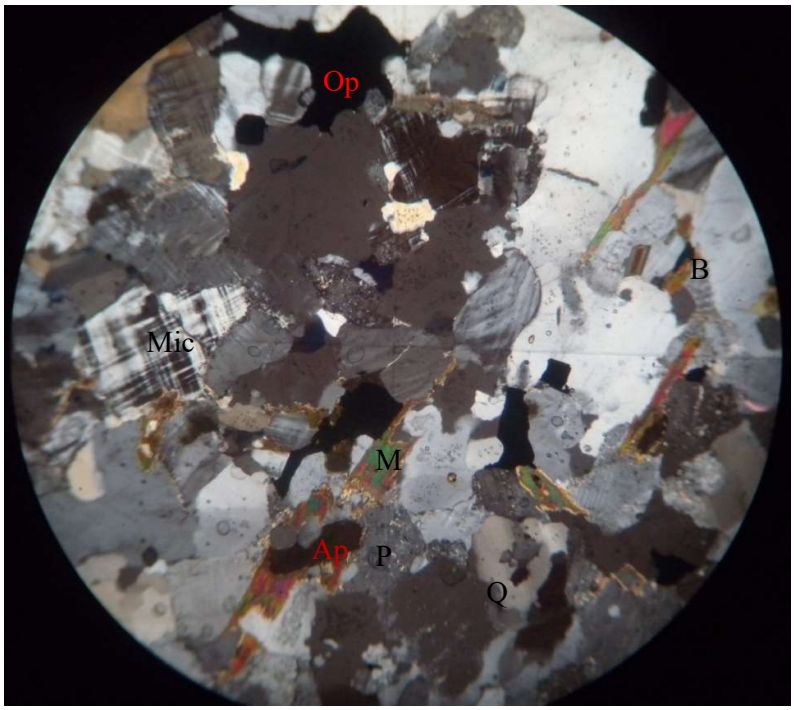

Fig 4.8 Typical Photomicrograph of Quartz Schist in Transmitted Light. *(a) plane polarised (b) cross polarised light (x40): indicating platy biotite (B) and muscovite (M) sparsely aligned in the grains of anhedral quartz (Q) and microcline (Mic), opaque mineral(Op) sericitized plagioclase feldspar (P) and apatite (Ap). Sample shared boundary with the muscovite garnet schist (Coordinate: N07^{o} 33.717', E 03^{o} 58.961')*

a

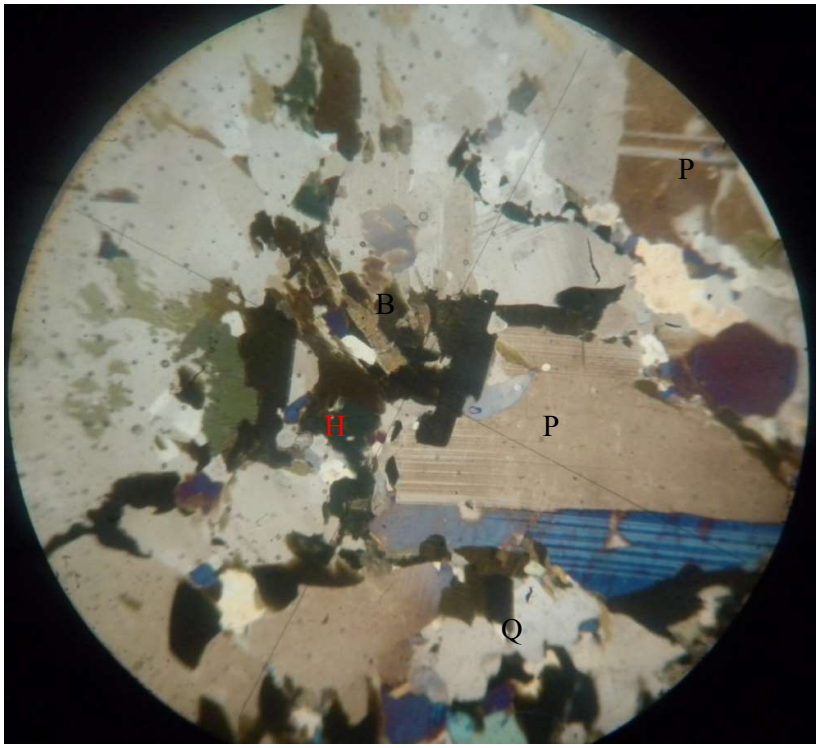

b

Fig 4.9 Typical Photomicrograph of Quartz Schist in Transmitted Light *(a) plane polarised (b) cross polarised light (x40): showing euhedral porphyroblast of plagioclase (P), quartz (Q), and green hornblende (H.) Sample shared boundary with biotite hornblende gneiss at north- eastern part of the area. (Coordinate: N07^{o} 40.383', E 03^{o} 57.203')*

a

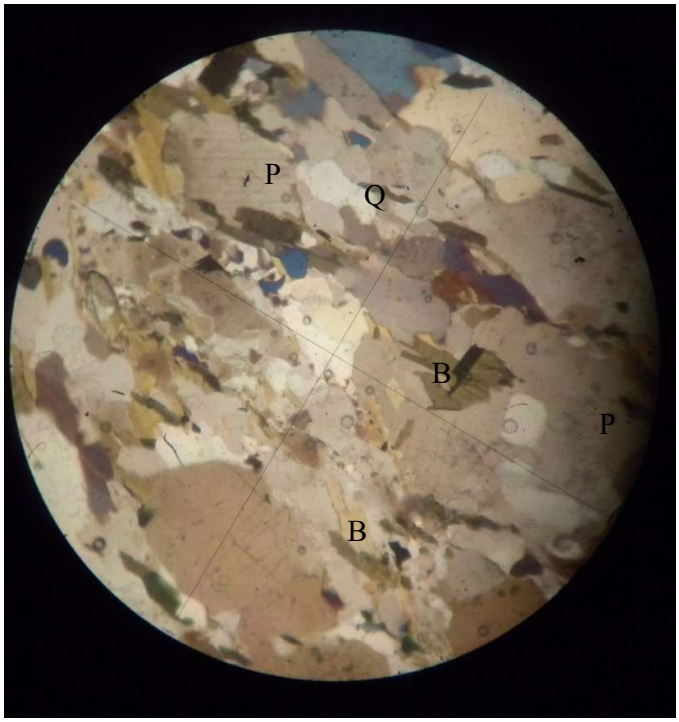

b

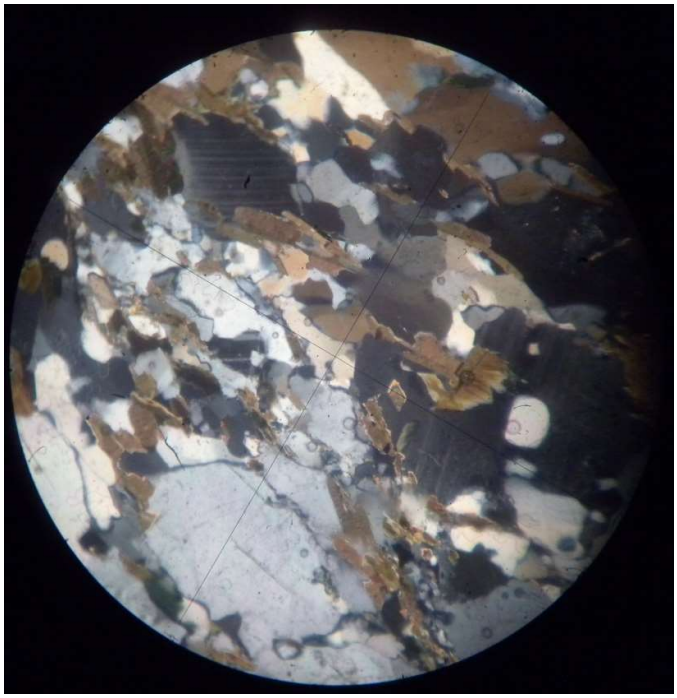

Fig 4.10 Typical Photomicrograph of Quartz Schist in Transmitted Light *(a) plane polarised (b) cross polarised light (x10): showing numerous lath-like grains of biotite (B) defining the schistosity plane, subhedral plagioclase feldspars (P) and quartz (Q). Sample shared boundary with biotite granite gneiss at south-western part of the area. (Coordinate: N07^{o} 31.514', E 03^{o} 45.401')*

4.1.2.2 Muscovite Garnet Schist

The muscovite garnet schist was found occurring within the quartz schist in the eastern part of the study area. They were exposed as small hill trending N-S with moderately dipping schistose planes (Fig.4.11). The muscovite garnet schist is coarse grained and light grey in colour. It contains high percentage of quartz, large crystals of muscovite and plagioclase feldspars in recrystallized granular quartz matrix. Garnet is common (Fig.4.12) and other opaque minerals were sometimes present. Muscovite crystals occur along the planes of parting in the muscovite garnet schists, which give rise to particular flaggy rocks (Fig.4.13).

The modal composition reveals: quartz (30-45%), orthoclase feldspar (12-18%), muscovite (16-20%), biotite (6-10%) and albite plagioclase (5-8%). Significant amount of garnet (8-12%), chlorite (4-5%) and opaque mineral (1-2%) were observed (Table 4.3).

The muscovite garnet schist displayed in-equant texture which comprises of anhedral quartz exhibiting coarse crystals with suture boundaries as well as sub-grains which show undulose extinctions (Fig.4.14 to 4.16). Deformed quartz also displays bending (Fig.4.15 and 4.16). Subhedral to anhedral porphyroblastic plagioclase feldspar shows polysynthetic twinning with few quartz inclusions.

Muscovite flakes occur as large lenticular grains and as fine grains smeared at the grains boundary of plagioclase feldspar and muscovite (Fig.4.15). High proportion of muscovite may be due to the close association of the muscovite garnet schist with the quartz-schist in the eastern corner of the area.

Biotite sometime show alteration to chlorite and display pleochroism from brown to dark brown colour. Isotropic garnet crystals occur as fine grains and not very conspicuous in the thin section as in the hand specimen.

Fig.4.11 Field Expression of Muscovite Garnet Schist.

(coordinate: N07^{o} 31.947', E 03^{o} 57.246')

Fig.4.12 Hand Specimen of Muscovite Garnet Schist.

(coordinate: N07^o 39.564', E 03^o 58.275')

Fig. 4.13 Hand Specimen of Muscovite Garnet Schist Showing Muscovite Flakes.
(coordinate: N07^{o} 32.729', E 03^{o} 59.470')

Table 4.3 Modal Composition of Minerals in Muscovite Garnet Schist in the Study Area

Sample No → / Mineral ↓	**GS1**	**GS2**	**GS3**	**Range**
Quartz	40	30	45	30-45
Orthoclase	15	18	12	12-18
Muscovite	16	20	20	16-20
Albite Plagioclase	5	8	6	5-8
Chlorite	5	4	-	4-5
Biotite	10	8	6	6-10
Garnet	8	10	10	8-10
Opaque	1	2	1	1-2
Total	100	100	100	

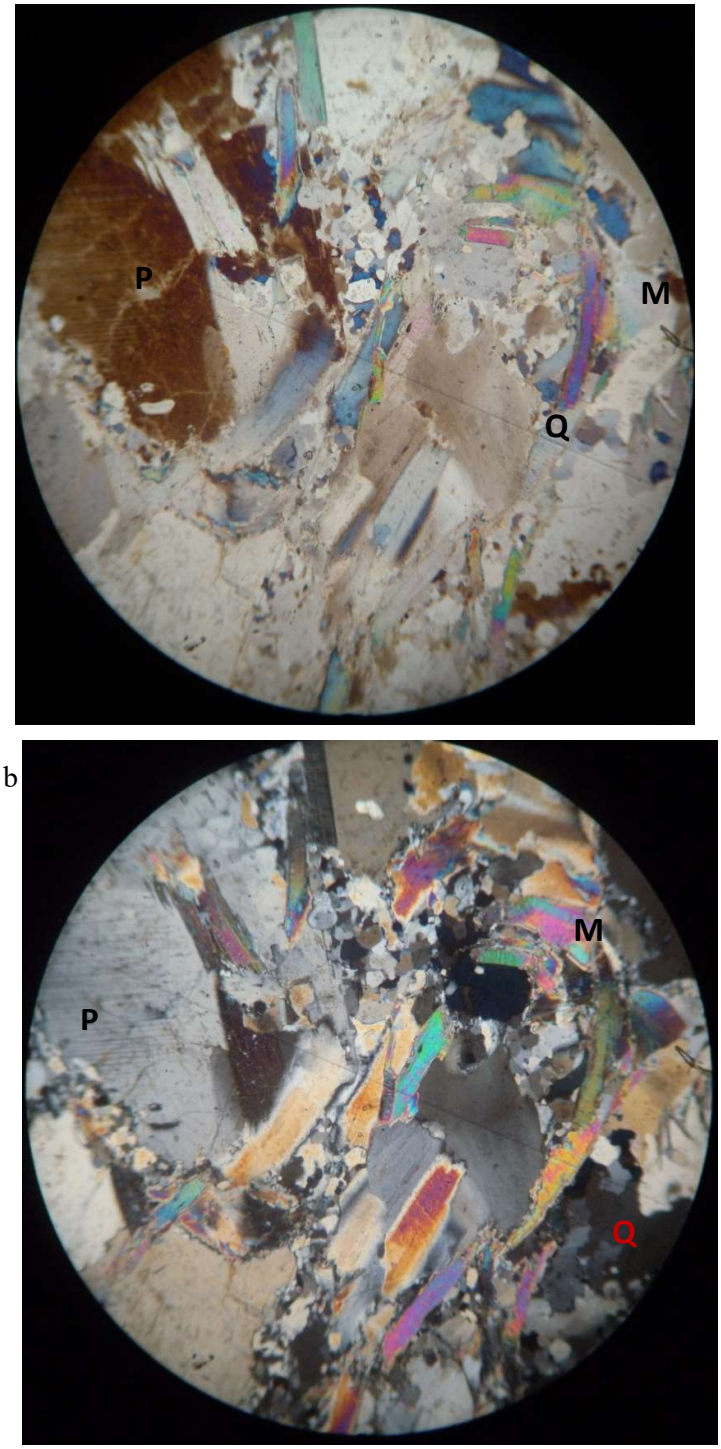

Fig. 4.14 Typical Photomicrograph of Muscovite Garnet Schist in Transmitted Light *(a) plane polarised (b) cross polarised light (x40): indicating in equant texture displaying sub-grains of quartz with suture boundary (Q), poikiloblastic plagioclase feldspar (P) enclosing muscovite, and numerous lath-like muscovite (M) grains. (coordinate: N07^o 39.564', E 03^o 58.275')*

a

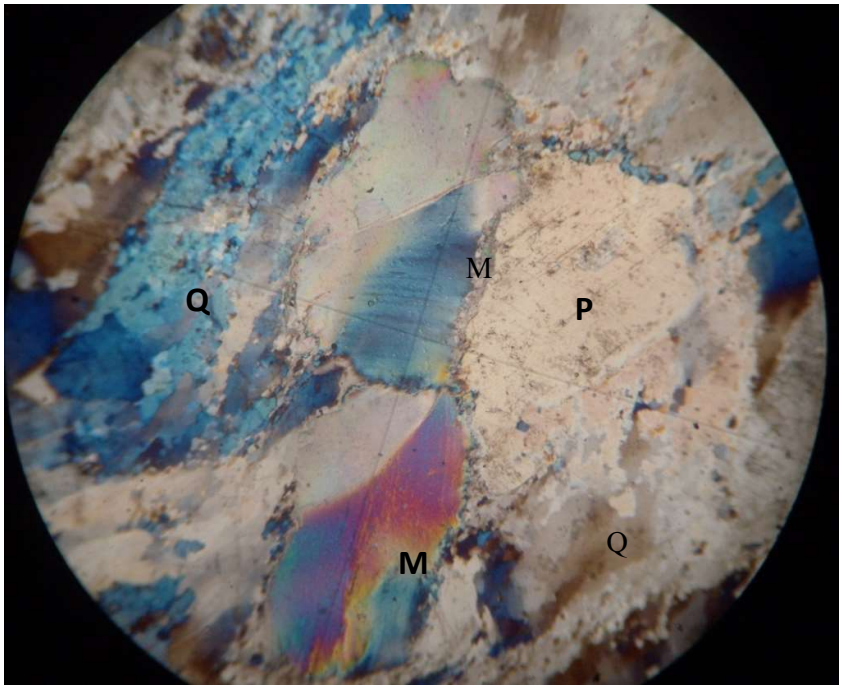

b

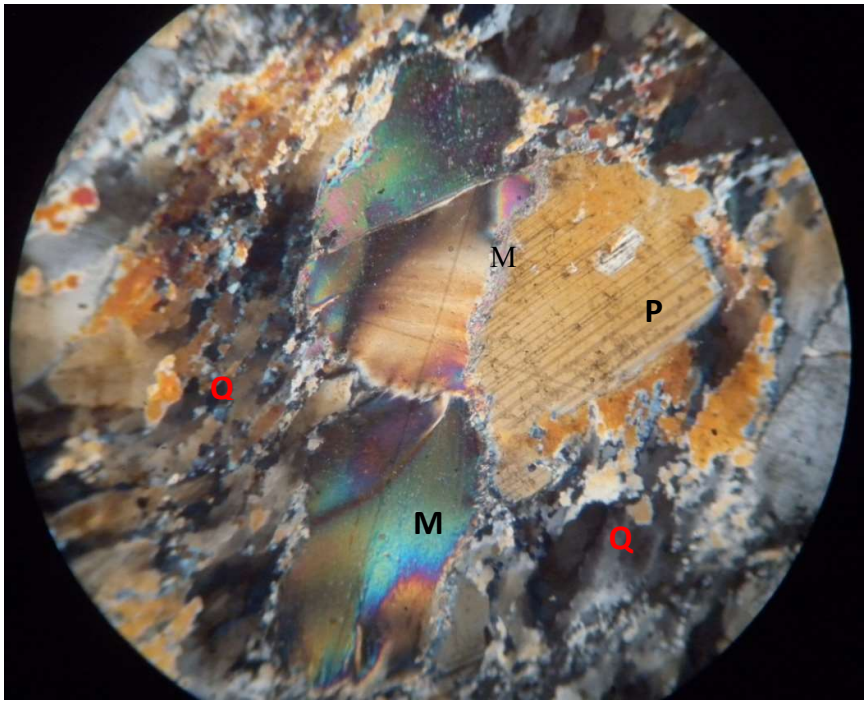

Fig. 4.15 Typical Photomicrograph of Muscovite Garnet Schist in Transmitted Light *(a) plane polarised (b) cross polarised light (x40): indicating strained grains of quartz with undulose extinction (Q), muscovite matrix smeared around the margin of porphyroblastic crystals of muscovite (M) and plagioclase feldspar(P) (coordinate: N07^o 32.729', E 03^o 59.470')*

a

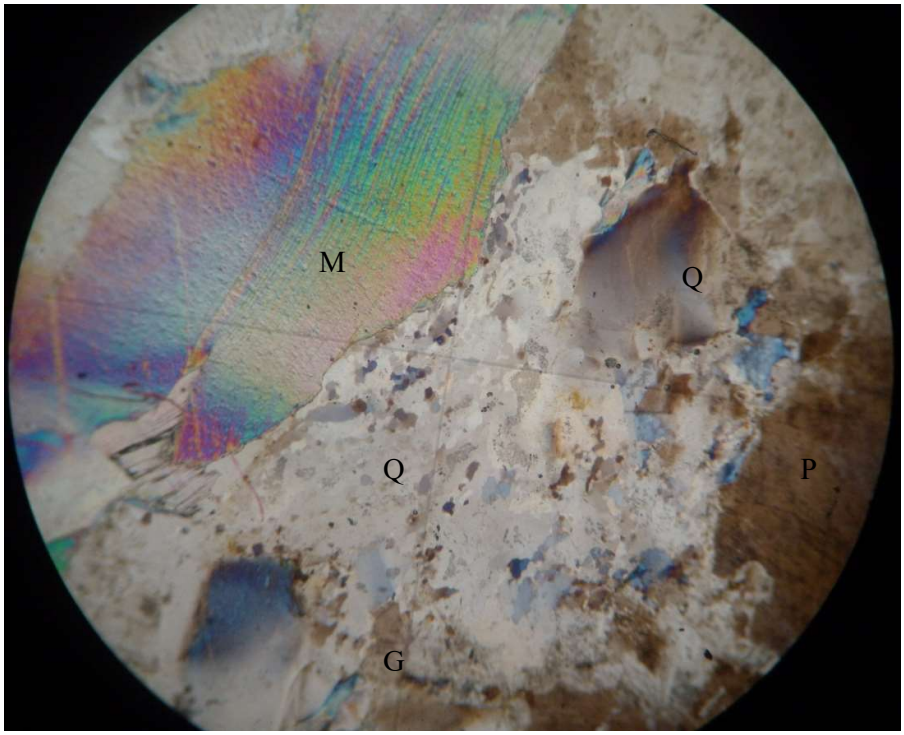

b

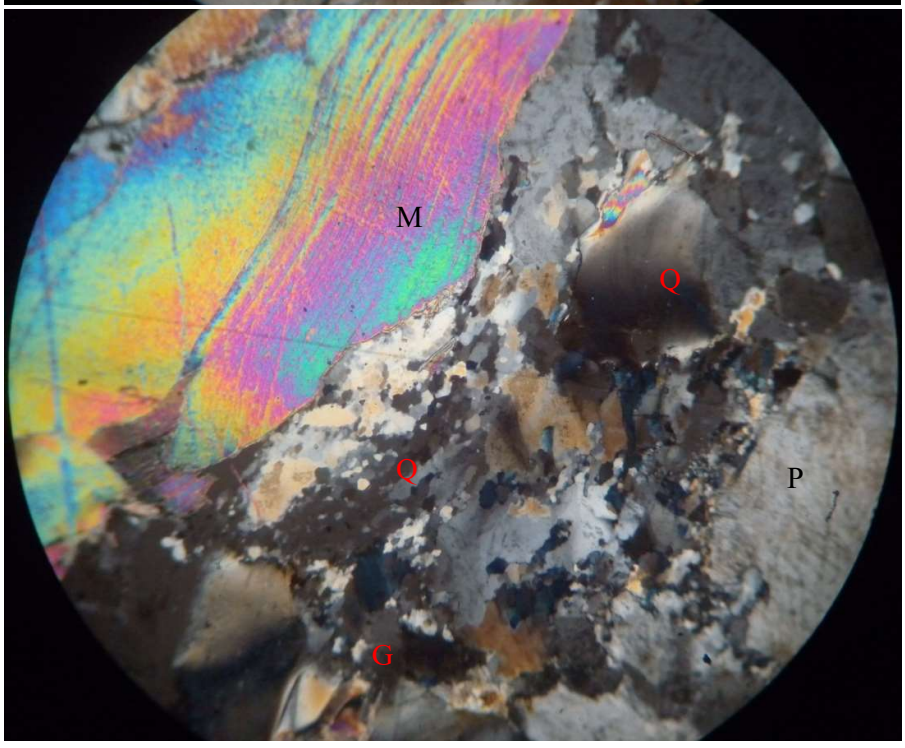

Fig. 4.16 Typical Photomicrograph of Muscovite Garnet Schist in Transmitted Light *(a) plane polarised (b) cross polarized light (x40): displaying coarse grain and finer sub-grains of quartz showing undulose extinction(Q), porphyroblastic muscovite grain(M), plagioclase feldspars(P) and garnet(G). (coordinate: N07^o 32.729', E 03^o 59.470')*

4.1.2.3 Geochemistry of the Schistose Rock (Quartz and Muscovite Garnet Schists)

4.1.2.3.1 Major Oxides

The concentrations of silica (SiO_2), alumina (Al_2O_3), Ferric oxide (Fe_2O_3) and magnesia (MgO)in the schistose rock ranged from 63.15 to 73.33%: 13.01 to 18.59%: 1.60 to 6.05% and 0.41 to 1.92% respectively (Table 4.4). The result also shows the concentrations of lime (CaO), Soda (Na_2O) and potash (K_2O) ranged: 1.22 to 4.80%: 3.30 to 4.66% and 1.73 to 4.92% respectively. Minor oxides of TiO_2, MnO, P_2O_5, and Cr_2O_3 revealed the concentration ranges from 0.23 to 0.58%, 0.02 to 0.13%, 0.08 to 0.35% and <0.002 to 0.005%. Loss on ignition (LOI) values ranged from 1.6 to 2.8.

The quartz and the muscovite garnet schist samples yielded similar values for all the major and minor oxides except for the slightly lower ferric oxide (Fe_2O_3) value of 1.76% and slightly higher value of K_2O (4.85%) in the muscovite garnet schist. This is conformable with the mineralogical study of the muscovite garnet schist having little mafic minerals but more of felsic minerals which comprises of the grey feldspars and muscovite minerals (Fig.4.12 and 4.13)

The concentrations of SiO_2 for the quartz and muscovite garnet schist samples were slightly lower than the values obtained from most quartz schist from Nigeria Metasedimentary belts (Okonkwo, 2005, Okunlola *et al*. 2009) but higher than Igbeti quartz schist (Akinola *et al.* 2014), Post Archean terrigeneous shale and Archean mudstone. Similarly, Al_2O_3, CaO, K_2O and Na_2O contents of the quartz schist are comparable similar to Igbeti Quartz schist and Archean mudstone but significantly higher than that Ibadan (Okunlola *et al*, 2009), Jebba area (Okonkwo, 2005) and Okemesi (Okunlola *et al*, 2009, Table 4.5).

Table 4.4 Result of Major Oxide Analyses of Pelitic Schist Unit.

Sample No→ Major Oxide(wt%)↓	QS1	QS2	QS3	QS4	QS5	QS6	QS7	QS8*	GS1	Range	Average
SiO_2	69.89	73.33	69.67	69.86	63.15	63.95	73.38	68.54	70.4	63.15-73.38	69.13
TiO_2	0.30	0.53	0.23	0.36	0.57	0.50	0.49	0.58	0.30	0.23-0.58	0.43
Al_2O_3	14.71	13.03	15.19	15.09	16.75	17.84	13.01	18.59	14.96	13.01-18.59	15.46
Fe_2O_3	2.24	1.89	1.60	1.81	6.01	4.73	1.98	5.90	1.76	1.60-6.05	3.10
MnO	0.02	0.02	0.02	0.02	0.13	0.11	0.02	0.12	0.02	0.02-0.13	0.05
MgO	0.51	0.41	0.51	0.53	1.89	1.43	0.41	1.92	0.53	0.41-1.92	0.09
CaO	1.58	1.26	1.61	1.57	4.75	4.39	1.22	4.80	1.53	1.22-4.80	2.52
Na_2O	4.43	3.31	4.66	3.65	3.74	4.23	3.3	3.71	3.71	3.30-4.66	3.86
K_2O	3.69	3.01	4.12	4.92	1.73	1.79	2.98	2.42	4.85	1.73-4.92	3.28
P_2O_5	0.10	0.12	0.13	0.09	0.35	0.32	0.12	_	0.08	0.08-0.35	0.16
Cr_2O_3	0.005	0.004	0.003	0.003	<0.002	<0.002	0.005	_	0.002	0.002-0.005	0.004
Loi	2.20	2.80	2.00	1.80	0.70	0.60	2.80	_	1.60	0.60-2.80	1.81
Sum	99.81	99.84	99.84	99.84	99.70	99.89	99.83	106.20	99.85	99.70-106.20	100.53

Major oxide contents with sample symbol * are determined by X-ray fluorescence (XRF).Elements with dash were not determined.

GS1 represent Garnetiferous Schist sample.

Table 4.5 Comparison of Major Oxide of the Quartz Schist in the Study Area with Other Area within the Basement Complex of Nigeria.

Major Oxide(wt%)	This study	Ibadan area	Jebba	Okemesi	Igbeti	PAS	AM
SiO_2	69.13	95.00	75.33	84.38	63.40	62.80	60.40
TiO_2	0.43	0.13	0.42	0.23	0.30	1.00	0.80
Al_2O_3	15.46	1.54	12.46	8.15	14.23	18.90	17.10
Fe_2O_3	3.10	0.42	3.67	1.20	6.58	6.50	9.50
MnO	0.05	0.01	0.03	0.01	0.05	0.11	0.10
MgO	0.09	0.05	1.43	0.59	1.85	2.20	4.30
CaO	2.52	0.71	0.32	0.19	3.43	1.30	3.20
Na_2O	3.86	0.11	1.41	0.50	2.18	1.20	2.10
K_2O	3.28	0.32	3.46	2.85	3.50	3.70	2.30
P_2O_5	0.16	0.04	0.13	0.14	_	0.16	_

Ibadan Area – Okunlola, *et.al*. (2009)

Jebba - Okonkwo (2005)

Okemesi – Okunlola, *et.al*. (2009)

Igbeti – Akinola, *et.al* (2014)

PAS – Post Archean Terrigeneous Shale

AM – Archean Mudstone

Discriminant diagram of Na_2O/Al_2O_3 against K_2O/Al_2O_3 established the petrogenetic character of the arenaceous rocks (Garrels and Mackenzie, 1971). The plots revealed that the dominant origin of the quartz and muscovite garnet schist is sedimentary (Fig.4.17).

The geochemical classification of Herron, (1988) for discriminating between terrigineous shale and sandstones using the plot of $\log(Fe_2O_3/K_2O)$ versus $\log(SiO_2/Al_2O_3)$ was plotted for the pelitic schist samples. The diagram shows that the samples plotted in the wacke and arkose fields (Fig.4.18), thus defining a arkosic protolith for the samples which is in conformity with the schist of Lafiaji and Osi (Adedoyin, *et. al*.2014).

The SiO_2 versus K_2O/Na_2O diagram have been used to determine tectonic setting of sandstone and mudstone suite by Roser and Korsch (1988). The quartz schist and muscovite garnet schist precursor data plot on the passive margin field where igneous activity were not taken place (Fig.4.19).

In order to determine the degree of weathering of the protolith of the rock, the chemical index of alteration (CIA) proposed by Nesbitt and Young (1982) defined as $CIA= Al_2O_3/ (Al_2O_3+CaO+Na_2O+K_2O)*100$ was used. The examined samples have average CIA value of 61.26 lower than those obtained from average shales (70-75) (Nesbitt and Young, 1982) indicating low degree of chemical weathering or relatively immature source rock (Wu *et al*., 2012). Differential weathering degree was further confirmed on the ternary plot of molecular proportions: Al_2O_3 (A) – $CaO+Na_2O$ (CN) –K_2O (K) after McLennan e*t. al*. (1985). A-CN-K system is also useful for evaluating fresh rock composition (Nesbitt and Young, 1984).

In comparison, quartz schist from Igarra area have an average CIA value of 53.9 (Okeke and Meju, 1985), those of Jakura area (Elueze and Okunlola, 2003) have an average CIA value of 62.1, those of Jebba area (Okonkwo, 2005) have an average CIA value 64.89 and quartz schist in Ibadan area and Okemesi (Okunlola *et. al*. 2009) have average CIA values of 57 and 69.7 respectively. Therefore, the protoliths of the quartz schist in the study area show slightly moderately degree of weathering than those of Igarra and Ibadan area quartz schist and lower than those of the Jebba, Jakura and Okemesi quartz schist.

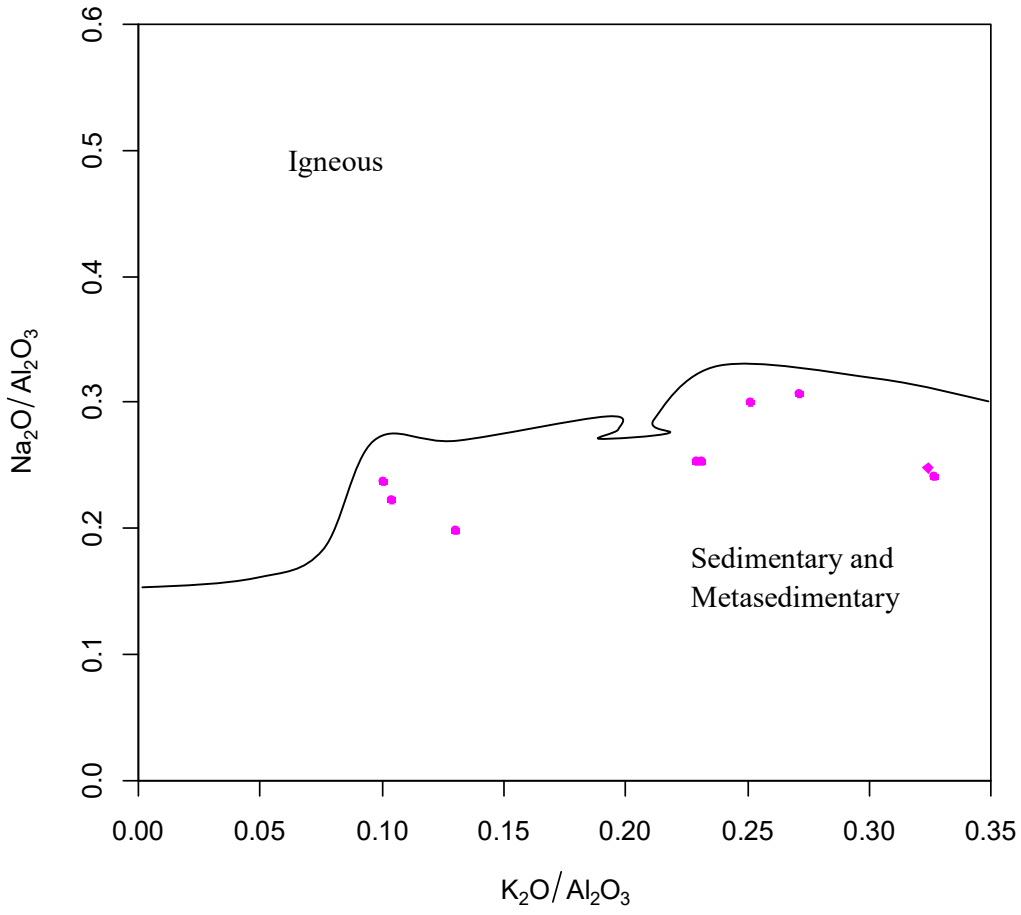

Fig.4.17 Na_2O/Al_2O_3 versus K_2O/Al_2O_3 Variation Diagram of Quartz and Muscovite Garnet Schist (After Garrels and Mackenzie, 1971).

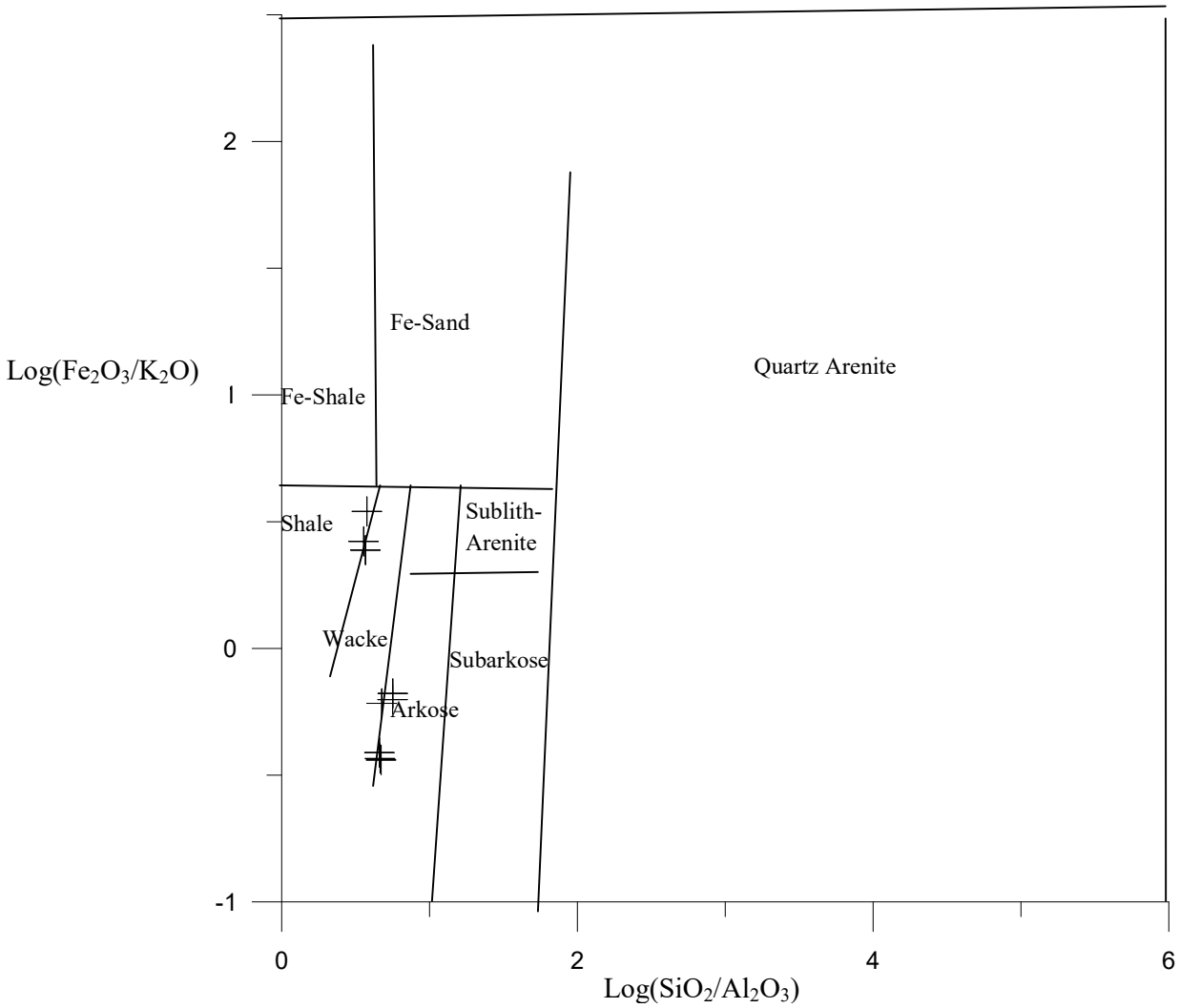

Fig.4.18 Plot of log (Fe_2O_3/K_2O) versus log (SiO_2/Al_2O_3) Diagram for Quartz and Muscovite Garnet Schist Samples (after: Herron, 1988).

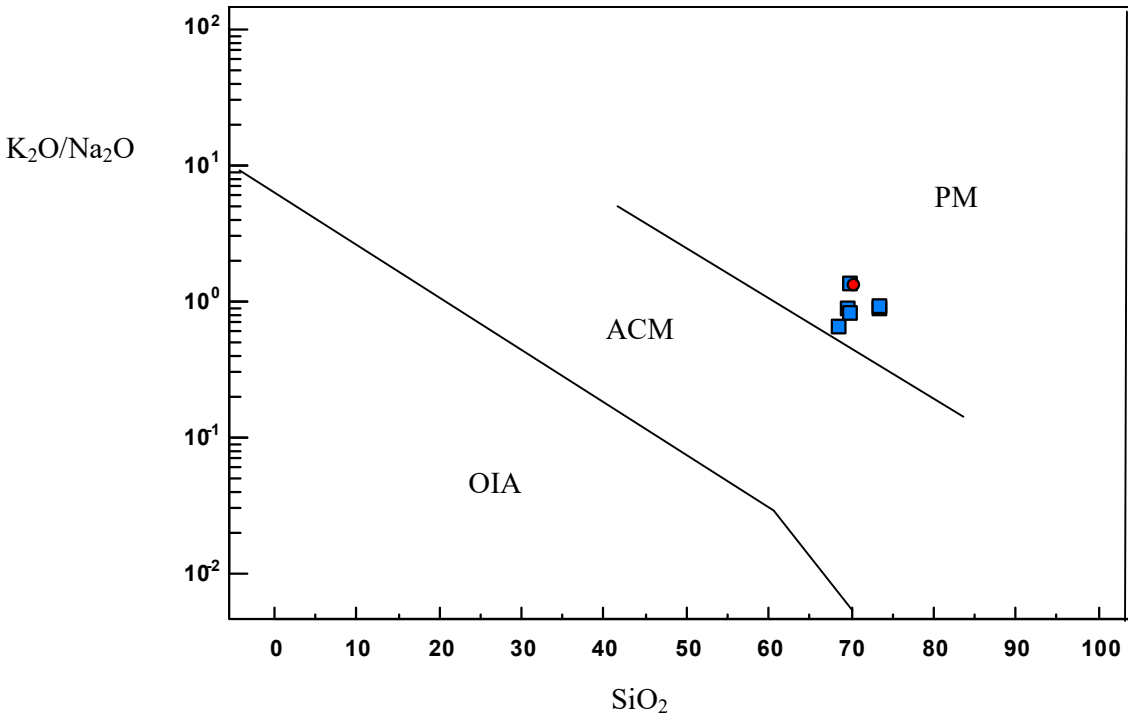

Fig.4.19 Plot of K_2O/Na_2O versus SiO_2 Tectonic Discrimination Plot for the Analysed Quartz and Muscovite Garnet Schist Samples (after: Roser and Korsch, 1988).

PM- Passive Margin,

ACM-Active Continental Margin,

OIA- Oceanic Island Arc.

The SiO_2-Al_2O_3-MgO-FeO-K_2O-H_2O (KFMASH) system was adopted to illustrate character and type of progenitor for the pelitic schist on the AKF diagram (Fig.4.20) designed by Thompson (1957) for pelitic rock. All the samples of the schist fell in the low Al pelite field.

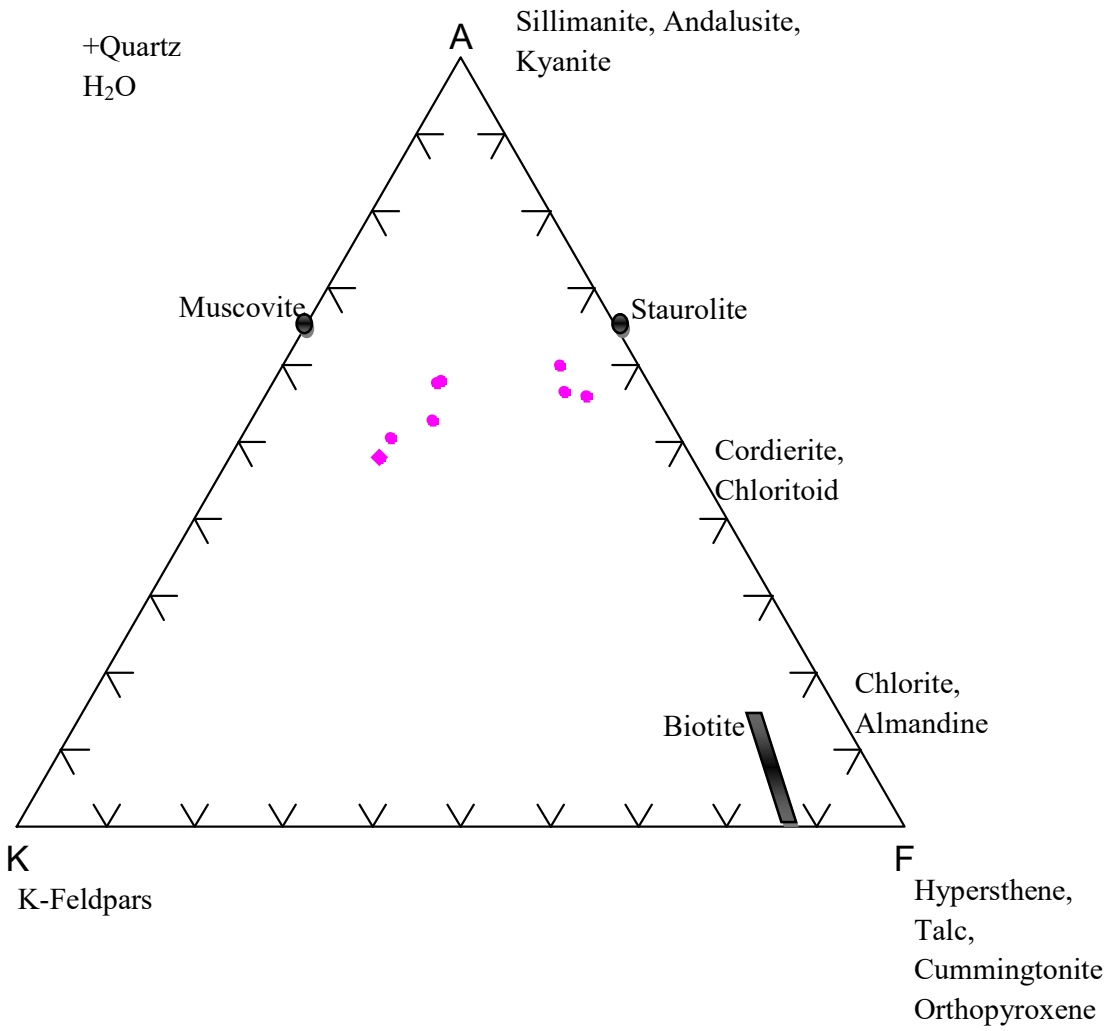

Fig.4.20 AKF Diagram for the Silica-saturated Low Pressure Pelitic Schist (Thompson, 1957)

4.1.2.3.2 Trace Element

The trace element concentrations for the pelitic schistose rock (Table 4.6) revealed enrichment of some Large Ion Lithophile Elements (LILE) (Ba, 399.8 to 966.0ppm; Rb, 60.2 to 167.3ppm and Sr, 259.2 to 818.4ppm) which typically behave mobile in fluid phase, indicates the contribution of feldspars components in the source rock.

The concentrations of the High Field Strength (HFS) elements (Sc, Y, Th, U, Hf, Nb - 9iand Ta) in the schists are relatively low except Zirconium which ranged from 110.6 to 315.0ppm. However, the result also revealed depletion in the transition metals like V.

Normalisation using upper continental crustal values of Taylor and McLennan (1985) and that of Weaver and Tarney, (1984) showed signatures that defined upper continental crust derived materials (Fig.4.21). Negative anomalies were observed for Nb, P and Ta. The plot also revealed enrichment in Rb, Ba, Th and U.

Table 4.6 Results of Trace Element Analyses of Pelitic Schist Unit.

Sample No → / Trace Element ↓ (ppm)	QS1	QS2	QS3	QS4	QS7	GS1	Range	Average
Ba	826.0	668.0	905.0	979.0	671.0	966.0	399.8-966.0	704.3
Sc	2.0	3.0	2.0	3.0	3.0	3.0	2.0-3.5	4.5
Be	<1	3.0	18.0	<1	<1	<1	<1.0-18	10.5
Co	3.9	3.4	3.6	2.5	3.4	2.0	2.0-3.9	3.1
Cs	6.4	4.9	5.9	3.9	5.0	3.9	3.9-6.4	5.0
Ga	18.3	17.3	19.0	17.7	16.0	17.6	16.0-19.0	17.7
Hf	5.7	8.2	3.4	5.8	7.2	5.6	3.4-8.2	6.0
Nb	5.9	11.8	4.1	18.9	13.4	11.0	4.1-19.0	11.6
Rb	131.1	103.7	140.8	167.3	101.1	163.0	60.2-167.3	123.9
Sn	4.0	5.0	1.0	5.0	5.0	4.0	1.0-5.0	4.0
Sr	786.7	584.9	816.4	573.6	586.4	573.0	259.2-816.4	532.5
Ta	0.6	0.9	0.3	1.5	0.9	0.9	0.3-1.5	0.9
Th	46.5	9.4	13.6	26.4	25.0	16.4	9.4-46.5	22.9
U	13.6	4.4	24.9	7.2	5.1	5.2	4.4-24.9	10.1
V	20.0	29.0	21.0	20.0	31.0	18.0	18.0-70.3	29.9
W	<0.5	<0.5	<0.5	0.9	<0.5	0.6	<0.5-0.9	0.8
Zr	221.1	314.7	116.9	204.9	297.2	199.4	110.6-315.0	229.1

Table 4.6 (cont.) Results of Trace Element Analyses of Pelitic Schist Unit.

Sample No → Trace Element ↓ (ppm)	QS1	QS2	QS3	QS4	QS7	GS1	Range	Average
Y	5.5	5.1	4.6	15.5	7.1	12.6	4.6-34.0	14.3
Mo	0.7	0.7	0.8	0.6	0.8	0.8	0.7-0.8	0.7
Cu	24.0	19.3	8.5	20.2	43.3	18.6	8.5-43.3	19.0
Pb	31.7	24.3	3.4	4.6	23.7	4.3	3.4-32.5	17.8
Zn	128.0	76.0	41.0	33.0	81.0	31.0	31.0-128.0	64.5
Ni	12.9	9.8	7.5	5.0	9.8	4.9	4.7-12.9	7.8
As	<0.5	0.8	0.5	<0.5	0.8	<0.5	<0.5-3.5	1.4
Sb	1.0	0.3	0.1	0.1	0.4	0.1	0.1-1.0	0.5
Ag	<0.1	<0.1	<0.1	<0.1	<0.1	<0.1	<0.1	
Au	3.0	3.3	0.6	30.8	3.9	16.8	0.6-30.8	9.2
Hg	0.1	0.1	<0.01	<0.01	0.1	<0.01	<0.01-0.08	0.1
Th/Sc	23.3	3.1	6.8	8.8	8.3	5.5	3.1-23.3	10.1
Zr/Sc	110.6	104.9	58.5	68.3	99.1	66.5	22.5-110.6	66.9
Rb/Sr	0.2	0.2	0.2	0.3	0.2	0.3	0.2-0.3	0.2
Th/U	3.4	2.1	0.5	3.7	4.9	3.2	0.5-4.9	3.0

GS1 represent Garnetiferous Schist sample.

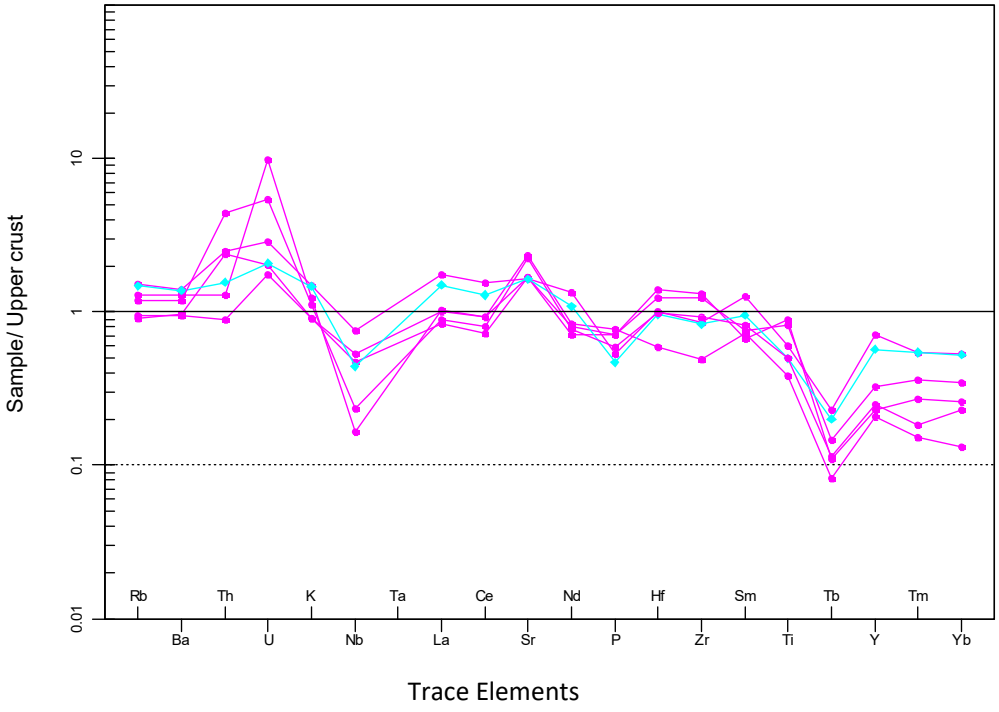

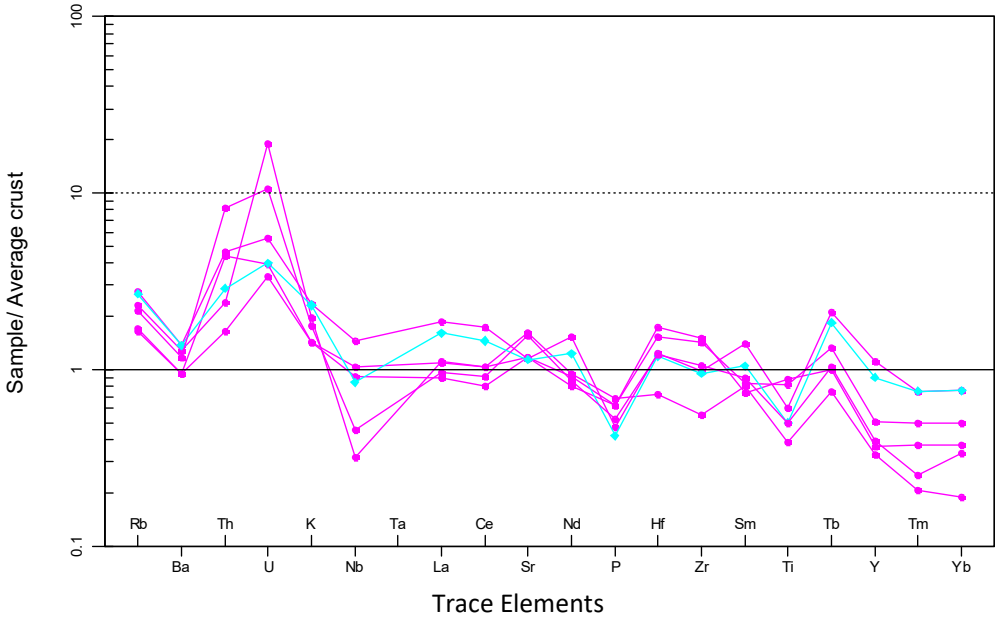

Fig.4.21 Chondrite Normalized Plots of the Trace Elements in the Pelitic Schist (after; (a) Taylor and McLennan, 1995; (b) Weaver and Tarney, 1984).

The plot of Th/Sc against Zr/Sc (Fig.4.22) was used to evaluate the source composition and sediment recycling processes (McLennan, *et al*., 1993 and Xiao, *et al*., 2012). It can be inferred from the plot that metamorphic differentiation processes occurred due to compositional variation with little or no sediment recycling. Th/Sc ratio is an indicator of igneous chemical differentiation processes since Th is typically an incompatible element whereas Sc is compatible in igneous system (McLennan, 1989a and McLennan, *et al*., 1993).

The ratio of Th/U increases due to successive cycles of weathering and redeposition and thus it is used as marker of these processes. Sedimentary recycling in oxidising conditions usually results in Th fractionation while U is readily oxidised during wethearing (McLennan and Taylor, 1980). Th/U ratios of the pelitic schist from the study area ranged from 0.5 to 4.9 with an average of 3.0 (Table 4.6) suggesting a simple cycling history. This was further confirmed by very low Rb/Sr ratios of the schist in the study area which ranged from 0.2 to 0.3 also suggesting a simple recycling history. Weathering and diagenetic processes can often lead to a significant increase in Rb/Sr ratios, and high Rb/Sr values have been interpreted to be indicators of strong weathering and sediment recycling (McLennan *et al*., 1993).

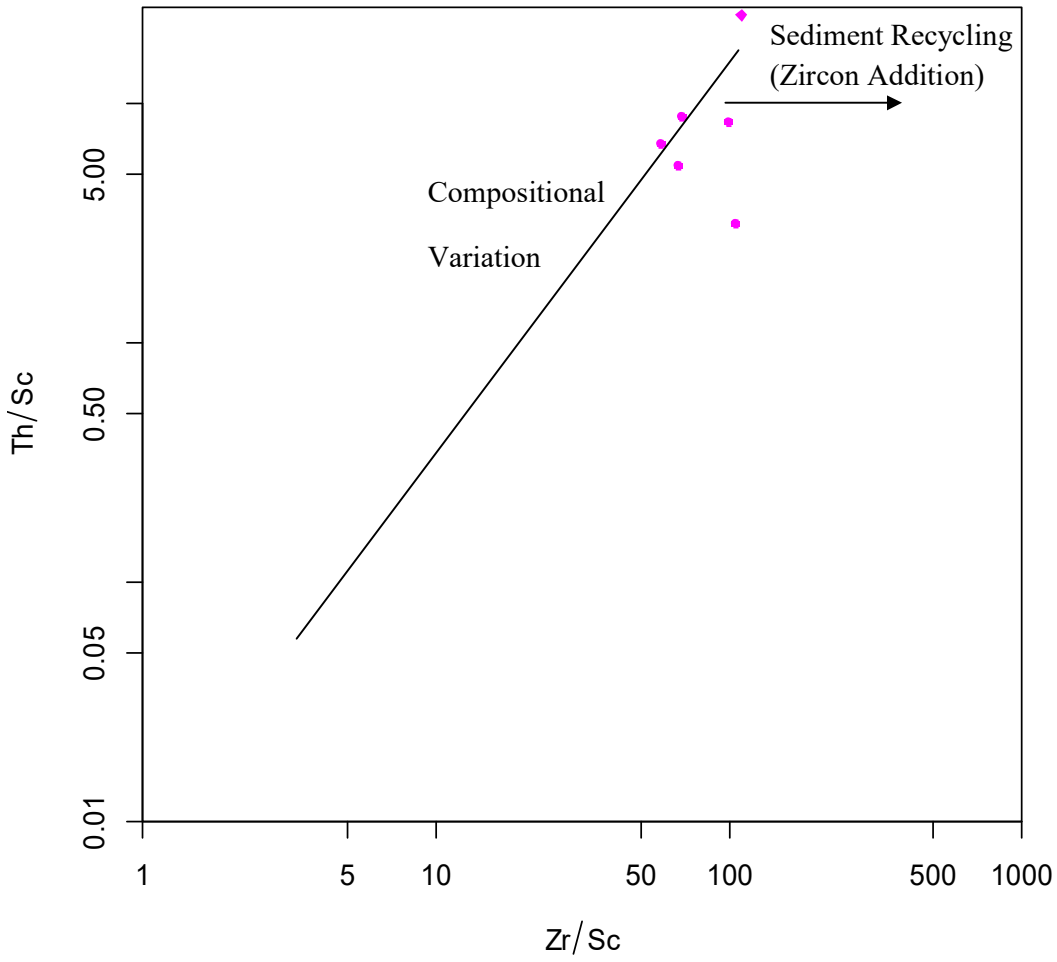

Fig. 4.22 Plot of Th/Sc against Zr/Sc for the Pelitic Schist (Adopted from McLennan *et.al*, 2015).

4.1.2.3.3 Rare Earth Elements

Rare Earth Element (REE) concentration of the pelitic schist (Table.4.7) revealed moderately enrichment of the Light Rare Earth Elements (LREE) such as Lanthanum (La, 25 to 58.24ppm), Cerium (Ce, 46.2 to 110.3ppm) and Neodymium (Nd,18.5 to 95.7ppm) and relatively depleted heavy rare earth elements (HREE).

Europium (Eu) concentration ranged from 0.5 to 1.1ppm with negative Eu anomalies (Eu/E*; 0.4 to 0.8, average 0.6) due to the extractions of Eu by plagioclase crystallisation during fractionation under reducing condition as exemplified by high value of Strontium in the trace elements.

Chondrite normalised plots (Nakumura, 1974) revealed negative Eu and LREE enrichment and depleted HREE pattern (Fig.4.23).

Table 4.7 Results of Rare Earth Element Analyses of Pelitic Schist Unit.

Sample No → REE (ppm) ↓	QS1	QS2	QS3	QS4	QS7	GS1	Range	Average
La	26.9	25.0	31.0	52.5	30.3	45.1	25.0-52.5	38.4
Ce	51.6	46.2	59.0	98.8	58.9	82.7	46.2-98.8	72.5
Pr	5.6	5.2	6.2	10.2	6.1	8.1	5.2-10.2	7.5
Nd	20.0	18.5	21.7	35.3	20.9	28.2	18.5-28.2	34.3
Sm	3.7	3.0	3.3	5.7	3.4	4.3	3.0-5.7	4.4
Eu	0.6	0.5	0.7	1.1	0.6	0.9	0.5-1.1	0.8
Gd	2.2	2.0	1.8	4.0	2.5	3.1	1.8-3.1	3.6
Tb	0.3	0.2	0.2	0.5	0.3	0.4	0.2-0.4	0.5
Dy	1.3	1.2	0.9	2.7	1.4	2.2	0.9-2.7	1.8
Ho	0.2	0.2	0.1	0.5	0.3	0.5	0.1-0.5	0.1
Er	0.5	0.5	0.4	1.3	0.8	1.2	0.4-1.3	1.1
Tm	0.1	0.1	0.1	0.2	0.1	0.2	0.1-0.2	0.1
Yb	0.5	0.6	0.3	1.2	0.8	1.2	0.3-1.2	0.9
Lu	0.1	0.1	0.1	0.2	0.1	0.2	0.1-0.2	0.2
Eu/Eu*	0.6	0.7	0.8	0.7	0.6	0.7	0.4-0.8	0.6
La_N/Yb_N	35.6	29.6	72.1	30.3	26.9	26.2	25.0-72.1	35.1
La_N/SmN	4.6	5.3	6.0	5.8	5.6	6.6	4.6-6.6	5.6
∑LREE	104.1	94.9	117.9	196.8	116.2	164.1	95.0-196.8	152.8
∑HREE	1.2	1.3	0.8	2.8	1.8	2.7	0.8-2.8	2.2
∑REE	113.39	103.33	125.56	214.00	126.51	178.23	103-214.0	166.4

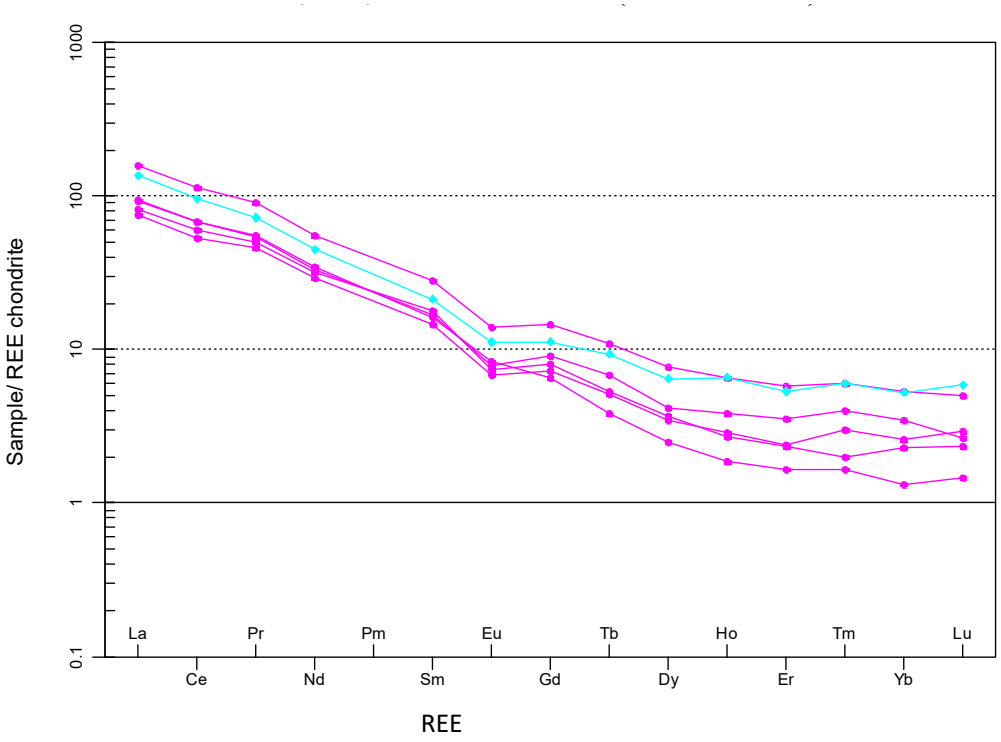

Fig.4.23 REE Chondrite Normalized Plots for the Pelitic Schist (After Nakamura, 1974)

4.1.3 Gneissose Rocks

4.1.3.1 Biotite Hornblende Gneiss (bHG)

The Biotite-Hornblende gneisses underlie a substantial part of the study area. Outcrops occur as extensive rigdes and low-lying bodies covering the central part from the north to south of the area. The outcrops essentially exhibit NNW-SSE foliation trends and are generally steep dip to the east. They are dark coloured rocks and medium to coarse grained in size with pronounced gneissic texture. Individual parallel bands vary in thickness from few centimetres to about 10-12 centimetres (Fig.4.24a). Generally, within the biotite-hornblende gneisses, pockets of granites, quartzites and granite gneiss were observed. The gneiss also inter-bands with quartz schist and muscovite garnet schist at the eastern part. Numerous quartzo-feldspartic, pegmatitic veins and dioritic dyke of varying sizes were found as intrusions and mafic xenoliths were present within the outcrops (Fig.4.24b).

The mafic bands comprise of biotite and hornblende, whereas the felsic bands which are mostly pegmatitic in nature are essentially quartz and plagioclase feldspars. Rahaman (1988) reported that the crystalline rocks have been metamorphosed, migmatised and granitised. Evidence of migmatisation was recognised on few of the biotite-hornblende gneiss as irregular felsic bands cutting across the earlier bands and also by the accumulation of felsic band in dilatant shear surface (Fig.4.25 and 4.26).

a

b

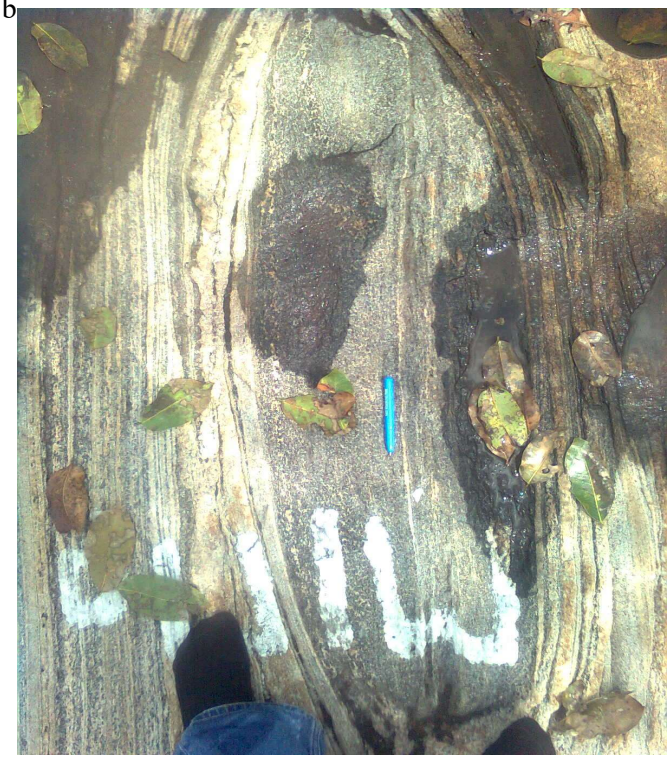

Fig.4.24 Outcrop of Biotite Hornblende Gneiss Showing: (a) Compositional Parallel Bands *(coordinate: N07^{o} 30.106", E 03^{o} 56.491")* (b) Mafic Xenolith within Outcrop (*coordinate: N07^{o} 35.109", E 03^{o} 55.270")*

Fig.4.25 Outcrop of Biotite Hornblende Gneiss Displaying Irregular Felsic bands at Alapata Village, Arulogun ***(coordinate: N07^{o} 30.106", E 03^{o} 56.491")***

Fig 4.26 Outcrop of Biotite Hornblende Gneiss Sample Showing Felsic Accumulation in Dilatant Shear Surface (coordinate: N07^{o} 32’ 269”, E 03^{o} 55’ 703”)

The mineralogy is dominantly composed of quartz (20-45%), plagioclase feldspar (5-30%), biotite (15-22%), hornblende (5-20%). Significant amount of microcline (2-10%), muscovite (2-10%), orthoclase feldspar (3-15%) and opaque mineral (1-5%) are present in some hornblende-biotite gneiss (Table 4.8).

Aggregates of aligned lath-like euhedral biotite flakes were the most prominent within the mafic bands defining the foliation in the biotite hornblende gneiss. The biotite displays pleochroism from light greenish brown to dark brown in colour. The greenish colouration suggested increased Fe^{2+}/Fe^{3+} concentrations. The biotite hornblende gneiss showed predominance of biotite and hornblende as the main mafic phases (Fig. 4.27 and 4.28) due to biotite having favourable site for nucleation of Fe-Mg minerals. Muscovite flakes were observed on few slides.

Hornblende occurs as subhedral coarse grained textures. It appeared as deep green crystal in cross polar and pale green in plane polar (Fig.4.29). Hornblende was found closely associated with biotite.

Plagioclase is abundant in addition to quartz in biotite hornblende gneiss, up to 30 percent of the rock. Most of the feldspars grains are euhedral to subheral in shape and occurred as clear elongated to granoblastic crystals. Plagioclase feldspar displays polysynthetic and simple twinning (Fig.4.28). Zoning is rare in the plagioclase due to homogenisation at higher temperature. K-feldspars sometimes occur in a mosaic of quartz in the leucocratic bands of the biotite-hornblende gneiss.

Anhedral to subhedral quartz grains are ubiquitous in the biotite hornblende gneiss. Some quartz grains were recrystallised as elongated or polygonised crystals strongly aligned parallel to the foliation of the rock (Fig.4.30).

Table 4.8 Modal Composition of Minerals in Biotiite Hornblende Gneiss (BHG) in the Study Area

Sample No → / **Mineral ↓**	bH1	bH2	bH3	bH4	bH5	bH6	bH7	bH8	bH9	bH10	bH11	Range
Quartz	29	20	40	45	30	30	35	30	35	30	35	20-45
Plagioclase	5	25	20	9	25	20	25	15	20	20	16	5-30
Microcline	2	-	5	10	2	3	3	-	4	-	-	2-10
Hornblende	15	15	5	3	15	15	13	10	10	20	18	5-20
Muscovite	4	10	2	3	3	4	3	8	5	4	5	2-10
Biotite	20	20	15	21	17	15	15	15	20	20	22	15-22
Orthoclase Feldspar	15	10	10	7	5	8	4	10	5	5	3	3-15
Opaque	2	-	3	-	3	5	2	4	1	1	1	1-5
Chlorite	-	-	-	2	-	-	-	8	-	-	-	2-8
Epidote	8	-	-	-	-	-	-	-	-	-	-	
Total	100	100	100	100	100	100	100	100	100	100	100	

Migmatitic portion-bH10 and bH11

a

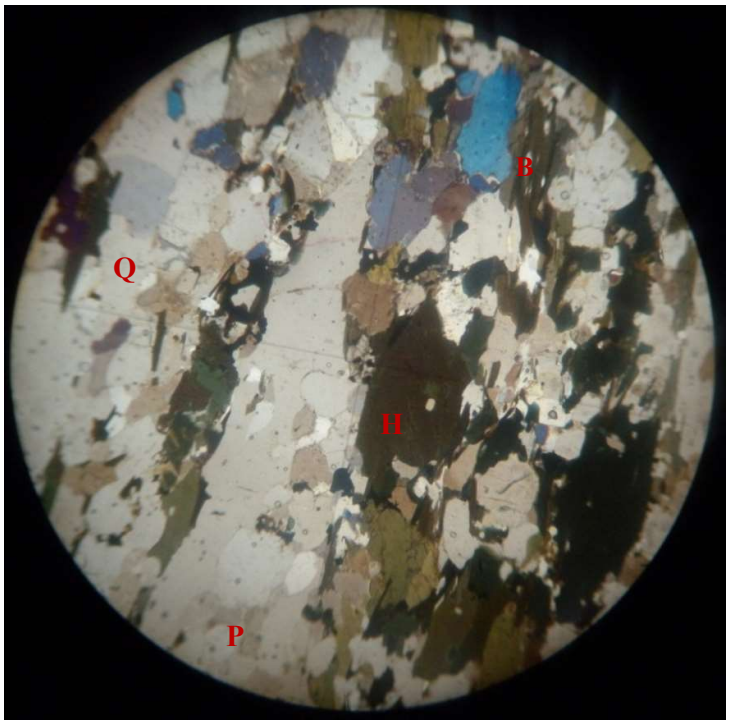

b

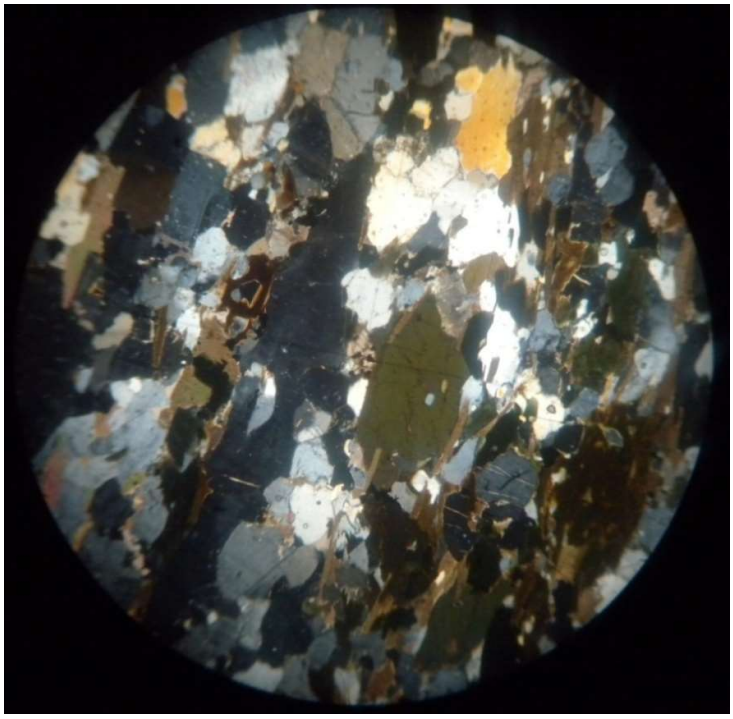

Fig 4.27 Typical Photomicrograph of Biotite Hornblende Gneiss in Transmitted Light ***(a)*** *plane polarised (b) cross polarised light (x40): showing compositional banding defined by anhedral grains of hornblende (H) and biotite grains (B), in the matrix of subhedral quartz (Q), and plagioclase (P). (coordinate: N07^{o} 35.218', E 03^{o} 55.201').*

a

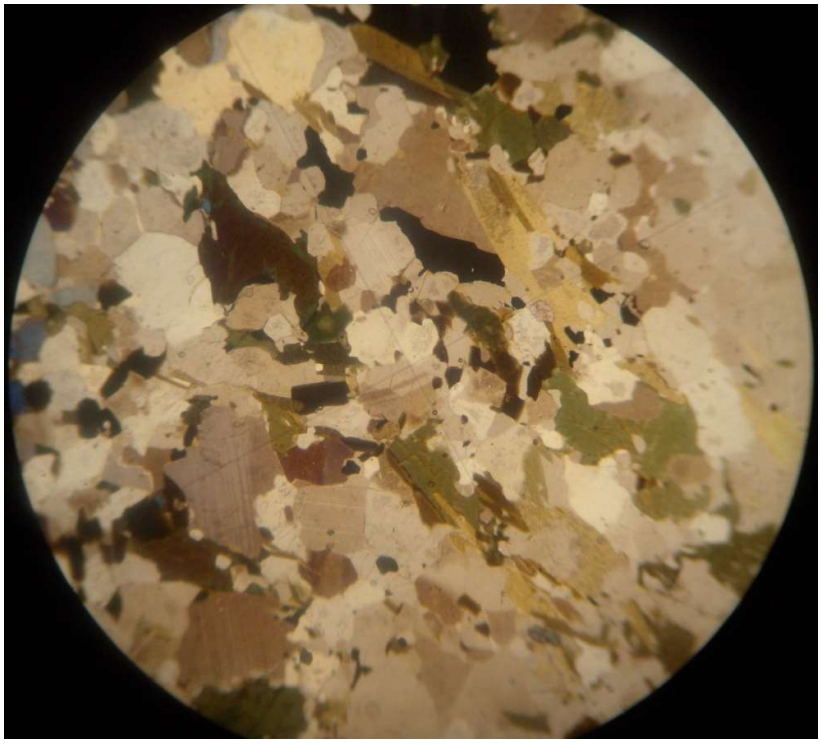

b

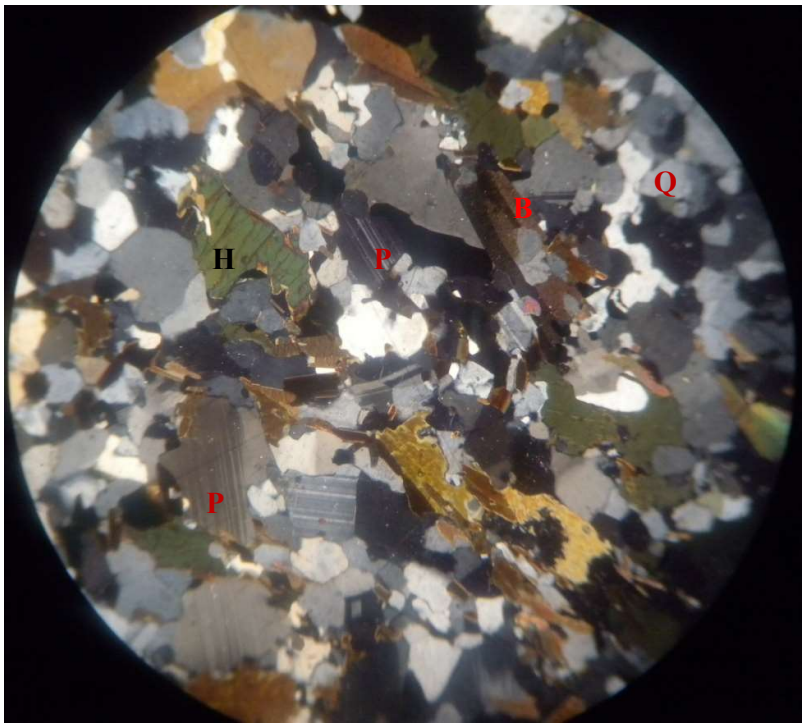

Fig 4.28 Typical Photomicrograph of Biotite Hornblende Gneiss in Transmitted Light*(a) plane polarised (b) cross polarised light (x40): showing compositional banding defined by euhedral grains of hornblende (H) and biotite grains (B), in the matrix of subhedral quartz (Q), and plagioclase (P) with polysynthetic twinning. (coordinate: N07^{o} 34.004', E 03^{o} 51.823').*

a

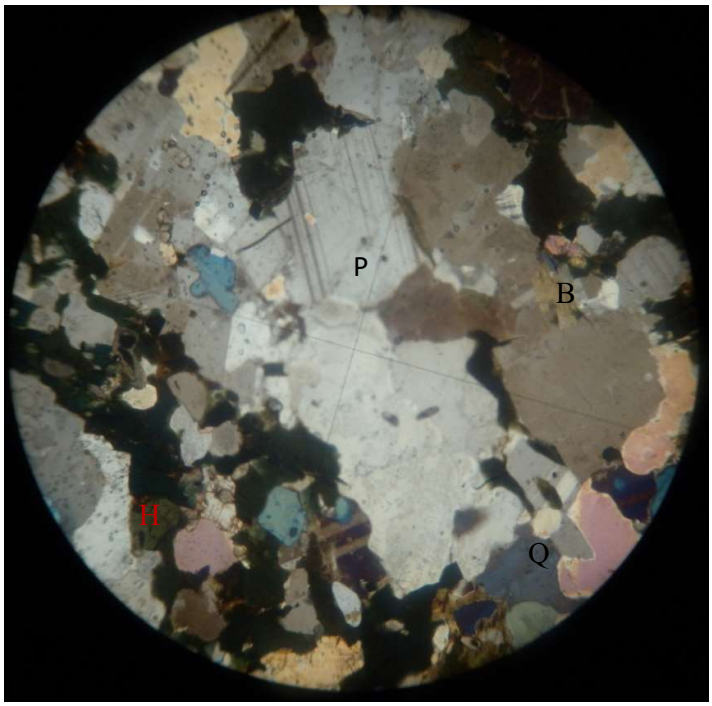

b

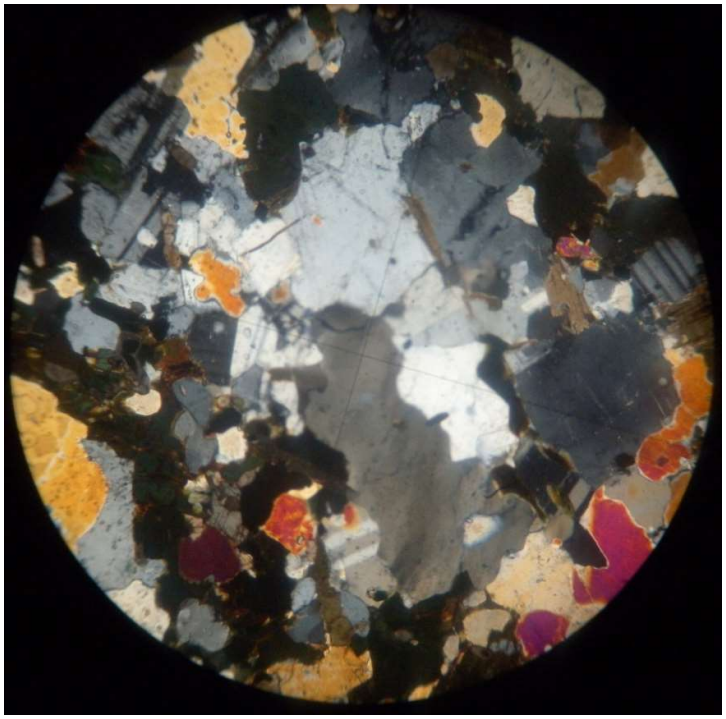

Fig 4.29 Typical Photomicrograph of Biotite Hornblende Gneiss in Transmitted Light ***(a)*** *plane polarised (b) cross polarised light (x40): indicating granoblastic texture with compositional banding subhedral grains of green hornblende and lath-like biotite flakes (B), quartz (Q), and plagioclase (P). (co-ordinate:N07^{o} 32.309', E 03^{o} 55.607').*

a

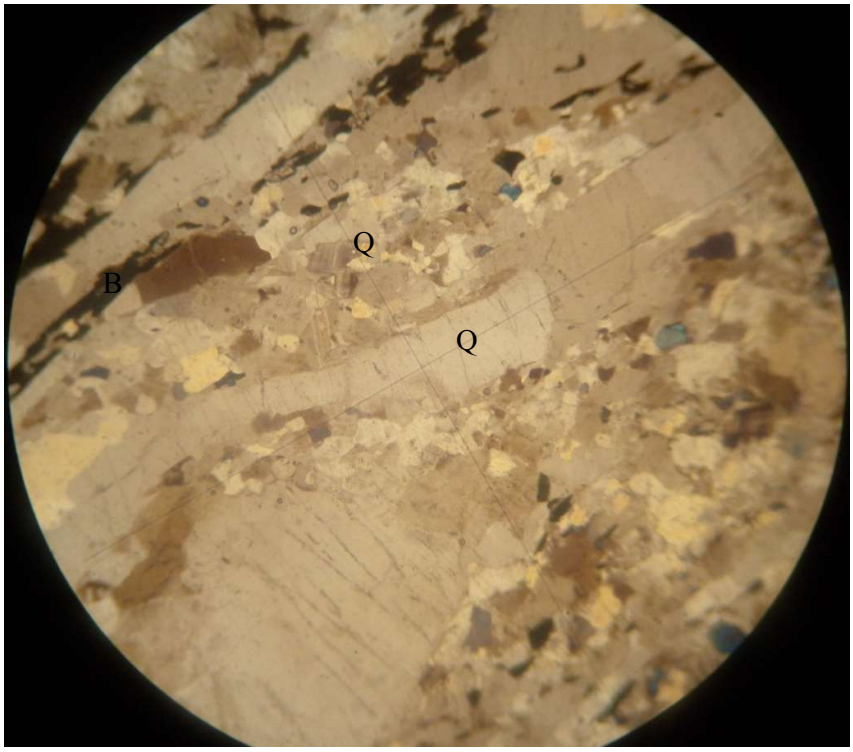

b

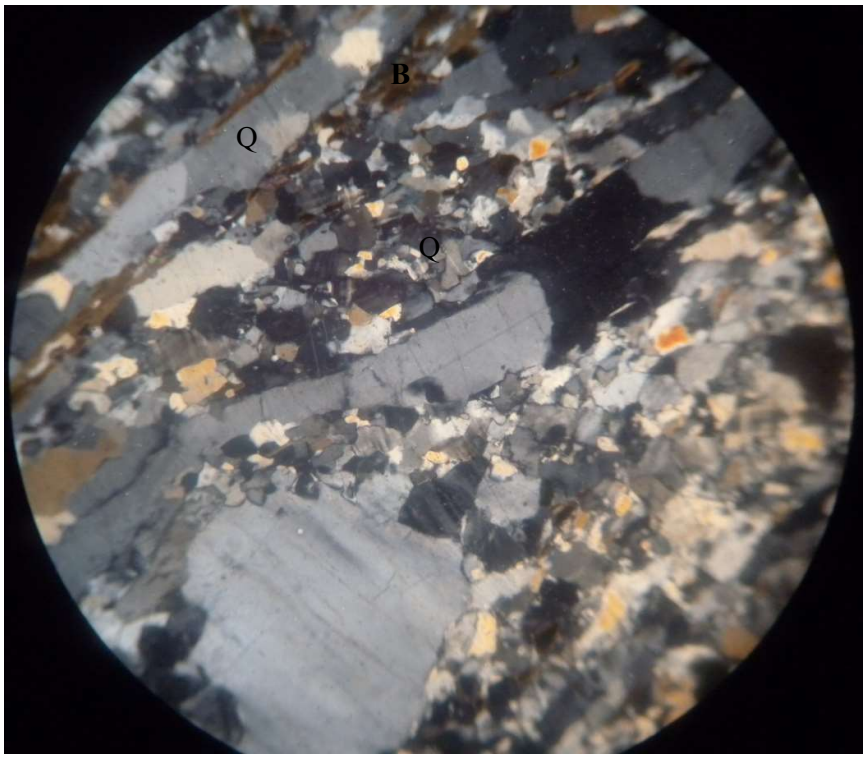

Fig 4.30 Typical Photomicrograph of Biotite Hornblende Gneiss in Transmitted Light ***(a)*** *plane polarised (b) cross polarised light (x40): indicating in-equant texture with recrystallized elongated quartz (Q) and lath-like biotite flakes (B) strongly aligned parallel to the foliation (co-ordinate:N07^{o} 35.743', E 03^{o} 51.249').*

4.1.3.2 Geochemistry of the Biotite-Hornblende Gneiss.

4.1.3.2.1 Major Oxide

Major oxides composition of biotite hornblende gneiss vary between broad limit revealed the concentrations of SiO_2 (62.23 to 73.80%), TiO_2 (0.81 to 0.78%), Al_2O_3 (12.08 to 18.98%), Fe_2O_3 (0.86 to 6.47%), MnO (0.01 to 0.09%) MgO (0.21 to 1.93%), CaO (1.19 to 5.61%), Na_2O (1.65 to 4.79%), K_2O (2.71 to 4.83%), P_2O_5 (0.09 to 0.58%), Cr_2O_3 (<0.002 to 0.01%) and Loi varies from 1.60 to 2.80% (Table 4.9a). The biotite hornblende gneiss sample bH3* represent the felsic portion while bH15* represent the mafic portion of the whole rock unit and both samples have virtually different chemistry (Table 4.9b). The felsic oxides compositions have similar values to that of the whole rock composition.

Discriminate diagram of Na_2O/Al_2O_3 against K_2O/Al_2O_3 of Garrels and Mackenzie (1971) were constructed to predict the precursor materials for the biotite hornblende gneiss rock which revealed mixed origin for the protolith of biotite hornblende gneiss (Fig.4.33). This conformed to the proposed mixed origin of the protholiths of the Precambriam migmatite gneiss of Nigeria (Rahaman, 1988, Oyawoye, 1972 and Ekwueme, 2003).

The plot of R1-R2 diagram (Fig.4.32) of De la Roche et al. (1980) and Na_2O+K_2O versus SiO_2 diagram (Fig.4.33) of Middlemost (1994) indicate that majority of the analysed samples occupy the granite field while mafic sample fell in the gabbro field.

The Aluminium Saturated Index (ASI) ie $Al_2O_3/ (CaO+K_2O+Na_2O)>1$ for the whole rock data of the biotite-hornblende gneiss samples, indicating corundum normative, thus most of the gneiss are mildly peraluminous while the mafic component fell in strongly metalluminous portion (Fig.4.34).

The average composition values of the major oxides (Table 4.10) for this area compared favourably well with those of hornblende-biotite gneiss from Obudu Plateau area (Agbi and Ekwueme, 2018).

Table 4.9a Results of Whole-Rock Oxide Analyses of the Biotite Hornblende Gneiss.

Sample No► Major Oxide(wt%)▼	bH1	bH2	bH4	bH5	bH6*	bH7	bH8	bH9	bH10	bH11	bH12*	bH13	bH14	Range	Average
SiO_2	69.73	69.55	69.90	73.80	73.68	70.08	69.65	73.25	69.81	70.12	62.23	69.66	63.08	62.23-73.80	69.58
TiO_2	0.25	0.33	0.23	0.59	0.18	0.27	0.36	0.53	0.25	0.32	0.63	0.31	0.78	0.18-0.78	0.39
Al_2O_3	15.13	14.89	15.07	12.83	13.68	15.19	14.80	13.00	15.22	14.97	18.98	14.65	16.47	12.83-18.98	14.99
Fe_2O_3	1.54	2.34	1.57	1.92	0.86	1.57	2.17	1.91	1.50	1.90	5.96	2.32	6.47	0.86-6.47	2.46
MnO	0.02	0.02	0.02	0.02	0.01	0.02	0.02	0.02	0.02	0.02	0.09	0.02	0.09	0.01-0.09	0.03
MgO	0.50	0.53	0.48	0.41	0.21	0.55	0.53	0.42	0.51	0.56	1.68	0.53	1.93	0.21-1.93	0.68
CaO	1.61	1.59	1.62	1.19	1.28	1.62	1.59	1.26	1.65	1.55	5.61	1.64	2.82	1.19-5.61	1.93
Na_2O	4.62	4.47	4.70	3.23	1.95	4.69	4.44	3.41	4.79	3.60	3.99	4.43	3.81	1.95-4.79	4.01
K_2O	4.21	3.84	4.08	2.96	7.37	4.02	3.79	3.02	4.06	4.83	4.08	3.73	2.71	2.71-4.83	4.05
P_2O_5	0.12	0.10	0.12	0.12		0.12	0.11	0.11	0.12	0.09	0.37	0.13	0.58	0.09-0.58	0.16
Cr_2O_3	0.00	0.00	0.003	0.01		<0.002	0.00	0.00	0.00	0.00		0.00	0.01	<0.002-0.01	0.00
Loi	2.00	2.10	2.00	2.70		1.60	2.30	2.80	1.80	1.80		2.30		1.60-2.80	2.14
Sum	99.84	99.82	99.79	99.84	99.10	99.84	99.83	99.83	99.85	99.84	103.30	99.80	98.75	98.75-103.30	99.98

Major and trace element contents with sample symbol * were determined by X-ray fluorescence (XRF). Elements with blank space were not determined.

Table 4.9b Results of Major Oxide Analyses of the Mafic and Felsic Portion of Biotite Hornblende Gneiss.

Sample No → Major Oxide (wt%) ↓	bH3* (felsic)	bH15* (mafic)
SiO_2	80.01	47.82
TiO_2	0.37	1.33
Al_2O_3	12.08	14.38
Fe_2O_3	3.28	20.23
MnO	0.03	0.26
MgO	0.46	7.14
CaO	1.57	10.63
Na_2O	1.65	2.39
K_2O	5.80	1.25
P_2O_5	0.06	0.60
Sum	105.10	105.30

Major and trace element contents with sample symbol * were determined by X-ray fluorescence (XRF).

Table 4.10 Comparison of Major Oxide Geochemistry of this Study with Other Areas within the Basement Complex of Nigeria.

Major Oxide(wt%)	This study	Ilesha	W.Nigeria	Obudu Plateau
SiO_2	69.58	64.41	62.54	71.53
TiO_2	0.39	0.81	1.01	0.46
Al_2O_3	14.99	14.33	14.90	14.03
Fe_2O_3	2.46	6.84	7.86	2.66
MnO	0.03	0.11	0.13	0.03
MgO	0.68	2.71	3.09	0.96
CaO	1.93	3.28	4.21	1.91
Na_2O	4.01	1.79	2.85	3.28
K_2O	4.05	3.88	2.54	4.01
P_2O_5	0.16	0.12	0.39	0.10

Ilesha- Afolabi, (2018)

W.Nigeria- Elueze, (1982)

Obudu Plateau- Agbi and Ekwueme, (2018)

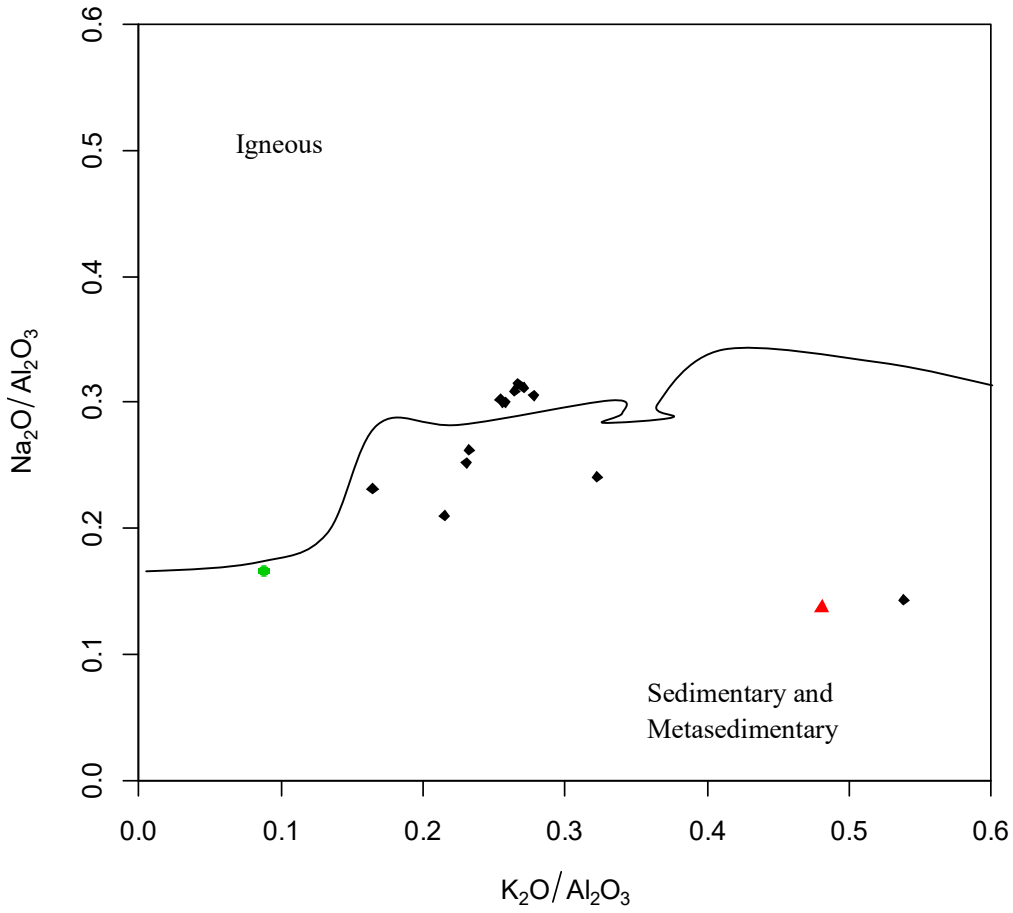

Fig.4.31 Na_2O/Al_2O_3 versus K_2O/Al_2O_3 Variation Diagram of Biotite Hornblende Gneiss (After Garrels and Mackenzie, 1971).

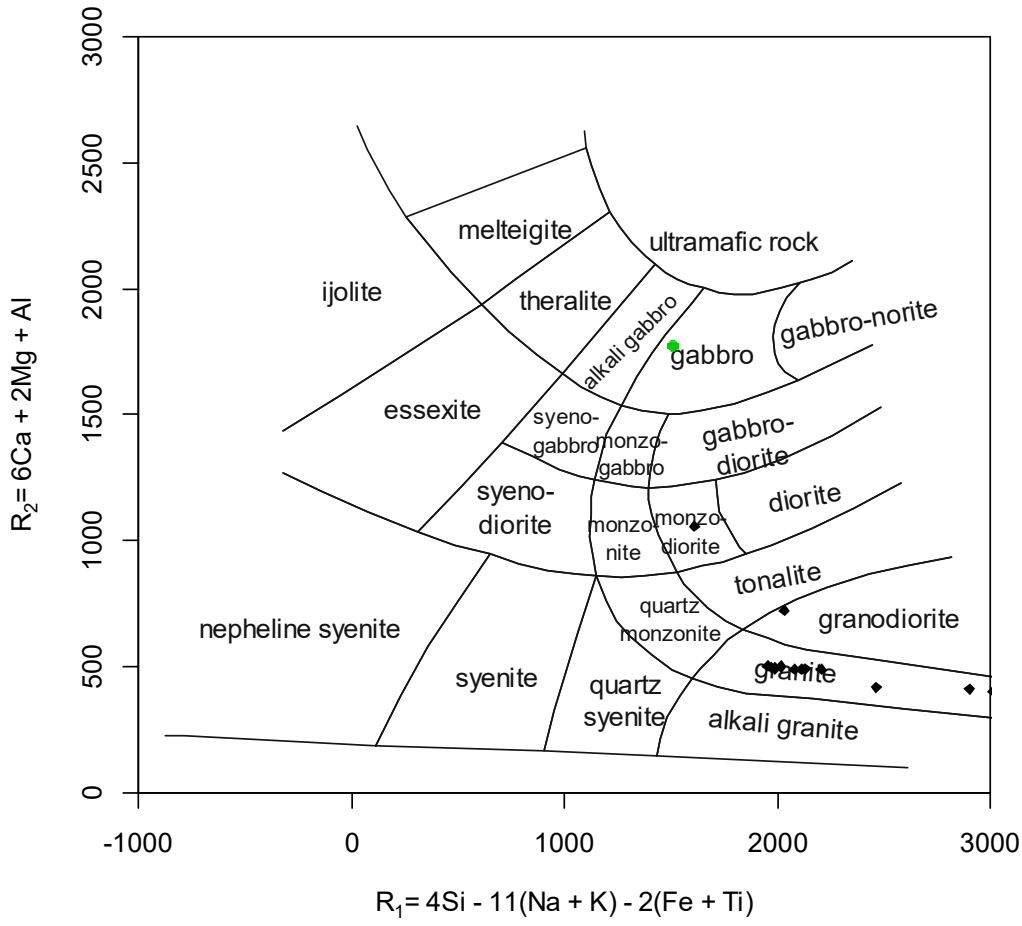

Fig.4.32 R1-R2 Plot of Biotite Hornblende Gneiss indicating granitic origin (After De la Roche *et.al*, 1980).

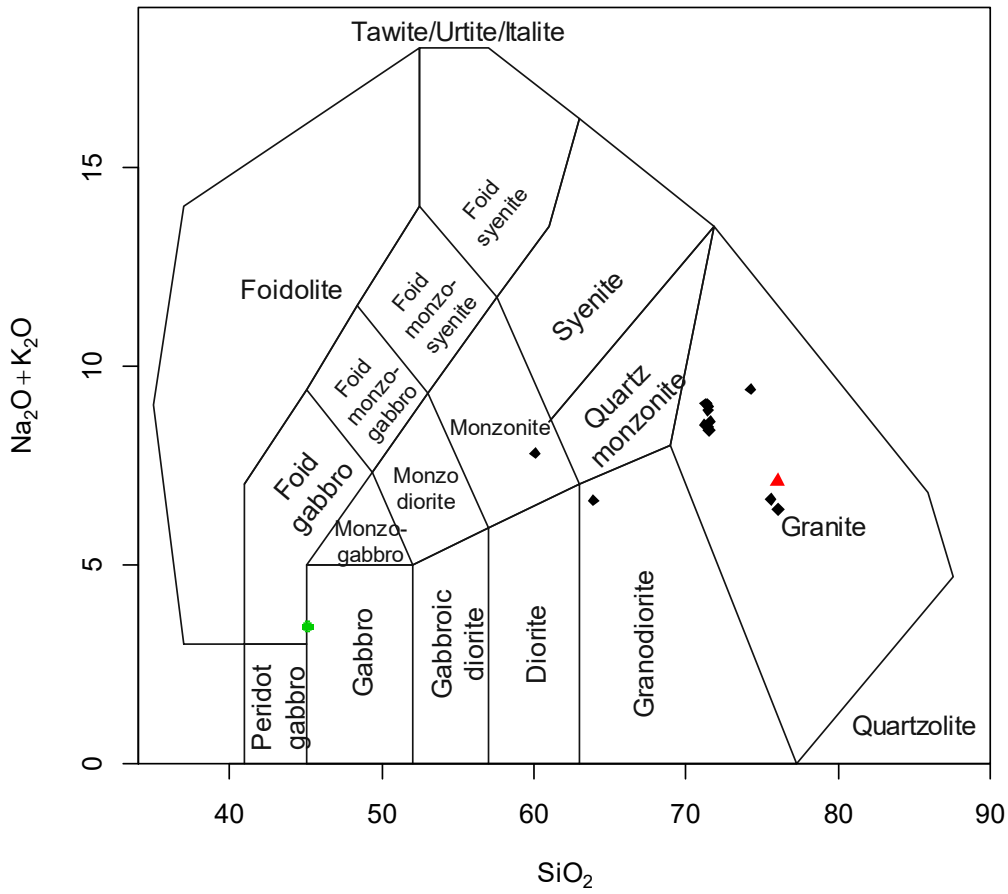

Fig.4.33 Classification Diagram of Biotite Hornblende Gneiss base on Na_2O+K_2O versus SiO_2 (After Middlemost, 1994).

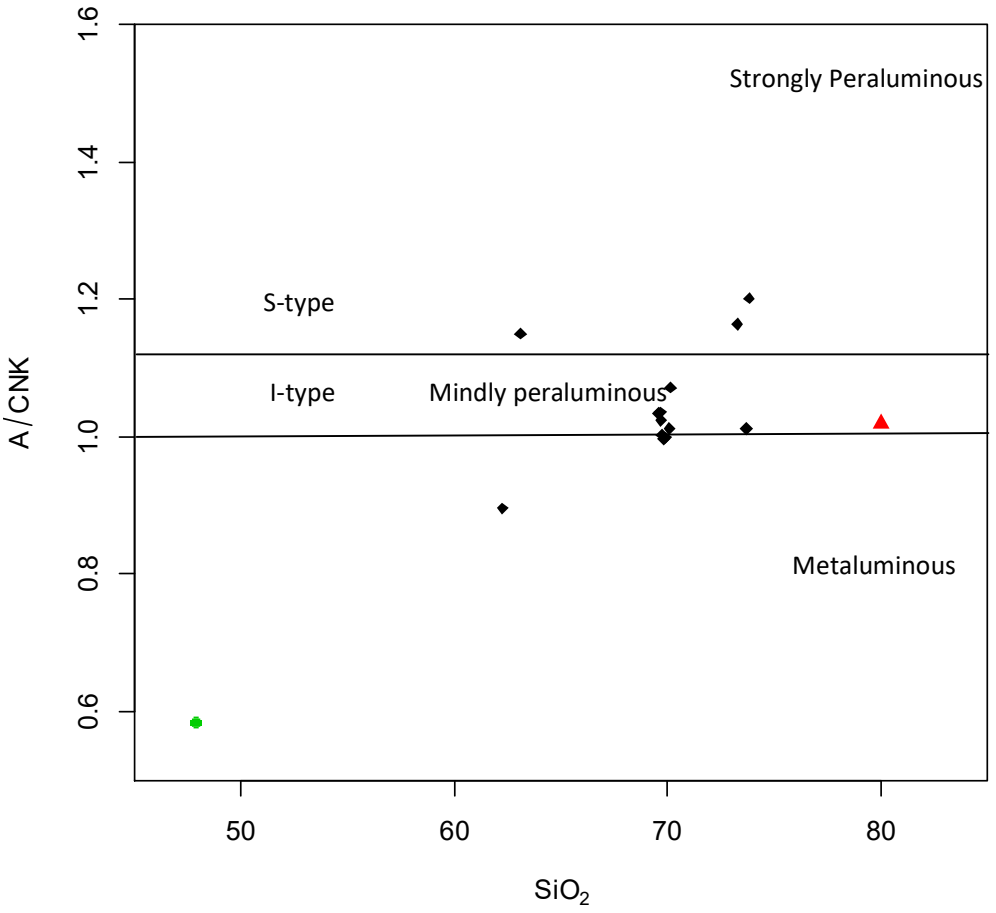

Fig.4.34 Al_2O_3/ ($CaO+Na_2O+K_2O$) versus SiO_2 Binary Diagram of the Biotite Hornblende Gneiss (After Chappel and White, 1974)

4.1.3.2.2 Trace Elements

There is wide range of variation in trace element contents of the biotite hornblende gneiss especially Ba (289.4 to 2310ppm), Sr (239.3 to 1130ppm), Zr (110.7 to 325.7ppm) and Nb (4.6 to 16.6ppm) (Table 4.11), which strongly supports a mixture of igneous rock types input as exemplified by the major oxides composition.

Elevated concentration of Cr (373.3ppm) and V (274.6ppm) in the mafic portion indicate derivation of the parent magma from basaltic rock source. The biotite hornblende gneiss is characterized by low concentrations of High Field Strength (HFS) elements (Nb, Ta). However, the concentrations of transition elements like Sc, V, Cr, Co and Ni show depletion, while high proportion of the Large Ion Lithophile Element (LILE) such as Ba, Sr and Rb due to their concentration in the melt phase of the parent magma.

The binary plot of log(Zr/Y) against log(Zr) (Pearce *et al*., 1983) revealed that all the biotite hornblende gneiss samples fell within the continental arc field, except the mafic portion which falls in the oceanic arc field (Fig.4.35).

The log(Nb) against log(Y) discrimination diagram(Pearce *et al*., 1984) revealed that the biotite hornblende gneiss plotted in volcanic arc-syn collision granites field (Fig. 4.36). The drawback of such diagram however is that they are based on concentrations rather than ratio hence may be strongly affected by differentiation and fractionation processes (Pearce *et al*. 1984). This effect may be responsible for the plot of the samples in volcanic – arc field. The plot of R1-R2 diagram for the biotite hornblende gneiss (Batchelor and Bowden, 1985) indicate that majority of the analysed samples occupy the syn-collision granite field (Fig.4.37).

Spider plot of normalized chondrite of trace elements of the biotite hornblende gneiss samples confirm that Thorium (Th), Barium (Ba), Rubidium (Rb) and Potassium (K) had the high peaks due to their mobility in the calc-alkali magma (Pearce *et al*., 1983) while thulium (Tm) had lowest concentration (Fig.4.38).

Table 4.11 Results of Trace Element Analyses of Biotite Hornblende Gneiss.

Sample No → Trace Element ↓ (ppm)	bH1	bH2	bH4	bH5	bH7	bH8	bH9
Ba	957	845	867	693	890	835	673
Sc	2	2	2	3	2	2	3
Be	3	<1	<1	<1	5	5	5
Co	3.2	4.7	2.7	2.8	3.4	4	3.2
Cs	6.2	6	5.9	4.8	6.5	6.5	4.5
Ga	18.5	19	19.7	16.1	18.5	19.7	16.6
Hf	3.5	6.7	3.6	7.3	3.5	5.1	8.1
Nb	5	6.5	4.6	16.6	4.9	7.2	12.3
Rb	144.4	135.1	139.6	102.4	140.1	133.6	105.5
Sn	2	4	1	3	2	3	3
Sr	823.6	767.7	801.9	588.7	813.1	775.8	601
Ta	0.5	0.7	0.3	1.1	0.5	0.6	0.9
Th	11.5	9.4	10.2	16.9	10.1	10.3	10.3
U	7.4	6.9	5.8	6.2	5.2	5.6	5.1
V	21	30	19	30	21	25	31
W	<0.5	<0.5	<0.5	1	<0.5	<0.5	<0.5
Zr	115.5	244.3	117.6	288.4	120	188.1	325.7
Y	4.2	6.9	3.6	5.8	4.4	4.7	5.9
Mo	0.8	0.8	0.8	0.7	0.5	0.8	0.7
Cu	7.8	22.7	8.3	21.7	7.2	23.3	17.7
Pb	3.4	22.4	3.2	22.9	3.3	28.1	26.6
Zn	41	110	42	84	45	111	77
Ni	7.5	12.4	7.5	13.7	7.2	11.9	10.3
As	<0.5	0.9	<0.5	0.8	<0.5	0.9	0.8
Cd	<0.1	<0.1	<0.1	0.1			0.8
Sb	0.3	0.1	0.2	0.4			0.9
Ag	<0.1	<0.1	<0.1	<0.1	<0.1	<0.1	<0.1
Au	<0.5	5	<0.5	4.4	<0.5	1.6	3.8

Elements with blank space were not determined

Table 4.11(cont.) Results of Trace Element Analyses of Biotite Hornblende Gneiss.

Sample No→ Trace Element(ppm)↓	bH10	bH11	bH13	Range	Average
Ba	898	976	840	289.4-898	847.4
Sc	2	3	2	2.0-3.0	2.3
Be	3	5	3	<1.0-5.0	4.1
Co	3.6	2.1	4.5	2.1-4.7	3.4
Cs	6.1	4.0	5.9	4.0-6.5	5.6
Ga	19.1	17.3	18.3	12.2-19.7	18.3
Hf	3.6	5.2	5.7	3.2-8.1	5.2
Nb	4.6	10.3	6.8	4.6-16.6	7.9
Rb	139.7	164	133.9	23.8-164.0	133.8
Sn	1	5	9	1.0-9.0	3.3
Sr	829.3	538.5	764.6	239.3-829.3	730.4
Ta	0.6	0.9	0.7	0.5-1.1	0.7
Th	9.9	28.0	9.3	9.3-28.0	12.6
U	5.3	7.4	5.1	5.1-7.4	6.0
V	21	22	23	20.0-70.1	24.3
W	<0.5	0.6	<0.5	<5-0.6	0.8
Zr	116.5	197.3	203.4	110.7-325.7	191.7
Y	4.2	14.4	4.9	4.2-14.4	5.9
Mo	0.6	0.8	0.8	0.5-0.8	0.7
Cu	7	20.9	26.8	7.0-26.8	16.3
Pb	3.1	4.5	30.6	3.0-30.6	14.8
Zn	45	34	132	34.0-132.0	72.1
Ni	7.1	4.8	13.4	4.8-13.4	9.6
As	<0.5	<0.5	0.7	<0.5-0.9	0.8
Cd	<0.1	<0.1	0.8	<0.1-0.8	0.6
Sb	0.1	0.1	1.1	0.1-1.1	0.4
Ag	<0.1	<0.1	0.1	<.1-0.1	0.1
Au	<0.5	12.3	1.3	<0.5-12.3	4.7

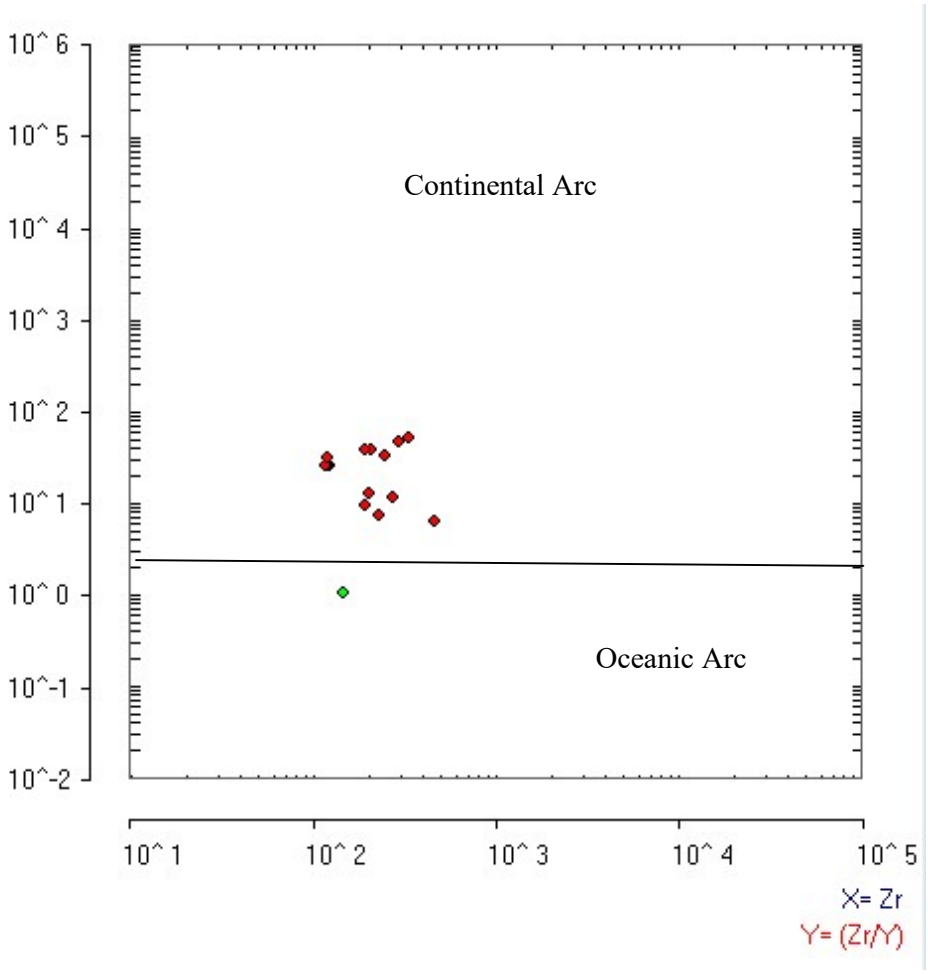

Fig.4. 35 Binary Diagram of Log(Zr/Y) vs Log(Zr) for the Biotite Hornblende Gneiss (After Pearce, 1983).

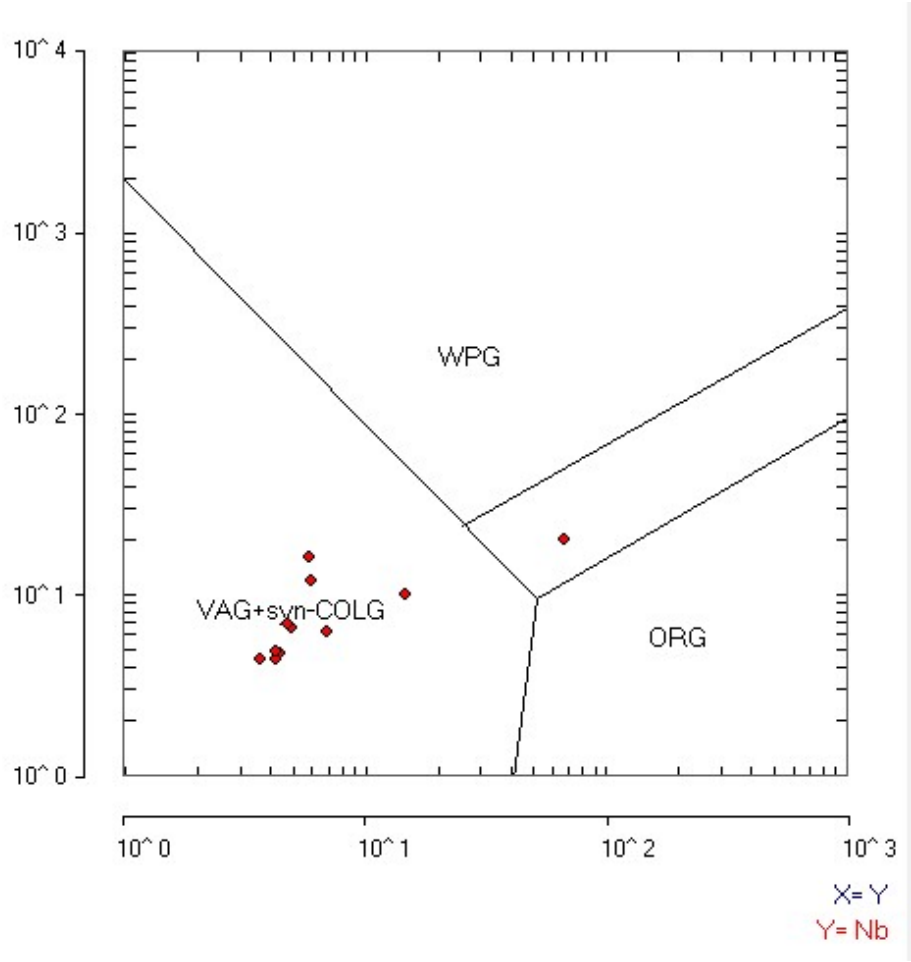

Fig.4.36 Discriminate Binary Diagram of Log(Nb) versus Log(Y). (After Pearce *et. al*. 1984)

Syn-COLG: syn-collision granites, WPG: within-plate granites, VAG: volcanic-arc granites, ORG: ocean-ridge granites

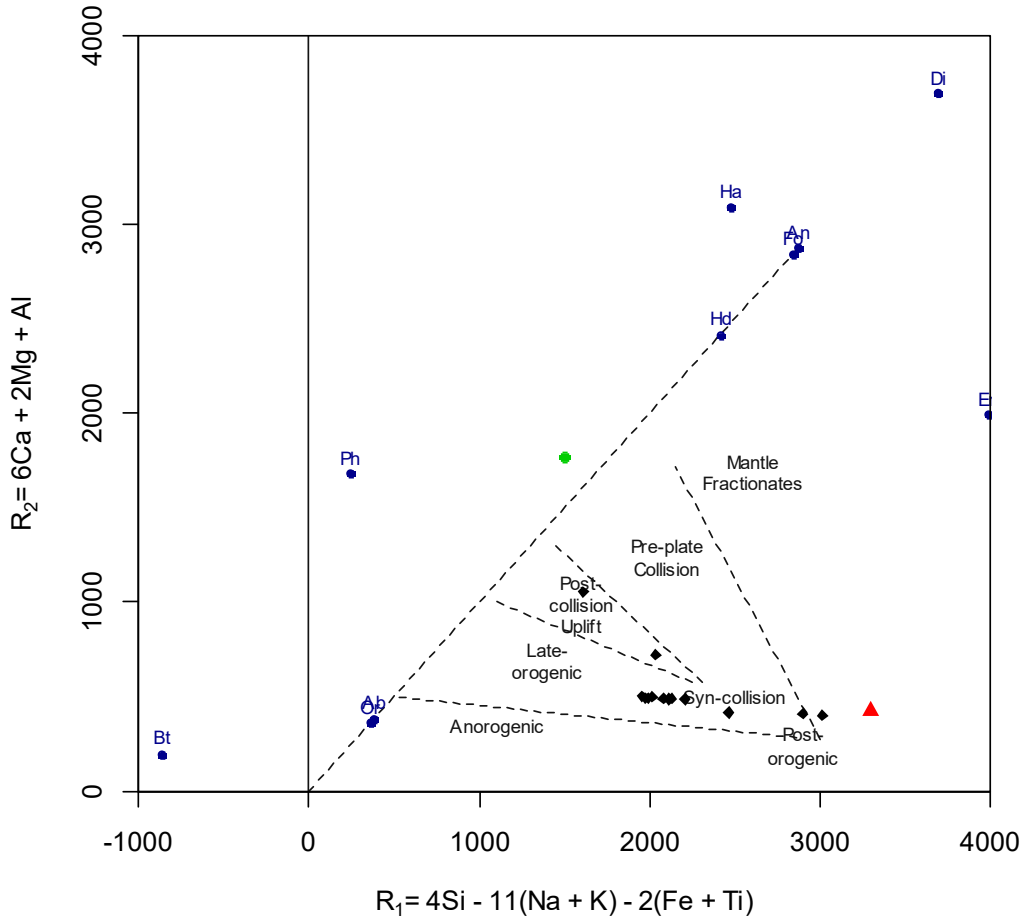

Fig.4.37 Discriminate Binary Diagram of R1 versus R2 for Biotite Hornblende Gneiss. (After Batchelor and Bowden, 1985)

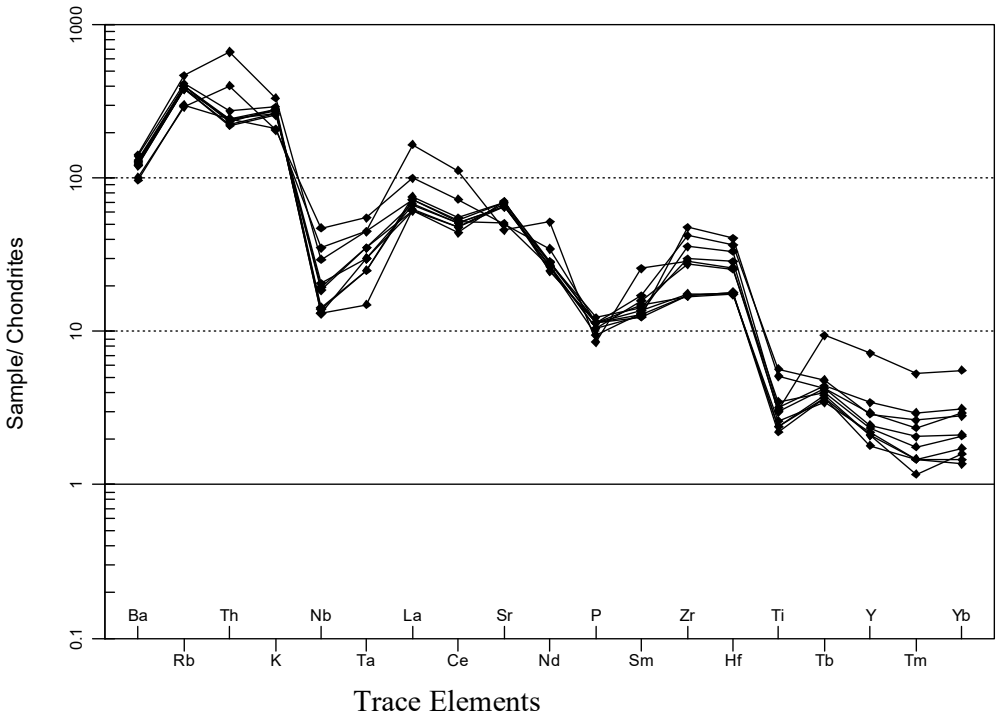

Fig.4.38 Chondrite Normalized Plot of the Trace Elements in the Biotite Hornblende Gneiss (After Thompson, 1982).

.

4.1.3.2.3 Rare Earth Elements

The biotite hornblende gneiss samples in the study area were enriched in light rare earth elements (LREE) concentrations (average; 25.38) but showed relatively depleted heavy rare earth elements (HREE) (average; 0.32, Table 4.12). Europium (Eu) concentration ranged from 0.50 to 0.96ppm having negative Eu anomalies (Eu/Eu*; 0.66 to 0.87, average 0.78).

The chondrite normalized plot of rare earth element (REE)) (Boynton, 1984) for the biotite hornblende gneiss revealed high values for the light rare earth elements (LREE) and moderately low values for the Heavy rare earth elements (HREE) with negative Eu (Fig.4.39). This extreme depletion of HREE relative to LREE may be indication of the presence of garnet and zircon in the source rock, moreso that LREE are more concentrated in the crust (Rollinson, 1993).

Table 4.12 Results of Rare Earth Element Analyses of Biotite Hornblende Gneiss Unit.

Sample No → REE Element ↓ (ppm)	RK45	RK47	RK53	RK56	RK71	RK88	R3K	41	44	49	Range	Average
La	20.1	54.6	22.6	32.9	24.8	22.1	23.7	23.8	20.4	20.6	7.18-54.60	26.56
Ce	38.1	96.9	43.9	62.9	47.8	43.9	44.9	45.7	41.3	41.2	16.53-96.90	50.66
Pr	4.4	9.87	4.79	6.28	4.89	4.73	4.7	4.84	4.34	4.37	1.23-9.87	5.321
Nd	15.6	32.7	17.8	21.8	18	17.1	16.6	17.8	16.8	15.6	15.60-32.70	18.98
Sm	2.64	5.24	2.89	3.47	2.77	3.23	2.56	3.04	2.65	2.52	2.31-5.24	3.101
Eu	0.63	0.96	0.58	0.59	0.6	0.59	0.5	0.64	0.6	0.57	0.50-0.96	0.626
Gd	1.86	3.67	1.86	2.18	1.82	1.77	1.77	1.78	1.73	1.64	1.73-3.86	2.008
Tb	0.2	0.49	0.22	0.25	0.18	0.21	0.22	0.19	0.23	0.19	0.18-0.49	0.238
Dy	0.75	2.52	1.04	1.18	0.82	1.01	1.05	0.87	1.15	0.88	0.62-2.52	1.127
Ho	0.12	0.5	0.17	0.22	0.14	0.16	0.2	0.13	0.25	0.11	0.12-0.50	0.2
Er	0.41	1.32	0.48	0.57	0.29	0.42	0.66	0.35	0.8	0.34	0.29-1.01	0.564
Tm	0.04	0.18	0.07	0.09	0.05	0.06	0.08	0.05	0.1	0.05	0.04-0.10	0.077
Yb	0.35	1.23	0.47	0.62	0.32	0.46	0.65	0.38	0.69	0.3	0.32-1.23	0.547
Lu	0.04	0.17	0.07	0.1	0.04	0.05	0.09	0.06	0.09	0.04	0.04-0.53	0.075
Eu/Eu*	0.87	0.67	0.77	0.66	0.82	0.76	0.72	0.85	0.86	0.86	0.66-0.87	0.78
La_N/Yb_N	38.29	29.59	32.06	35.38	51.67	32.03	24.31	41.75	19.71	45.78	19.71-51.67	35.06
La_N/Sm_N	4.68	6.41	4.81	5.83	5.51	4.21	5.69	4.82	4.74	5.03	4.21-6.41	5.17
ƩLREE	19.55	48.52	22.27	30.97	23.87	21.96	22.46	23.04	20.71	20.44	19.55-48.52	25.38
ƩHREE	0.21	0.73	0.27	0.35	0.18	0.25	0.37	0.21	0.42	0.18	0.18-0.73	0.32

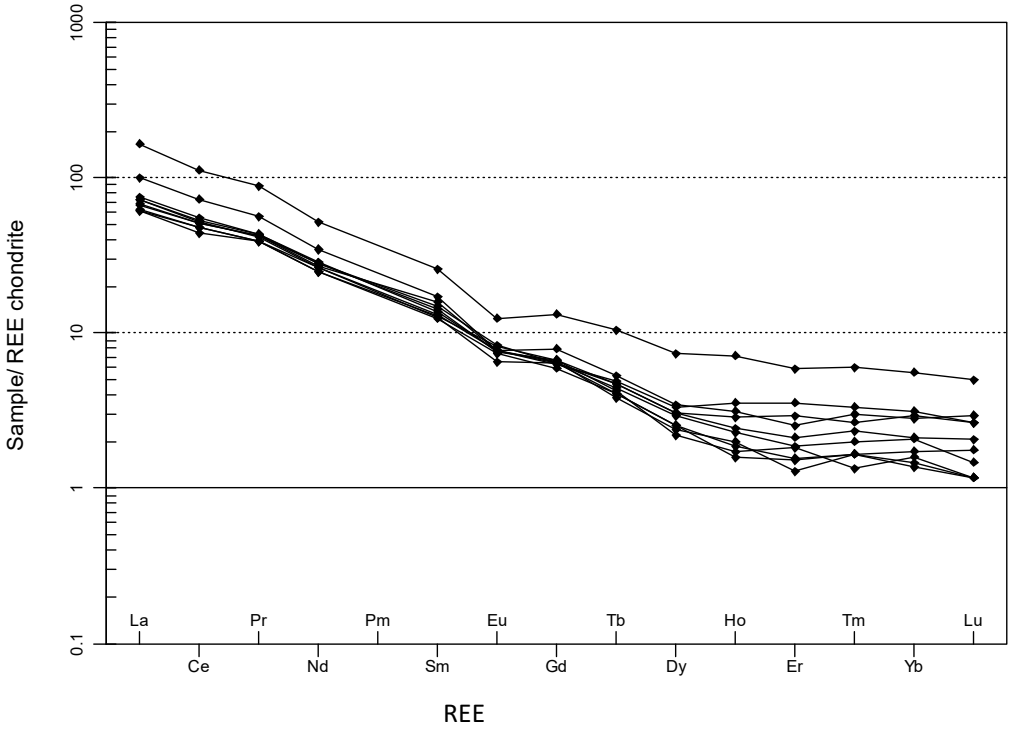

Fig.4.39 Chondrite Normalized Plot of Rare Earth Elements (REE) in the Biotite Hornblende Gneiss (After Boynton, 1984).

4.1.3.3 Granodioritic Gneiss

The granodioritic gneisses underlie a small part in the southern end of the study area. They are mostly found outcropping as moderate extensive elongated bodies (Fig.4.40). The outcrops essentially exhibit a NNW-SSE trend and generally dip to the east (Fig.4.41). Buried outcrop of granodioritic gneiss that were exposed as a result of quarry activities in part of the area (Fig.4.42 and 4.43). The granodioritic gneisses are grey coloured and coarse grained in size with less distinct gneissic texture (Fig.4.44 and 4.45).The mafic bands comprise biotite and hornblende, whereas the felsic bands are essentially quartz and plagioclase feldspars. The granodioritic gneisses are closely associated with the biotite hornblende gneiss in the field and they have been suggested to be part of the migmatite-gneiss complex of Ibadan area (Rahaman, 1976).

The mineralogy is dominantly composed of quartz (30-40%), plagioclase feldspar (24-35%), biotite (6-20%), hornblende (2-12%). Microcline (3-8%), muscovite (3-10%), orthoclase feldspar (4-8%), and opaque mineral (2-4%) are present insignificant amount in the gneiss (Table 4.13).

Quartz and plagioclase feldspars are the dominant minerals in the granodioritic gneiss. Grain of quartz appeared as subhedral phenocrysts (Fig.4.46).

K-feldspars were mostly microcline, which are subordinate to plagioclase feldspar. It occurs as tabular or rectangular large crystal displaying the cross hatch twinning (Fig.4.47). Some of the microcline crystal exhibit perthitic intergrowth.

Biotite is the dominant mafic mineral in the granodioritic gneiss and it mainly responsible the foliations shown. Biotite displays strong pleochroism from green to light brown colour (Fig.4.48). Subhedral hornblende is sometimes intimately associated with biotite, epidote and chlorite forming the foliation bands.

Plagioclase is mostly common, showing wide albite twinning. Alteration of plagioclase to sericite is more profound. Sericitization appeared as overall dusting patches, which almost render the crystal opaque (Fig.4.49). Cubic crystals of garnet were observed in few slides.

Fig.4.41 Outcrop of Granodioritic Gneiss Displays the Compositional Banding (coordinate: N07^{o} 32.744′, E 03^{o} 53.102′)

Fig.4.42 Exposure of Granodioritic Gneiss Showing Level of Overburden in an Active Quarry Site. (Coordinate: N07^{o} 33.829′, E 03^{o} 54.295′)

Fig. 4.43 Outcrop of Buried Granodioritic Gneiss in an Abandoned RCC Quarry Site, Moniya Area. (Coordinate: N07^{o} 30.793′, E 03^{o} 55.134′)

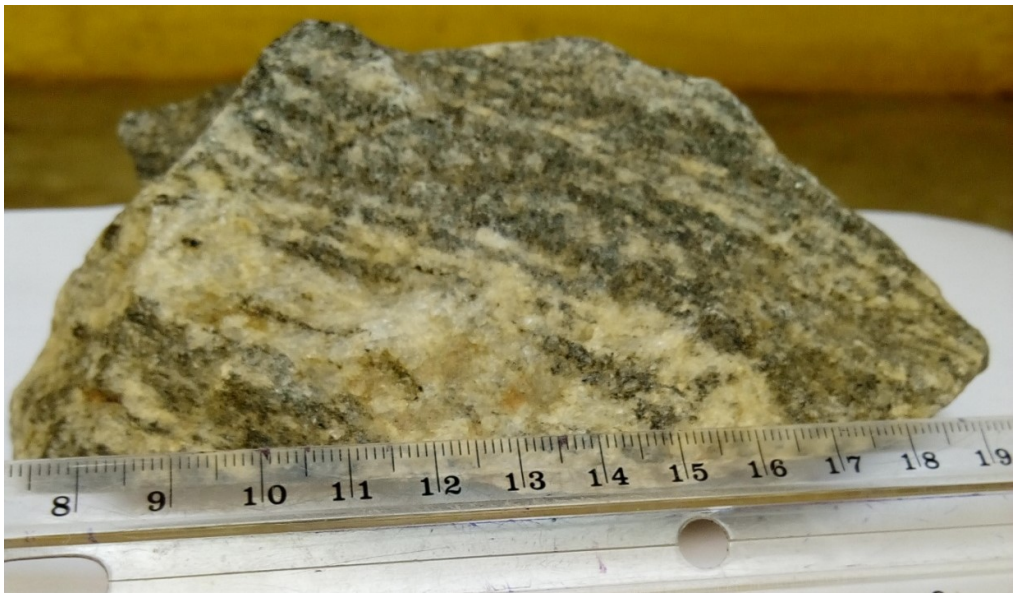

Fig.4.44 Hand Specimen of Granodioritic Gneiss. ***(Coordinate: N07^{o} 32.130', E 03^{o} 53.326'))***

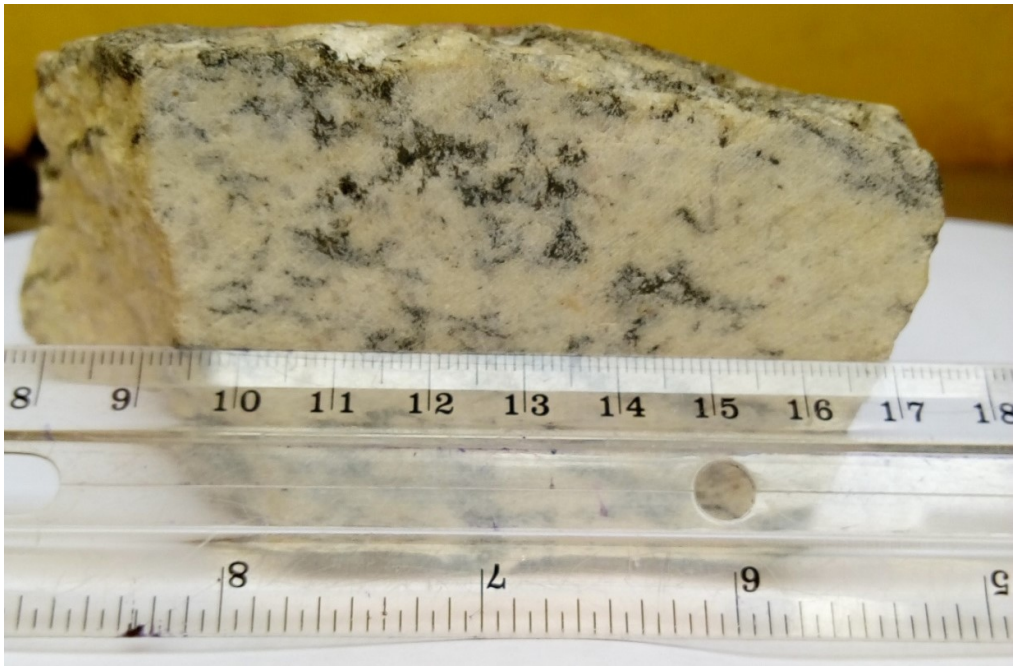

Fig.4.45 Hand Specimen of Granodioritic Gneiss. ***(Coordinate: N07^{o} 32.419', E 03^{o} 53.171')***

Table 4.13 Modal Composition of Minerals in Granodioritic Gneiss in the Study Area

Sample No → / **Mineral ↓**	G1	G2	G3	G4	G5	G6	G7	Range
Quartz	35	35	30	38	40	31	30	30-40
Plagioclase	26	25	24	30	35	30	25	24-35
Microcline	-	8	3	-	5	5	5	3-8
Hornblende	5	8	12	10	-	3	5	2-12
Muscovite	10	6	5	-	4	3	10	3-10
Biotite	20	10	12	15	6	12	10	6-20
Alkali Feldspar	4	4	8	5	8	8	6	4-8
Opaque	-	2	4	2	2	2	3	2-4
Chlorite	-	-	2	-	-	6	4	2-6
Epidote	-	-	-	-	-	-	2	
Garnet	-	2	-	-	-	-	-	
Total	100	100	100	100	100	100	100	

a

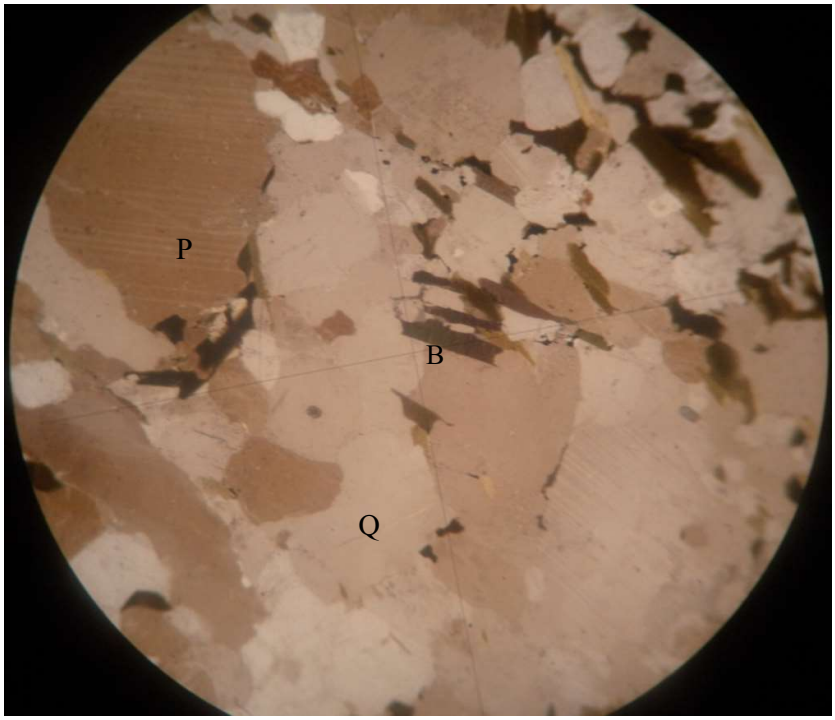

b

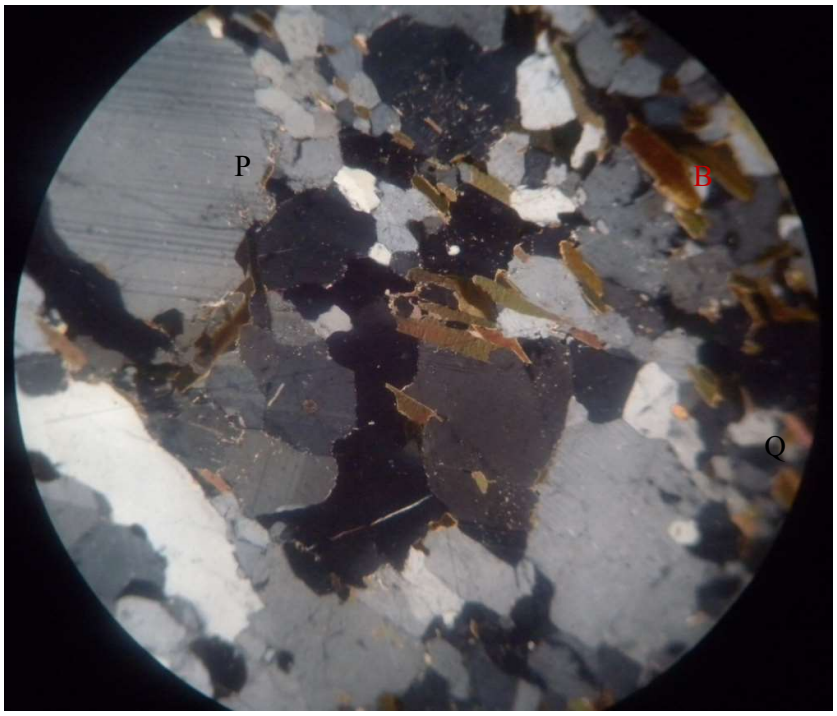

Fig 4.46 Typical Photomicrograph of Granodioritic Gneiss in Transmitted Light

(a) plane polarised (b) cross polarised light (x40): showing granoblastic texture of coarse grains of plagioclase feldspars (P) and quartz (Q), and thin flakes of biotite (B) in the felsic portion of the rock (coordinate: N07^{o} 32.130', E 03^{o} 53.326')

a

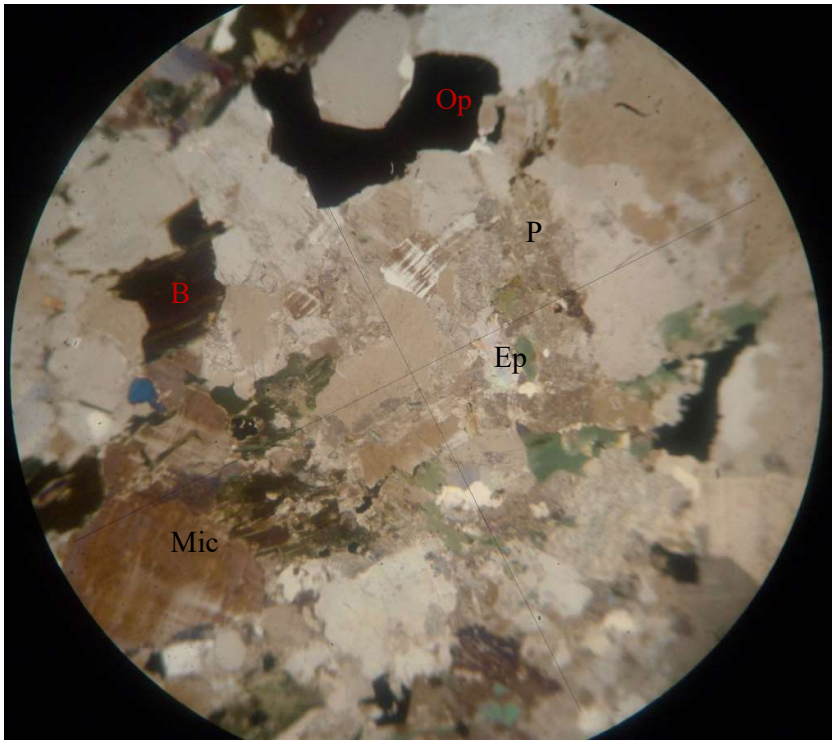

b

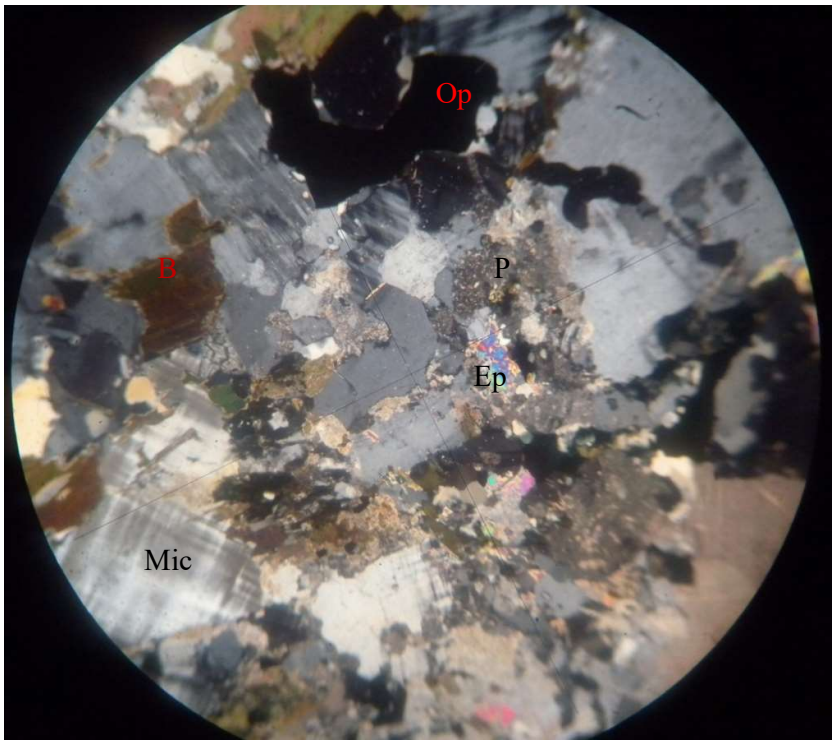

Fig 4.47 Typical Photomicrograph of Granodioritic Gneiss in Transmitted Light

(a) plane polarised (b) cross polarised light (x40): Showing microcline (Mic) having tartan twining, Epidote (Ep), chloritized biotite (B) and opaque mineral (Op) and sericite plagioclase (P) (coordinate: N07^{o} 32.419', E 03^{o} 53.171')

a

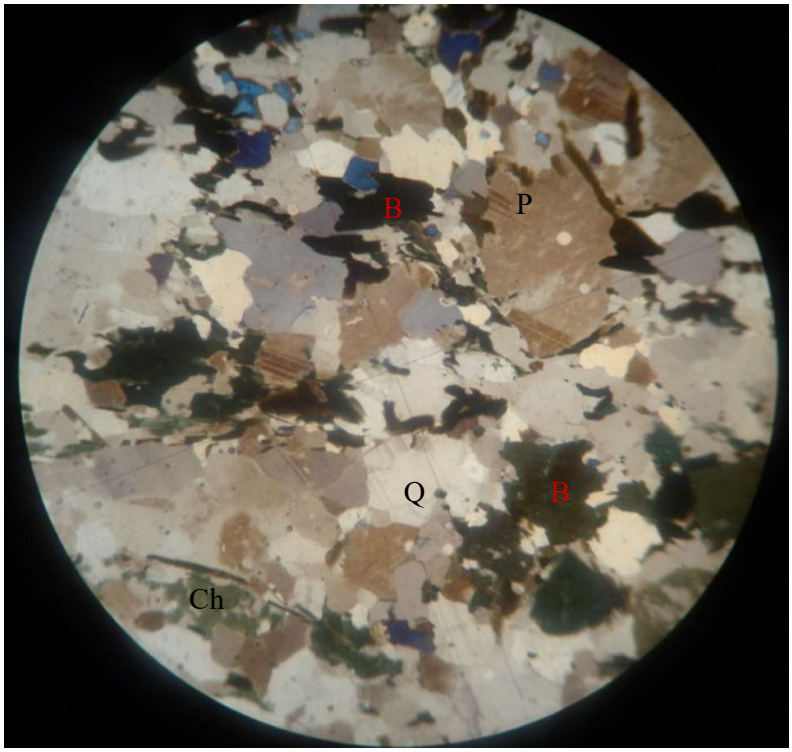

b

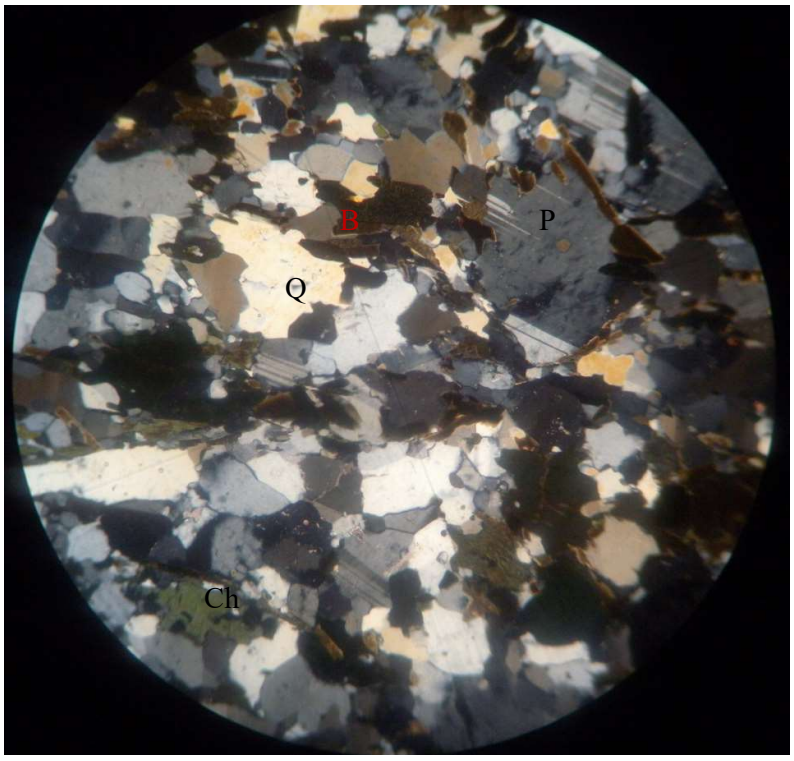

Fig 4.48 Typical Photomicrograph of Granodioritic Gneiss in Transmitted Light *(a) plane polarised (b) cross polarised light (x40): indicating biotite (B) and chlorite (Ch) minerals in a mosaic of quartz (Q) and plagioclase feldspar (P). (coordinate: N07^o 30.863', E 03^o 52.830')*

a

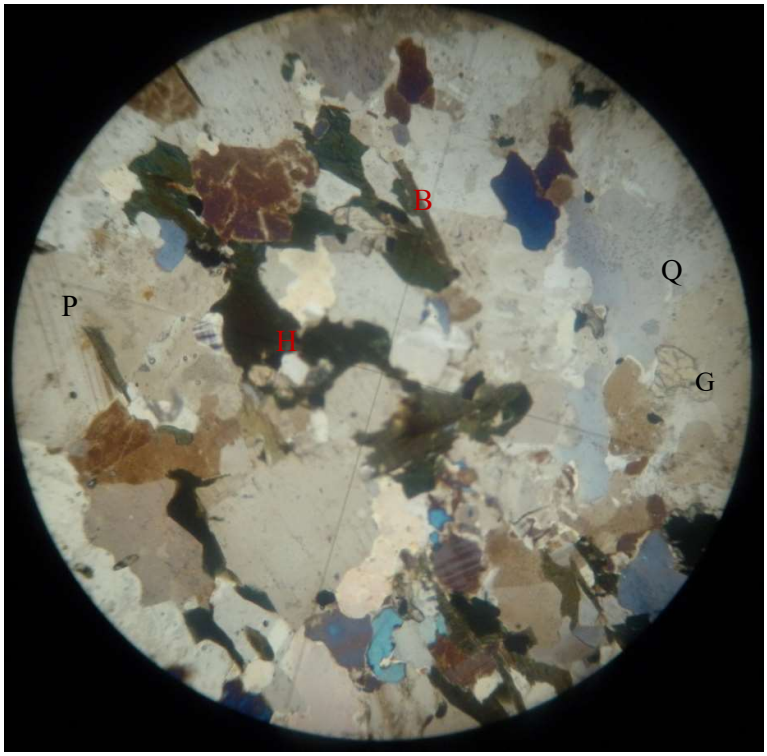

b

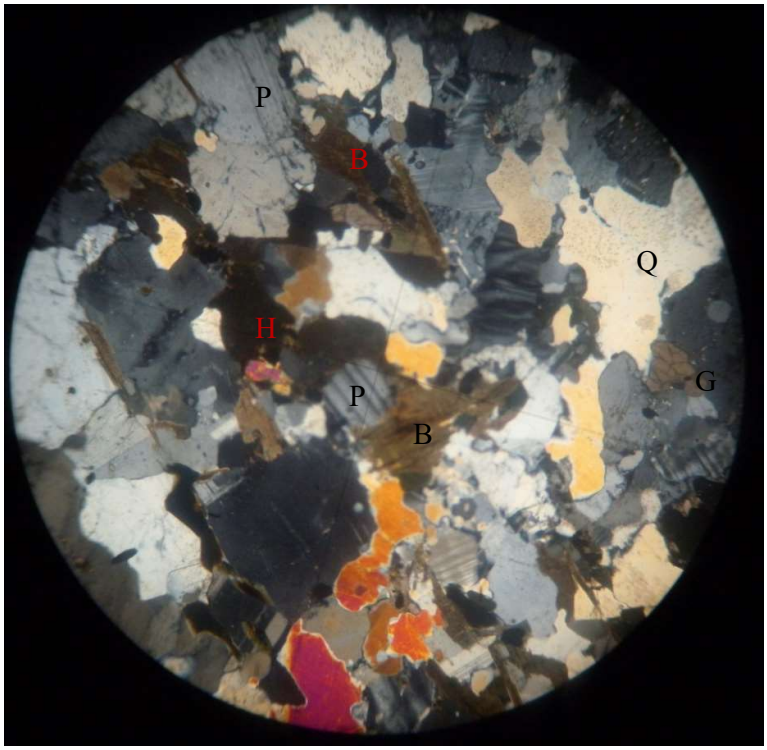

Fig 4.49 Typical Photomicrograph of Granodioritic Gneiss in Transmitted Light *(a) plane polarised (b) cross polarised light (x40): showing distinct thin foliation band of subhedral biotite flakes (B) and hornblende (H), suhedral quartz (Q), plagioclase feldspars (P) and euhedral garnet (G). (coordinate: N07^o 30.200', E 03^o 55.259')*

X-Ray Diffractograms of the granodioritic gneiss (Fig.4.50 and 4.51) also revealed conspicuous peaks of quartz and plagioclase feldspars with subordinate biotite, microcline and epidote corroborating the minerals obtained from petrographic studies of the granodioritic gneiss. The modal composition of the two representative samples of granodioritic gneiss is presented in Table 4.14.

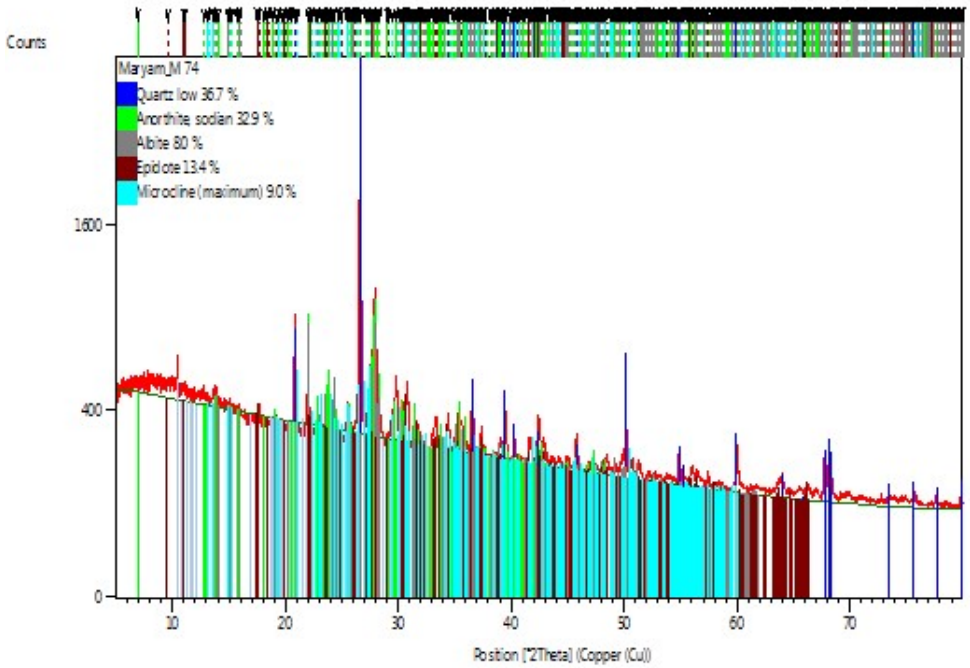

Fig.4.50 Diffractogramof Granodioritic Gneiss Depicting Predominant Quartz, Anorthite, Albite, Epidote and Microcline Peaks *(coordinate: N07^o 30.904', E 03^{o}54.522')*

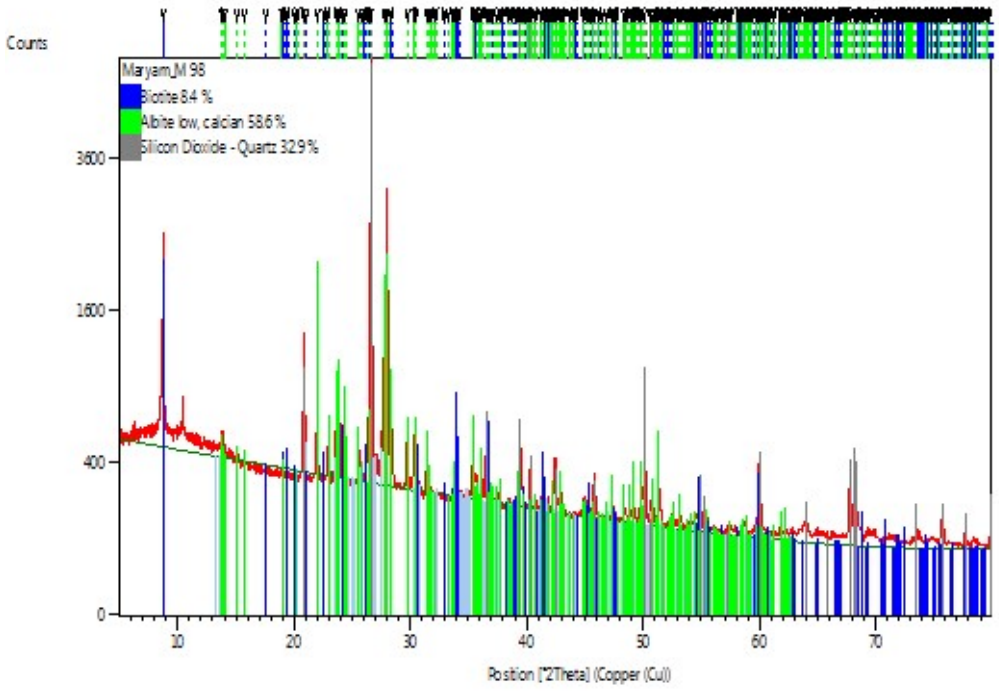

Fig.4.51 Diffractogramof Granodioritic Gneiss Depicting Predominant Quartz, Albite and Biotite Peaks *(coordinate: N07^o 34.096', E 03^o 54.168')*

Table 4.14 Modal Composition of X-Ray Diffractograms of Representative Samples of Granodioritic Gneiss in the Study Area.

Sample no.	Mineralogy (%)					
	Quartz	**Albite**	**Anorthite**	**Biotite**	**Microcline**	**Epidote**
G5	32.9	58.6	-	8.4	-	-
G8	36.7	8.0	32.9	-	9.0	13.4
Mean	53.15	33.3	32.9	8.4	9.0	13.4

4.1.3.4 Geochemistry of the Granodioritic Gneiss

4.1.3.4.1 Major Oxide

The major oxide of the granodioritic gneiss revealed the composition of silica (SiO_2) ranged from 50.37 to 71-81% with average composition of 65.65%. Al_2O_3 values ranged from 12.18 to 23.04% with average concentration of 16.31%. CaO values ranged from 1.25 to 12.60%, Fe_2O_3 values ranged from 2.66 to 14.12% and MgO values ranged from 0.50 to 6.68%. The average composition of CaO, Fe_2O_3 and MgO were 5.26, 5.52 and 1.68 respectively. Na_2O concentration ranged from 1.79 to 5.09% while K_2O ranged from 1.30 to 8.77% with respective average concentration of 3.34 and 3.55. Minor oxide elements TiO_2, MnO P_2O_5 and Cr_2O_3 yielded average concentration of 0.68, 0.08, 0.32 and 0.02 calculated from each composition values ranging from 0.25 to 1.11%, 0.04 to 0.23%, 0.11 to 0.91% and <0.002 to 0.06%. Loss on ignition varies from 0.5 to 1.0% (Table 4.15).

A plot of Na_2O/Al_2O_3 against K_2O/Al_2O_3 (Garrels and Mackenzie 1971) indicates that mixed precursor materials may be suggested for the granodioritic gneiss (Fig.4.52).

The classification diagram of (Na_2O+K_2O) against SiO_2 (Middlemost, 1994) revealed that majority of the granodioritic gneiss samples plotted in granodiorite portion, with minor in granite, gabbro and diorite portion (Fig.4.53). Triangular diagram proposed by O'Connor (1965) for the granodioritic gneiss, their calculated CIPW normative data indicate that majority of the data are tonalite - granodiorite protolith (Fig.4.54).

Triangular variation diagram (Irvine and Baragar, 1971) indicated the geotectonic setting between the tholeiitic and cal-alkaline environment of the granodioritic gneiss. Most of the data that plotted within the cal-alkaline series are relatively enriched in silica and alkali but depleted in iron oxide. The samples plotted in the tholeiitic environment show moderate silica content and enrichment in iron and magnesium oxide (Fig.4.55). Most samples that plotted in the cal-alkaline environment were peraluminous. The other samples in tholeiitic setting are metaluminous which reflects the presence of Al-poor biotite (Fig.4.56).

The R1-R2 diagram proposed by De la Roche *et al* (1980) with it field defined by Batchelor and Bowden (1985) established the geotectonic environment of the granodioritic gneiss to be pre-plate and syn-collision portion (Fig.4.57).

Table 4.15 Results of Whole-Rock Analyses of Granodioritic Gneiss Unit.

Sample No→ Major Oxide(wt%)↓	G1 *	G2	G3	G5 *	G6	G8 *	G9	G10 *	G11 *	Range	Average
SiO_2	64.09	71.60	50.37	71.81	73.35	65.90	66.80	58.10	68.80	50.37-73.35	65.65
TiO_2	0.50	0.76	1.03	0.46	0.51	1.11	0.71	0.75	0.25	0.25-1.11	0.68
Al_2O_3	21.16	12.21	12.18	17.88	13.11	14.89	13.45	23.04	18.88	12.18-23.04	16.31
Fe_2O_3	3.76	3.32	14.12	3.67	1.86	6.66	6.28	7.38	2.66	2.66-14.12	5.52
MnO	0.04	0.05	0.23	0.04	0.02	0.14	0.11	0.05	0.04	0.04-0.23	0.08
MgO	1.21	0.82	6.98	1.17	0.41	1.37	0.50	1.87	0.81	0.50-6.68	1.68
CaO	5.28	2.43	9.58	4.21	1.25	12.60	3.01	4.22	4.75	1.25-12.60	5.26
Na_2O	5.09	1.79	2.29	4.08	3.41	3.02	2.55	3.09	4.78	1.79-5.09	3.34
K_2O	1.74	5.89	1.79	2.55	3.04	1.49	5.37	8.77	1.30	1.30-8.77	3.55
P_2O_5	0.18	0.91	0.34		0.11	0.30	0.26	0.13		0.11-0.91	0.32
Cr_2O_3		0.01	0.06		0.005		<0.002			<0.002-0.06	0.02
Loi		0.6	0.7		2.7		0.5			0.5-1.0	1.13
Sum	103.06	100.39	99.67	105.85	99.78	107.5	99.54	107.39	102.27	99.54-107.5	102.83

Major oxide contents with sample symbol * were determined by X-ray fluorescence (XRF). Elements with blank space were not determined

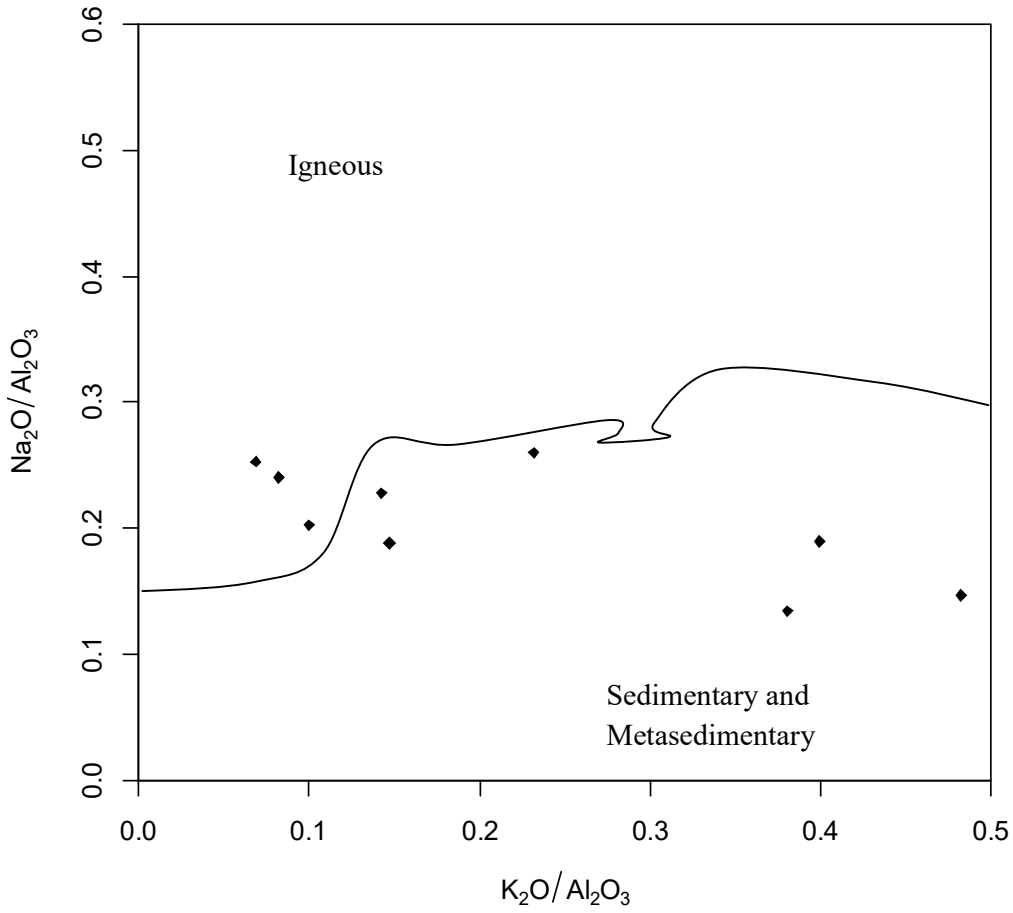

Fig.4.52 Binary Plot of Na_2O/Al_2O_3 versus K_2O/Al_2O_3 for Granodioritic Gneiss Samples. (After Garrels and Mackenzie 1971).

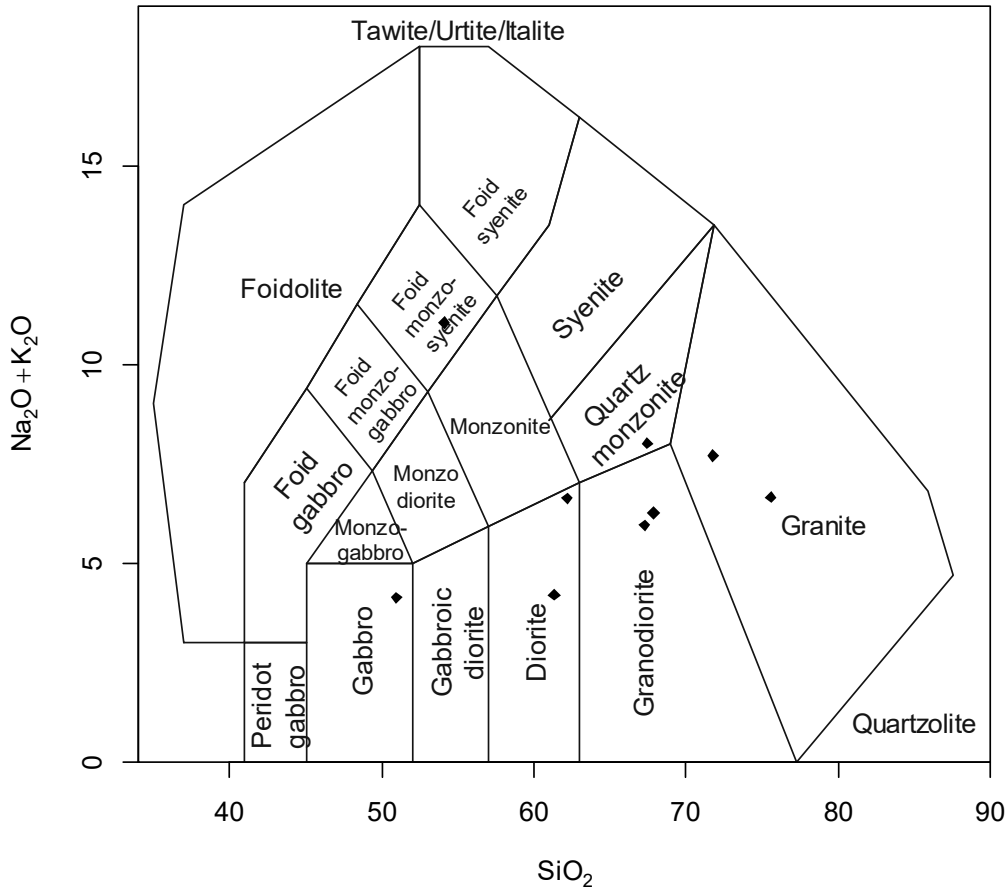

Fig.4.53 Plot of (Na_2O+K_2O) versus SiO_2 for Granodioritic Gneiss on Classification Diagram (after: Middlemost, 1994).

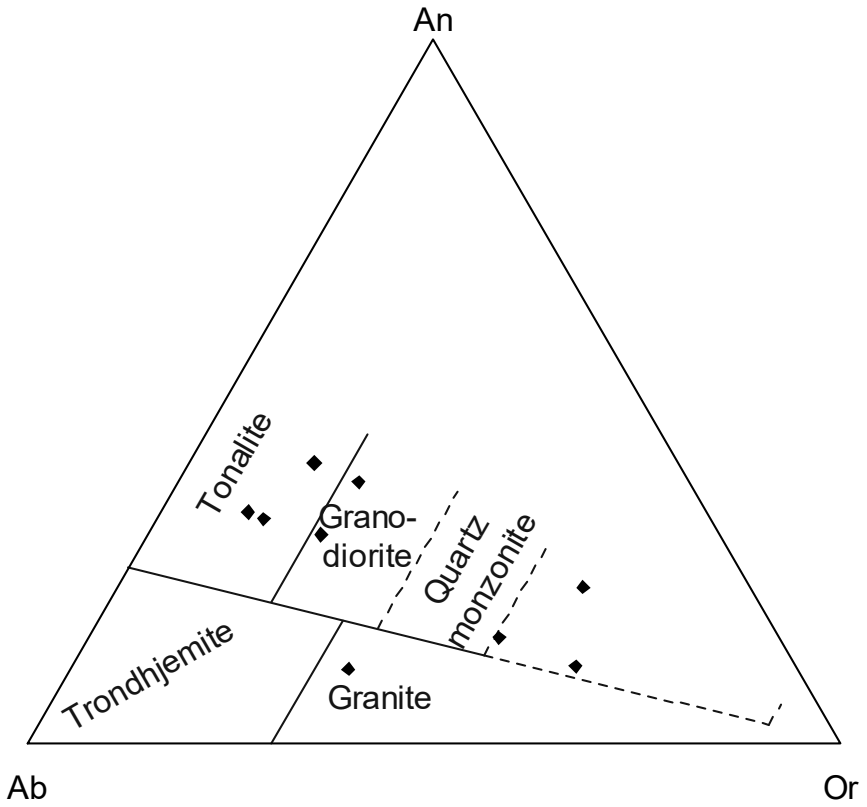

Fig.4.54 Ternary Diagram Based on Combination of Ab (Albite), An (Anothite) and Or (Orthoclase feldspar) for Granodioritic Gneiss. CIPW normative data as proposed by O'Connor (1965).

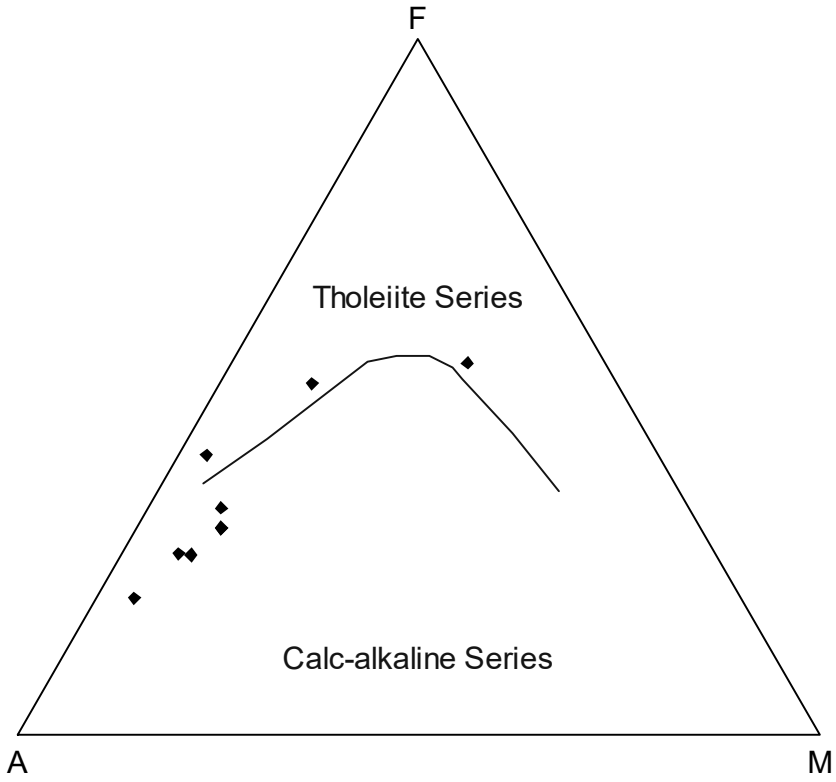

Fig.4.55 Plot of A.F.M. Ternary Diagram for Granodioritic Gneiss (After Irvine and Baragar, 1971). The A, F, and M are defined as follows:

A = (K_2O + Na_2O) wt %

F = FeO total wt %

M = MgO wt %

A+F+M = 100%

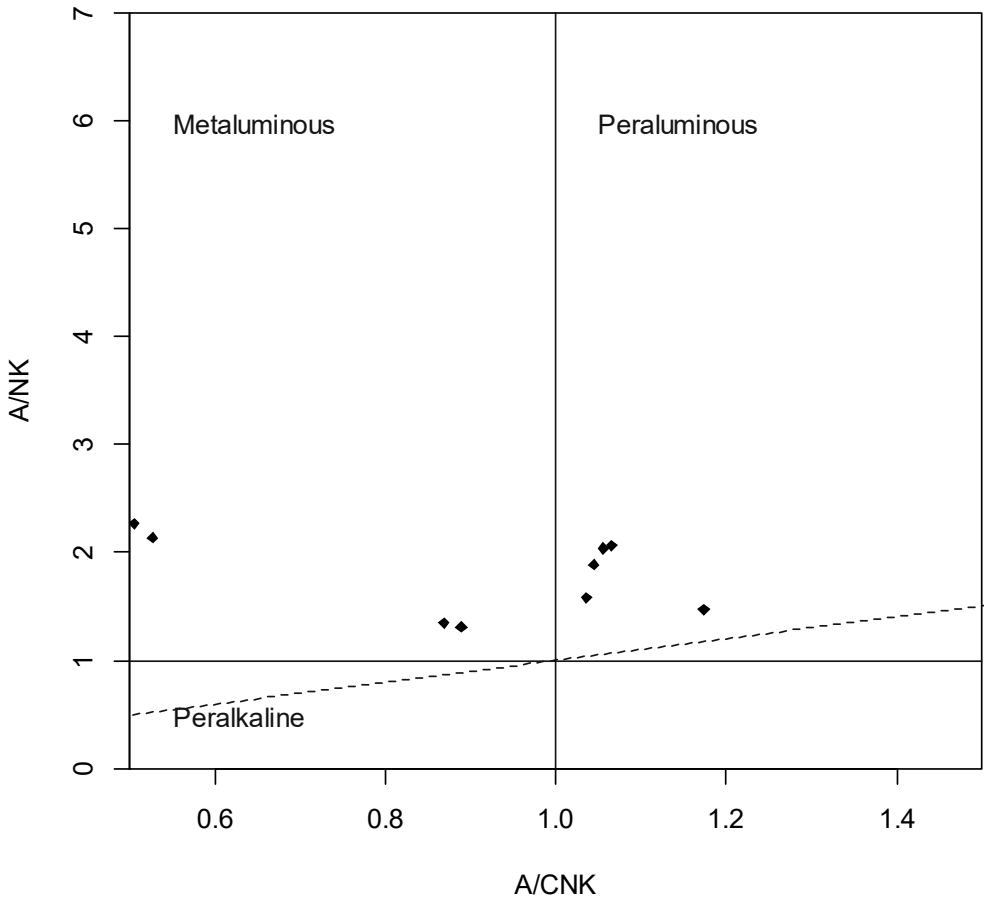

Fig.4.56 A/NK versus A/CNK plot of Shand (1943) Discriminating Metaluminous, Peraluminous and Peralkaline Composition for the Granodioritic Gneiss.

A/CNK = $Al_2O_3/(CaO+Na_2O+K_2O)$ (mol.%)

A/NK = $Al_2O_3/(Na_2O+K_2O)$ (mol.%)

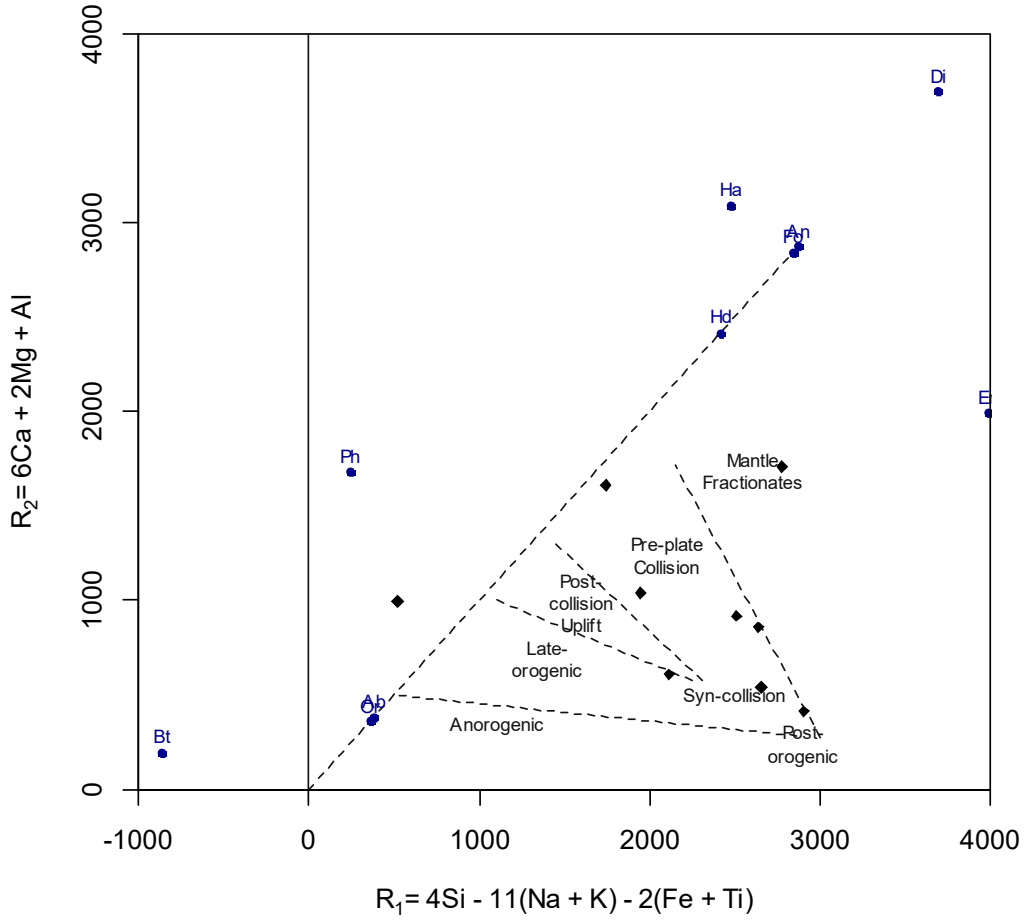

Fig.4.57 Plot of R1-R2 Diagram for Granodioritic Gneiss (After De La Roche *et al*. 1980, with field defined Batchelor and Bowden 1985).

4.1.3.4.2 Trace Elements

The wide range of variationin some of Large Ion Lithophile Elements (LILE) (Ba, 354.2 to 1644 ppm; Rb, 16.6 to 320.9 ppm and Sr, 131.7 to 665.9 ppm) and Zirconium (Zr) composition of the granodioritic gneiss strongly suggest mixed protoliths input as exemplified by the major oxide discrimination diagram (Table 4.16).

The plot of Nb against Y for the granodioritic gneiss (Fig.4.58) indicates that all the samples fell in the syn-collision and within-plate granite portion. The plot confirmed the major oxide binary plot of R1-R2 (Fig.4.57).

Figure 4.61 show separate spider diagrams for cal-alkaline peraluminous and tholeiitic metaluminous samples for the granodioritic gneiss after Thompson, (1982). Higher concentrations of trace elements like Ba, Rb, Th and K occur in the cal-alkaline peraluminuos samples with compare to the tholeiitic metaluminuos samples while Zr content is higher in the tholeiitic metaluminuos samples of the granodioritic gneiss.

Table 4.16 Results of Trace Elements Analyses of Granodioritic Gneiss Unit.

Sample No→ Trace Element (ppm) ↓	G1 *	G2	G3	G5 *	G6	G8 *	G9	G10 *	G11 *	Range	Average
Ba	930.3	1644.0	686.0	687.9	673.0	354.2	1623.0	1635.0		354.2-1644.0	1026.2
Sc		8.0	29.0		3.0	0.7	16.0	11.0		0.7-29.0	11.3
Ga	21.5				17.7	16.5		31.1	18.1	16.5-31.1	21.0
Nb		36.0	7.0		12.4		35.0			7.0-36.0	22.6
Rb	32.3			67.0	105.5	26.2		320.9	16.6	16.6-320.9	94.8
Sn	46.7				3.0			58.5	40.3	40.3-58.5	37.1
Sr	665.9	248.0	138.0	318.3	594.0	270.9	296.0	131.7	609.9	131.7-665.9	363.6
V	27.1			23.9	30.0	71.9		47.9	23.8	23.8-71.9	37.4
Zr	140.9	562.0	175.0	113.9	297.7	214.6	1332.0	307.0	114.1	114.1-1332.0	361.9
Y		77.0	28.0	7.4	6.6	27.3	81.0	19.5		6.6-81.0	35.3
Zn	50.1			46.2	75.0	71.1		122.3	34.4	34.4-122.3	66.5
Cu					17.9	-0.6				-0.6-17.9	8.60
Pb					20.8	8.2		43.3		8.2-43.3	24.10
Ni		<20	137		11	6.1	<20			<20.0-137.0	51.4
As					0.6	1.5				0.6-1.5	1.1
Sb					0.3	0.9				0.3-0.9	0.6
Au					2.7	9.9				2.7-9.9	6.3

Trace element contents with sample symbol * are determined by X-ray fluorescence (XRF). Elements with blank space were not determined.

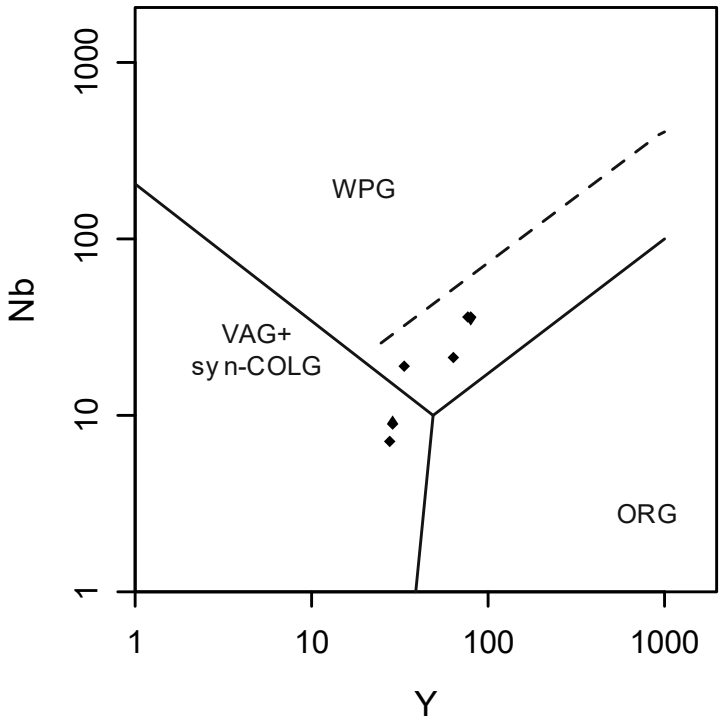

Fig.4.58 Discriminate Diagram of Nb versus Y for the Granodioritic Gneiss samples (After Pearce *et. al*. 1984).

Syn-COLG: syn-collision granites, WPG: within-plate granites, VAG: volcanic-arc granites, ORG: ocean-ridge granites

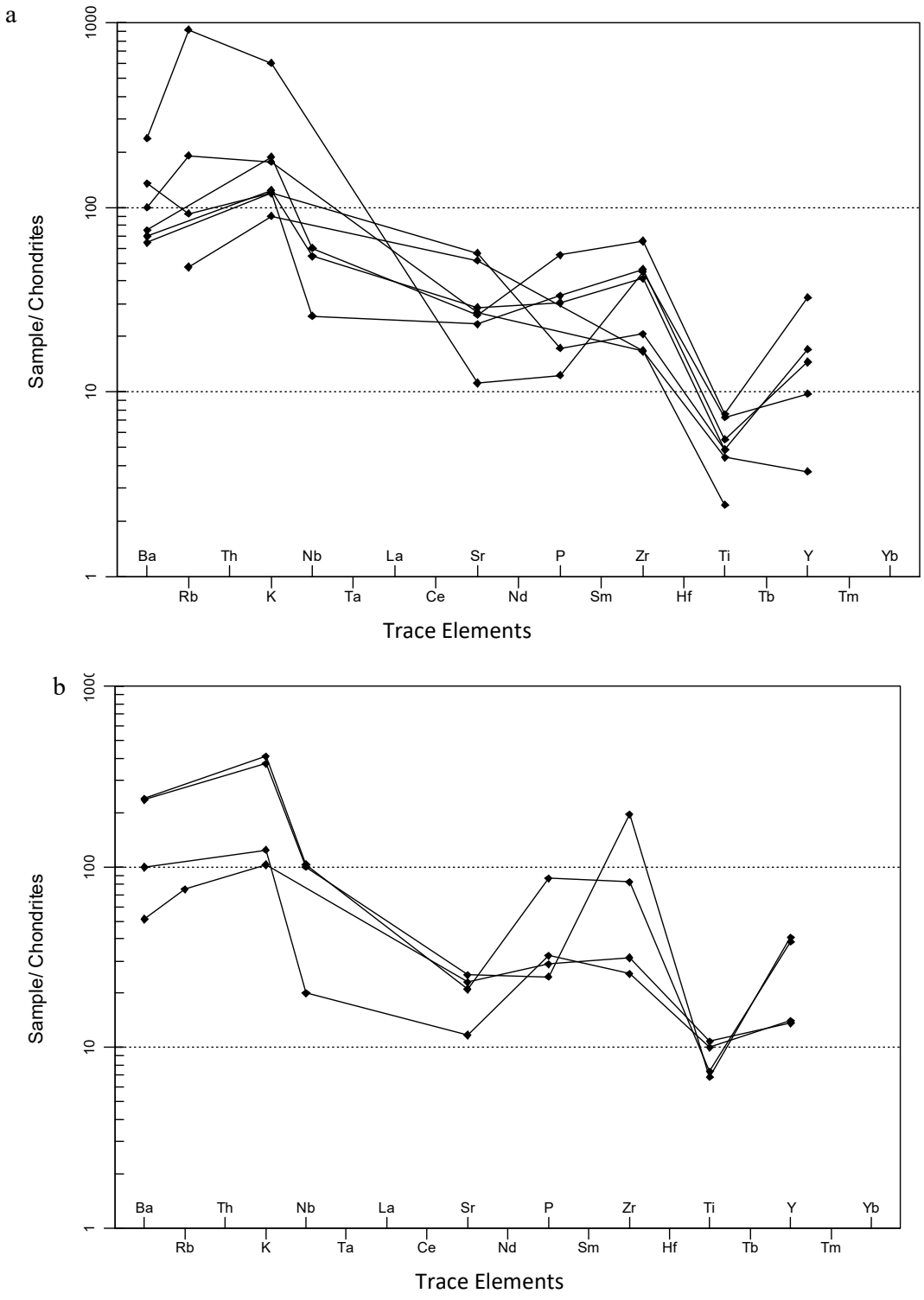

Fig4.59 Spider Diagrams for Selected Trace Elements for the Granodioritic Gneiss (a) Cal-alkaline Peraluminuos Samples (b) Tholeiitic Metaluminous Samples (After Thompson, 1982).

4.1.3.4.3 Rare Earth Elements

Rare Earth Element (REE) concentration of the granodioritic gneiss revealed enriched light rare earth elements (LREE) concentrations but showed relatively depleted heavy rare earth elements (HREE) (Table.4.17).

Chondrite normalised plots of Nakamura, (1974) revealed slightly negative Eu anomaly (Eu/Eu*:0.73) and LREE enrichment (Fig.4.60).

Table 4.17 Results of Rare Earth Element Analyses of Granodioritic Gneiss Unit.

Sample No → **REE Element (ppm) ↓**	G6
La	30.2
Ce	55.1
Pr	5.72
Nd	21
Sm	3.06
Eu	0.61
Gd	2.11
Tb	0.26
Dy	1.34
Ho	0.23
Er	0.67
Tm	0.1
Yb	0.69
Lu	0.12
Eu/Eu*	0.73
La_N/Yb_N	29.5
La_N/Sm_N	6.2

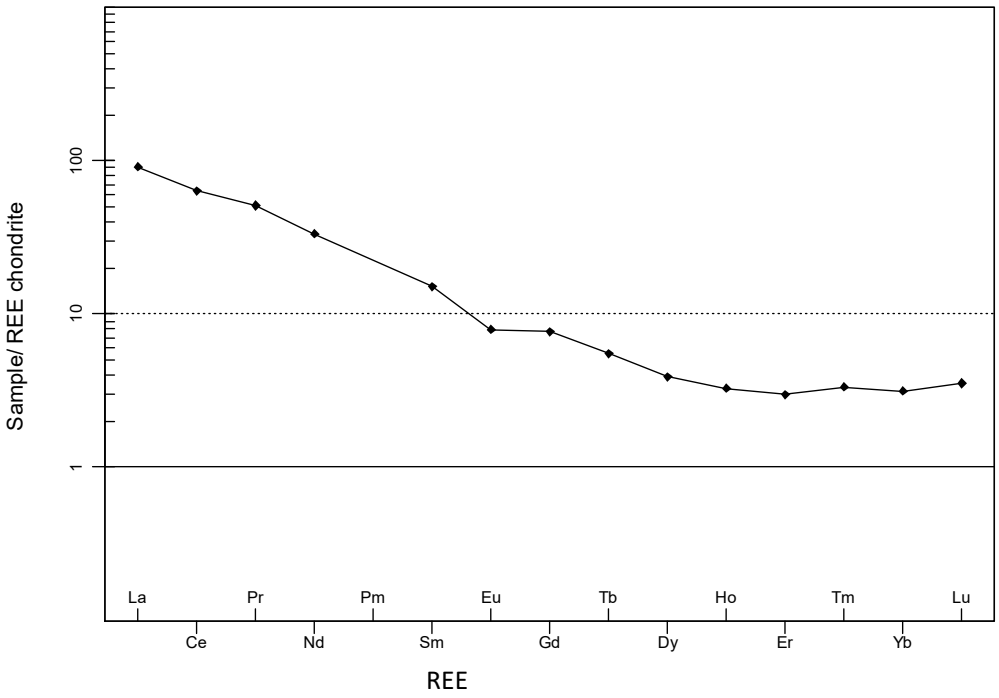

Fig.4.60 Chondrite Normalized Plot of Rare Earth Elements (REE) in the Granodioritic Gneiss (after; Nakamura, 1974).

4.1.3.5 Biotite Granite Gneiss

The biotite granite gneiss (bGG) underlies the north-western to the south-western part of the study area inter-banded with the biotite-hornblende gneiss. It outcrops as good exposures forming batholithic and elongated moderately hilly bodies trending N-S with moderately dipping gneissosity (Fig. 4.61a and 4.62). Biotite granite gneiss is of medium to coarse grained in size and moderately to weakly foliated (Fig.4.61b).

The gneiss is characterized by migmatitic and tectonized features. The medium to coarse grained quartzo-feldspartic felsic band stripes along banding forming compositional layering. Towards the northern part, the felsic bands were gradually transformed into lenses, augens and streaks aligned within medium grained mafic portion forming porphyroblasts (Fig. 4.63 and 4.64). It was observed that moderately hilly exposures of garnetiferous gneiss were found in closed association with the biotite granite gneiss at the same location in just two places (Fig.4.65). Generally, the biotite granite gneisses were intruded by numerous quartzo-feldspartic and pegmatite veins of varying thickness and which sometimes form micro-folds. The intrusions are mostly concordant to the regional foliation.

(a)

(b)

Fig.4.61 (a) Over-View of an Elongated Biotite Granite Gneiss Along Idiroko-Imini Road. (b) Hand Specimen *(coordinate: N07^{o} 40.349', E 03^{o} 48.154')*

Fig 4.62a Overview of Biotite Granite Gneiss Outcrop at Adubiare, in Ilora Village. ***(coordinate: N07^{o} 42.438' , E 03^{o} 50.520')***

Fig.4.62b Overview of Low-lying Biotite Granite Gneiss Outcrop at Adubiare, in Ilora village. ***(coordinate: N07^{o} 42.522' , E 03^{o} 50.556')***

Fig 4.63 Coarse Grained Sample of Biotite Granite Gneiss at Adejumo Village, off Iseyin-Ibadan Road. ***(co-ordinate: N07^{o} 42.282', E 03^{o} 47.004')(Exposure contain augen feldspars outcropping at the north-western corner of the study area).***

Fig 4.64 Coarse Grained Sample of Biotite Granite Gneiss Along Ijaye- Iseyin Road. ***(co-ordinate: N07^{o} 43.541', E 03^{o} 46.330') (Exposure contains small phenocrysts feldspars outcropping at the north-western corner of the study area).***

Fig. 4.65 Coarse Grained Sample of Garnetiferous Gneiss Associated with the Biotite Granite Gneiss at Ori-Oke MuyideenKasali Church. ***(coordinate: N07^{o} 38.179', E 03^{o} 48.508').***

Significant amount of quartz (20-35%), plagioclase feldspar (oligoclase: 5-28%), biotite (5-30%), hornblende (5-15%), microcline (5-30%), orthoclase-feldspar (5-22%), muscovite (2-8%) and opaque mineral (1-5%) are present in the rock (Table 4.18). Garnet, epidote and zircon occur as accessory minerals in some the biotite granite gneiss, while chlorite is occasionally present as secondary alteration product.

The thin sections of the biotite granite gneisses in the study area are in-equant, medium to coarse grained and exhibit moderate foliations.

The biotite occurs as lath-like and euhedral to subhedral in shape. The thin sheet of the biotite appeared strained and deformed as it breaks into flakes and bends (Fig. 4.66 and 4.69). Biotite shows pleochroism from light brown to dark brown and sometimes altered to olive green chlorite. Biotite occurs as sheared structure warped around the augen of orthoclase-feldspars (Fig.4.67).

Suhedral green hornblende grains are sometimes associated with biotite which both made up the mafic portion in the gneiss, while prismatic hornblende displayed pleochroism from dark green to light brown.

The plagioclase feldspars occur as subhedral to anhedral large and medium grained displaying polysynthetic and simple twinning. Antiperthitic plagioclase occasionally occur (Fig.4.73) in the biotite granite gneiss

Microcline and orthoclase-feldspars mostly occur as porphyroblasts forming augen in the gneiss (Fig. 4.67). K-feldspars were the conspicuous feldspars in the biotite granite gneiss. Inclusions of quartz were observed in microcline (Fig.4.68). Perthite exsolution intergrowth texture on microcline mineral was present (Fig.4.72). Fig.4.74 show large grain of orthoclase feldspars with simple or albite twin in the matrix of quartz and microcline.

Subhedral to anhedral quartz grains is ubiquitous and display undulatory extinction. The quartz grains are recrystallised as slightly elongated grains aligned parallel to the foliations of the rock (Fig. 4.70). It also developed sub-grains indicating that the gneiss had been moderately strained.

Euhedral poikiloblastic garnet minerals with quartz inclusion were observed in some of the biotite granite gneiss (Fig. 4.66) as well as in the garnetiferous gneiss associated with the biotite granite gneiss outcrop (Fig.4.73). Epidote mineral grain was present as accessory minerals.

X-Ray Diffractograms of the biotite granite gneiss (Fig.4.75) revealed conspicuous peaks of quartz (29.5%) and albite low, calcian feldspars (59.2%) with subordinate biotite (6.9%), and actinolite (4.4%).

Table 4.18 Modal Composition of Minerals in Biotite Granite Gneiss (bGG) in the Study Area

Sample No → / **Mineral ↓**	b1	b2	b3	b4	b5	b6	b7	b8	b9	b10	b11	b12*	b13*	b14*	Range
Quartz	30	30	30	30	35	20	30	35	40	30	33	30	30	30	20-35
Plagioclase	15	25	10	12	10	10	25	15	18	10	5	10	25	28	5-28
Microcline	5	-	30	15	6	5	-	25	5	25	20	15	-	5	5-30
Muscovite	-	3	-	2	5	3	2	-	-	-	-	-	-	-	2-8
Biotite	24	25	5	10	10	30	10	5	12	5	9	20	25	15	5-30
Orthoclase	8	5	5	10	15	5	10	10	15	20	22	15	10	5	5-22
Hornblende	10	5	15	15	8	11	15	-	-	-	-	5	-	12	5-15
Opaque	3	1	3	2	3	2	1	2	5	2	3	2	5	2	1-5
Garnet	-	-	-	5	8	-	-	-	-	-	-	-	-	-	5-8
Sphene	-	-	2	-	-	-	2	-	-	-	-	-	-	-	-
Epidote	-	-	-	-	-	4	-	-	-	-	-	-	-	-	-

a

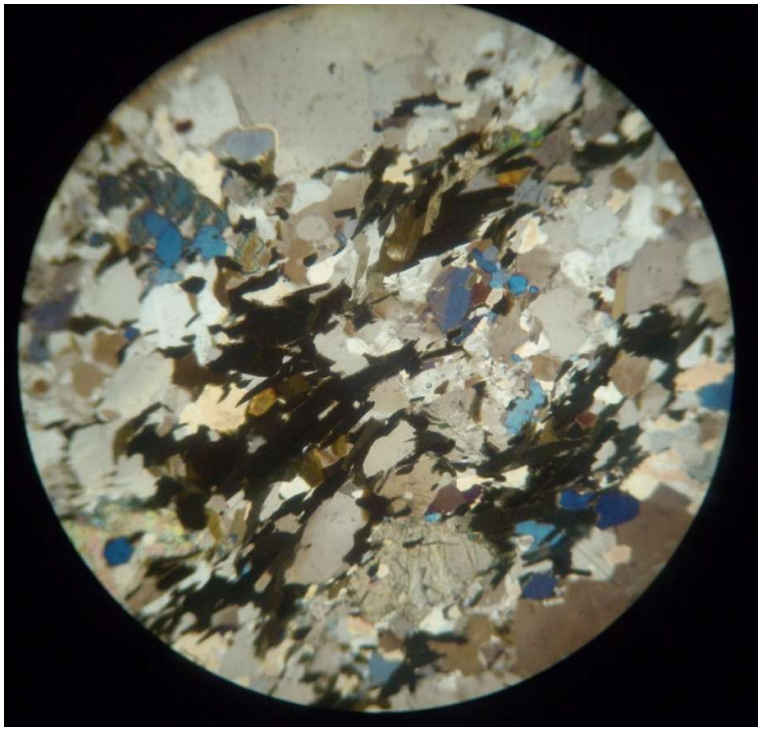

b

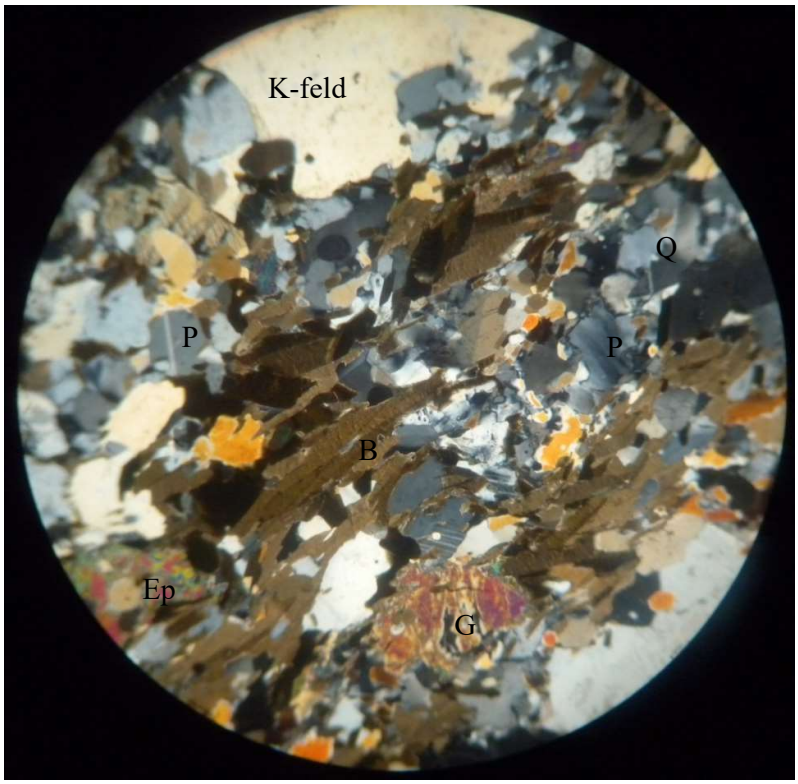

Fig 4.66 Typical Photomicrograph of Biotite Granite Gneiss in Transmitted Light
(a) plane polarised (b) cross polarised light (x40):showing foliation defined by the bending of aligned biotite grains (B), sub-grains of quartz (Q), k-feldspars(K-Feld), plagioclase(P), Epidote(Ep) and garnet(G),(coordinate: N07^{o} 37.619', E 03^{o} 47.270')

a

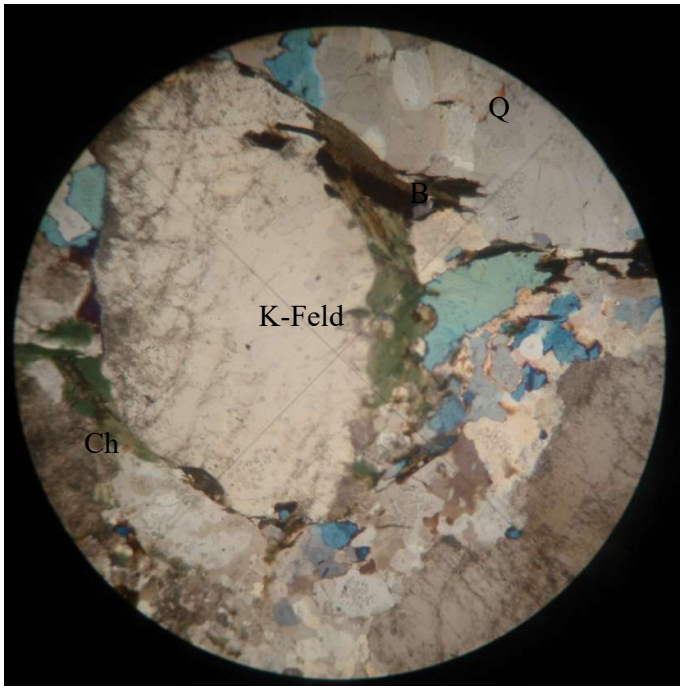

b

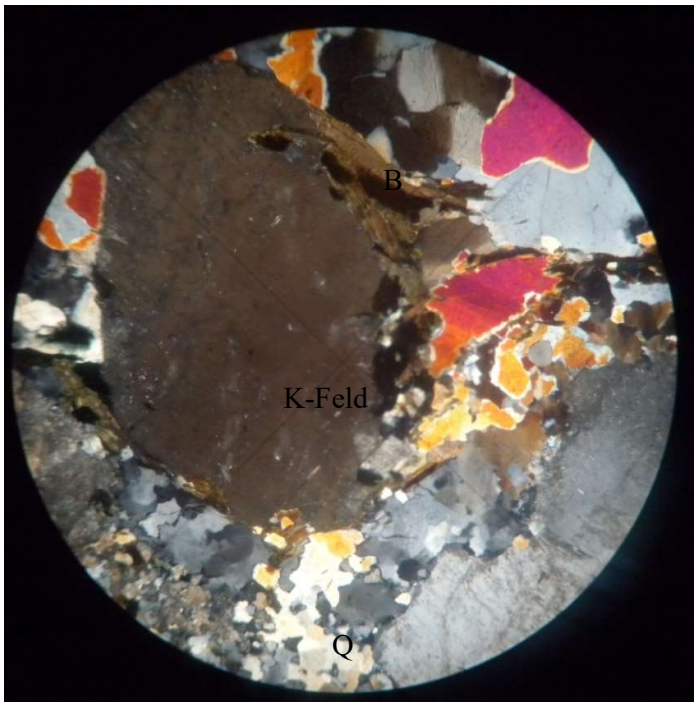

Fig.4.67 Typical Photomicrograph of Biotite Granite Gneiss in Transmitted Light ***(a)*** *plane polarised (b) cross polarised light (x40):showing the orthoclase-feldspars porphyroblast (K-Feld) forming augen eye with a rim of brown biotite lath(B) (coordinate: N07^{o} 42.282', E 03^{o} 47.004')*

a

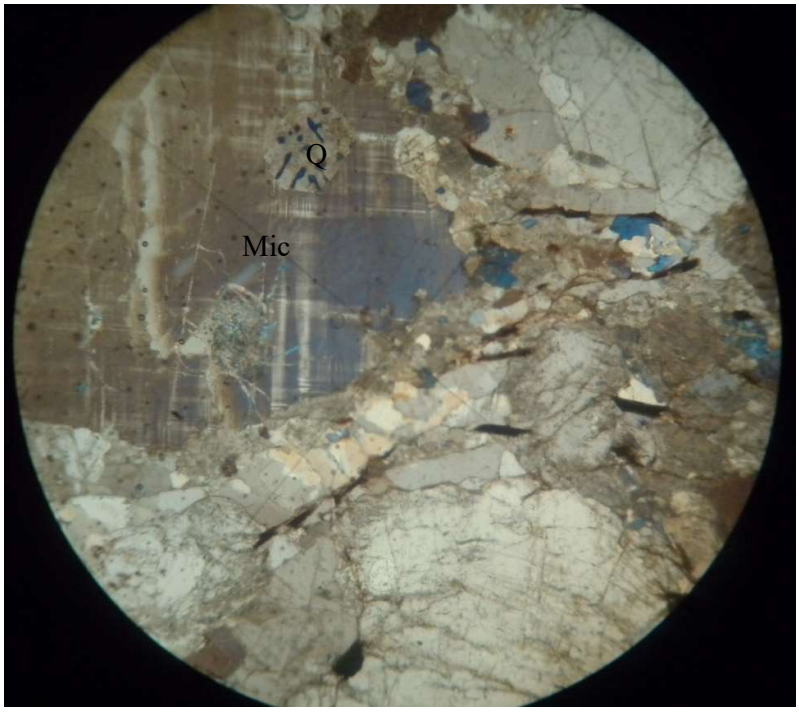

b

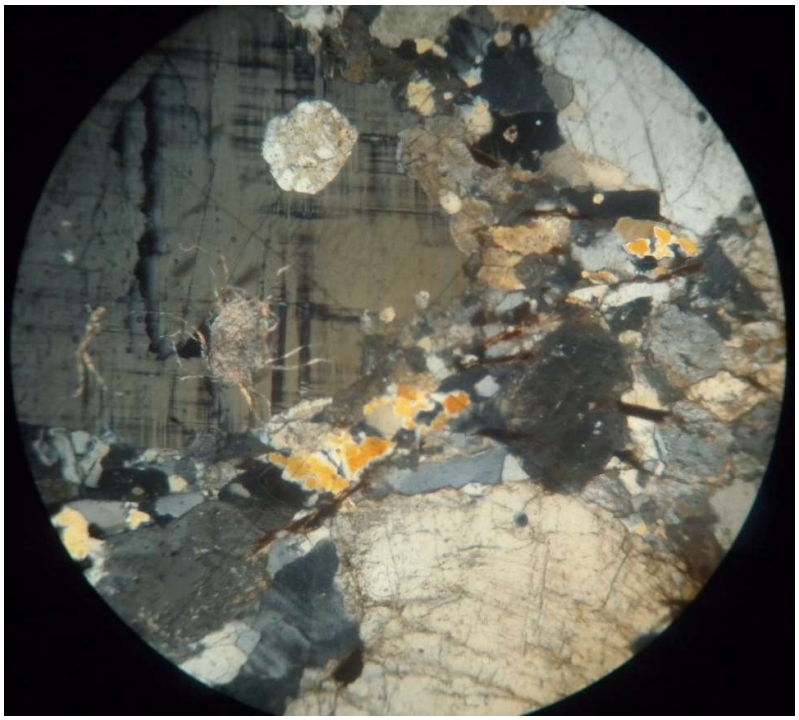

Fig.4.68 Typical Photomicrograph of Biotite Granite Gneiss in Transmitted Light ***(a)*** *plane polarised (b) cross polarised light (x40): showing the microcline porphyroblast (Mic) with inclusion of quartz(Q) (coordinate: N07^{o} 42.421', E 03^{o} 45.802')*

a

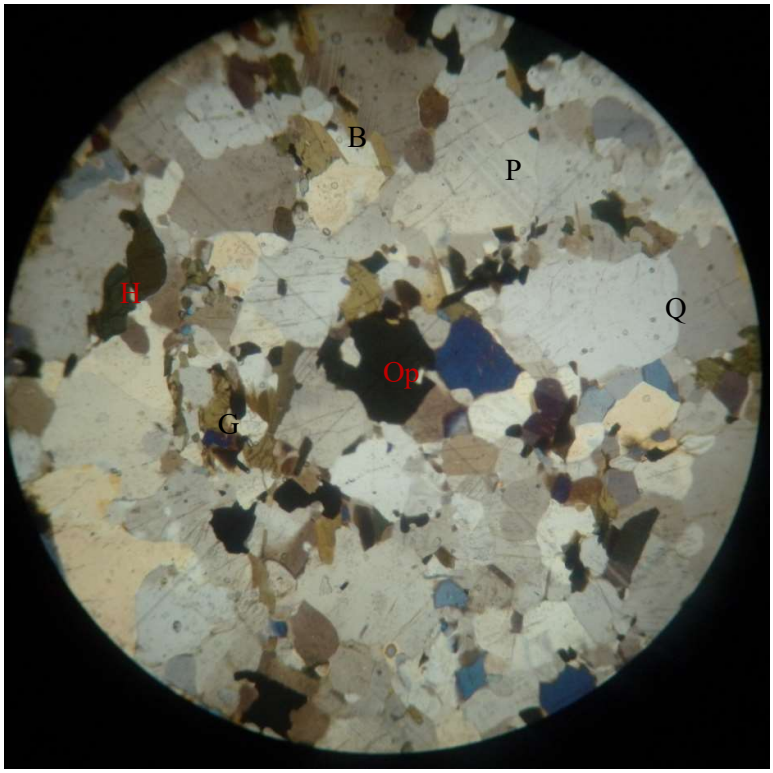

b

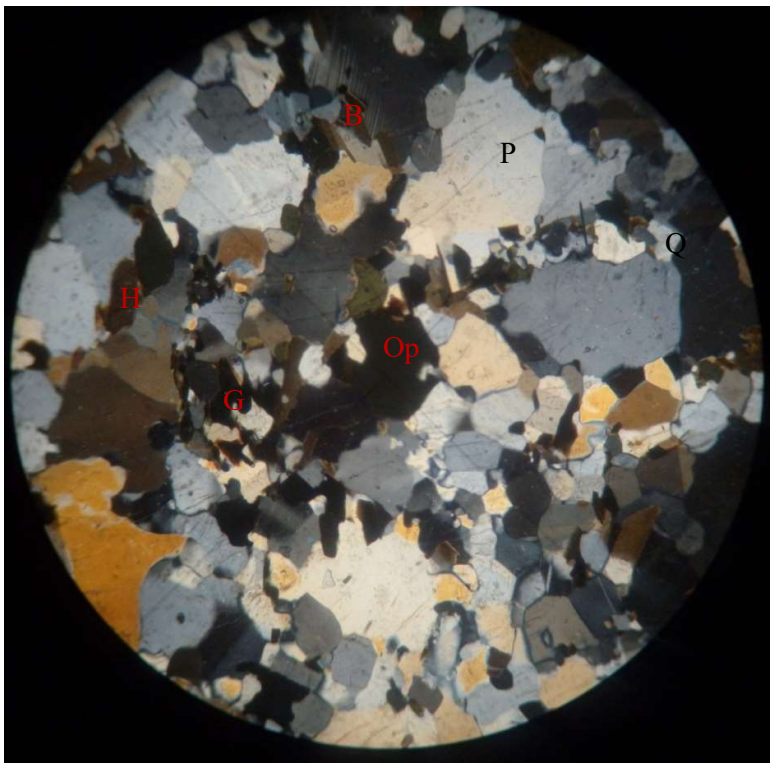

Fig 4.69 Typical Photomicrograph Coarse Biotite Granite Gneiss in Transmitted Light *(a) plane polarised (b) cross polarised light (x40): showing coarse grains of plagioclase feldspar(P), subhedral quartz(Q) and opaque mineral (Op) in the tiny flakes of biotite(B),hornblende (H) and garnet (G). (Coordinate: N07^o 42.553', E 03^o 49.980')*

a

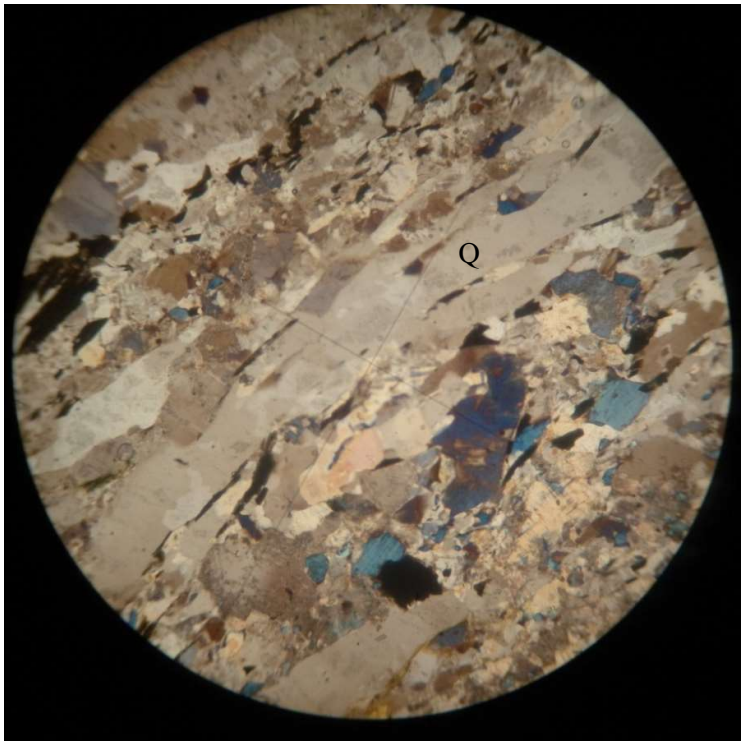

b

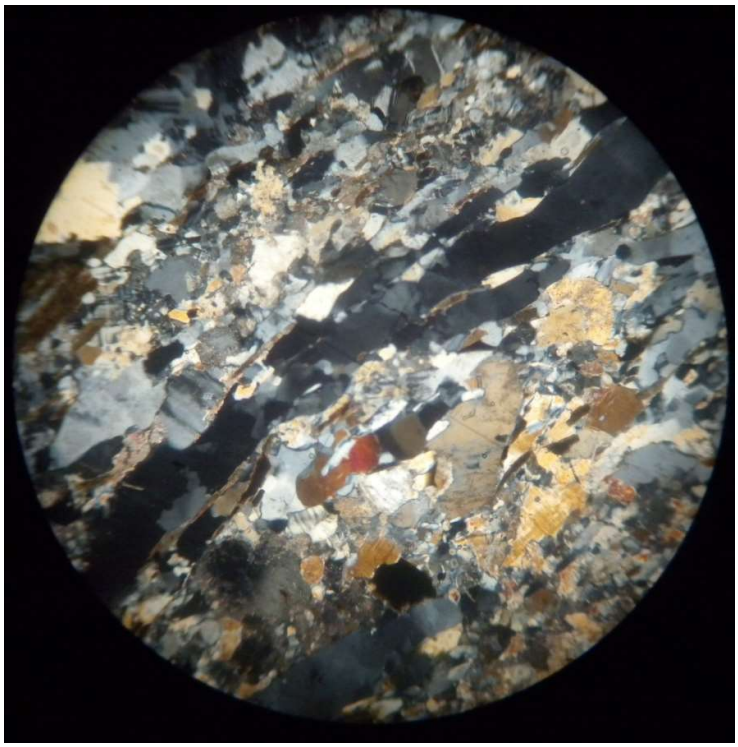

Fig.4.70 Typical Photomicrograph of Biotite Granite Gneiss in Transmitted Light ***(a)*** *plane polarised (b) cross polarised light (x40): showing aligned elongated quartz grains (Q) with undulose extinctions forming the foliation. (coordinate: N07^{o} 40.349', E 03^{o} 48.154')*

a

b

Fig.4.71 Typical Photomicrograph of Biotite Granite Gneiss in Transmitted Light ***(a)*** *plane polarised (b) cross polarised light (x40): displaying euhedral garnet porphyroblast (Gar) with quartz inclusions. (coordinate: N07^{o} 38.179', E 03^{o} 48.508')*

a

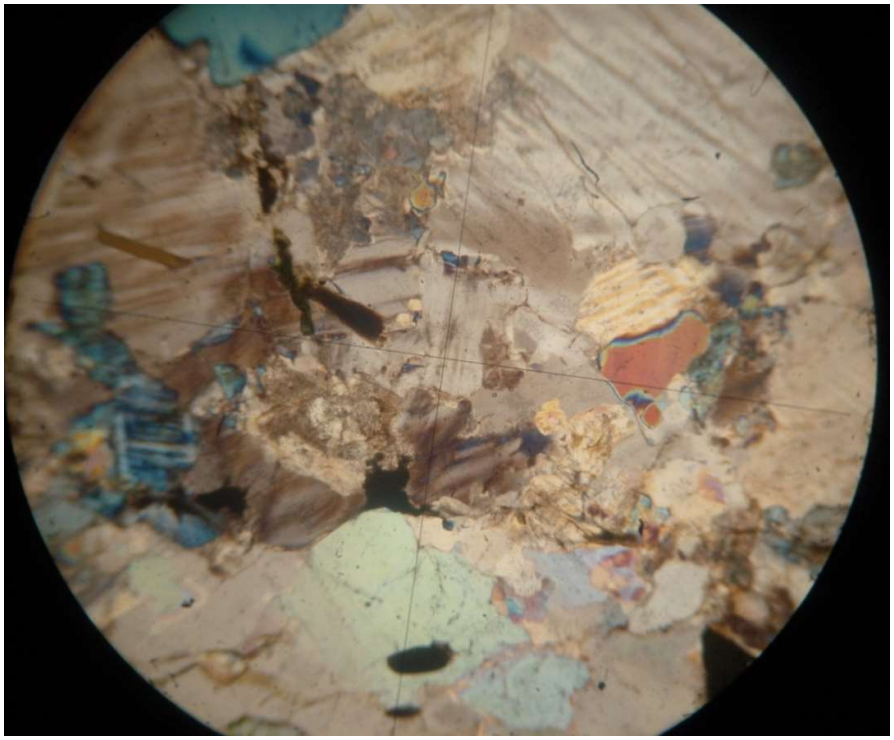

b

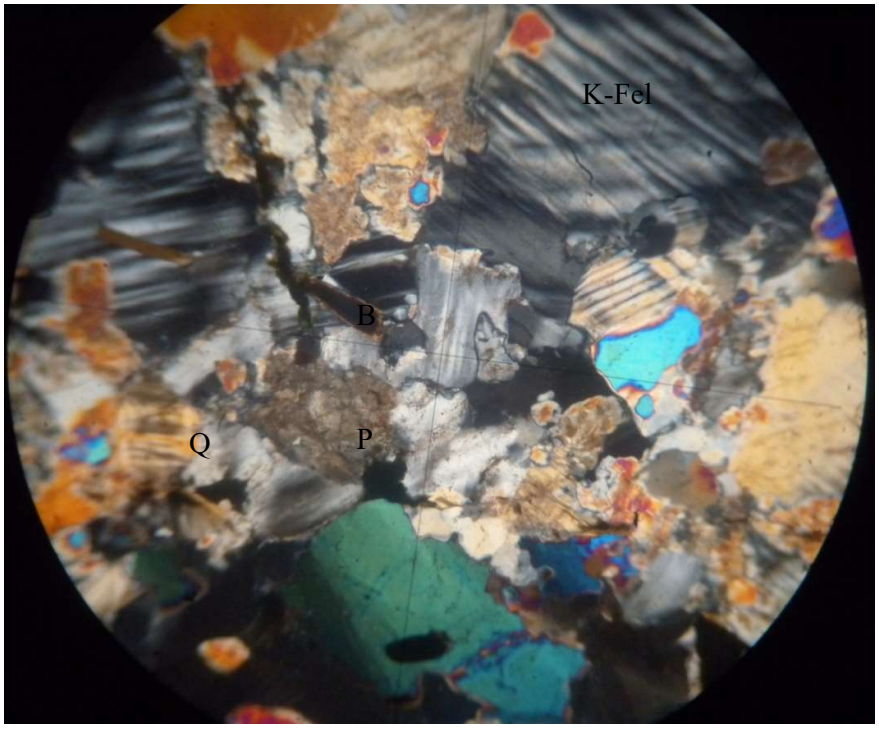

Fig.4.72 Typical Photomicrograph of Biotite Granite Gneiss in Transmitted Light *(a)* *plane polarised (b) cross polarised light (x40): showing perthitic orthoclase-feldspar(K-Feld), biotite(B), and quartz(Q) grains, sericite plagioclase feldspar(P). (coordinate: N07^o 44.351', E 03^o 59.077')*

a

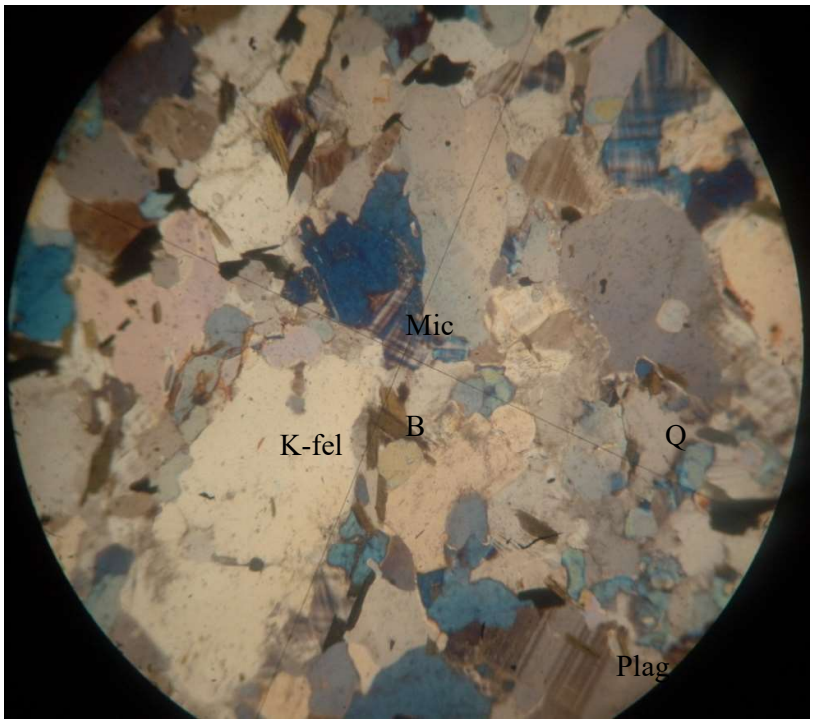

b

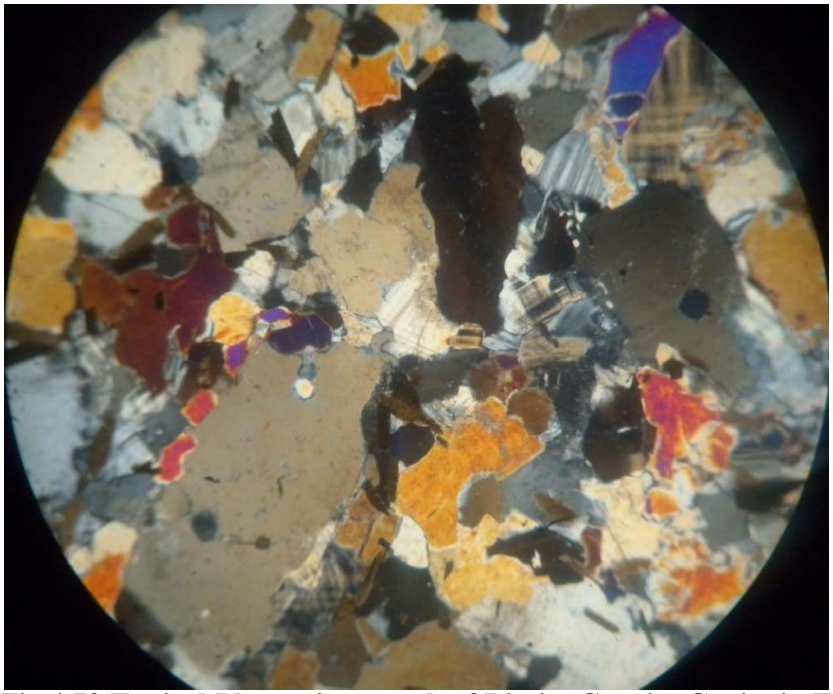

Fig.4.73 Typical Photomicrograph of Biotite Granite Gneiss in Transmitted Light ***(a)*** *plane polarised (b) cross polarised light (x40): displaying coarse grains of plagioclase(P) showing polysynthetic twinning and k-feldspars(K-fel) in the matrix of quartz(Q), biotite(B) and microcline grains (Mic). (coordinate: N07^{o} 39.142', E 03^{o} 55.468')*

a

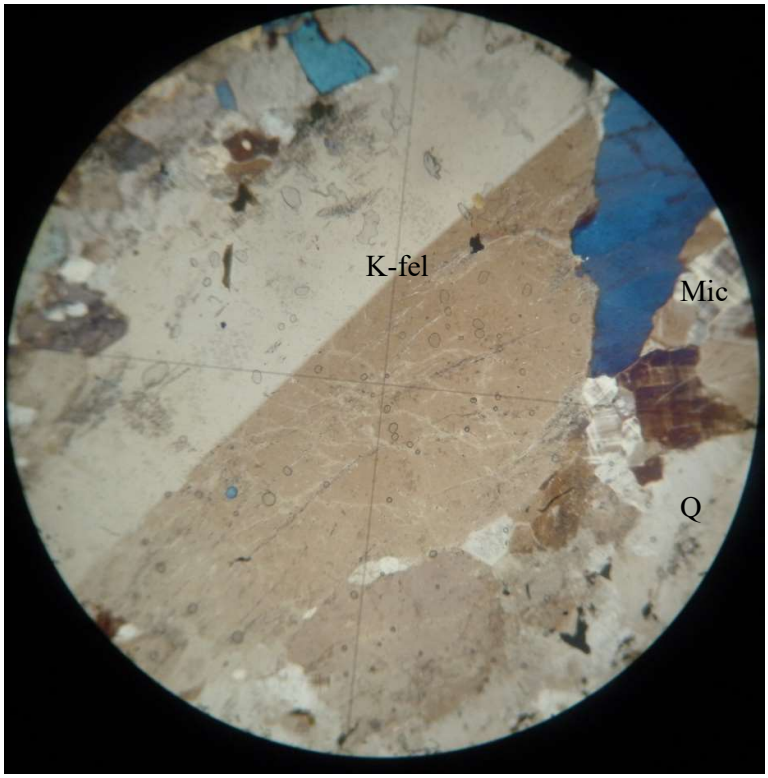

b

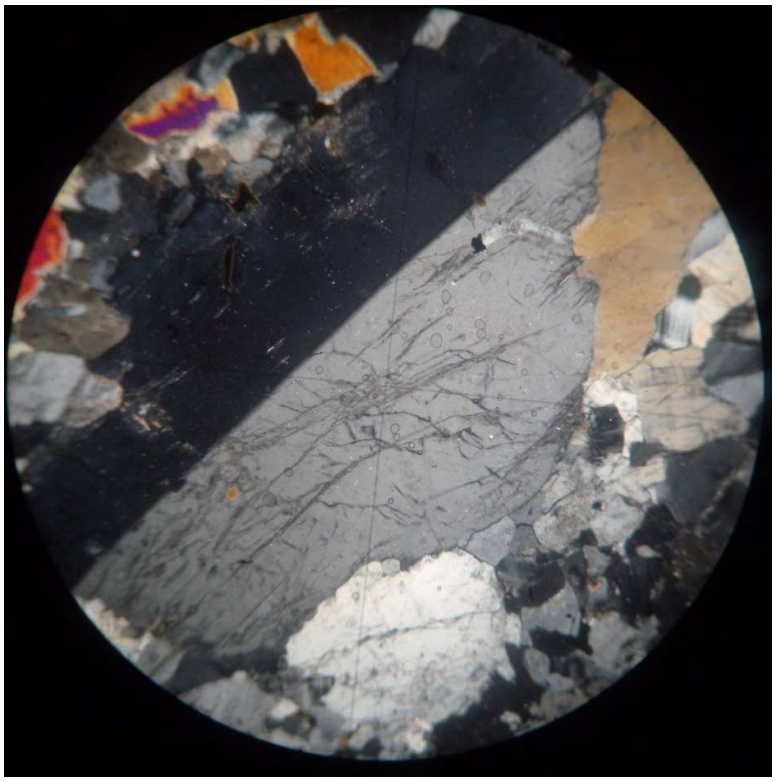

Fig.4.74 Typical Photomicrograph of Coarse Biotite Granite Gneiss in Transmitted Light *(a) plane polarised (b) cross polarised light (x40): displaying large grain of orthoclase k-feldspars showing a simple twinning, subhedral quartz(Q) and microcline (Mic)(Coordinate: N07^{o} 42.522', E 03^{o} 50.556')*

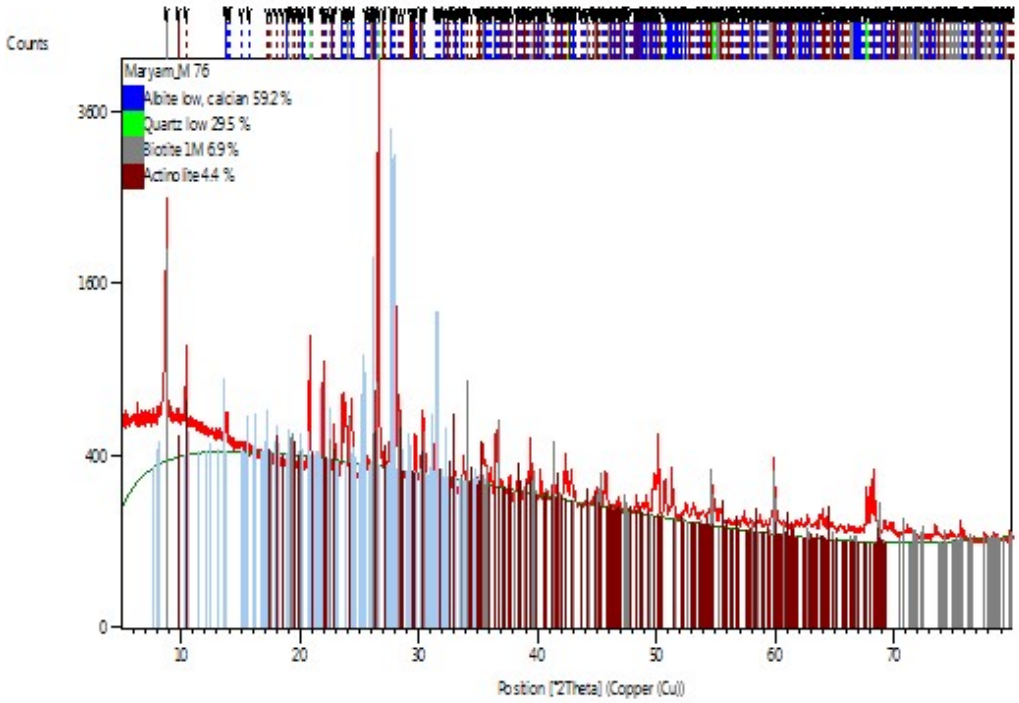

Fig.4.75 Diffractogram of Biotite Granite Gneiss Sample Depicting Predominant Quartz, Albite and Biotite and Actinolite Peaks *(coordinate: N07^{o} 42.553', E 03^{o} 49.980')*

4.1.3.6 Geochemistry of the Biotite Granite Gneiss

4.1.3.6.1 Major Oxides

The composition of major oxides for the biotite granite gneiss varies between broad limit. The concentration of silica (SiO_2), Alumina (Al_2O_3) and Ferric oxide (Fe_2O_3) ranged from 62.47 to 75.92%; 12.67 to 19.03% and 1.21 to 5.68% respectively. Lime (CaO), Soda (Na_2O) and potash (K_2O) values ranged from 1.24 to 5.31%; 2.88 to 4.76% and 1.40 to 6.05% respectively. Magnesia (MgO) values ranged 0.25 to 1.47%. The concentration oxides of minor elements, TiO_2, MnO, $P_2O_5$and Cr_2O_3 ranged from 0.14 to 0.71%; 0.02 to 0.06%; 0.09 to 0.14% and <0.002 to 0.004% respectively. Loialso varies from 1.70 to 2.60% (Table 4.19).

Discriminate diagram of Na_2O/Al_2O_3 versus K_2O/Al_2O_3 of Garrels and Mackenzie (1971) was plotted to predict between igneous and sedimentary protolith of the biotite granite gneiss. All the biotite granite gneiss fell within the field of igneous origin (Fig.4.76).

Using the plot of Na_2O+K_2O versus SiO_2 diagram (Fig.4.77) of Middlemost (1994) and R1-R2 diagram (Fig.4.78) of De la Roche *et. al.* (1980), the biotite granite gneiss samples plotted mainly in the granite field and minor in the granodiorite field.

The plot of Na_2O versus K_2O (Klemenn and Twist, 1989) gneiss indicated I-type granite character (Fig4.79). Majority of the biotite granite gneiss were also mildly paraluminous according to the Aluminium Saturated Index (ASI) ie $Al_2O_3/(CaO+K_2O+Na_2O)>1$ diagram plotted for the samples (Fig.4.80). A/CNK against SiO_2 diagram of Chappel and White (1974) was further used to confirm I-type granite and mildly paraluminous nature of the biotite granite gneiss (Fig.4.81). Discrimination diagram of R1 against R2 for granite (Batchelor and Bowden, 1985) indicated that majority of the biotite granite gneiss occupy the syn-collision to pre plate collision granite field (Fig.4.82).

Low ratio values of CaO/Na_2O and $CaO/(Na_2O+K_2O)$ (Table 4.20) implicated calcic plagioclase depletion in the mineralogy of the biotite granite gneiss. The whole rock unit showed high ratio values of K_2O/Na_2O and differentiation indices (DI) inferring to predominance abundant of the total alkali feldspars.

Average SiO_2 value compare well with those from Arigidi area (Odunyemi *et.al*. 2011) while average values of CaO, TiO_2 and MgO compared favourable with the granitic gneiss in Jos Plateau (Wright, 1971). Major oxide concentration for the granitic gneisses in Abeokuta area (Elueze e*t.al*. 2004) agreed well (Table 4.21) with average composition of Al_2O_3 and K_2O for the study.

Table 4.19 Results of Whole-Rock Major Oxide Analyses of Biotite Granite Gneiss Unit.

Sample No→ Major Oxide(wt%)↓	b1	b2	b3	b4	b5	b6	b7	b8	b9	b10	b11
SiO_2	69.8	70.17	69.65	69.47	70.23	69.93	74.05	69.59	69.85	70.01	69.75
TiO_2	0.25	0.26	0.26	0.30	0.30	0.24	0.49	0.23	0.26	0.34	0.32
Al_2O_3	15.13	15.02	15.18	14.91	14.93	15.09	12.67	15.47	15.17	15.02	14.77
Fe_2O_3	1.50	1.53	1.56	2.14	1.78	1.49	1.83	1.51	1.53	1.94	2.13
MnO	0.02	0.02	0.02	0.02	0.02	0.02	0.02	0.02	0.02	0.02	0.02
MgO	0.5	0.49	0.49	0.55	0.52	0.49	0.38	0.49	0.50	0.57	0.55
CaO	1.62	1.64	1.65	1.64	1.54	1.61	1.24	1.64	1.63	1.55	1.57
Na_2O	4.70	4.64	4.69	4.55	3.79	4.72	3.37	4.76	4.66	3.61	4.45
K_2O	4.13	4.14	4.18	3.79	4.78	4.15	2.87	4.22	4.11	4.87	3.80
P_2O_5	0.12	0.13	0.14	0.13	0.09	0.12	0.13	0.12	0.13	0.10	0.11
Cr_2O_3	0.002	0.003	0.002	0.004	0.003	<0.002	0.004	0.002	0.002	0.003	0.004
Loi	2.00		1.90	2.20	1.70	1.90	2.60	1.70	1.90	1.70	2.20
Sum	99.84		99.84	99.83	99.84	99.84	99.76	99.84	99.84	99.84	99.82

Table 4.19 cont.) Results of Whole-Rock Major Oxide Analyses of Biotite Granite Gneiss Unit.

Sample No→ **Major Oxide(wt%)↓**	b12 *	b13 *	b14 *	b15 *	Range	Average
SiO_2	75.92	73.41	70.81	68.60	69.47-75.92	70.75
TiO_2	0.33	0.32	0.38	0.71	0.14-0.71	0.33
Al_2O_3	17.03	17.41	17.87	19.03	12.67-19.03	15.65
Fe_2O_3	2.60	2.61	2.82	5.68	1.21-5.63	2.18
MnO	0.03	0.02	0.03	0.06	0.02-0.06	0.02
MgO	0.60	0.71	1.13	1.47	0.25-1.71	0.63
CaO	1.99	2.86	3.45	5.31	1.24-5.31	2.06
Na_2O	3.20	3.61	3.87	4.61	2.88-4.76	4.22
K_2O	6.05	4.95	3.43	1.61	1.40-6.05	4.07
P_2O_5				0.26	0.09-0.14	0.13
Cr_2O_3					<0.002-0.004	0.00
Loi					1.70-2.60	1.32
Sum	107.6	105.8	103.60	107.00	99.76-106.1	94.82

Trace element contents with sample symbol * are determined by X-ray fluorescence (XRF). Elements with blank space were not determined.

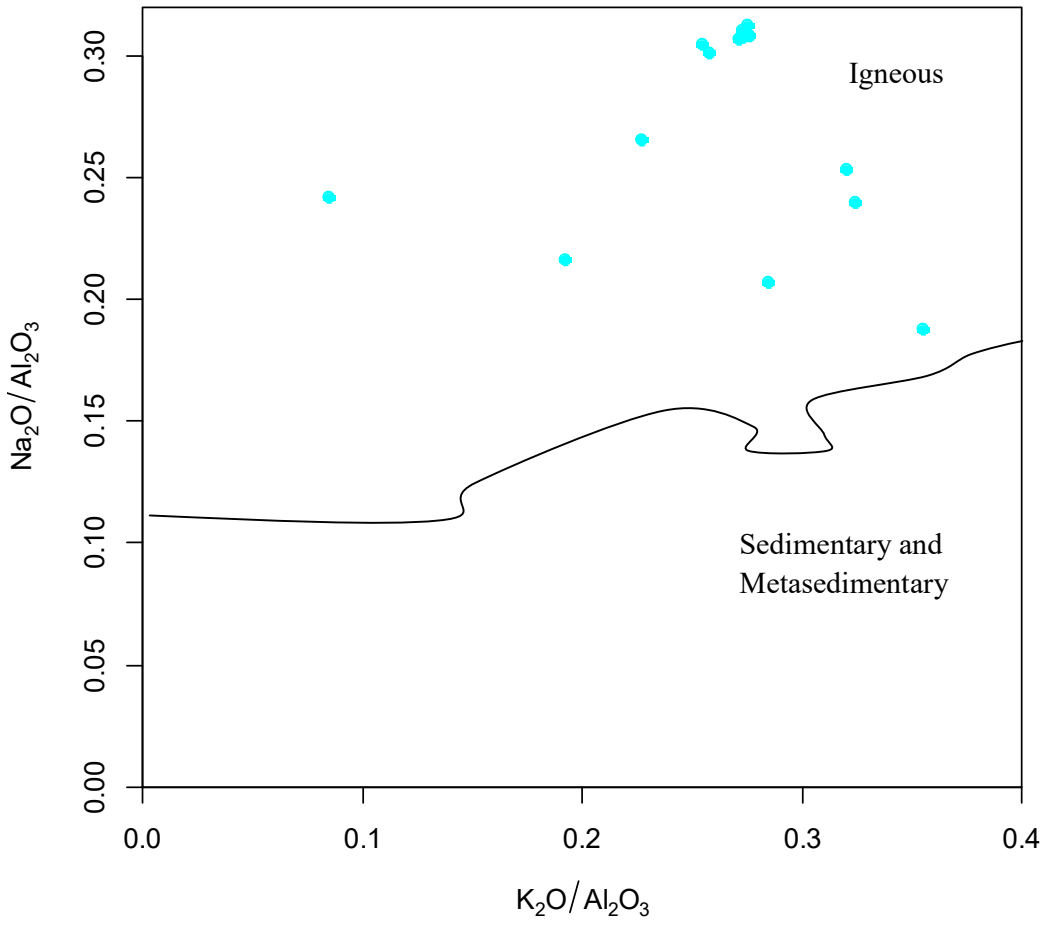

Fig.4.76 Na_2O/Al_2O_3 versus K_2O/Al_2O_3 Variation Diagram of Biotite Granite Gneiss (After Garrels and Mackenzie, 1971).

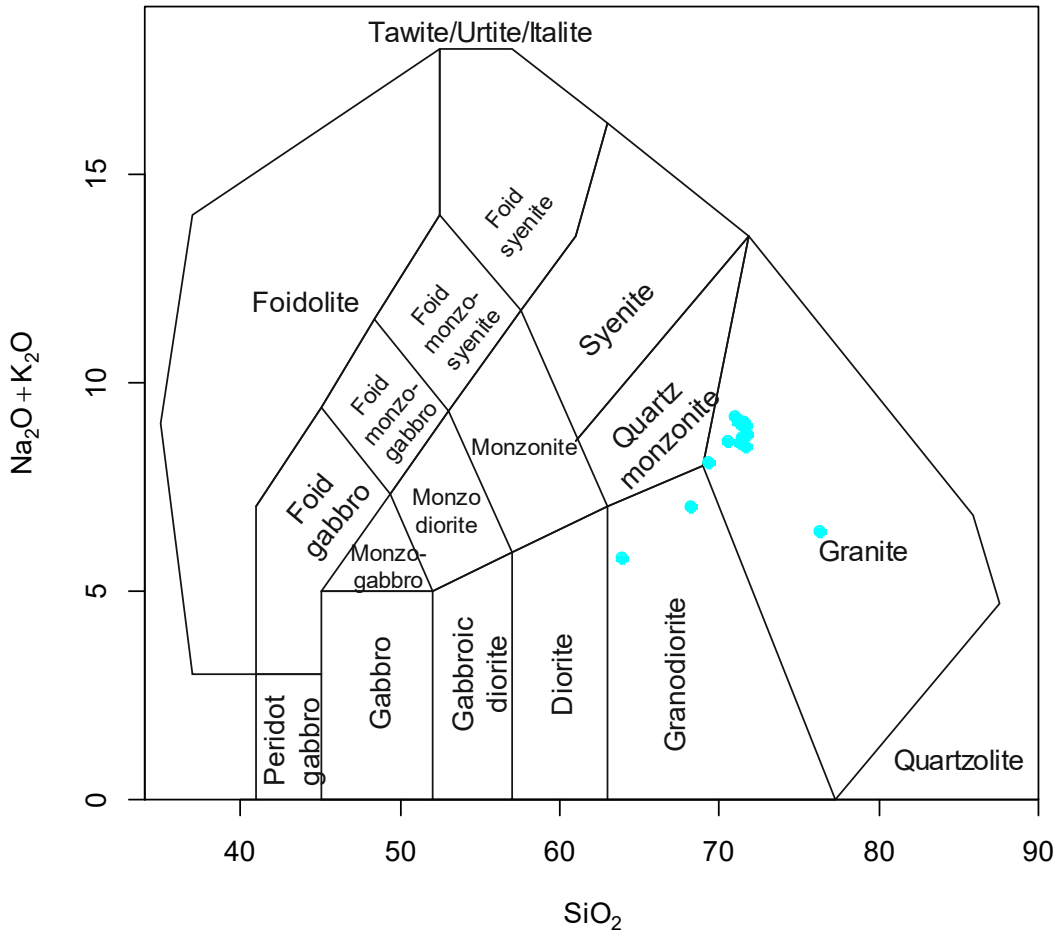

Fig.4.77 Classification Diagram of Biotite Granite Gneiss Samples Base on Na_2O+K_2O versus SiO_2 (After Middlemost, 1994).

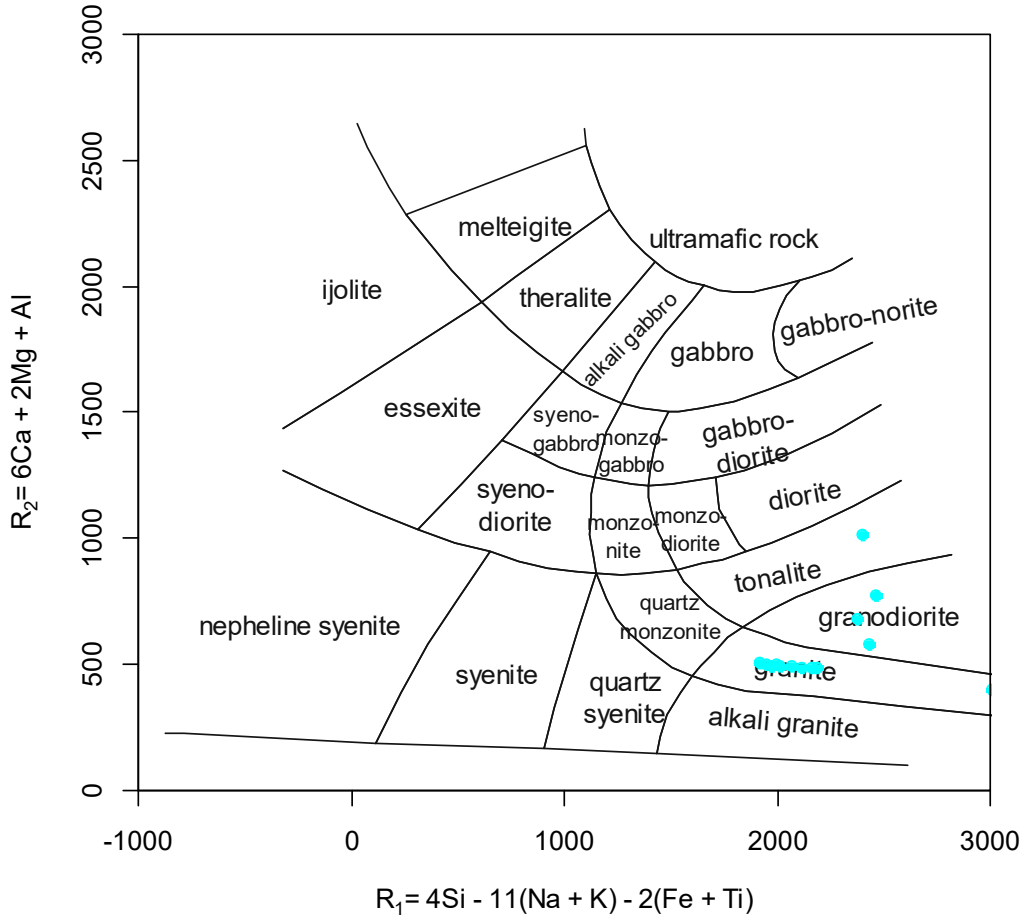

Fig.4.78 R1-R2 Plot of Biotite Granite Gneiss Samples (After De la Roche *et. al.*, 1980).

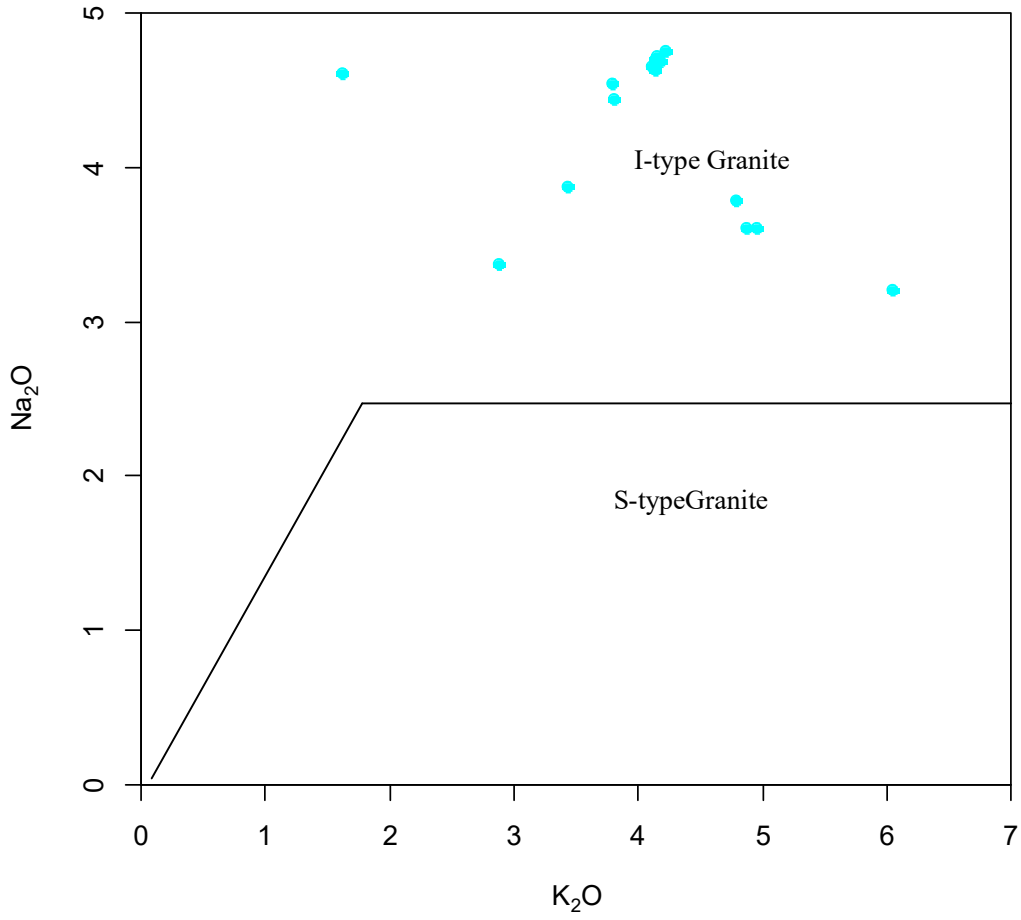

Fig.4.79 Binary Plot of Na_2O against K_2O Showed I-type Granitoid for the Biotite Granite Gneiss (After Klemenn and Twist, 1989).

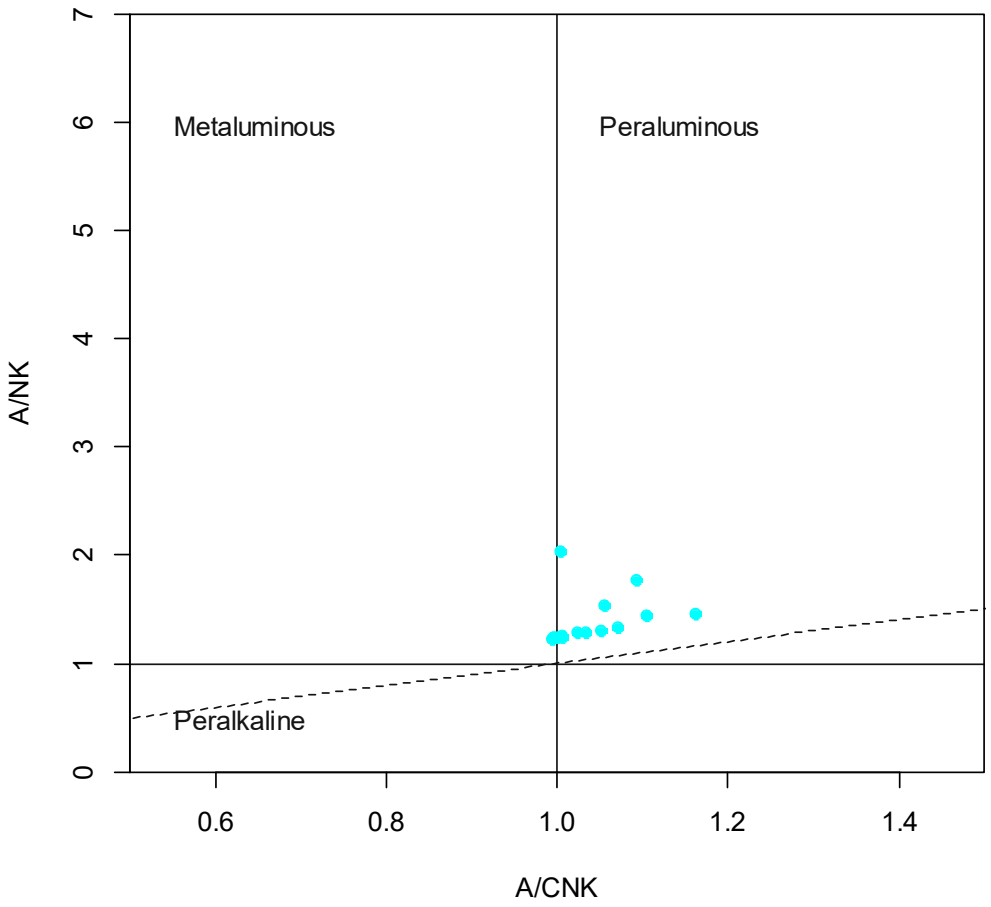

Fig.4.80 A/NK versus A/CNK Plot Discriminating Metaluminous, Peraluminous and Peralkaline Composition for the Biotite Granite Gneiss (Shand, 1943).

A/CNK = Al_2O_3/(CaO+Na_2O+K_2O) (mol.%)

A/NK = Al_2O_3/(Na_2O+K_2O) (mol.%)

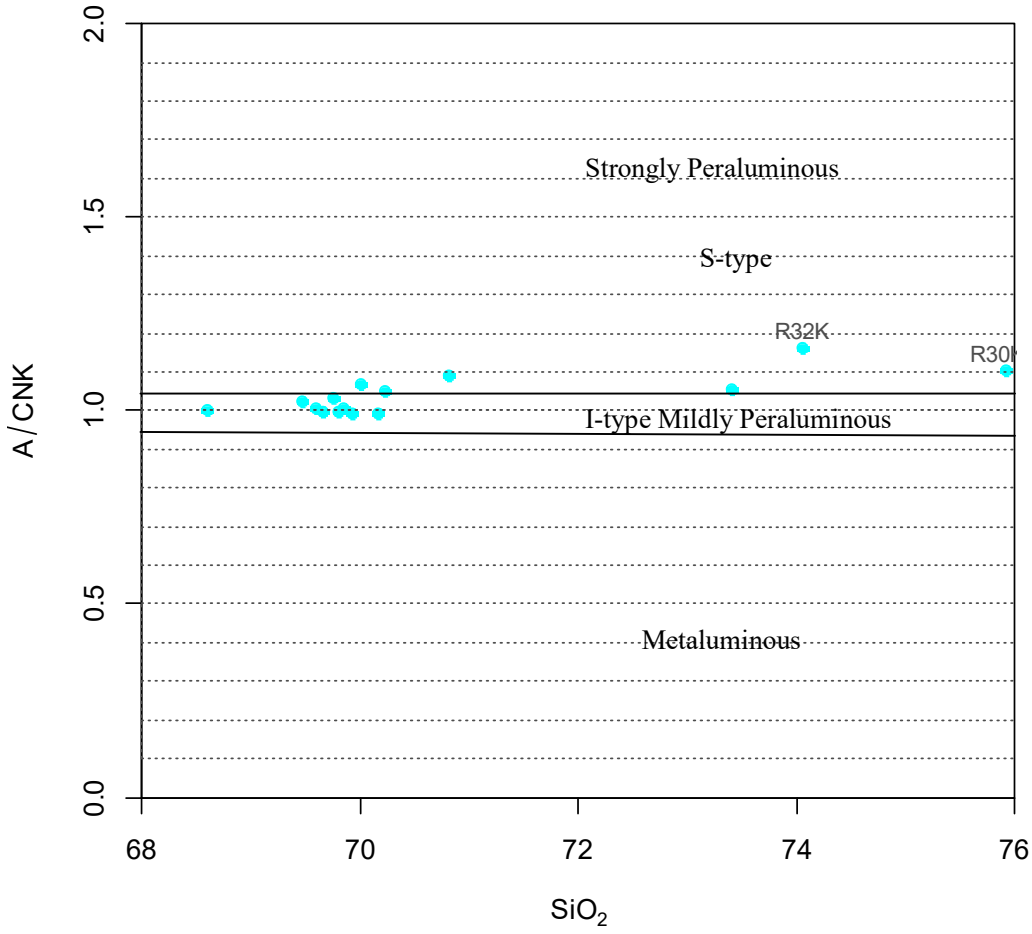

Fig.4.81 Al_2O_3/ ($CaO+Na_2O+K_2O$) versus SiO_2 Binary Diagram of the Biotite Gneiss (After Chappel and White, 1974)

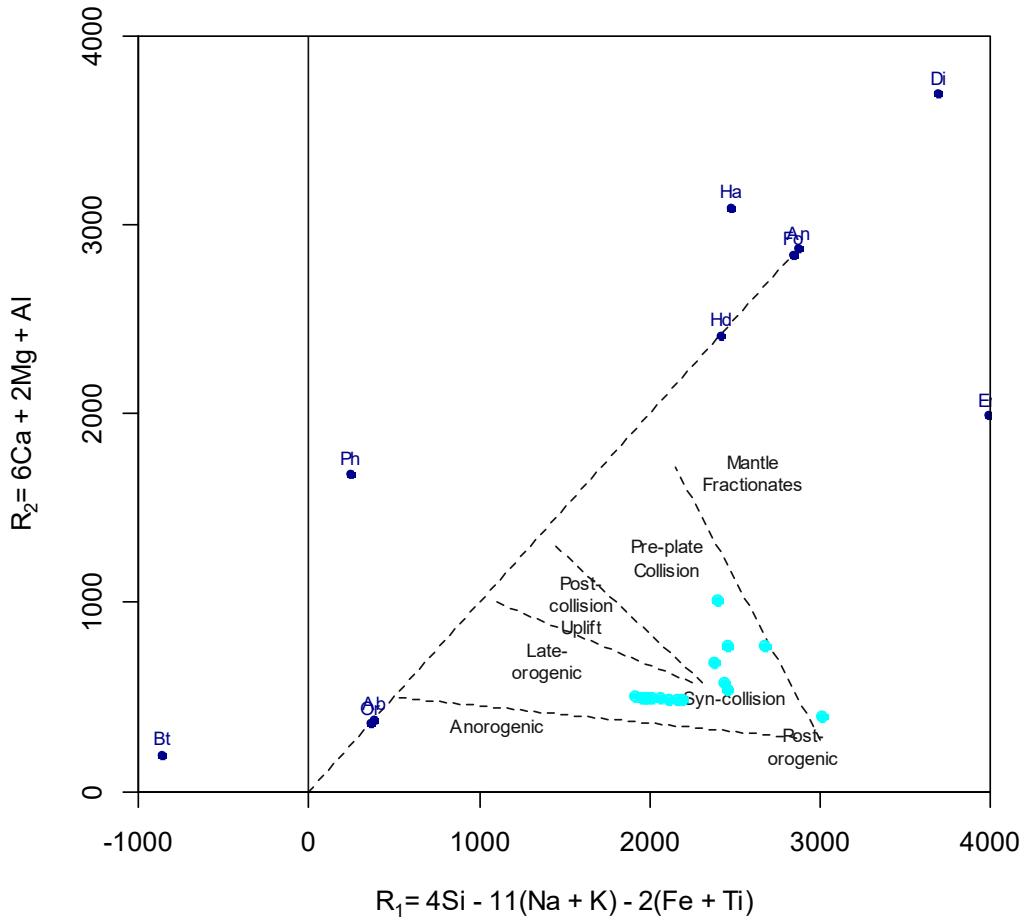

Fig.4.82 R1 versus R2 Discriminate Diagram for Biotite Granite Gneiss (After Batchelor and Bowden, 1985).

Table4.20 Ratio Calculations and Differentiation Indice from Major Oxides of the Biotite Granite Gneiss Unit.

Sample No→ Mineral Ratio↓	**b1**	**b2**	**b3**	**b4**	**b5**	**b6**	**b7**	**b8**	**b9**	**b10**	**b11**	**b12***	**b13 ***	**b14 ***	b15 *
CaO/Na_2O	0.34	0.35	0.35	0.36	0.41	0.34	0.37	0.34	0.35	0.43	0.35	0.62	0.79	0.89	1.15
CaO/Na_2O+K_2O	0.18	0.19	0.19	0.20	0.18	0.18	0.20	0.18	0.19	0.18	0.19	0.21	0.33	0.47	0.85
K_2O/Na_2O	0.88	0.89	0.89	0.83	1.26	0.88	0.85	0.89	0.88	1.35	0.85	1.89	1.37	0.88	0.35
DI	86.96	87.19	86.897	85.44	86.40	87.22	86.09	87.07	86.87	85.82	85.57	91.84	86.09	79.11	71.31

DI = Normative Q+Or+Ab+Ne+Ks+Lc

Table 4.21 Comparison of the Average Major Oxides of the Biotite Granite Gneiss in the Study Area with Other Area.

Major Oxide(wt%)	This study	Jebba	Abeokuta	Arigidi	Jos Plateau	India
SiO_2	70.75	76.11	65.12	70.92	70.36	64.60
TiO_2	0.33	0.29	0.81	0.45	0.32	0.54
Al_2O_3	15.65	11.84	15.10	13.09	14.42	17.00
Fe_2O_3	2.18	2.81	5.51	6.08	0.66	3.60
MnO	0.02	0.02	0.09	0.32		
MgO	0.63	0.11	1.08	1.11	0.90	1.58
CaO	2.06	0.42	3.57	3.20	2.03	3.48
Na_2O	4.22	3.53	3.35	1.81	3.35	4.17
K_2O	4.07	7.43	3.82	1.45	5.38	3.48
P_2O_5	0.13	0.03	0.33			

Jebba: Okonkwo *et.al*. (2012)

Abeokuta: Elueze *et.al*. (2004)

Arigidi: Odunyemi *et.al*. (2011)

Jos Pateau: Wright, (1971)

India: Condie *et.al* (1982)

4.1.3.6.2 Trace Elements

The wide range of variations in trace element contents of biotite granite gneiss, especially that of Barium (Ba, 611.0 to 984.0ppm), Rubidium (Rb, 13.9 to 163.5ppm), Strontium (Sr, 223.7 to 819.4ppm) and Zircon (73.9 to 273.8ppm) strongly support a mixture of igneous rock types inputs as exemplified by the major oxide variation and discrimination diagrams (Table 4.22).

Variation diagram of the concentration of selected elements normalized by chondrite values as documented by Thompson (1982) was plotted for the biotite granite gneiss samples (Fig.4.83). The trace elements exhibit a pattern characterized by Rb, Th and K enrichment relative to depleted Ti Y, Tm and Yb.

The plot of Nb against Y discrimination diagram (Pearce *et. al.,* 1984) revealed that the parent rock of the biotite granite gneiss fell within the volcanic-arc to syn-collision granite field (Fig.4.84).

The original magmatic rock of the biotite granite gneiss were emplaced within a fairly thickened Pan African crust setting (>30km) as exemplified on the diagram of Rb versus Sr of Condie, (1973) (Fig.4.85).

Table 4.22 Results of Trace Element Analyses of Biotite Granite Gneiss Unit

SampleNo → Trace Element ↓ (ppm)	b1	b2	b3	b4	b5	b6	b7	b8	b9
Ba	890.0	902.0	891.0	819.0	964.0	902.0	611.0	984.0	910.0
Sc	2.0	2.0	2.0	2.0	3.0	2.0	3.0	2.0	2.0
Be	2.0	9.0	5.0	<1	5.0	4.0	<1	5.0	1.0
Co	2.5	2.8	3.1	3.8	2.3	2.6	2.8	2.7	2.8
Cs	5.8	6.2	5.3	6.5	4.0	5.8	4.2	6.3	6.4
Ga	20.1	19.5	19.8	19.8	16.9	22.0	18.2	19.2	18.1
Hf	3.5	3.2	3.4	4.0	5.3	3.6	9.7	3.3	3.7
Nb	5.7	5.2	5.6	6.1	9.4	5.3	12.2	4.6	5.1
Rb	141.4	144.3	141.7	135.4	162.5	141.4	99.4	141.5	135.6
Sn	1.0	2.0	1.0	3.0	4.0	1.0	3.0	1.0	1.0
Sr	792.0	806.7	809.0	770.6	592.1	801.9	572.8	819.4	790.8
Ta	0.6	0.6	0.5	0.4	0.7	0.5	1.0	0.5	0.6
Th	12.8	14.6	13.1	8.4	22.9	17.5	9.1	16.8	11.7
U	6.8	24.0	6.2	3.8	6.3	5.6	3.9	5.9	10.0
V	20.0	20.0	20.0	21.0	17.0	20.0	27.0	21.0	19.0
Zr	118.0	110.7	116.0	144.9	191.6	116.2	384.9	113.4	132.0
Y	5.0	4.5	4.3	4.5	14.2	5.0	6.6	5.2	4.5
Mo	0.7	0.7	0.7	0.9	0.8	0.7	0.7	0.6	0.6
Cu	7.9	8.1	9.3	26.6	20.0	8.6	64.2	10.8	10.4
Pb	3.2	3.0	3.1	30.0	4.9	3.1	21.9	3.6	3.4
Zn	44.0	41.0	42.0	122.0	37.0	42.0	76.0	41.0	41.0
Ni	7.6	7.2	7.5	13.0	5.2	7.7	9.9	7.0	7.2
As	<0.5	<0.5	<0.5	<0.5	<0.5	<0.5	0.7	<0.5	<0.5
Cd	<0.1	<0.1	<0.1	0.8	<0.1	<0.1	0.2	<0.1	<0.1
Sb	0.1	0.1	0.1	0.8	0.1	0.1	0.4	0.1	0.1
Ag	<0.1	<0.1	<0.1	<0.1	<0.1	<0.1	<0.1	<0.1	<0.1
Au	<0.5	0.9	0.5	1.3	5.8	1.2	7.7	<0.5	<0.5
Tl	0.3	0.3	0.3	0.4	0.3	0.3	0.3	0.3	0.3

Table 4.22 (continue) Results of Trace Element Analyses of Biotite Granite Gneiss Unit.

Sample No → Trace Element ↓ (ppm)	b10	b11	Range	Average
Ba	986.0	819.0	611-984.0	879.82
Sc	4.0	3.0	2.0-5.2	2.45
Be	3.0	1.0	<1.0-5.0	3.89
Co	2.2	6.7	2.3-3.8	3.12
Cs	3.8	6.7	4.0-6.5	5.55
Ga	17.0	17.6	13.0-20.1	18.93
Hf	5.8	4.3	3.4-9.7	4.53
Nb	13.5	5.9	5.3-12.2	7.15
Rb	163.5	129.9	13.9-163.5	139.69
Sn	6.0	4.0	1.0-50.8	2.45
Sr	549.1	744.6	223.7-819.4	731.73
Ta	1.2	0.5	0.4-1.0	0.65
Th	21.5	10.3	9.1-22.9	14.43
U	5.5	5.3	3.8-6.2	7.57
V	22.0	21.0	17.0-27.0	20.73
Zr	212.5	153.4	73.9-273.8	163.05
Y	19.0	3.7	3.4-18.8	6.95
Mo	0.9	1.0	0.7-0.9	0.75
Cu	20.1	25.6	7.9-64.2	19.24
Pb	4.4	39.5	3.1-41.8	10.92
Zn	32.0	136.0	18.6-122.0	59.45
Ni	4.8	14.6	1.8-9.9	8.34
As	<0.5	0.6	<0.5-3.1	0.65
Cd	<0.1	0.9	<0.1-0.8	0.63
Sb	0.2	1.4	0.1-1.4	0.32
Ag	<0.1	<0.1	<0.1	
Au	6.9	2.6	<0.5-7.7	3.36
Tl	0.3	0.4	0.3-0.4	0.32

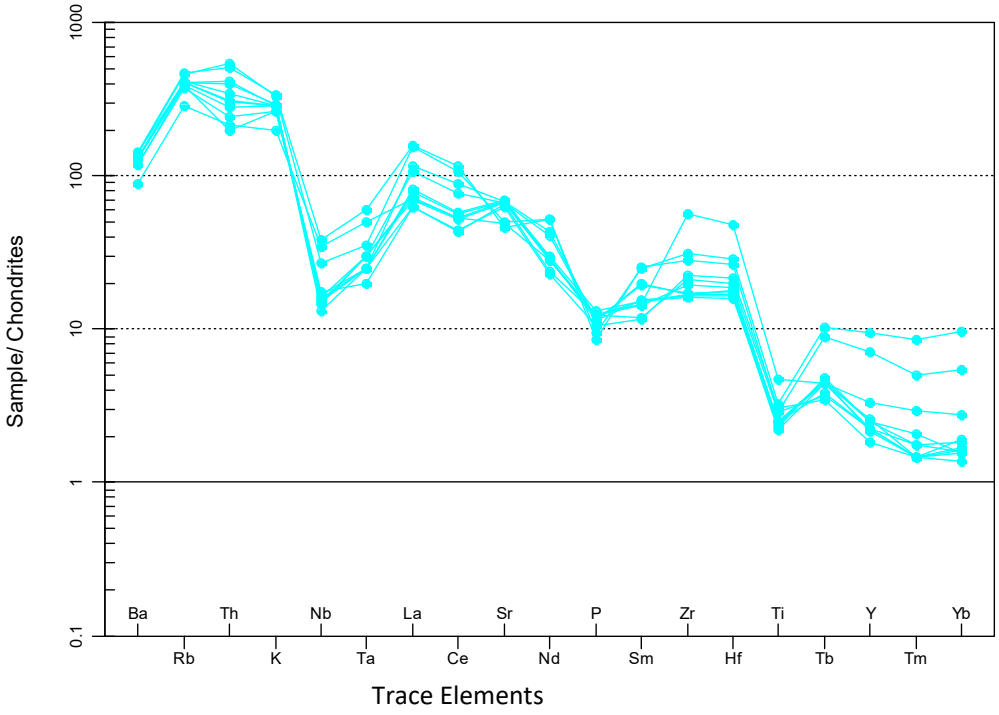

Fig.4.83 Plot of Normalized Mean Concentration of Trace Element with Chondrite in Biotite Granite Gneiss (Thompson, 1982).

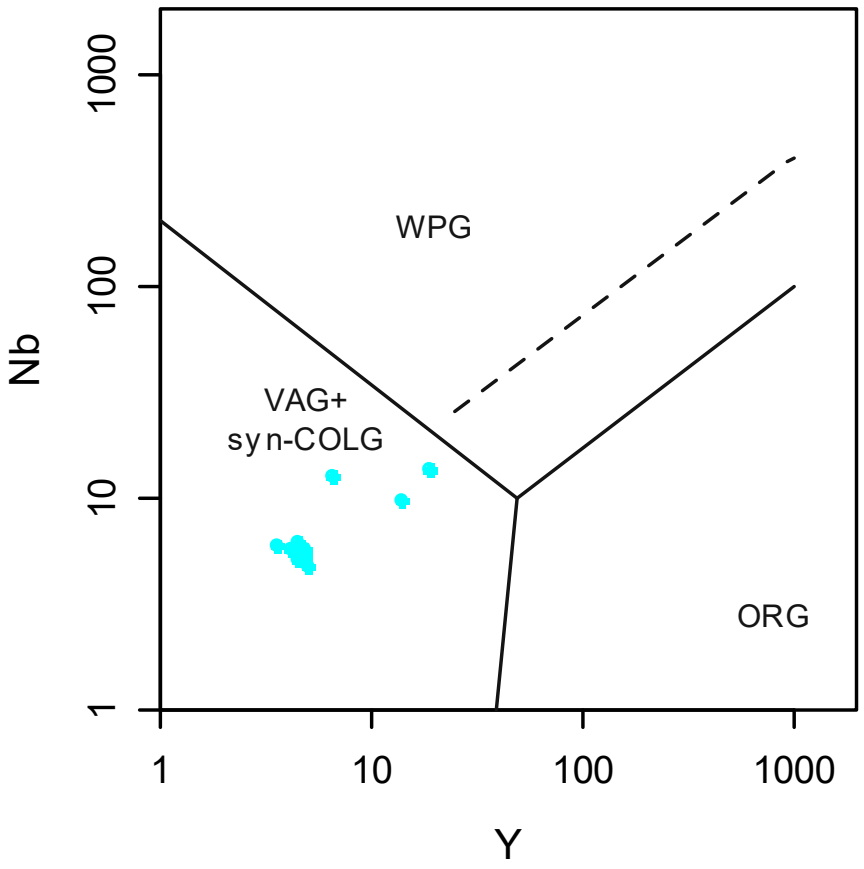

Fig.4.84 Nb versus Y Discriminate Diagram for Biotite Granite Gneiss (After Pearce *et al.*, 1984).

Syn-COLG: syn-collision granites, WPG: within-plate granites, VAG: volcanic-arc granites, ORG: ocean-ridge granites

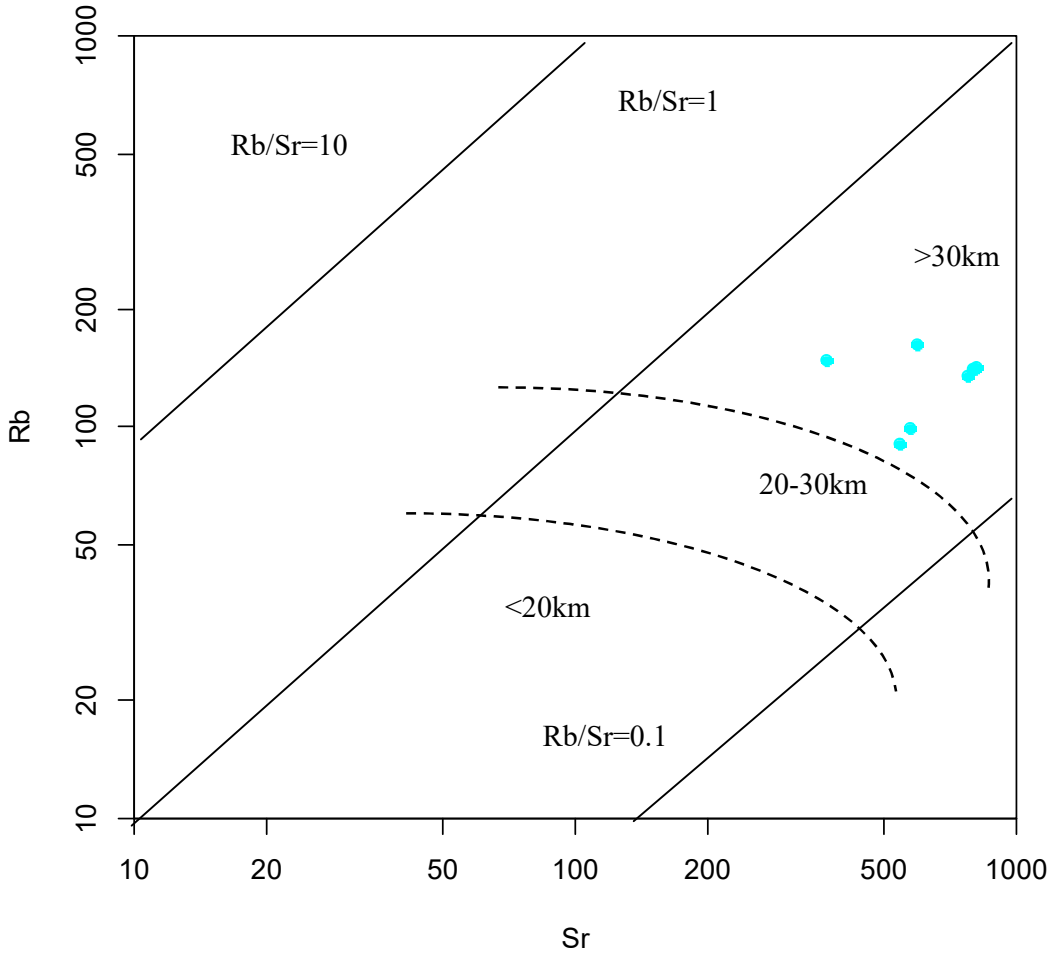

Fig.4.85 Biotite Granite Gneiss in the Rb against Sr crustal thickness grid.(Condie, 1973)

4.1.3.6.3 Rare Earth Elements

The biotite granite gneiss samples are enriched in light rare earth elements (LREE) concentrations (average; 137.59) but showed relatively depleted heavy rare earth elements (HREE) (average; 1.93)(Table.4.23).

The biotite granite gneiss samples from the study area showed negative Eu anomalies (Eu/E*; 0.58 to 0.85, average 0.76) while La_N/Yb_N ranged from 4.41 to 75.29ppm.

The chondrite normalized plot of rare earth element (REE) for the biotite granite gneiss revealed high values for the light rare earth elements (LREE) and moderately low values for the Heavy rare earth elements (HREE) (Fig.4.86).

Table 4.23 Results of Rare Earth Element Analyses of Biotite Granite Gneiss Unit.

Sample No → REE Element (ppm) ▼	b1	b2	b3	b4	b5	b6	b7	b8	b9	b10	b11	Range	Average
La	35.10	24.00	26.00	20.80	50.50	38.40	23.40	27.20	22.90	51.80	20.80	23.4-51.80	33.84
Ce	66.50	46.40	48.70	37.40	92.90	76.70	45.70	49.90	45.10	99.60	38.20	37.4-99.60	62.76
Pr	7.12	5.05	5.22	4.12	9.44	7.96	4.79	5.30	4.72	9.81	4.08	4.12-9.81	6.87
Nd	25.60	18.00	18.90	15.10	32.80	27.50	17.70	18.30	17.60	33.10	14.40	15.10-33.10	34.12
Sm	3.92	3.10	3.11	2.43	5.13	4.00	2.98	3.15	2.90	5.09	2.38	2.43-5.13	3.76
Eu	0.70	0.68	0.65	0.53	0.95	0.74	0.50	0.67	0.63	0.94	0.53	0.50-0.95	0.81
Gd	2.13	1.99	2.14	1.54	3.55	2.22	1.85	1.90	1.79	3.69	1.56	1.54-3.69	3.14
Tb	0.24	0.23	0.24	0.19	0.46	0.25	0.23	0.23	0.20	0.53	0.18	0.19-0.53	0.47
Dy	0.98	1.06	1.00	0.94	2.51	1.11	1.17	0.94	0.85	3.27	0.83	0.94-3.27	1.38
Ho	0.16	0.17	0.16	0.14	0.47	0.16	0.23	0.16	0.15	0.67	0.12	0.16-0.67	0.10
Er	0.37	0.44	0.42	0.34	1.24	0.37	0.70	0.40	0.40	1.99	0.38	0.34-1.99	0.99
Tm	0.06	0.06	0.05	0.05	0.17	0.07	0.10	0.05	0.05	0.29	0.05	0.05-0.29	0.04
Yb	0.35	0.40	0.37	0.42	1.19	0.34	0.61	0.34	0.36	2.11	0.30	0.34-2.11	0.71
Lu	0.05	0.05	0.06	0.06	0.17	0.05	0.11	0.04	0.05	0.34	0.05	0.05-0.34	0.19
Eu/Eu*	0.74	0.84	0.77	0.84	0.68	0.76	0.65	0.84	0.85	0.67	0.85	0.58-0.85	0.76
La_N/Yb_N	66.86	40.00	46.85	33.02	28.29	75.29	25.57	53.33	4.41	16.37	46.22	4.41-75.29	37.66
La_N/Sm_N	5.51	4.76	5.14	5.27	6.06	5.91	4.83	5.31	4.86	6.26	5.38	4.76-8.27	5.58
ƩLREE	134.32	93.45	98.82	77.42	185.64	150.56	91.59	100.70	90.32	194.31	77.48	77.4-185.6	137.59
ƩHREE	0.83	0.95	0.90	0.87	2.77	0.83	1.52	0.83	0.86	4.73	0.78	0.8-4.73	1.93

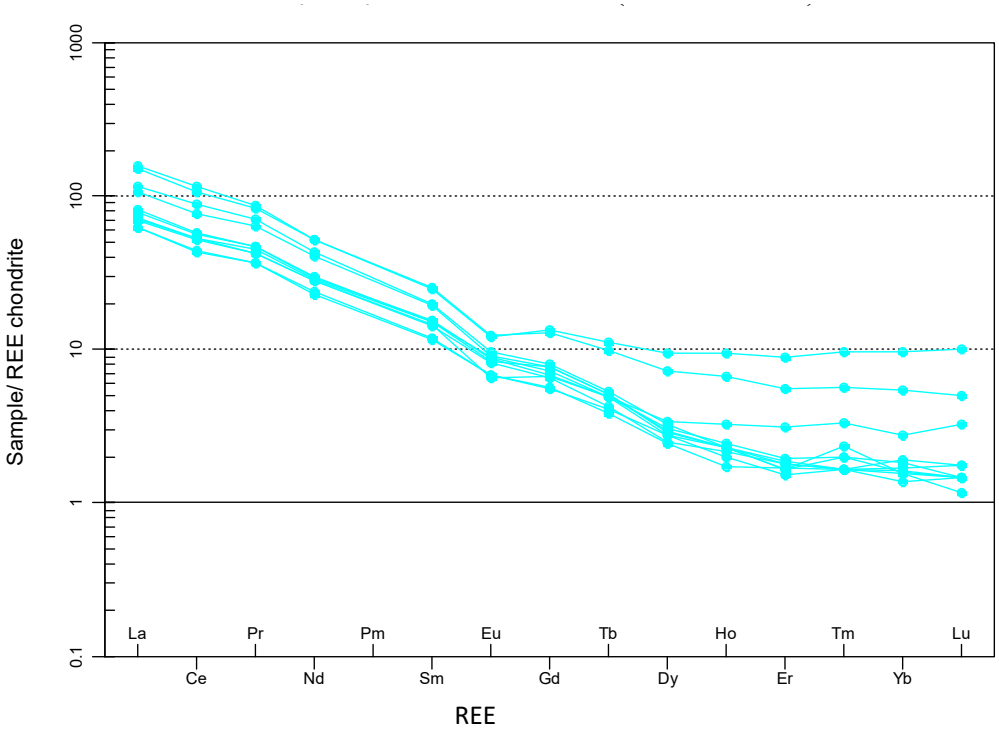

Fig.4.86 REE Chondrite Normalized Plots for the Biotite Granite Gneiss (After Nakamura, 1974),

4.1.4 Leucogranite

Leucogranite outcrop as isolated low lying units occupying few locations at the central part of the area with a north to south trending. The leucogranite is fine grained in size, whitish in colour and it outcropped only at four locations (Fig.4.87).

The leucogranite consists of abundant amount of the following minerals: Quartz (35-42%), plagioclase (8-10%), microcline (20-35%), and alkali feldspars (15-20%). Significant amount of muscovite (3-8%), biotite (3-6%), and opaque (1-2%) are present in the rock (Table4.24).

Microcline displayed diagnostic cross-hatched tartan twinning with perthite occurring as lighter irregular stripes in the leucogranite. Subhedral Microcline crystal also exhibits zoning (Fig.4.88).

Biotite occurs as tiny flakes displaying pleochroism from light brown to dark brown. Quartz crystal is subhedral to anhedral grains (Fig.4.89).

Fig.4.87 Hand Sample Displaying Whitish Grey Leucocratic Granite *(Coordinate: N07^{o} 37.105', E 03^{o} 51.534')*

Table 4.24 Modal Composition of Minerals in Leucogranite in the Study Area.

Sample No → / Mineral ↓	R1	R2	R3	Range
Quartz	40	42	35	35-42
Plagioclase	10	8	5	8-10
Microcline	20	22	35	20-35
Muscovite	7	8	3	3-8
Biotite	6	3	6	3-6
Orthoclase Feldspar	15	16	20	15-20
Opaque	2	1	1	1-2
Total	100	100	100	

a

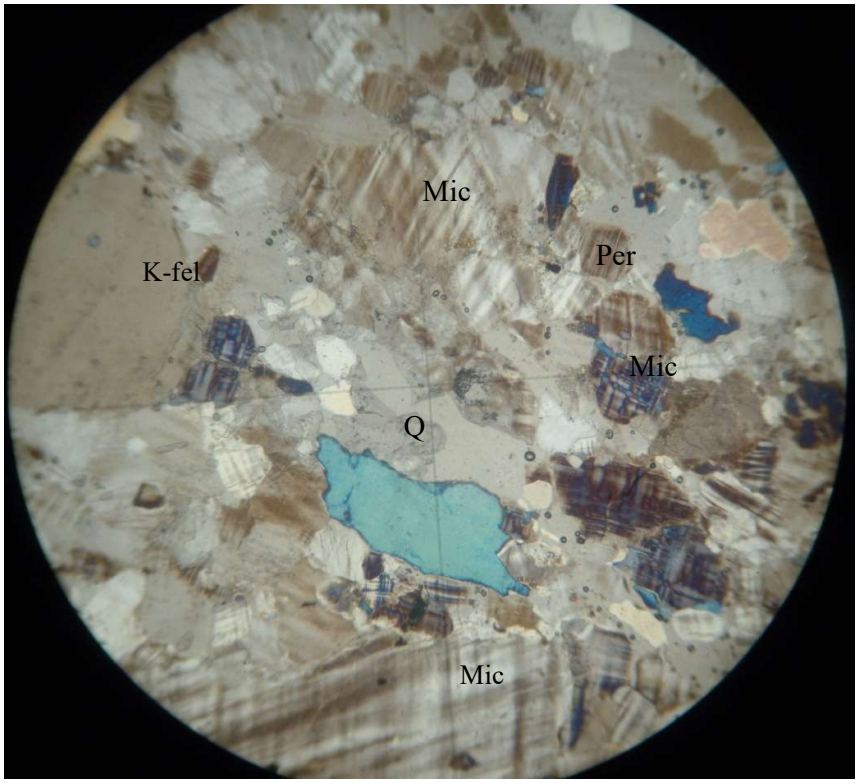

b

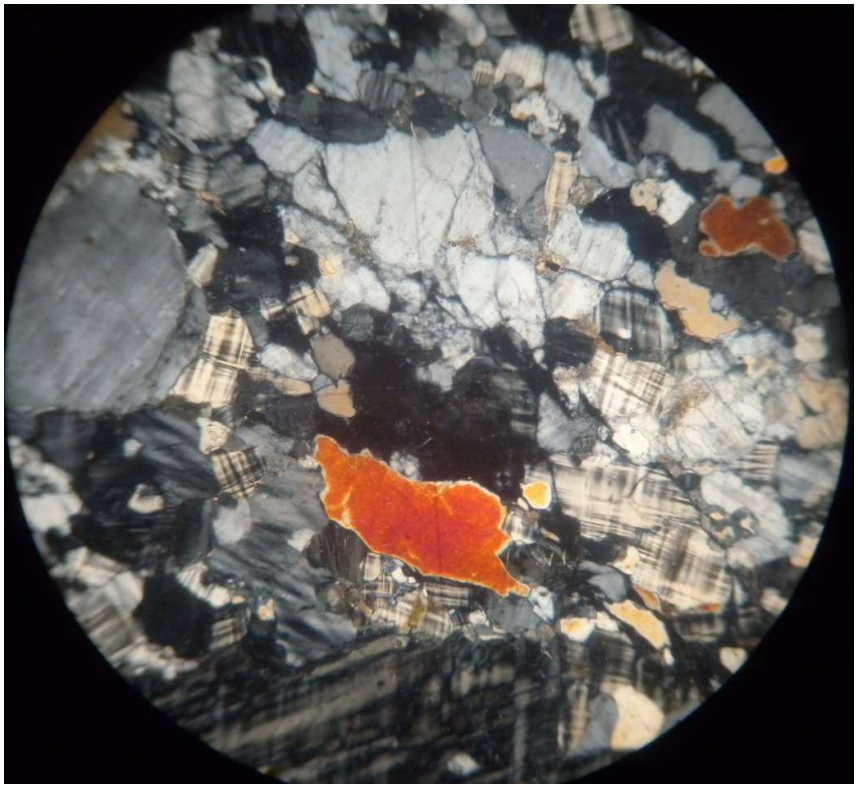

Fig 4.88 Typical Photomicrograph of Leucocratic Granite in Transmitted Light *(a) plane polarised (b) cross polarised light (x40): indicating subhedral zoned microcline (Mic) showing tartan twinning, k-feldspar (K-fel), perthite (Per) and quartz (Q) (Coordinate: N07^o 38.769', E 03^o 51.839')*

a

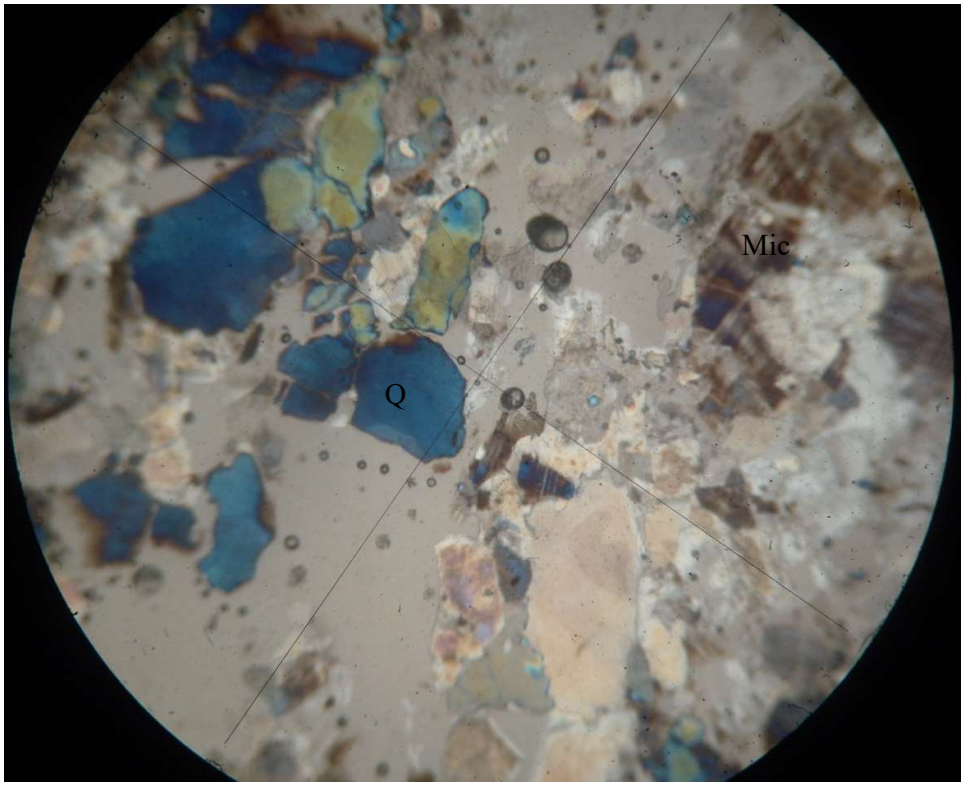

b

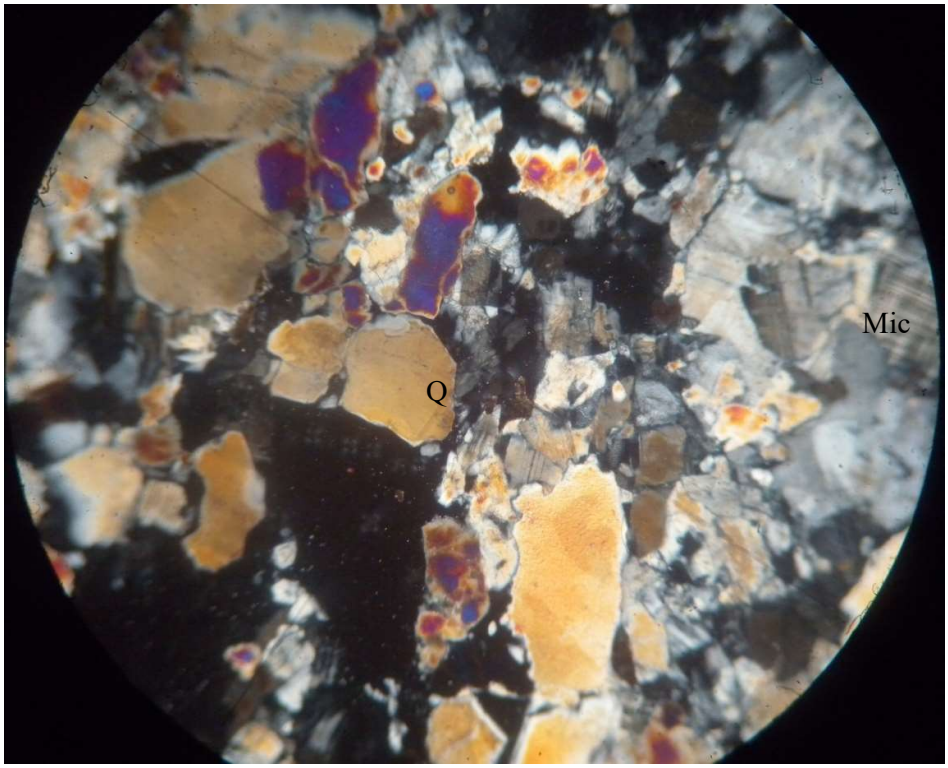

Fig 4.89 Typical Photomicrograph of Leucocratic Granite in Transmitted Light *(a) plane polarised (b) cross polarised light (x40): indicating subhedral microcline (Mic) showing tartan twinning, interlocking with subhedral quartz (Q) (Coordinate: N07^o 37.105', E 03^o 51.534')*

4.1.5 Minor Rocks

4.1.5.1 Pegmatite

Pegmatite are frequently found mostly associated with the gneiss as veins and sometimes displaying minor folds. Many of these pegmatite mapped varies from 3 centimeters to 15 centimeters in dimension and they are usually found to be discordant or concordant with their host rocks (Fig4.90 and 4.91).

Massive exposure of pegmatite body were found at the eastern end (Elede village, coordinate: N07^{o} 37.004', E 03^{o} 58.136'), dome-shaped outcrops at south-eastern (Okefunfun, coordinate: N07^{o}31.139', E 03^{o} 57.626') and north-eastern part (Amosun village, coordinate: N07^{o} 39.683', E 03^{o} 57.289') in close association with quartzite and biotite-hornblende gneiss. A moderately exposed hilly pegmatite body which had been greatly weathered was found at the south western part (Elehinfunfun village, coordinate: N07^{o} 33.508', E 03^{o} 46.334').

The pegmatite is typically coarse grained, Graphic intergrowth of quartz with alkali-feldspars and numerous muscovite minerals were observed on the pegmatite in the study area. Macroscopic sharp contact and alignment of tourmaline minerals usually occur at the border of the vein-type pegmatite and the host rock.

The modal analysis of thin section of pegmatite samples in transmitted light is contained in Table 4.25. Petrographic studies showed that the pegmatite displayed graphic intergrowth texture (Fig.4.92). Perthitic-microcline of characteristic cross-hatched twinning ranging from 40 to 55% by volume, Albite ranging from 20 to 25%, subhedral quartz grain (10-20%) and zoning of the absorption colour in tourmaline mineral (approximately 10%) are present in the section (Fig.4.93).

X-Ray Diffractograms of the pegmatite sample (Fig.4.94) revealed conspicuous peaks of quartz low (36.7%) and microcline (38.6%) and anorthite, sodian (21.8%). Potassic paragasite (Ti-bearing) of 2.9% was also shown. This was in conformity with the mineralogical studies of the pegmatite.

Fig.4.90 Concordant Pegmatite Vein (*Coordinate: N07^{o} 32.776', E 03^{o} 53.840')*

Fig.4.91 Discordant Pegmatite Vein Intruded the Biotite Granite Gneiss (*Coordinate: N07^{o} 38.745', E 03^{o} 48.843')*

Table 4.25 Modal Composition of Minerals in Pegmatite in the Study Area

Sample No → / Mineral ↓	P1	P2	Range
Quartz	20	10	10-20
Microcline	40	55	40-55
Albite	20	25	20-25
Orthoclase-Feldspars	10	-	10
Tourmaline	-	10	10

a

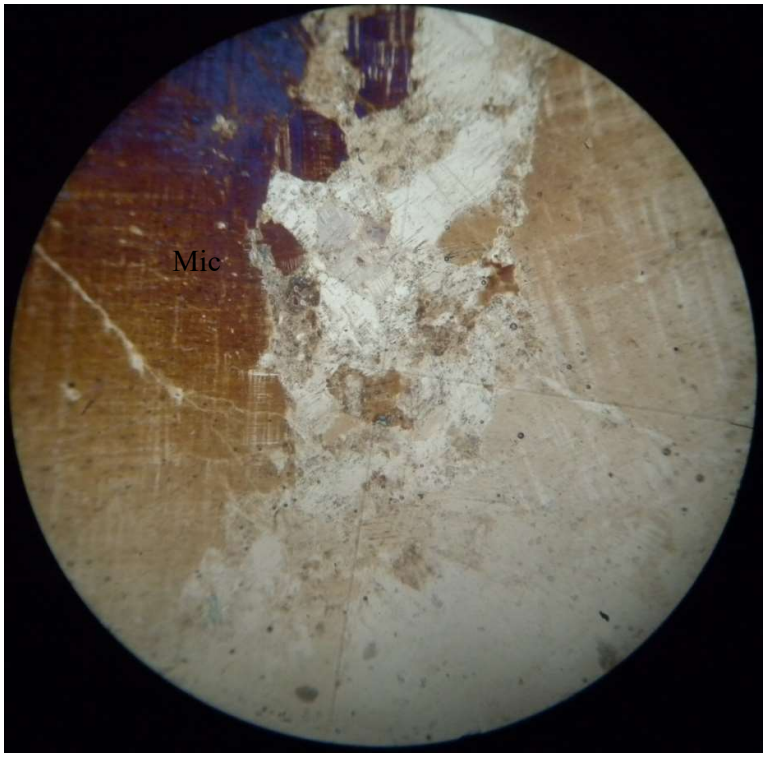

b

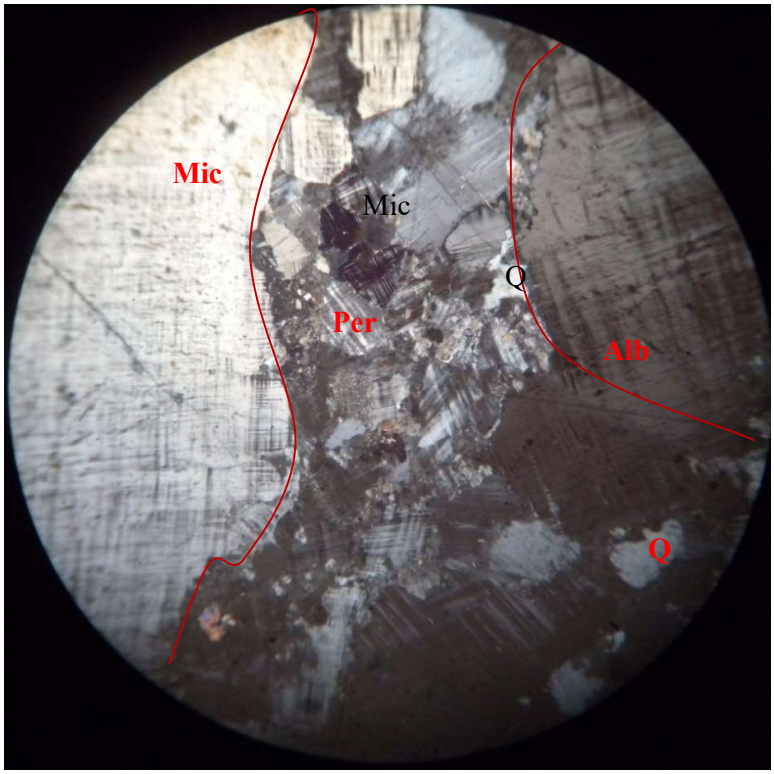

Fig 4.92 Typical Photomicrograph of Pegmatite in Transmitted Light *(a) plane polarised (b) cross polarised light (x40): displaying coarse grain of microcline (Mic) showing tartan twinning, Albite (Alb) subhedral rounded quartz(Q) inclusion in microcline (Mic) exhibit graphic texture, and perthite (Per) (Coordinate: N07^{o} 31.139', E 03^{o} 57.626')*

a

b

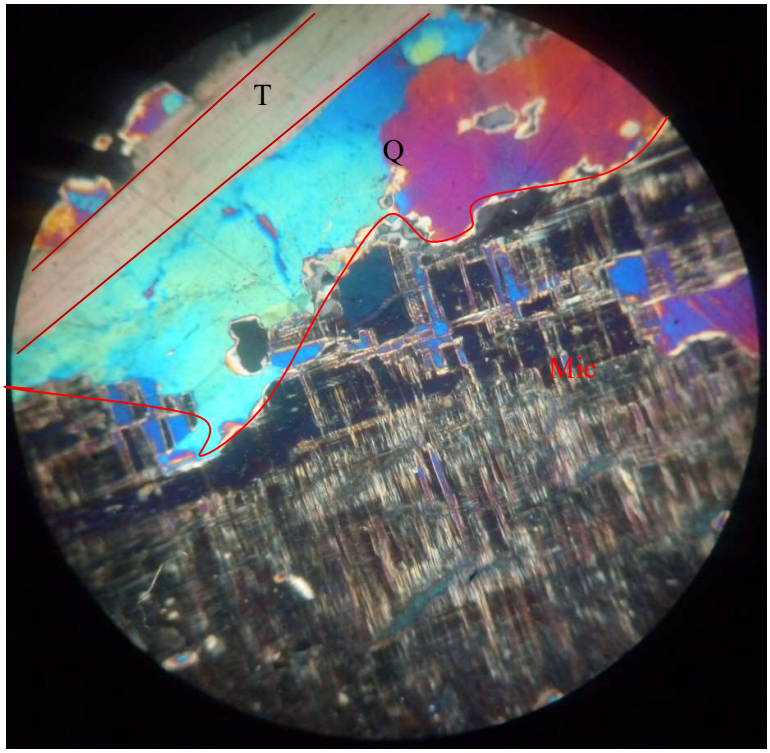

Fig 4.93 Typical Photomicrograph of Pegmatite in Transmitted Light *(a) plane polarised (b) cross polarised light (x40): displaying coarse grain of microcline showing a tartan twinning, subhedral quartz(Q) and zoned tourmaline (T) (Coordinate: N07^{o} 39.638', E 03^{o} 57.289')*

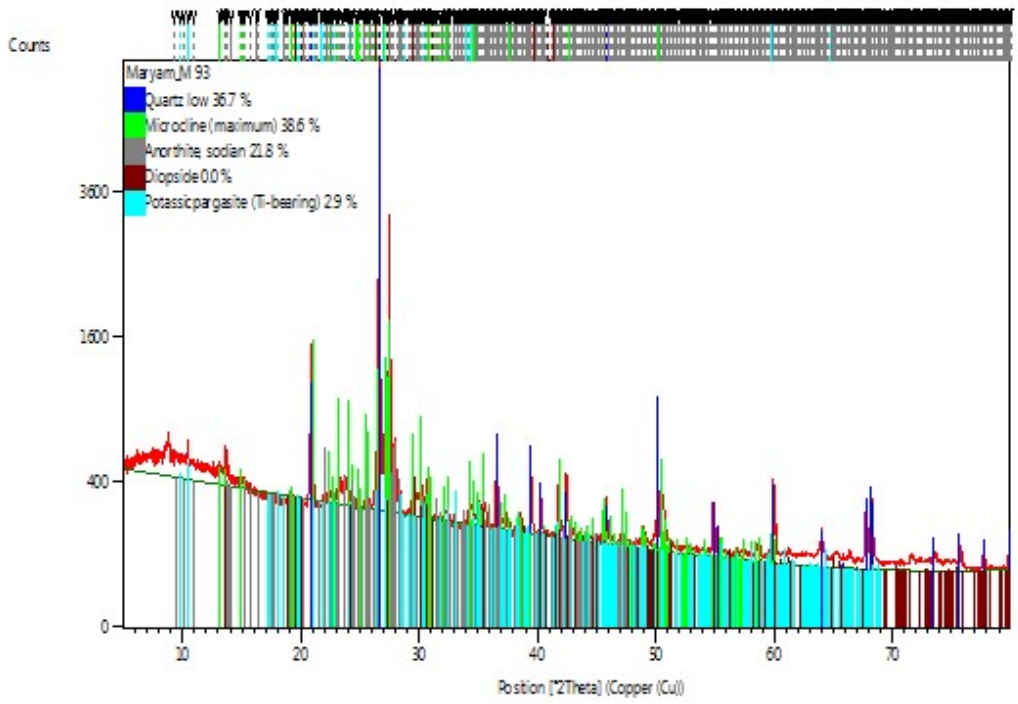

Fig.4.94 Diffractogram of Pegmatite Sample Depicting Predominant Quartz, Microcline, Anorthite Sodian and Potassic Pargasite Peaks *(coordinate: N07^o 32.487', E 03^o 54.661')*

4.1.5.2 Geochemistry of the Pegmatitic Rocks

4.1.5.2.1 Major Oxides

The major oxide geochemical composition of the pegmatite samples revealed that Silica (SiO_2), Alumina (Al_2O_3), and Ferric oxide (Fe_2O_3), concentrations ranged from 70.56to 75.55%; 14.67 to 15.27% and 2.07 to 4.85%, while Magnesia (MgO) and lime (CaO) ranged from 0.31 to 0.52% and 1.48 to 2.47%, respectively (Table 4.26). Soda (Na_2O) concentration ranged from 1.40 to 2.64% whereas patash (K_2O) values ranged from 5.55 to 9.33% Minor oxides of TiO_2, MnO,P_2O_5, and Cr_2O_3 yielded values ranging from 0.39 to 0.57%, 0.02 to 0.05%, 0.06 to 0.11% and 0.003 to 0.18% respectively.

The plot of molar Al_2O_3/Na_2O+K_2O against $Al_2O_3/CaO+Na_2O+K_2O$ indicate that the pegmatite samples that were associated with the pelitic schist in the south eastern part of the study area are mildly peraluminous while intrusive vein sample which is found within the metaluminous granodioritic gneiss is also metaluminuos in nature (Fig.4.95).

Figure 4.96 illustrates that the pegmatite samples have total alkalis (Na_2O+K_2O) greater than MgO indicating calc-alkaline magma origin.

Table 4.26 Results of Whole-Rock Major Oxide Analyses of Pegmatite Unit.

Sample No→ / Major Oxide(wt%)↓	P1 (Rock)	P2 * (Rock)	P3 * (Vein)	Range	Average
SiO_2	70.56	75.55	72.58	70.56-75.55	72.90
TiO_2	0.39	0.57	0.55	0.39-0.57	0.50
Al_2O_3	14.67	15.27	15.03	14.67-15.27	14.99
Fe_2O_3	2.07	4.85	3.00	2.07-4.85	3.31
MnO	0.02	0.05	0.04	0.02-0.05	0.04
MgO	0.52	0.31	0.70	0.31-0.52	0.51
CaO	1.48	1.99	2.47	1.48-2.47	1.98
Na_2O	2.63	2.64	1.40	1.40-2.64	2.22
K_2O	5.55	6.40	9.33	5.55-9.33	7.09
P_2O_5	0.06		0.11	0.06-0.11	0.09
Cr_2O_3	0.003		0.18	0.003-0.18	0.09
Sum	99.84	107.40	105.00	99.84-107.40	104.08

Major oxide contents with sample symbol * are determined by X-ray fluorescence (XRF). Elements with blank space were not determined.

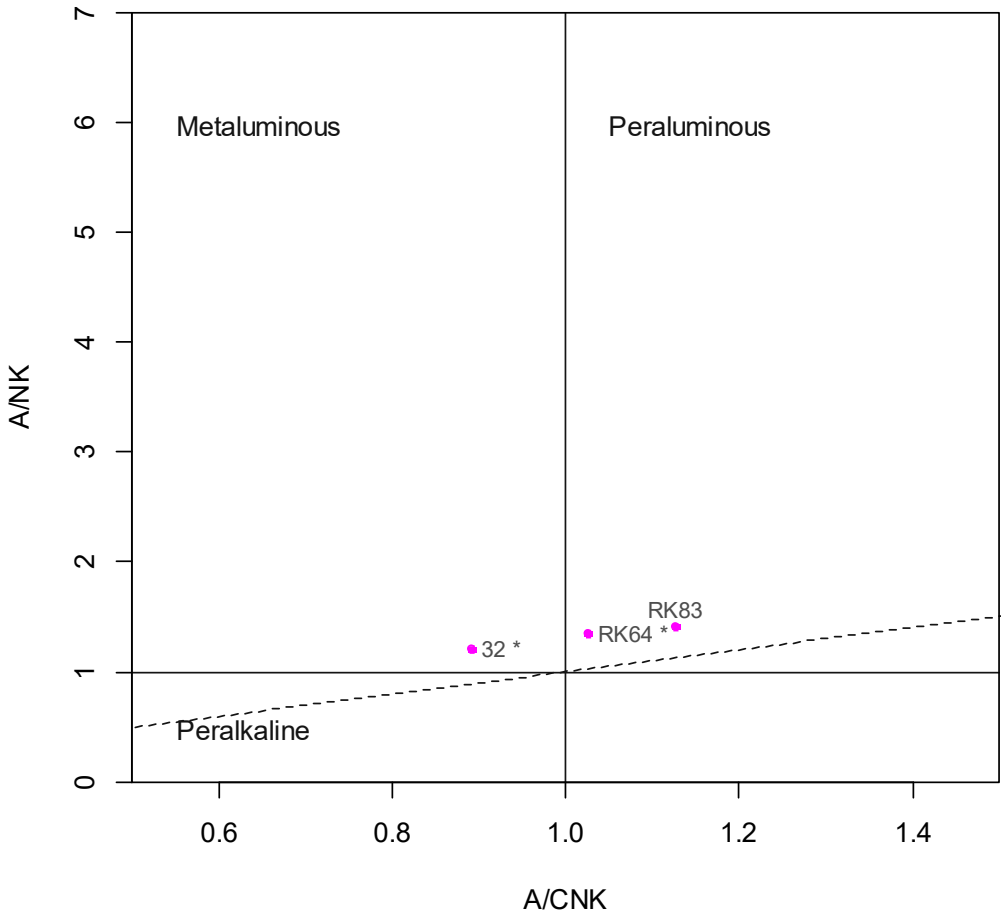

Fig.4.95 A/NK versus A/CNK Diagram Discriminating Metaluminous, Peraluminous and Peralkaline Composition for the Pegmatitic Samples (after: Shand, 1943).

A/CNK = Al_2O_3/(CaO+Na_2O+K_2O) (mol.%)

A/NK = Al_2O_3/(Na_2O+K_2O) (mol.%)

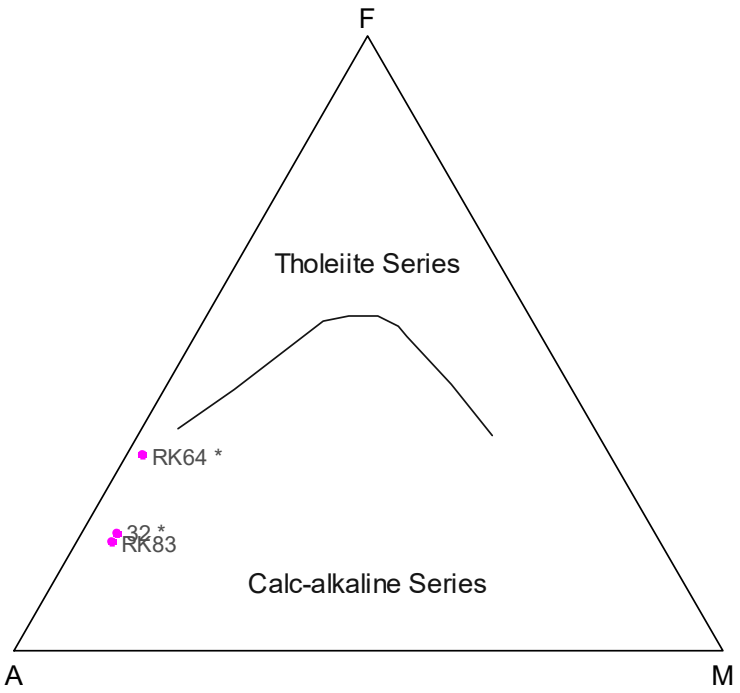

Fig.4.96 Plot of A.F.M. Ternary Diagram for Pegmatitic Samples (after: Irvine Baragar, 1971). The A, F, and M are defined as follows:

A = (K_2O + Na_2O) wt %

F = FeO total wt %

M = MgO wt %

A+F+M = 100%

4.1.5.2.2 Trace Elements

Trace element concentrations for the pegmatite samples revealed enriched Large Ion Lithophile Elements (LILE) such as Barium (Ba, 935.5 to 1800ppm), Rubidium (Rb, 156.0 to 271.9ppm) and Strontium (Sr, 182.4 to 312.3ppm), and Zircon, (Zr,305.4 to 505.5ppm) (Table 4.27). High values of Ba and Rb confirmed the abundant present of K-feldspars in the pegmatitic samples.

The values of transition metals (Cu, Zn, Ni and Sn) ranged from Cu, 0.7 to 32.0ppm; Zn, 21.0 to 81.5ppm; Ni, 2.4 to 7.4ppm, Sn, 8.0 to 52.0ppm and Au, 7.2 to 15.3ppb, respectively.

The pegmatite samples belong to non mineralized muscovite class on plot of K/Rb against Ba diagram (Fig.4.97).

Spider plot of normalized concentration of selected elements of pegmatitic samples with Chondrite (Thompson, 1982) revealed Rb and Ba enrichment as well as significant depletion of Yb, Tm and Y (Fig.4.98).

Table 4.27 Results of Trace Element Analyses of Pegmatite Samples.

Sample No→ Trace Element ↓ (ppm)	P2 * (Rock)	P3 * (Vein)
Ba	935.6	1800.0
Sc	2.8	
Ga	18.7	16.8
Nb		16.8
Rb	156.0	271.9
Sn	52.0	
Sr	182.4	184.2
Zr	505.5	411.2
Y	57.0	45.5
Cu	0.7	
Pb	32.7	33.4
Zn	81.5	80.0
Ni	7.4	
As	1.0	13.5
Sb	0.9	
Au(ppb)	7.2	

Trace element contents with sample symbol * are determined by X-ray fluorescence (XRF). Elements with blank space were not determined.

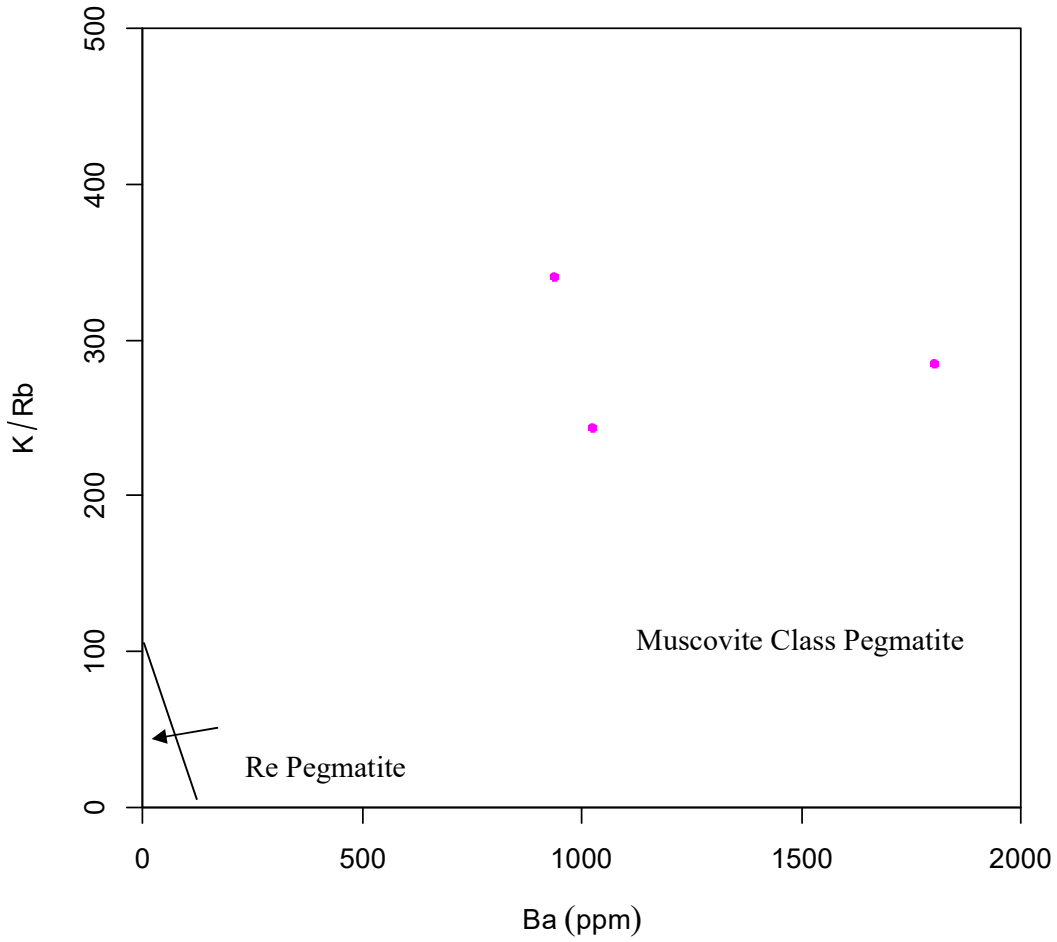

Fig.4.97 Binary Diagram Showing the Mineralization Potentials and Classification of the Pegmatite Samples (after: Cerny and Burt, 1984).

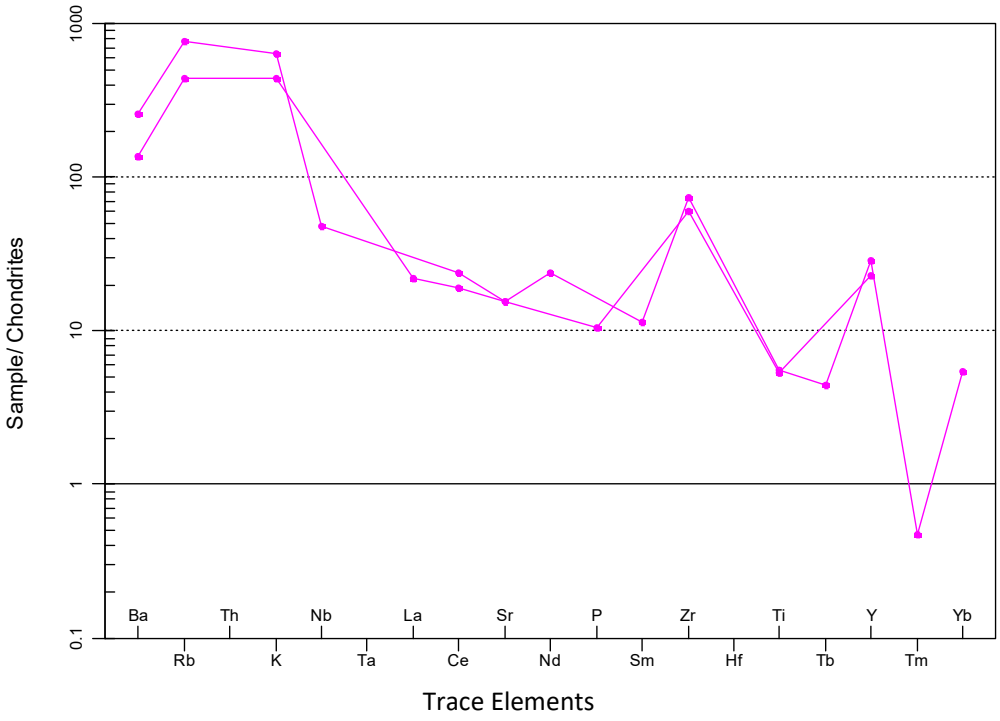

Fig.4.98 Plot of Normalized Mean Concentration of Trace Elements with Chondrite (Thompson, 1982) in Pegmatite Samples.

4.1.5.2.3 Rare Earth Elements

The pegmatitic sample from the study area showed negative Eu anomaly (Eu/E*; 0.62,) and depleted Heavy rare earth elements (HREE) relative to light rare earth elements (LREE) (Table.4.28). The chondrite normalized plot of rare earth element (REE) for the pegmatite samples revealed high values for the light rare earth elements (LREE) and moderately low values for the Heavy rare earth elements (HREE) (Fig.4.99).

Table 4.28 Result of Rare Earth Element Analyses of Pegmatite Sample

Sample No → / **REE (ppm) ↓**	P1 (Rock)
La	78.1
Ce	146.4
Pr	14.36
Nd	49.5
Sm	7.57
Eu	1.31
Gd	5.64
Tb	0.77
Dy	4.4
Ho	0.78
Er	2.52
Tm	0.33
Yb	2.18
Lu	0.33
Eu/Eu*	0.62
La_N/Yb_N	23.88
La_N/Sm_N	6.35
∑LREE	228.36
∑HREE	5.36

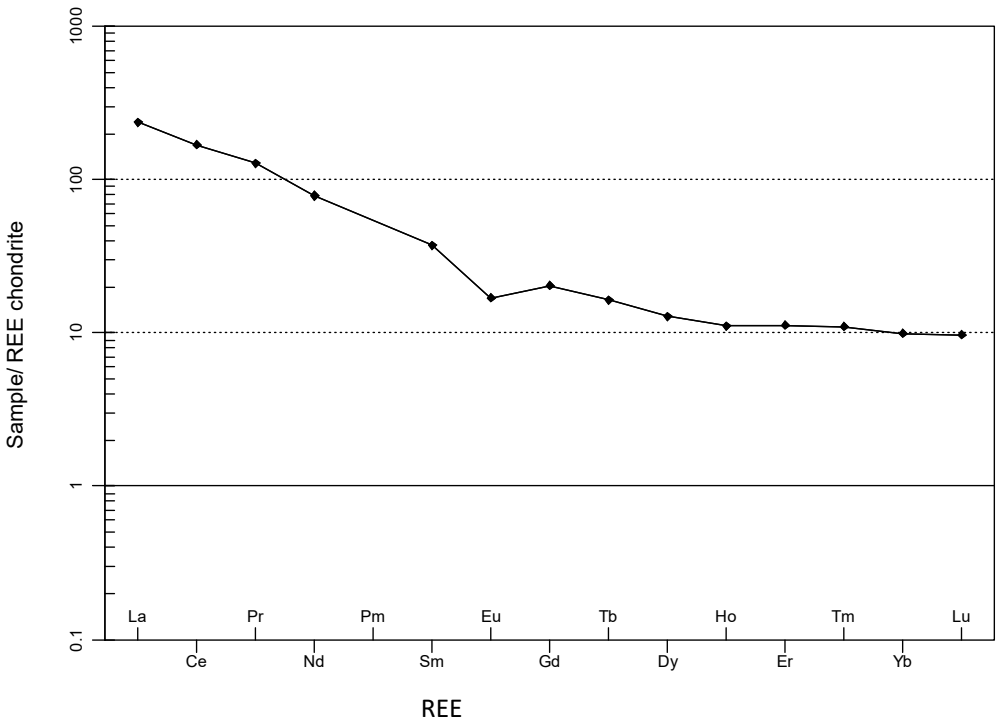

Fig.4.99 REE Chondrite Normalization of Pegmatite Sample (After Boynton, 1984).

4.1.5.3 Quartz Veins

Lenses and veins of quartz occurred abundantly in all the lithologic units in the study area. They varied in sizes and thickness with great irregularities in forms (Fig.4.100 and 4.101). Most of the quartz veins were concordant with the host rocks (Fig. 4.102).

4.1.5.4 Dolerite Dykes

Intrusion of dolerite dykes were found in some of the outcrops in the study area. They occurred as tabular and un-metamorphosed bodies crosscutting the foliated host rocks. Dolerite dykes found in the mapped area ranged from 3cm to 60cm in thickness. Some of the dyke contained rock xenoliths.

The dolerite dykes is usually black and fine grained. It makes sharp and chilled contact with the host rock and usually composed of mafic mineral. The dyke trends NE/SW (Fig. 4.103).

Fig.4.100 Irregular Exposure of Quartz Veins on the Granodioritic Gneiss. *Width ranges from 2-5cm. (Coordinate: N07^{o} 30.269', E 03^{o} 55.232')*

Fig.4.101 Quartz Phenocryst on the Granodioritic Gneiss. *About 30cm long, and 2cm thick. (Coordinate: N07^{o} 32.744', E 03^{o} 54.102')*

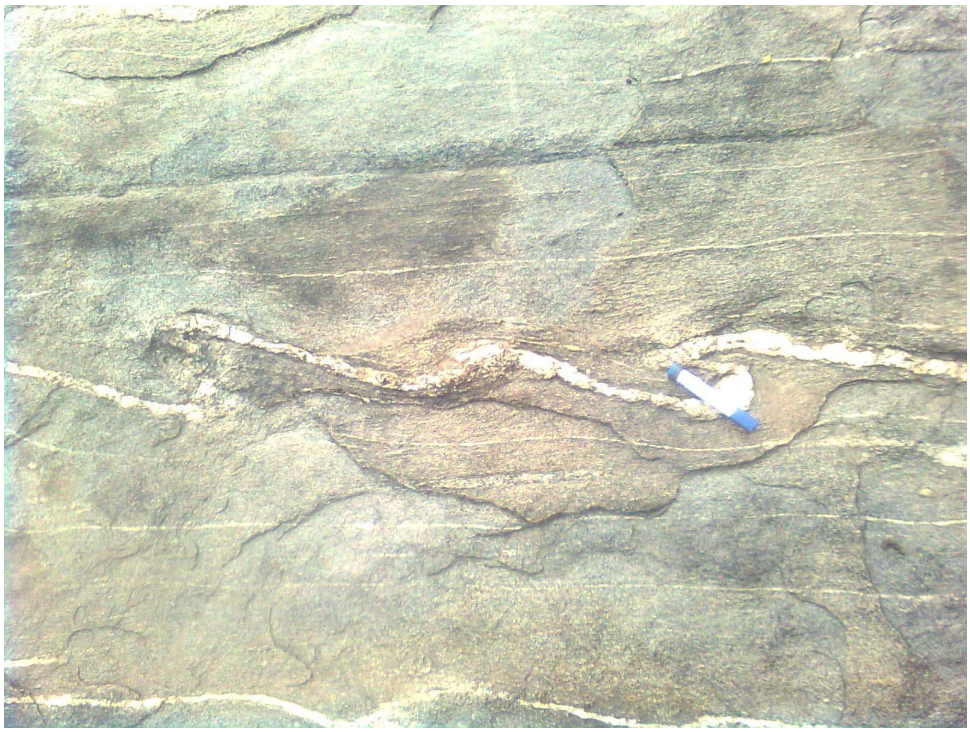

Fig.4.102 Concordant Quartz Vein diplaying ptygmatitic fold on the Biotite Hornlende Gneiss. *(Coordinate: N07^{o} 30.106', E 03^{o} 56.491')*

Fig. 4.103 Dolerite Dyke Intruded Biotite Hornblende Gneiss at Ositedo Village.
About 40cm thick and trending 80° NE. (Coordinate: N07° 30.106', E 03° 56.491')

4.2 Stuctural Elements

4.2.1 Regional Structural Orientation

The linear stuctural grains from aeromagnetic map showed the most defined lineaments are trending in NE – SW direction (Fig.4.104a) which was also confirmed on the Rose diagram plot (Fig.4.104b).

The residual magnetic intensity map (-118.1 to 82.6 nT) correspond to the various rock types in the study area which is directly related to thier susceptibilities (Fig.4.105).

4.2.2 Structures Observed on the Field

Foliation

In the gneissose rocks, the most conspicuous foliation surface is marked by parallel layers with alternating dark and light minerals (Fig. 4.106a). The foliation in the quartz schist are well developed schistosity defined by parallel alignment of mica and compositional banding while muscovite garnet schist only peeled off along micaceous laminae. The rocks are generally striking in NE-SW direction (Fig.1.106b) and are gentle to moderately dipping.

Crenulation cleavage is characteristised by earlier foliation (S_1) generally defined by preferred orientation of layer felsic minerals folded on a micro scale (Hobbs *et. al.*,1976). The fold (F_1) are assymetrical and recumbent (Fig. 4.107).

Lineation

Lineation occur as linear fabric elements that are repetitive on rock outcrops. The most common type of lineations found on the outcrops is mineral lineation. A mineral lineation is defined by preferred dimensional orientation of in-equant grains or by elongate mineral aggregates. In the gneisses, lineation is marked by linear arrangement of quartz minerals.

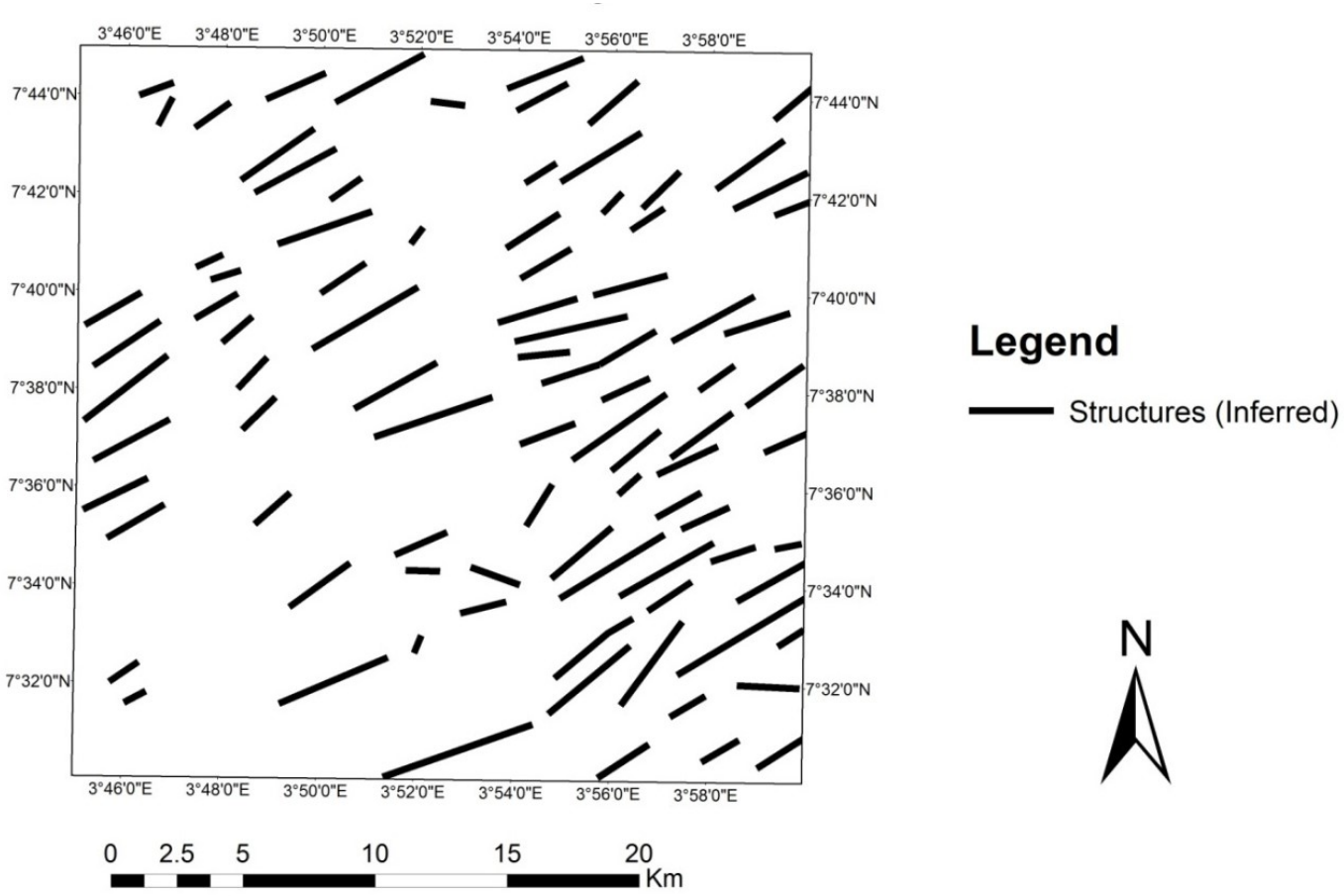

Fig.4.104a Lineaments Map of Sheet 241, Oyo SE from Aeromagnetic Map.

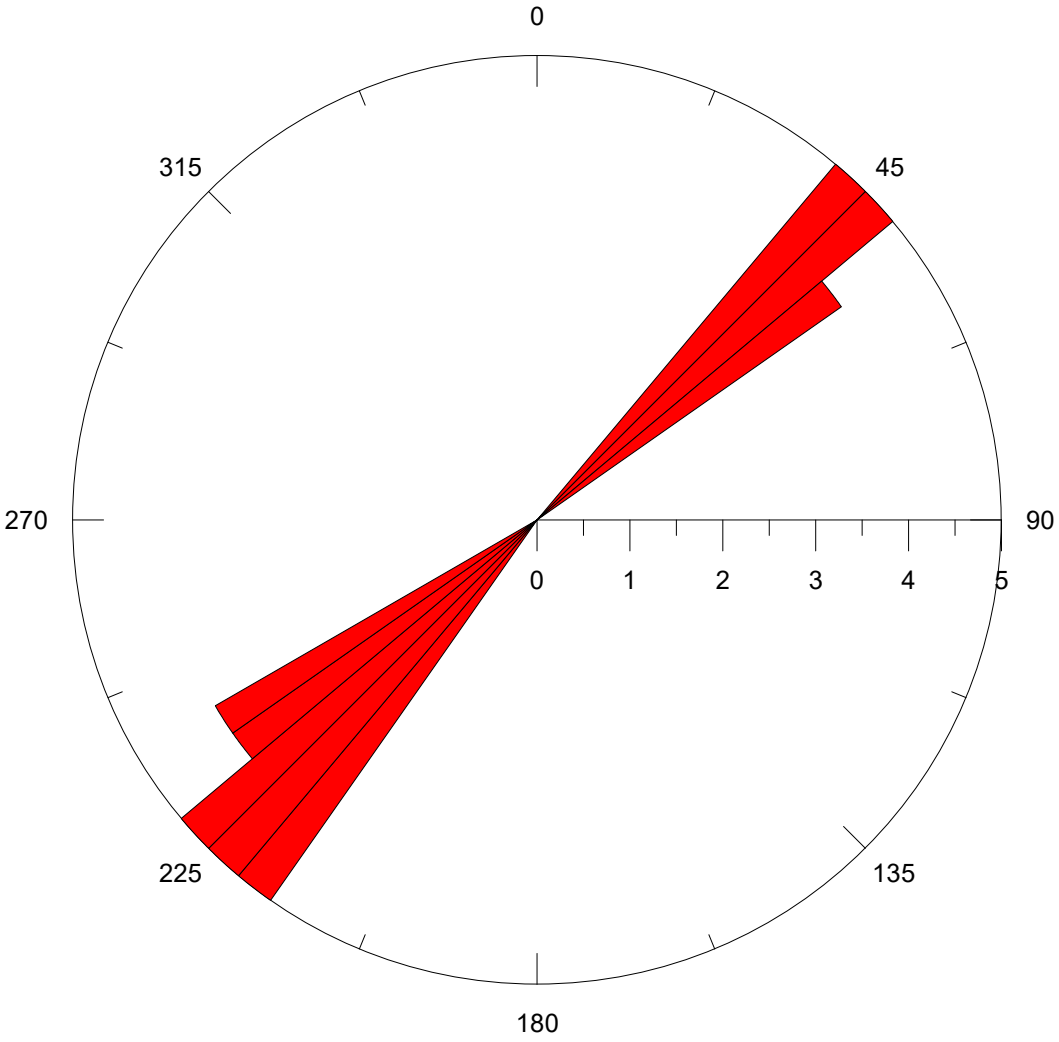

Fig.4.104b Rose Diagram for the Lineaments Map of Sheet 241, Oyo SE.

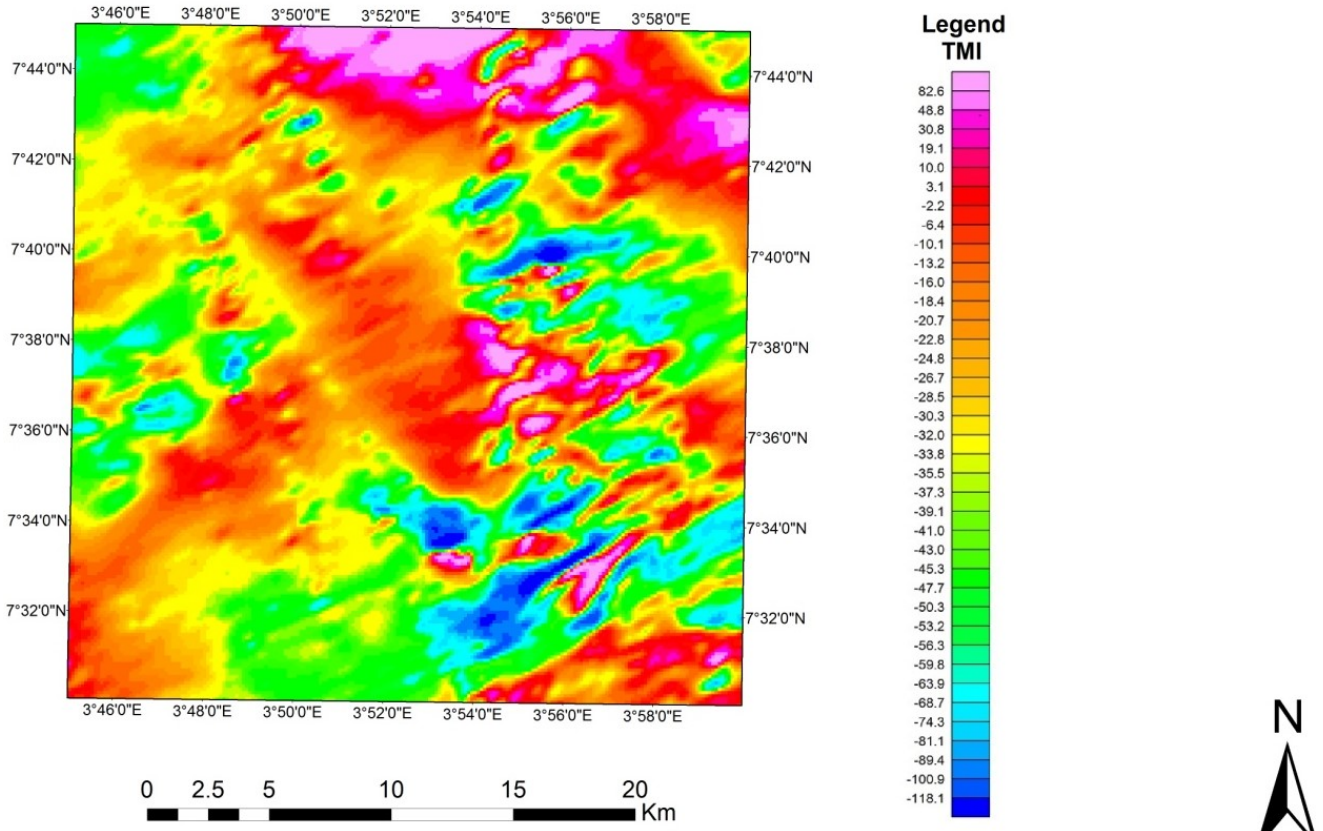

Fig.4.105 Regional Analytical Signal Map of Sheet 241, Oyo SE.

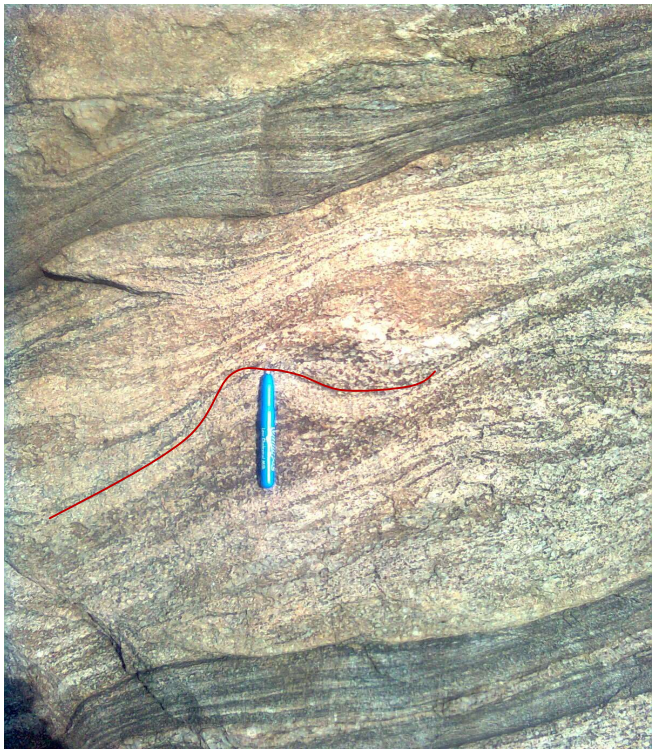

Fig.4.106a Migmatitic Biotite Hornblende Gneiss Outcrop Displaying Foliation Band Forming Symmetrical Fold. *(Coordinate: N07^{o} 30'20", E 03^{o} 55'29.9")*

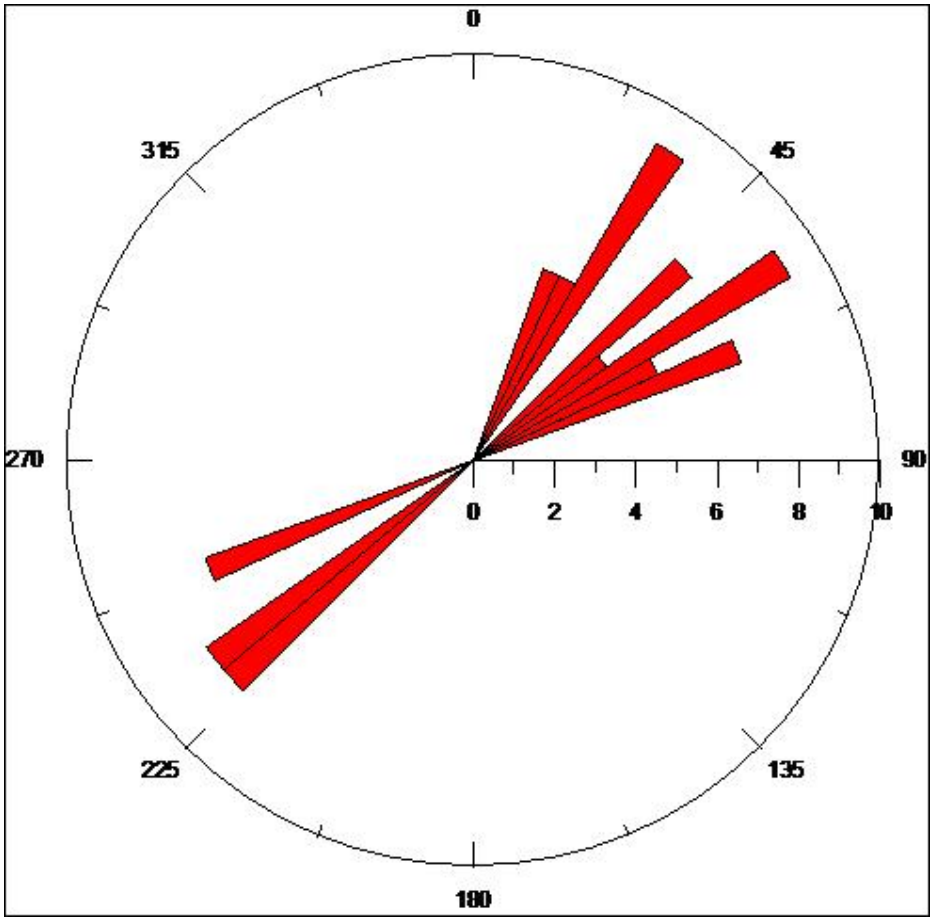

Fig. 4.106b Rose Diagram of Foliation Trends in the Quartz Schist and Gneissic Rocks (n=56).

Fig. 4.107 Biotite Hornblende Gneiss Outcrop Showing Crenulation Cleavage.
(Coordinate: N07^{o} 30.106', E 03^{o} 56.491')

Shear Zone

Shear zone occurs on region of localised ductile deformation on the gneiss outcrops (Fig. 4.108)

Folds

Sets of folds differing in styles are present in the study area. Minor folds were observed on outcrops of the gneisses and quartz schist. Figure 4.109 to 4.111 illustrate different fold styles that were observed in the field.

Joint

Joints were found on majority of the rock mapped. They are very notable on the gneisses (Fig.4.112). The rosette diagram for joint direction in the lithological units shows that the main direction is NW-SE and minor trending in NE-SW direction (Fig. 4.113).

Minor Fault

Minor faults were observed on the granite and gneiss outcrops. Strike slip sinistral fault (Fig. 4.114) which varies in displacement was mapped.

Fig 4.108 Shear Zone Trace Where Blocks of Rocks have been Displaced in a Fault like Manner, but without Prominent Development of Visible Faults in Biotite Hornblende Gneiss. *(Coordinate: N07^{o}32.400', E 03^{o} 55.894')*

Fig.4.109 Convolute Fold Trace in Quartz Schist.
(Coordinate: N07^{o}33.260', E 03^{o}.58.821')

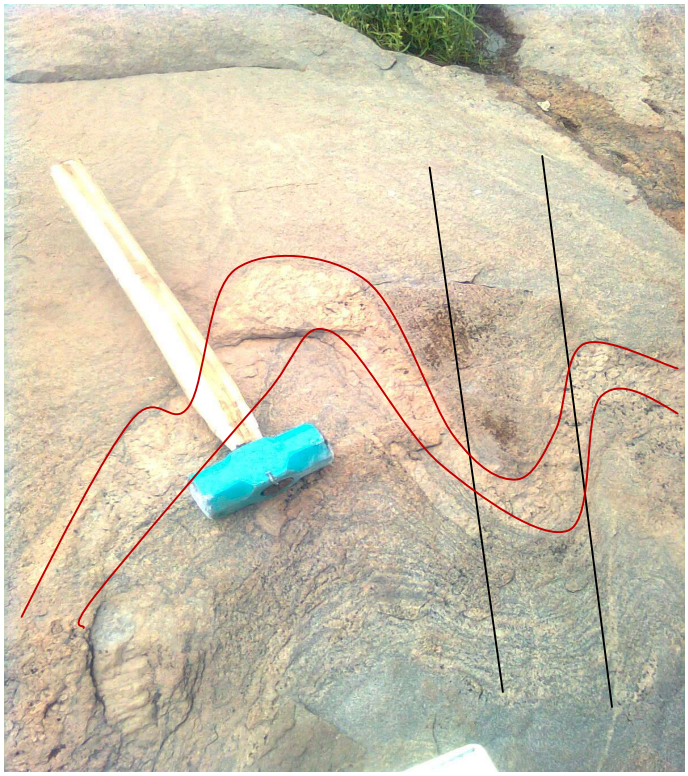

Fig.4.110 Symmetrical Fold in Biotite Hornblende Gneiss

Fig. 4.111a Parallel and Symmetrical Folds in Biotite Hornblende Gneiss Outcrop.

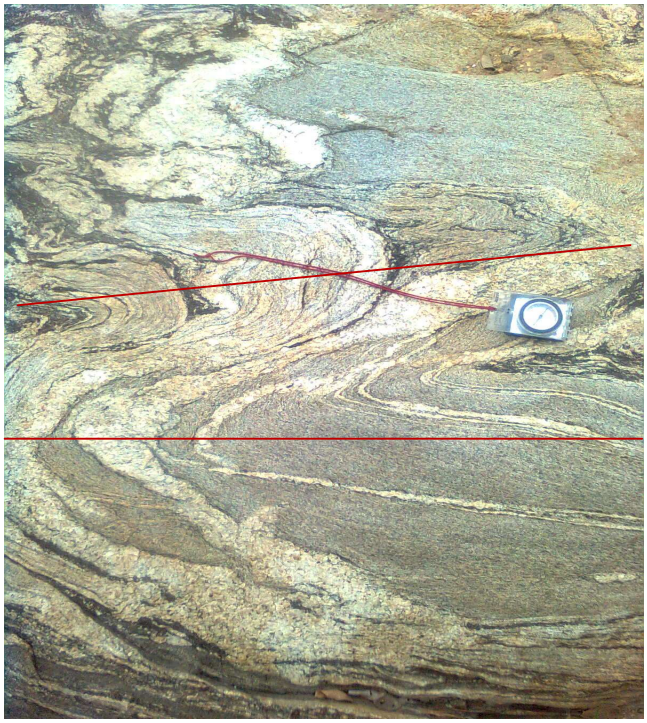

Fig. 4.111b Ptygmatic Folds caused by Ductile Deformation of Biotite Hornblende Gneiss.

Fig. 4.112 Joint on Migmatitic Biotite Hornblende Gneiss.

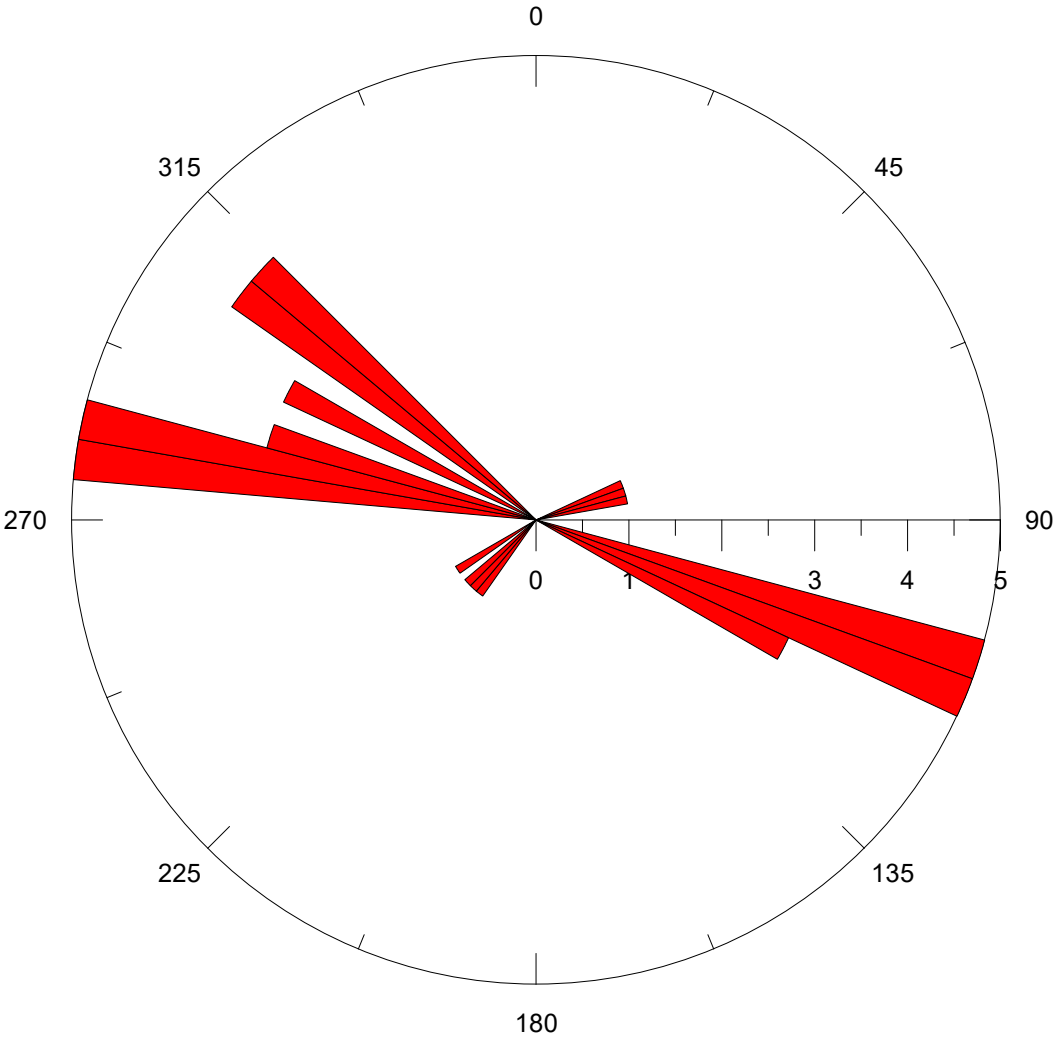

Fig. 4.113 Rose Diagram of Joint Trends in the Quartz Schist and Gneissous Rocks (n=45)

Fig. 4.114 Strike-slip Fault as Observed on Biotite Granite Gneiss. *(Coordinate: N07^{o}45.010', E 03^{o}.50.442')*

4.3 Geological Setting of the Study Area.

Field characteristics, petrography and geochemical study of the rocks in the study area revealed occurrences of quartzite, quartz and muscovite garnet schist, biotite hornblende gneiss, granodioritic and biotite granite gneisses, leucogranite, pegmatite and dolerite dyke.

The detained lithological information of the boundary delineation was deduced from ternary map of the Sheet 241, Oyo SE (Fig.4.115), which was used to produced the geology map of the study area on the scale of 1:50,000 (Fig.4.116). Lithological dimension which varies widely from small sizes to batholitic sizes were observed. Outcrops of bitiote granite gneiss, granodioritic gneiss, leucogranite and pocket of quartzite are distributed within the biotite hornblende gneiss on the western side. Quartz schist with minor occurrence of muscovite garnet schist and quartzite outcrop at the eastern side of the area (Fig.4.117).

The biotite granite gneiss was emplaced into the Migmatite-banded gneiss-quartzite complex of Ibadan area. This may be suggesting rocks of same age of Eburnean or older as obtained by Grant (1970) using a whole rock Rb-Sr isochron age of 2205 ± 70 m.y for Ibadan granite gneiss.

The produced map for the study area shows that biotite hornblende gneisses occupied a far more extensive area than any of the other rocks. It can be assumed that these gneisses were formed during the ancient granitic cycle (Rahaman, 1989). The gneisses were later intruded by granite rock during Pan African thermos-tectonic event (600 ± 150 Ma). The emplacement involved successive magmatism and differentiation.

On the bases of field relationship and association, quartz schist outcrops inter-banded with the gneisses. Quartzite can be suggested from the field relation to have been emplaced as rigdes within the quartz schist.

The dolerite dyke, quartz vein and pegmatite are un-metamorphosed. They are generally cross-cutting all pre-existing rocks of the study area. They are considered to be the youngest members.

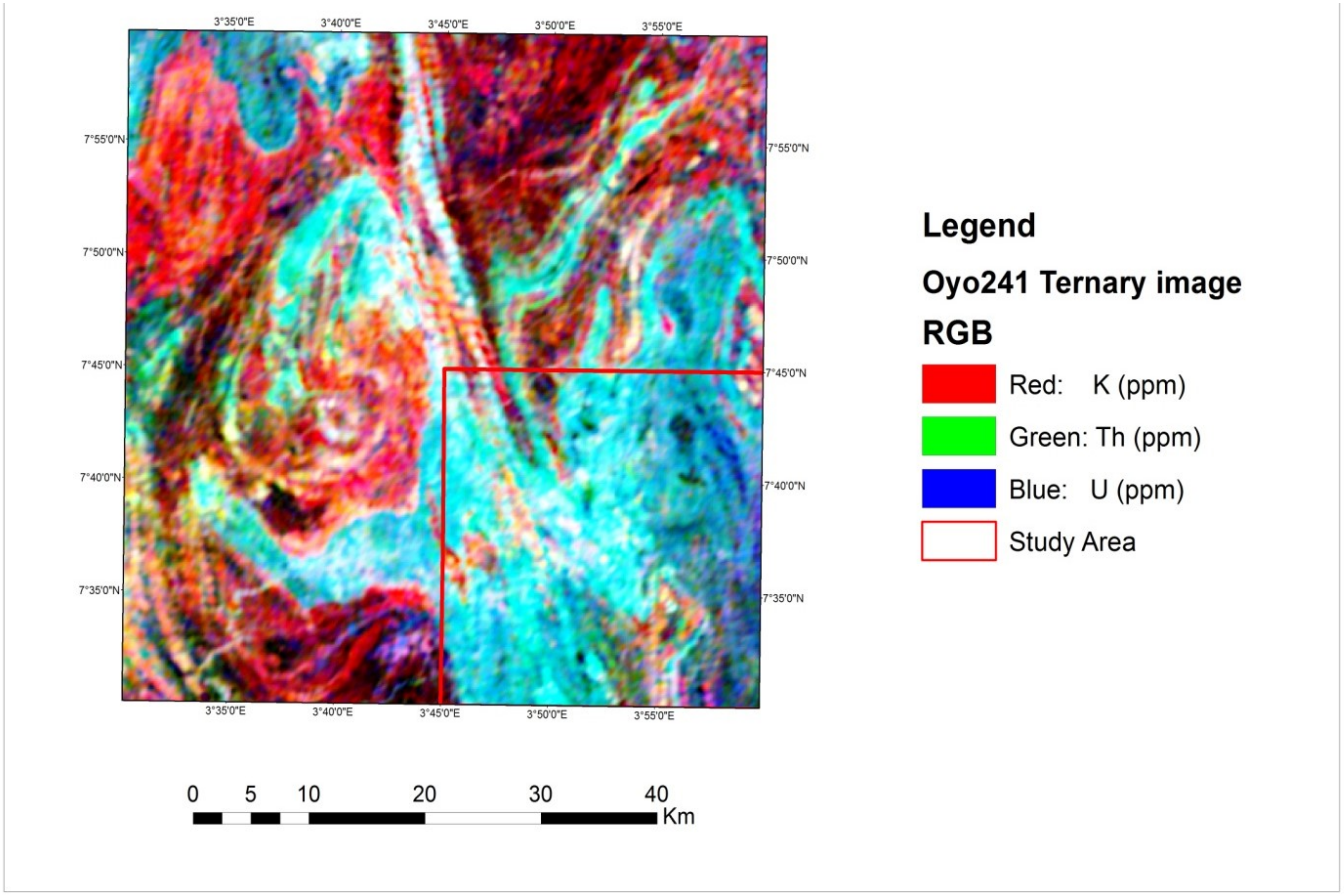

Fig.4.115 Ternary Image Map (K+Th+U) On Scale of 1:100 000

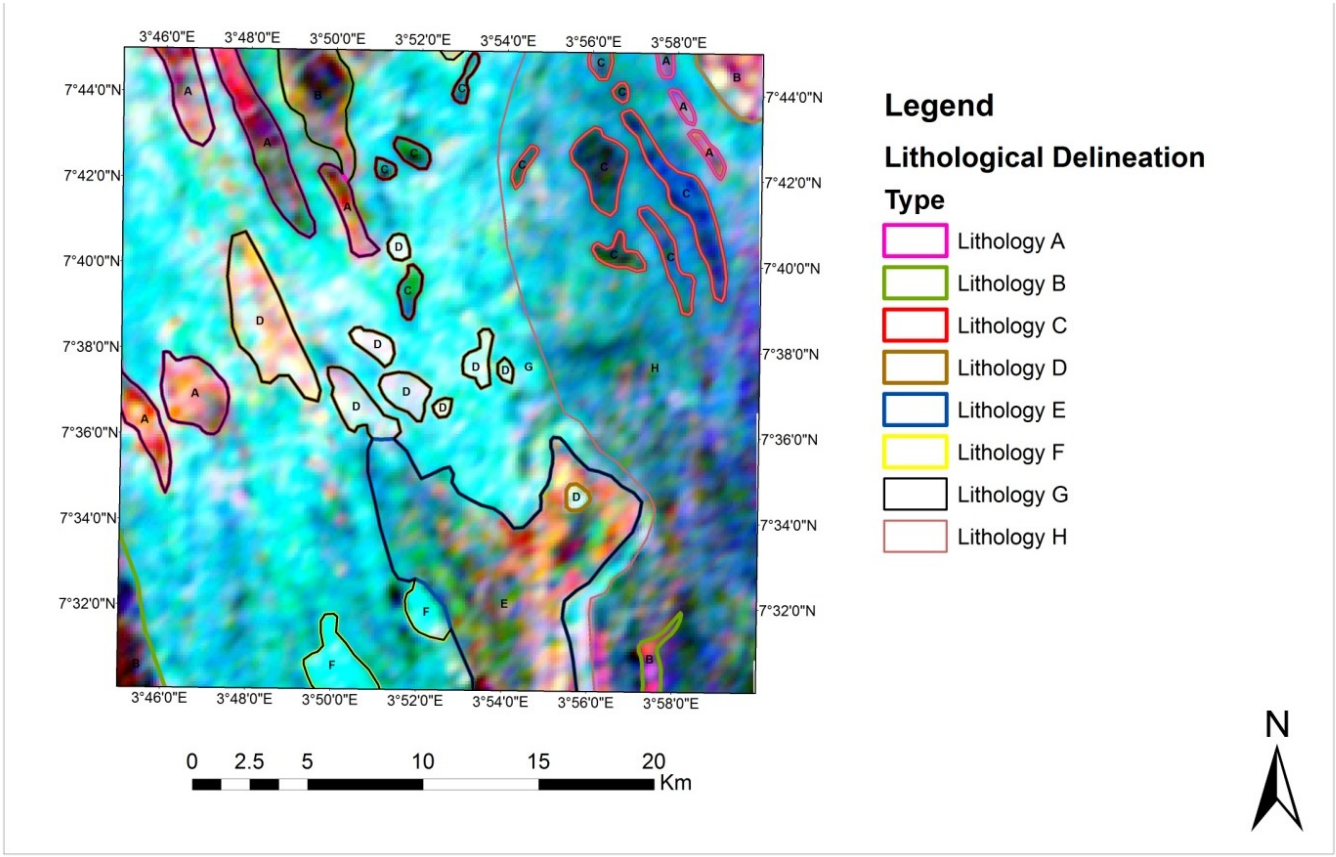

Fig.4.116 Ternary Image Map (K+Th+U) of the Study Area on Scale of 1:50 000.

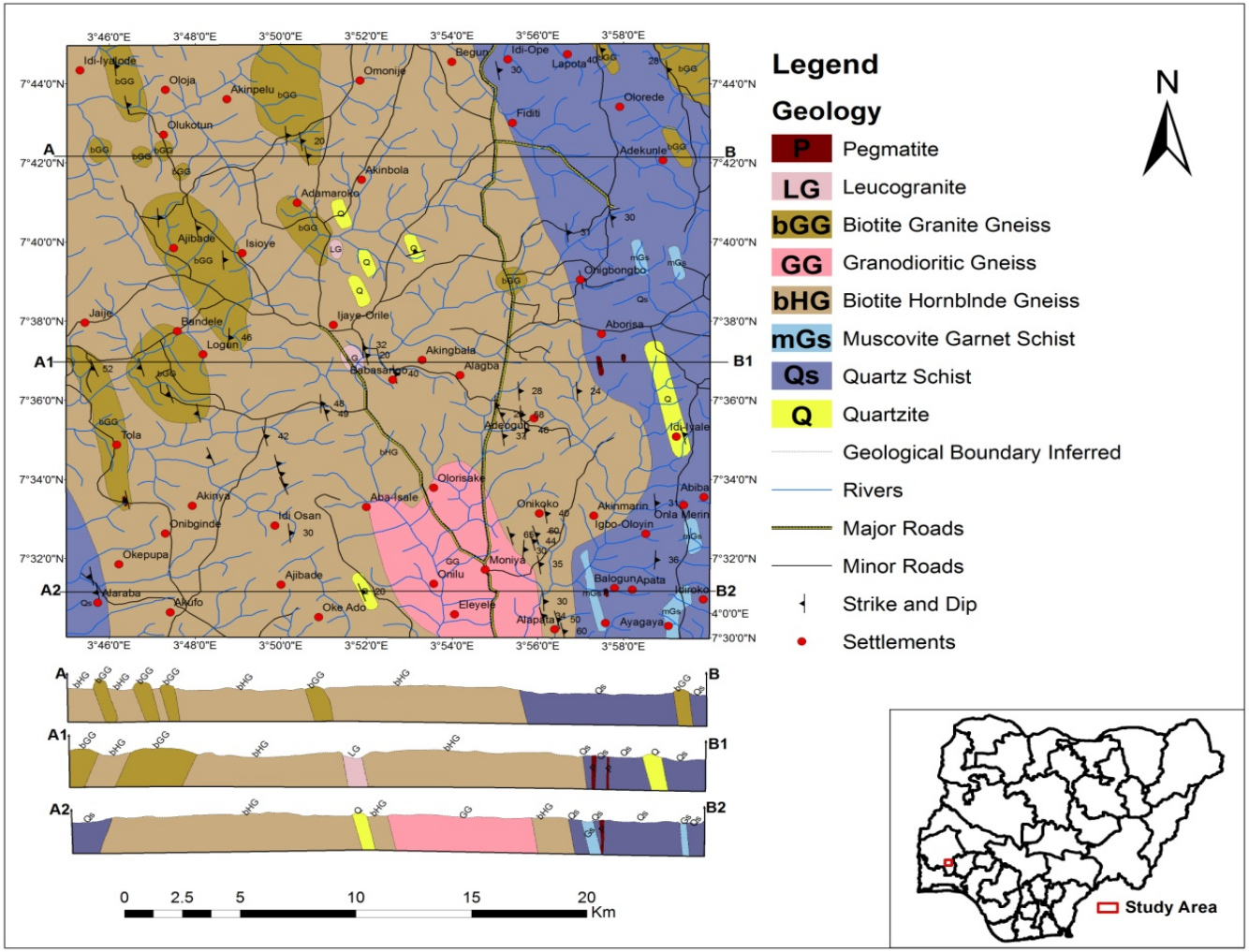

Fig.4.117 Geological map of the study area.

4.3.1 Metamorphism.

The mineralogical assemblages in each of the lithologic unit encountered in the field and in thin sections were employed to classify the degree of metamorphism. The quartzite composed quartz + plagioclase feldspar ± biotite ± sphene; quartz schist comprised quartz + plagioclase feldspar + biotite + muscovite ± microcline + chlorite + k-feldspar + hornblende ± apatite; while the muscovite garnet schist is comprised of quartz + plagioclase feldspar + muscovite + biotite + garnet ± chlorite. On the basis of mineral assemblage, the metapsammite (quartzite) and the metapelitic (schistose) rocks of the study area can be suggested to belong to the Epidote-Amphibolite Facies (due to the presence of almanditic garnet and chlorite.

The mineral assemblage of the gneissic rock is as follows: the biotite-hornblende gneiss comprises quartz + albite (oligoclase) + biotite + hornblende + orthoclase feldspars + muscovite ± microcline ± epidote; the granodioritic gneiss composed quartz + albite (oligolase to andesine) + biotite + hornblende ± muscovite+ orthoclase feldspar ± microcline ± epidote ± garnet; while the biotite granite gneiss composed of quartz + microcline + oligoclase ± hornblende ± muscovite ± garnet ± sphene ± epidote. The biotite-hornblende gneiss and the granodioritic gneiss can be suggested to belong to the Mid-Amphibolite Facies with conditions of pressure of 5-10 kbar and at temperature between 600-670^{0}C (Baker, 1998). Whereas, the biotite granite gneiss can be suggested to reach upper Amphibolite Facies condition (about 700^{0}C) due to the lack of muscovite and the presence of k-felspars that sometime occurs as pods or augens, discontinous segregation layers which arised from partial melting of the protholith rocks (Baker, 1998).

4.4 Mineral Chemistry

All the analysed rocks samples are composed of feldspars and biotites, while a sample of the granodioritic and biotite granite gneiss contain hornblende minerals in addition. There are garnet, chlorite, zircon, apatite, titanite (sphene), rutite and magnetite as accessory minerals in some of the samples of granodioritic and biotite granite gneiss.

4.4.1 Feldspars

The plagioclase feldspars crystals occur as subhedral laths and were closely in contact with quartz and K-feldsapars minerals (Fig.4.118 and 4.119).

Major oxide composition (Table 4.29 and Table 4.32) results generally showed higher content of SiO_2 varying from 59.82 to 66.56 wt.% and Al_2O_3 content varying from 20.37 to 23.41wt.%. The amount of TiO_2, K_2O and MgO contents were low. Concentration of FeO, CaO and Na_2O range from 0.0 to 1.83 wt.%, 2.47 to 6.56wt% and 6.49 to 11.19wt%, respectively. Chemical composition of the plagioclases was calculated on the basis of 32 O_2 atoms, using Ca-Na-K ratios and with all Fe as FeO (and solving for Fe^{3+}) (Table 4.30 and 4.33) showed the plagioclases were predominantly of oligoclase ($An_{10.43}$to $An_{27.82}$) to low andesine ($An_{31.42}$ to $An_{31.81}$) varieties (Table 4.31 and Table 4.34) in the granodioritic gneiss .

Alkali feldspars were few in the granodioritic gneiss (Tables 4.35). The values of SiO_2 varying from 63.70 to 69.15wt.% and Al_2O_3 varying from 16.77 to 18.26wt.% were analysed. The concentrations of TiO_2, FeO, CaO and MgO yielded low values. The content of BaO ranged from 0.32 to 0.96wt%, while Na_2O and K_2O ranged from 0.83 to 1.68wt% and 11.47 to 16.70wt% respectively. There is negligible value of anorthite (An) components (Tables 4.37), Orthoclase composition in the granodioritic gneiss ranged from $Or_{83.32}$ $Ab_{16.68}$ to $Or_{92.98}Ab_{7.02}$ (Fig.4.120).

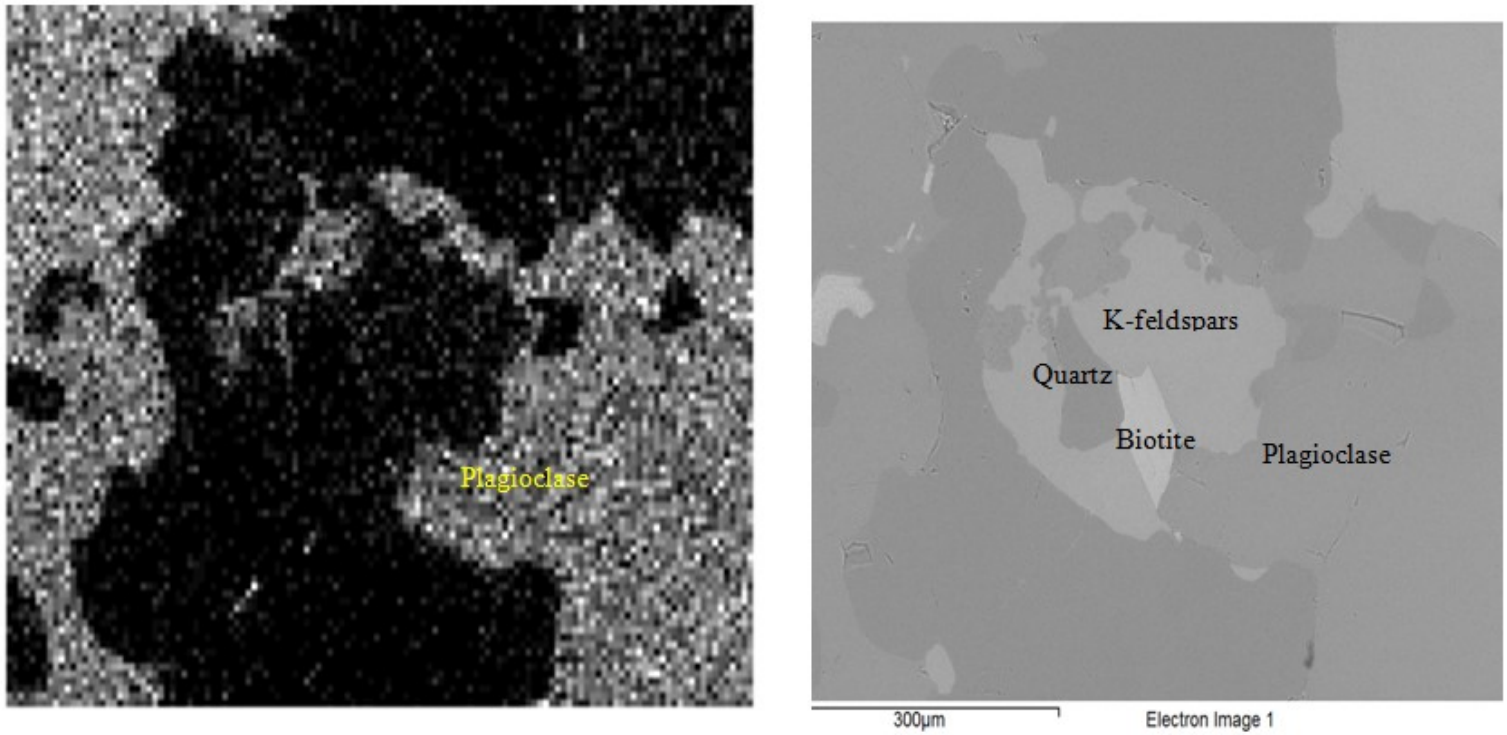

Fig.4.118 Micro-Probe Image of Plagioclase Feldspars of Oligoclase Composition ($An_{23.81}Ab_{71.21}Or_{4.98}$) and Orthoclase ($Or_{84.08}Ab_{15.02}$) in the Granodioritic Gneiss (coordinate: N07^o 30.887′, E 03^o 53.516′)

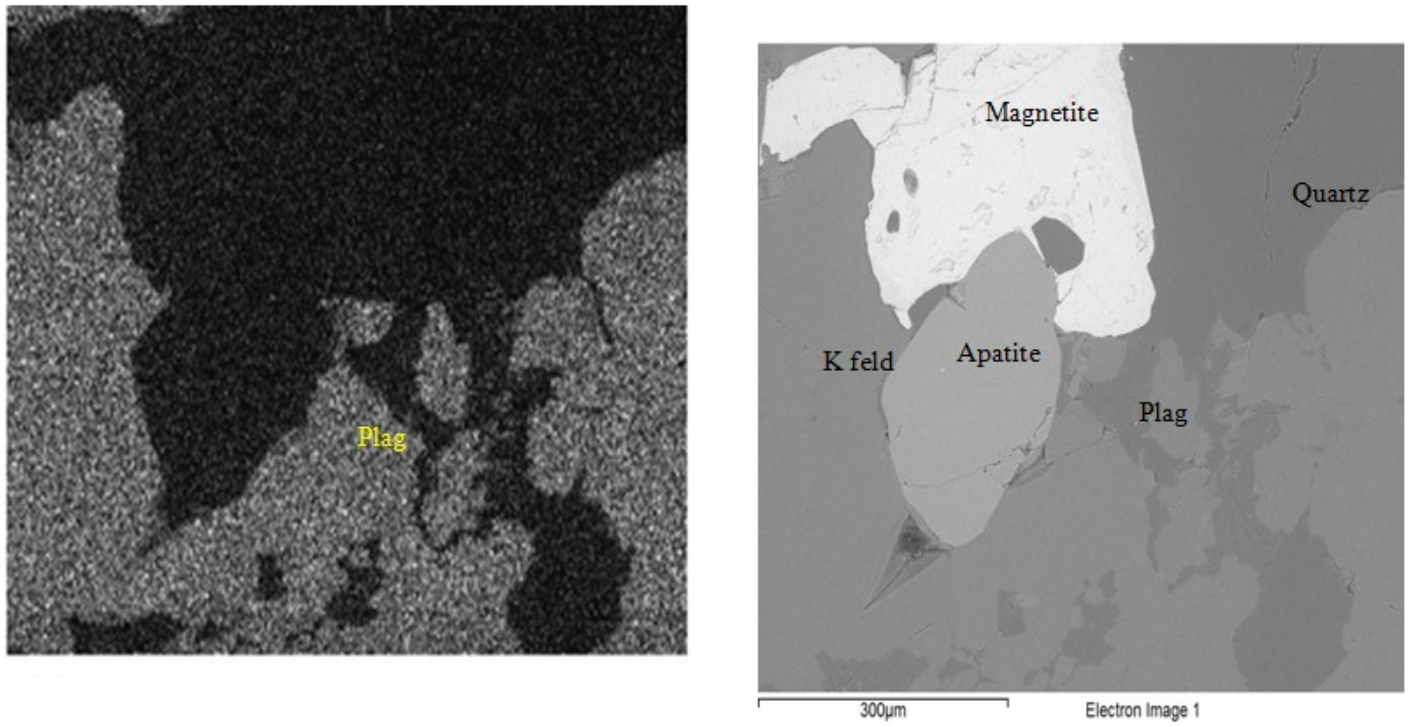

Fig.4.119 Micro-Probe Image of Plagioclase Feldspars of Oligoclase Composition ($An_{9.19}Ab_{73.90}Or_{16.90}$) and Orthoclase ($Or_{92.13}Ab_{7.87}$) in the Biotite Granite Gneiss (coordinate: N07^o 43.541′, E 03^o 46.330′)

Table 4.29 Representative Mineral Chemistry of Plagioclase Feldspars in Granodioritic Gneiss.

Sample no	G11														
Analyses	1	2	3	4	5	6	7	8	9	10	11	12	13	14	15
SiO_2	65.14	63.95	66.27	65.66	65.93	65.80	66.56	65.77	64.13	63.39	65.35	59.82	59.98	62.35	62.66
TiO_2	0.00	0.00	0.00	0.00	0.00	0.00	0.00	0.00	0.00	0.00	0.00	1.46	1.77	0.00	0.27
Al_2O_3	21.53	22.61	21.13	21.61	20.83	20.77	20.37	20.48	22.28	22.50	21.59	21.93	21.80	22.36	21.84
FeO	0.37				0.63	0.63	0.62	0.93	0.53	0.81	0.40	1.83	1.45	1.29	1.34
MgO						0.27	0.30	0.41				0.66	0.51	0.52	0.45
CaO	4.58	5.10	4.53	4.69	4.51	4.52	4.52	4.40	4.99	5.02	4.90	6.40	6.56	5.49	5.19
BaO															
Na_2O	7.58	7.91	7.13	7.80	7.13	6.92	6.49	6.85	7.78	7.84	7.33	7.39	7.48	7.65	7.81
K_2O	0.80	0.43	0.94	0.23	0.98	1.10	1.13	1.15	0.30	0.43	0.43	0.51	0.44	0.34	0.43
Total	100.00	100.00	100.00	100.00	100.00	100.00	100.00	100.00	100.00	100.00	100.00	100.00	100.00	100.00	100.00

Table 4.30 Structural Formulae of Plagioclase Feldspar in Granodioritic Gneiss.

Structural Formulae based on 32 O_2															
Sample no	**G11**														
Analyses	1	2	3	4	5	6	7	8	9	10	11	12	13	14	**15**
Si	2.92	2.86	2.98	2.94	2.97	2.97	3.01	2.97	2.87	2.84	2.94	2.69	2.70	2.79	2.81
Ti	0.00	0.00	0.00	0.00	0.00	0.00	0.00	0.00	0.00	0.00	0.00	0.05	0.06	0.00	0.01
Al	1.14	1.19	1.12	1.14	1.11	1.10	1.09	1.09	1.18	1.19	1.14	1.16	1.16	1.18	1.15
Fe^{+3}	0.00	0.00	0.00	0.00	0.00	0.00	0.00	0.00	0.00	0.00	0.00	0.01	0.00	0.00	0.00
Fe^{+2}	0.01	0.00	0.00	0.00	0.02	0.02	0.02	0.04	0.02	0.03	0.02	0.05	0.05	0.05	0.05
Mn	0.00	0.00	0.00	0.00	0.00	0.00	0.00	0.00	0.00	0.00	0.00	0.00	0.00	0.00	0.00
Mg	0.00	0.00	0.00	0.00	0.00	0.02	0.02	0.03	0.00	0.00	0.00	0.04	0.03	0.03	0.03
Ca	0.22	0.24	0.22	0.23	0.22	0.22	0.22	0.21	0.24	0.24	0.24	0.31	0.32	0.26	0.25
Ba	0.00	0.00	0.00	0.00	0.00	0.00	0.00	0.00	0.00	0.00	0.00	0.00	0.00	0.00	0.00
Na	0.66	0.69	0.62	0.68	0.62	0.61	0.57	0.60	0.68	0.68	0.64	0.64	0.65	0.66	0.68
K	0.05	0.02	0.05	0.01	0.06	0.06	0.07	0.07	0.02	0.02	0.02	0.03	0.03	0.02	0.02
tot. cat.	5.00	5.00	5.00	5.00	5.00	5.00	5.00	5.00	5.00	5.00	5.00	5.00	5.00	5.00	5.00
tot. oxy.	8.14	8.10	8.21	8.17	8.19	8.19	8.24	8.18	8.11	8.08	8.18	7.99	8.00	8.04	8.04

Table 4.31 End Member Composition of Plagioclase Feldspars in Granodioritic Gneiss

Sample no G11															
End Member	1	2	3	4	5	6	7	8	9	10	11	12	13	14	15
An	23.81	25.59	24.43	24.56	24.28	24.62	25.67	24.21	25.68	25.46	26.24	31.42	31.81	27.82	26.18
Ab	71.21	71.83	69.56	73.98	69.46	68.27	66.69	68.23	72.49	71.94	71.02	65.63	65.65	70.13	71.22
Or	4.98	2.58	6.01	1.45	6.26	7.11	7.63	7.56	1.83	2.59	2.74	2.96	2.54	2.05	2.60

Table 4.32 Representative Electron Microprobe Analyses of Plagioclase Feldspar in Granodioritic Gneiss.

Sample no	G6								
Analyses	1	2	3	4	5	6	7	8	9
SiO_2	61.88	63.01	62.63	62.45	61.25	61.55	63.41	64.51	65.22
TiO_2	0.00	0.00	0.00	0.00	0.00	0.00	0.00	0.00	0.00
Al_2O_3	23.37	22.75	22.72	22.78	23.41	23.21	22.34	21.21	21.26
Fe(O)t	0.00	0.00	0.00	0.00	0.00	0.00	0.00	0.12	0.00
CaO	5.19	4.05	4.37	4.38	5.16	5.01	3.90	2.97	2.37
BaO	0.00	0.00	0.00	0.00	0.00	0.00	0.00	0.00	0.00
Na_2O	9.55	10.42	9.90	10.02	9.36	9.49	10.26	11.01	11.19
K_2O	0.14	0.08	0.11	0.17	0.15	0.14	0.16	0.00	0.11
Total	100.13	100.30	99.73	99.79	99.34	99.39	100.08	99.83	100.14

Table 4.33 Structural Formulae of Plagioclase Feldspar in Granodioritic Gneiss.

Structural Formulae based on 32 O_2									
Sample no	G6								
Analyses	1	2	3	4	5	6	7	8	9
Si	2.72	2.75	2.76	2.75	2.72	2.73	2.78	2.83	2.84
Al	1.21	1.17	1.18	1.18	1.22	1.21	1.15	1.10	1.09
Fe3	0.00	0.00	0.00	0.00	0.00	0.00	0.00	0.00	0.00
Ca	0.24	0.19	0.21	0.21	0.25	0.24	0.18	0.14	0.11
Ba	0.00	0.00	0.00	0.00	0.00	0.00	0.00	0.00	0.00
Na	0.81	0.88	0.85	0.85	0.80	0.82	0.87	0.93	0.95
K	0.01	0.00	0.01	0.01	0.01	0.01	0.01	0.00	0.01
tot. cat.	5.00	5.00	5.00	5.00	5.00	5.00	5.00	5.00	5.00
tot. oxy.	7.92	7.89	7.92	7.91	7.92	7.92	7.92	7.91	7.91

Table 4.34 End Member Composition of Plagioclase Feldspars in Granodioritic Gneiss.

Sample no G6 End member									
An	22.92	17.60	19.48	19.28	23.18	22.42	17.21	12.99	10.43
Ab	76.34	81.97	79.92	79.84	76.00	76.86	81.94	87.01	88.99
Or	0.73	0.43	0.59	0.88	0.82	0.72	0.86	0.00	0.58

Table 4.35 Representative Electron Microprobe Analyses of Alkali Feldspar in Granodioritic Gneiss.

Sample no	G11							G6							
Analyses	1	2	3	4	5	6	7	1	2	3	4	5	6	7	8
SiO_2	68.43	68.29	67.49	69.15	67.80	67.32	67.03	63.70	63.81	63.97	64.47	64.14	63.84	63.81	64.23
TiO_2	0.00	0.00	0.00	0.00	0.00	0.00	0.00	0.00	0.00	0.00	0.00	0.00	0.00	0.00	0.00
Al_2O_3	17.18	17.32	17.31	16.77	17.62	17.08	17.09	17.81	18.09	18.26	18.25	18.38	18.11	18.10	18.23
FeO	0.30	0.00	0.83	0.40	0.00	1.07	1.24	0.15	0.00	0.00	0.00	0.00	0.00	0.00	0.00
MgO	0.00	0.00	0.00	0.00	0.00	0.39	0.50	0.00	0.00	0.00	0.00				
CaO	0.00	0.00	0.00	0.00	0.00	0.00	0.00	0.00	0.00	0.00	0.00	0.00	0.16	0.11	0.00
BaO	0.88	1.00	1.06	0.90	0.87	0.96	0.94	0.48	0.51	0.50	0.46	0.47	0.41	0.45	0.32
Na_2O	1.38	1.36	1.55	1.32	1.53	1.24	1.11	0.83	0.96	1.04	1.68	1.38	1.19	1.28	0.95
K_2O	11.83	12.03	11.76	11.47	12.18	11.94	12.07	16.70	16.65	16.41	15.19	15.74	16.39	16.27	16.43
Total	100.00	100.00	100.00	100.00	100.00	100.00	100.00	99.67	100.02	100.26	100.05	100.11	100.09	100.09	100.15

Table 4.36 Structural Formulae of Alkali Feldspar in Granodioritic Gneiss.

Structural Formulae based on 32 O_2															
Sample no	**G11**							**G6**							
Analyses	1	2	3	4	5	6	7	1	2	3	4	5	6	7	8
Si	3.20	3.19	3.15	3.24	3.16	3.15	3.14	2.95	2.94	2.94	2.96	2.95	2.94	2.94	2.96
Ti	0.00	0.00	0.00	0.00	0.00	0.00	0.00	0.00	0.00	0.00	0.00	0.00	0.00	0.00	0.00
Al	0.95	0.95	0.95	0.93	0.97	0.94	0.94	0.97	0.98	0.99	0.99	1.00	0.98	0.98	0.99
Fe^{+3}	0.00	0.00	0.00	0.00	0.00	0.00	0.00	0.01	0.00	0.00	0.00	0.00	0.00	0.00	0.00
Fe^{+2}	0.01	0.00	0.03	0.02	0.00	0.04	0.05	0.00	0.00	0.00	0.00	0.00	0.00	0.00	0.00
Mn	0.00	0.00	0.00	0.00	0.00	0.00	0.00	0.00	0.00	0.00	0.00	0.00	0.00	0.00	0.00
Mg	0.00	0.00	0.00	0.00	0.00	0.03	0.04	0.00	0.00	0.00	0.00	0.00	0.00	0.00	0.00
Ca	0.00	0.00	0.00	0.00	0.00	0.00	0.00	0.00	0.00	0.00	0.00	0.00	0.01	0.01	0.00
Ba	0.02	0.02	0.02	0.02	0.02	0.02	0.02	0.01	0.01	0.01	0.01	0.01	0.01	0.01	0.01
Na	0.12	0.12	0.14	0.12	0.14	0.11	0.10	0.07	0.09	0.09	0.15	0.12	0.11	0.11	0.08
K	0.71	0.72	0.70	0.68	0.72	0.71	0.72	0.99	0.98	0.96	0.89	0.92	0.96	0.95	0.96
tot. cat.	5.00	5.00	5.00	5.00	5.00	5.00	5.00	5.00	5.00	5.00	5.00	5.00	5.00	5.00	5.00
tot. oxy.	8.25	8.25	8.21	8.30	8.21	8.21	8.20	7.91	7.90	7.91	7.94	7.92	7.89	7.89	7.93

Table 4.37 End Member Composition of Alkali Feldspars in Granodioritic Gneiss.

Sample no G11																
End Member	1	2	3	4	5	6	7	G6 1	2	3	4	5	6	7	8
An	0.00	0.00	0.00	0.00	0.00	0.00	0.00	0.00	0.00	0.00	0.00	0.00	0.74	0.51	0.00
Ab	15.02	14.63	16.68	14.87	15.99	13.64	12.27	7.02	8.08	8.76	14.42	11.78	9.83	10.63	8.06
Or	84.98	85.37	83.32	85.13	84.01	86.36	87.73	92.98	91.92	91.24	85.58	88.22	89.43	88.86	91.94

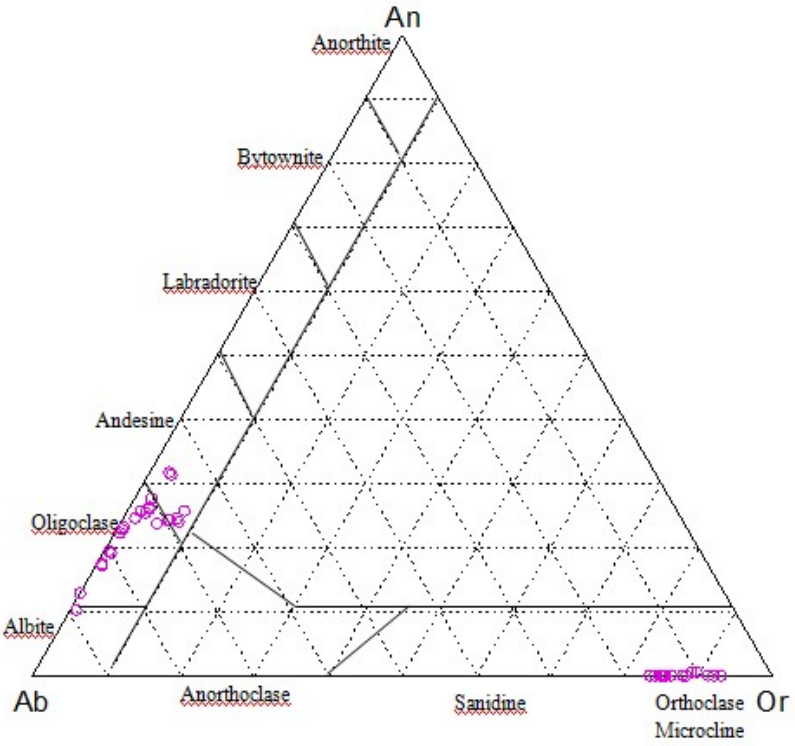

Fig.4.120 Plot of Ab-An-Or for Feldspars in the Granodioritic Gneiss (After Deer *et. al.*, 1963)

Major oxide composition of plagioclase feldspars in the biotite granite gneiss (Table 4.38 and Table 4.41) revealed that the concentration of SiO_2 ranged from 61.47 to 71.60wt.%; Al_2O_3: 16.57 to 24.5wt.% and CaO ranged from 0.45 to 5.32. The contents of Na_2O and K_2O ranged from 3.06 to 11.52wt% and 0.08 to 1.05wt%, respectively. Mineral chemistry of the plagioclase in the biotite granite gneiss were mainly of oligoclase composition ($An_{11.46}$ to $An_{27.82}$), with surbodinate high andesine ($An_{47.68}Ab_{49.66}Or_{2.66}$) and ranged of albite composition from $An_{2.28}Ab_{91.36}Or_{6.36}$ to $An_{9.46}Ab_{90.15}Or_{0.39}$ (Table 4.40 and Table 4.43, Fig.4.121).

Alkali feldspars were more visible in the biotite granite gneiss than in other rock units that were investigated in the study area (Tables 4.44 to 4.52). The values of SiO_2 ranged from 58.36 to 83.07wt.% and Al_2O_3 ranged from 9.60 to 31.05wt.%. The concentrations of Na_2O and K_2O ranged from 0.43 to 8.27wt% and 1.41 to 15.72wt%, respectively. Sodium rich microcline in the biotite granite gneiss samples, where the values of Ab increased from 73.90 to 81.46 mole percent ($Or_{14.05}Ab_{81.46}An_{4.49}$; $Or_{20.70}Ab_{73.93}An_{5.37}$ and $Or_{16.90}Ab_{73.90}An_{9.20}$) were observed. There is significant variation in microcline component with lower composition of $Or_{71.50}$ to higher composition of $Or_{95.26}$ in the biotite granite gneiss arising in perthitic microcline and with subordinate $Or_{47.37}Ab_{49.56}An_{3.08}$ (Fig.4.121).

Mineral chemistry of plagioclase feldspars in the biotite hornblende gneiss (Tables 4.53 to 4.55) revealed little variations in the range of concentrations of SiO_2 (64.69 to 65.18wt %); Al_2O_3 (21.11 to 21.40wt %); CaO (2.44 to 2.65wt %) and Na_2O (10.59 to 11.06wt %) in the plagioclase feldspars (Table 4.53). The composition of plagioclase in the biotite hornblende gneiss sample displays low oligoclase ($An_{11.15}$ to $An_{11.75}$) content (Fig.4.122).

Major oxide contents of the alkali feldspars in the biotite hornblende gneiss revealed concentrations of SiO_2 ranged from 64.18 to 64.62wt % and Al_2O_3 ranged from 17.96 to 18.20wt %. Na_2O and K_2O ranged from 0.90 to 2.91wt % and 14.13 to 16.46wt %, respectively (Table 4.53). The alkali feldspars showed that the orthoclase compositions ranged between $Or_{75.76}$ to $Or_{92.35}$ (Fig4.122). The presence of both sodic plagioclase and orthoclase or microcline in all the rock units suggests crystallization under a subsolvus condition and of medium to high temperatures of formation.

Table 4.38 Representative Electron Microprobe Analyses of Plagioclase Feldspar in Biotite Granite Gneiss.

Sample no	**b3**						**b4**									
Analyses	1	2	3	4	5	6	1	2	3	4	5	6	7	8	9	10
SiO_2	66.20	61.63	61.68	62.14	62.22	61.92	62.24	61.70	61.78	61.91	61.47	61.61	61.78	64.48	66.09	62.24
TiO	0.00	0.00	0.00	0.00	0.00	0.00	0.00	0.00	0.00	0.00	0.00	0.00	0.00	0.00	0.00	0.00
Al_2O_3	24.57	23.16	23.00	23.46	23.36	23.27	23.22	23.08	23.08	23.12	23.35	23.11	23.27	21.46	20.37	23.22
Fe_2O_3	0	0	0	0	0	0	0.00	0.00	0.00	0.00	0.00	0.00	0.00	0.00	0.00	0.00
Fe(O)t	0.17	0.14	0.00	0.14	0.00	0.13	0.16	0.16	0.14	0.00	0.00	0.00	0.00	0.00	0.00	0.16
MnO	0	0	0	0	0.14	0	0.00	0.00	0.00	0.00	0.00	0.00	0.00	0.00	0.00	0.00
CaO	5.32	5.10	5.00	5.05	5.07	5.15	4.82	4.94	5.02	4.80	4.95	4.98	4.92	2.90	1.51	4.82
BaO	0.00	0.00	0.00	0.00	0.00	0.00	0.00	0.00	0.00	0.00	0.00	0.00	0.00	0.00	0.00	0.00
Na_2O	3.06	9.24	9.23	9.15	9.36	8.71	9.54	9.58	9.35	9.56	9.41	9.57	9.33	10.77	11.52	9.54
K_2O	0.25	0.25	0.13	0.14	0.15	0.17	0.20	0.08	0.25	0.18	0.18	0.16	0.28	0.11	0.09	0.20
Total	99.57	99.51	99.04	100.09	100.29	99.35	100.2	99.54	99.61	99.57	99.37	99.44	99.58	99.71	99.57	100.2

Table 4.39 Structural Formulae of Plagioclase Feldspar in Biotite Granite Gneiss.

Structural Formulae based on $32O_2$																
Sample no	b3						b4									
Analyses	1	2	3	4	5	6	1	2	3	4	5	6	7	8	9	10
Si	3.09	2.73	2.75	2.74	2.74	2.76	2.74	2.73	2.74	2.74	2.73	2.73	2.74	2.83	2.87	2.89
Ti	0.00	0.00	0.00	0.00	0.00	0.00	0.00	0.00	0.00	0.00	0.00	0.00	0.00	0.00	0.00	0.00
Al	1.35	1.21	1.21	1.22	1.21	1.22	1.20	1.20	1.20	1.21	1.22	1.21	1.21	1.11	1.07	1.05
Fe^{+3}	0.00	0.01	0.00	0.01	0.00	0.00	0.01	0.01	0.01	0.00	0.00	0.00	0.00	0.00	0.01	0.00
Fe^{+2}	0.01	0.00	0.00	0.00	0.00	0.00	0.00	0.00	0.00	0.00	0.00	0.00	0.00	0.00	0.00	0.00
Mn	0.00	0.00	0.00	0.00	0.01	0.00										
Ca	0.27	0.24	0.24	0.24	0.24	0.25	0.23	0.23	0.24	0.23	0.24	0.24	0.23	0.14	0.10	0.07
Ba	0.00	0.00	0.00	0.00	0.00	0.00	0.00	0.00	0.00	0.00	0.00	0.00	0.00	0.00	0.00	0.00
Na	0.28	0.79	0.80	0.78	0.80	0.75	0.81	0.82	0.80	0.82	0.81	0.82	0.80	0.92	0.95	0.98
K	0.01	0.01	0.01	0.01	0.01	0.01	0.01	0.00	0.01	0.01	0.01	0.01	0.02	0.01	0.00	0.00
tot. cat.	5.00	5.00	5.00	5.00	5.00	5.00	5.00	5.00	5.00	5.00	5.00	5.00	5.00	5.00	5.00	5.00
tot. oxy.	8.62	7.94	7.95	7.96	7.94	7.99	7.93	7.92	7.93	7.93	7.93	7.92	7.93	7.92	7.93	7.93

Table 4.40 End Member of Plagioclase Feldspar in Biotite Granite Gneiss.

Sample no	b3						b4									
End member%																
An	47.68	23.08	22.90	23.19	22.85	24.38	21.59	22.09	22.57	21.52	22.30	22.13	22.22	12.88	9.46	6.71
Ab	49.66	75.59	76.39	76.03	76.35	74.64	77.35	77.47	76.12	77.55	76.71	77.01	76.25	86.52	90.15	92.82
Or	2.66	1.34	0.72	0.78	0.80	0.98	1.06	0.44	1.31	0.93	0.99	0.87	1.53	0.60	0.39	0.47

Table 4.41 Representative Electron Microprobe Analyses of Plagioclase Feldspar in Biotite Granite Gneiss.

Sample no	b16					b13		
Analyses	1	2	3	4	5	1	2	3
SiO_2	71.60	65.49	65.13	64.97	66.56	65.36	65.08	65.70
TiO_2	0.00	0.00	0.00	0.00	0.00	0.00	0.00	0.00
Al_2O_3	16.57	21.47	21.66	21.72	20.52	20.46	20.45	20.21
Fe_2O_3	0.00	0.00	0.00	0.00	0.00	0.00	0.00	0.00
FeO	0.38	0.22	0.31	0.48	0.57	1.01	1.12	0.91
MgO	0.00	0.00	0.00	0.00	0.00	1.00	1.04	0.95
CaO	0.45	3.36	3.01	3.52	2.32	4.20	4.46	4.29
Na_2O	9.94	8.49	9.04	8.84	9.61	7.12	6.94	7.02
K_2O	1.05	0.97	0.85	0.46	0.42	0.86	0.90	0.91
Total	100.00	100.00	100.00	100.00	100.00	100.00	100.00	100.00

Table 4.42 Structural Formulae of Plagioclase Feldspar in Biotite Granite Gneiss.

Structural Formulae based on 32 O_2								
Sample no	b16					b13		
Analyses	1	2	3	4	5	1	2	3
Si	3.18	2.92	2.89	2.89	2.95	2.94	2.93	2.96
Ti	0.00	0.00	0.00	0.00	0.00	0.00	0.00	0.00
Al	0.87	1.13	1.13	1.14	1.07	1.08	1.09	1.07
Cr	0.00	0.00	0.00	0.00	0.00	0.00	0.00	0.00
Fe3	0.00	0.00	0.00	0.00	0.00	0.00	0.00	0.00
Fe2	0.01	0.01	0.01	0.02	0.02	0.04	0.04	0.03
Mn	0.00	0.00	0.00	0.00	0.00	0.00	0.00	0.00
Mg	0.00	0.00	0.00	0.00	0.00	0.07	0.07	0.06
Ca	0.02	0.16	0.14	0.17	0.11	0.20	0.22	0.21
Ba	0.00	0.00	0.00	0.00	0.00	0.00	0.00	0.00
Na	0.86	0.73	0.78	0.76	0.83	0.62	0.61	0.61
K	0.06	0.06	0.05	0.03	0.02	0.05	0.05	0.05
tot. cat.	5.00	5.00	5.00	5.00	5.00	5.00	5.00	5.00
tot. oxy.	8.16	8.09	8.04	8.06	8.06	8.15	8.14	8.16

Table 4.43 End member of Plagioclase Feldspar in Biotite Granite Gneiss.

Sample no	b16					b13		
End member%								
An	2.28	16.90	14.75	17.55	11.46	23.20	24.65	23.73
Ab	91.36	77.28	80.28	79.69	86.08	71.17	69.43	70.29
Or	6.36	5.83	4.96	2.76	2.46	5.63	5.92	5.98

Table 4.44 Representative Electron Microprobe Analyses of Alkali Feldspar in Biotite Granite Gneiss.

Sample no	b3													
Analyses	1	2	3	4	5	6	7	8	9	10	11	12	13	14
SiO_2	64.91	65.32	64.98	65.40	65.41	65.59	65.29	65.42	65.11	64.88	64.71	64.80	65.36	63.97
TiO	0.00	0.00	0.00	0.00	0.00	0.00	0.00	0.00	0.00	0.00	0.00	0.00	0.00	0.00
Al_2O_3	18.16	18.51	18.40	18.38	18.44	18.35	18.54	18.36	18.21	18.46	18.13	18.41	18.43	18.12
Fe_2O_3	0.00	0.00	0.00	0.00	0.00	0.00	0.00	0.00	0.00	0.00	0.00	0.00	0.00	0.00
Fe(O)t	0.00	0.00	0.00	0.00	0.00	0.00	0.00	0.00	0.00	0.00	0.00	0.00	0.00	0.00
MnO	0.00	0.00	0.00	0.00	0.00	0.00	0.00	0.00	0.00	0.00	0.00	0.00	0.00	0.00
CaO	0.00	0.00	0.00	0.00	0.00	0.00	0.00	0.00	0.00	0.00	0.00	0.00	0.00	0.00
BaO	0.47	0.55	0.37	0.65	0.48	0.63	0.45	0.29	0.53	0.53	0.53	0.66	0.35	0.66
Na_2O	1.03	1.11	0.97	1.03	0.84	0.84	1.51	1.14	0.98	1.02	0.98	1.05	1.45	0.74
K_2O	14.97	15.15	15.13	14.95	15.25	14.50	14.56	14.97	15.18	14.84	15.20	14.84	14.60	15.72
Total	99.54	100.64	100.36	100.41	100.43	99.90	100.91	100.17	100.48	99.73	99.56	99.75	100.20	99.21

Table 4.45 Structural Formulae of Alkali Feldspar in Biotite Granite Gneiss.

Structural Formulae based on 32 O_2														
Sample no	**b3**													
Analyses	1	2	3	4	5	6	7	8	9	10	11	12	13	14
Si	3.02	3.00	3.01	3.02	3.02	3.05	3.00	3.02	3.01	3.01	3.01	3.01	3.01	2.99
Ti	0.00	0.00	0.00	0.00	0.00	0.00	0.00	0.00	0.00	0.00	0.00	0.00	0.00	0.00
Al	0.99	1.00	1.00	1.00	1.00	1.01	1.00	1.00	0.99	1.01	0.99	1.01	1.00	1.00
Ca	0.00	0.00	0.00	0.00	0.00	0.00	0.00	0.00	0.00	0.00	0.00	0.00	0.00	0.00
Ba	0.01	0.01	0.01	0.01	0.01	0.01	0.01	0.01	0.01	0.01	0.01	0.01	0.01	0.01
Na	0.09	0.10	0.09	0.09	0.08	0.08	0.13	0.10	0.09	0.09	0.09	0.09	0.13	0.07
K	0.89	0.89	0.89	0.88	0.90	0.86	0.85	0.88	0.90	0.88	0.90	0.88	0.86	0.94
tot. cat.	5.00	5.00	5.00	5.00	5.00	5.00	5.00	5.00	5.00	5.00	5.00	5.00	5.00	5.00
tot. oxy.	8.02	8.01	8.02	8.03	8.03	8.08	8.01	8.02	8.02	8.03	8.01	8.03	8.01	7.98

Table 4.46 End Member Composition of Alkali Feldspars in Biotite Granite Gneiss

Sample no	**b3**													
End Member														
Analyses	1	2	3	4	5	6	7	8	9	10	11	12	13	14
An	0.00	0.00	0.00	0.00	0.00	0.00	0.00	0.00	0.00	0.00	0.00	0.00	0.00	0.00
Ab	9.47	10.05	8.88	9.48	7.75	8.09	13.58	10.38	8.94	9.45	8.95	9.68	13.15	6.65
Or	90.53	89.95	91.12	90.52	92.25	91.91	86.42	89.62	91.06	90.55	91.05	90.32	86.85	93.35

Table 4.47 Representative Electron Microprobe Analyses of Alkali Feldspar in Biotite Granite Gneiss.

Sample no	b16														
Analyses	1	2	3	4	5	6	7	8	9	10	11	12	13	14	15
SiO_2	69.83	69.27	69.77	70.38	69.14	69.99	68.87	69.11	70.68	70.94	77.33	58.36	71.60	69.65	68.63
TiO_2	0.00	0.00	0.00	0.00	0.00	0.00	0.00	0.00	0.00	0.00	0.00	0.00	0.00	0.00	0.00
Al_2O_3	16.16	16.19	16.18	15.97	16.42	16.37	16.84	16.89	15.75	15.73	14.79	31.05	15.23	13.86	16.90
FeO	0.00	0.59	0.26	0.82	1.21	0.00	0.00	0.00	0.00	0.00	0.00	0.00	0.00	4.54	0.00
MgO	0.00	0.00	0.00	0.00	0.34	0.00	0.00	0.00	0.00	0.00	0.00	0.00	0.00	0.87	0.00
CaO	0.00	0.00	0.00	0.00	0.56	0.00	0.00	0.00	0.00	0.00	0.90	0.00	0.00	1.14	0.00
Na_2O	0.82	0.45	0.75	0.78	5.03	1.16	0.99	1.34	1.03	0.83	0.43	0.69	1.12	0.72	1.06
K_2O	13.20	13.49	13.04	12.05	7.30	12.48	13.30	12.66	12.54	12.50	5.50	9.90	12.06	9.23	13.41
Total	100.00	100.00	100.00	100.00	100.00	100.00	100.00	100.00	100.00	100.00	100.00	100.00	100.00	100.00	100.00

Table 4.48 Structural Formulae of Alkali Feldspar in Biotite Granite Gneiss.

Structural Formulae based on 32 O_2															
Sample no	b16														
Analyses	1	2	3	4	5	6	7	8	9	10	11	12	13	14	15
Si	3.25	3.24	3.26	3.30	3.15	3.26	3.20	3.21	3.30	3.31	3.73	2.68	3.34	3.30	3.19
Ti	0.00	0.00	0.00	0.00	0.00	0.00	0.00	0.00	0.00	0.00	0.00	0.00	0.00	0.00	0.00
Al	0.89	0.89	0.89	0.88	0.88	0.90	0.92	0.92	0.87	0.87	0.84	1.68	0.84	0.77	0.92
Fe^{+2}	0.00	0.02	0.01	0.03	0.05	0.00	0.00	0.00	0.00	0.00	0.00	0.00	0.00	0.18	0.00
Mn	0.00	0.00	0.00	0.00	0.00	0.00	0.00	0.00	0.00	0.00	0.00	0.00	0.00	0.00	0.00
Mg	0.00	0.00	0.00	0.00	0.02	0.00	0.00	0.00	0.00	0.00	0.00	0.00	0.00	0.06	0.00
Ca	0.00	0.00	0.00	0.00	0.03	0.00	0.00	0.00	0.00	0.00	0.05	0.00	0.00	0.06	0.00
Na	0.07	0.04	0.07	0.07	0.44	0.10	0.09	0.12	0.09	0.08	0.04	0.06	0.10	0.07	0.10
K	0.78	0.80	0.78	0.72	0.42	0.74	0.79	0.75	0.75	0.74	0.34	0.58	0.72	0.56	0.79
tot. cat.	5.00	5.00	5.00	5.00	5.00	5.00	5.00	5.00	5.00	5.00	5.00	5.00	5.00	5.00	5.00
tot. oxy.	8.27	8.26	8.28	8.34	8.16	8.28	8.22	8.23	8.31	8.34	8.96	8.20	8.35	8.38	8.20

Table 4.49 End Member Composition of Alkali Feldspars in Biotite Granite Gneiss

Sample no	b16														
End Member															
Analyses	1	2	3	4	5	6	7	8	9	10	11	12	13	14	15
An	0.00	0.00	0.00	0.00	3.08	0.00	0.00	0.00	0.00	0.00	10.95	0.00	0.00	8.50	0.00
Ab	8.59	4.81	8.01	8.98	49.56	12.36	10.17	13.85	11.14	9.16	9.54	9.62	12.34	9.69	10.71
Or	91.41	95.19	91.99	91.02	47.37	87.64	89.83	86.15	88.86	90.84	79.51	90.38	87.66	81.80	89.29

Table 4.50 Representative Electron Microprobe Analyses of Alkali Feldspar in Biotite Granite Gneiss.

Sample no	b13														
Analyses	1	2	3	4	5	6	7	8	9	10	11	12	13	14	15
SiO_2	58.80	65.81	65.93	68.44	67.65	68.65	69.32	69.98	70.86	65.54	65.21	65.25	83.07	66.48	67.75
TiO_2	0.00	0.00	0.00	0.30	0.27	0.36	0.00	0.00	0.00	0.00	0.00	0.50	0.00	0.00	0.00
Al_2O_3	27.00	17.13	17.13	16.40	16.76	16.57	15.90	15.54	15.41	17.40	17.12	17.22	9.60	18.59	18.09
Fe_2O_3	0.00	0.00	0.00	0.00	0.00	0.00	0.00	0.00	0.00	0.00	0.00	0.00	0.00	0.96	0.00
FeO	1.73	1.94	0.97	0.75	0.70	0.28	0.53	0.33	0.00	1.01	1.25	1.36	0.00	0.00	0.79
MgO	0.38	0.00	0.00	0.00	0.00	0.00	0.00	0.00	0.00	1.15	1.49	1.51	0.00	0.00	0.00
CaO	0.79	0.00	0.00	0.00	0.00	0.00	0.00	0.00	0.00	0.00	0.00	0.00	0.54	1.89	1.09
BaO	0.00	0.00	0.00	0.00	0.00	0.00	0.60	0.67	0.00	0.84	0.91	0.00	0.00	0.00	0.00
Na_2O	1.86	0.77	1.11	0.66	0.75	1.05	0.58	0.43	0.43	1.12	1.06	0.86	5.38	8.38	8.27
K_2O	8.75	13.72	13.34	13.45	13.88	13.09	13.07	13.06	13.29	12.94	12.95	13.31	1.41	2.91	3.52
Total	99.32	99.37	98.49	100.00	100.00	100.00	100.00	100.00	100.00	100.00	100.00	100.00	100.00	99.20	99.51

Table 4.51 Structural Formulae of Alkali Feldspar in Biotite Granite Gneiss.

Structural Formulae based on 32 O_2															
Sample no	b13														
Analyses	1	2	3	4	5	6	7	8	9	10	11	12	13	14	15
Si	2.72	3.09	3.10	3.20	3.15	3.20	3.25	3.29	3.32	3.05	3.03	3.02	3.87	2.99	3.04
Ti	0.00	0.00	0.00	0.01	0.01	0.01	0.00	0.00	0.00	0.00	0.00	0.02	0.00	0.00	0.00
Al	1.47	0.95	0.95	0.90	0.92	0.91	0.88	0.86	0.85	0.95	0.94	0.94	0.53	0.99	0.96
Fe^{+3}	0.00	0.00	0.00	0.00	0.00	0.00	0.00	0.00	0.00	0.00	0.00	0.00	0.00	0.00	0.00
Fe^{+2}	0.07	0.08	0.04	0.03	0.03	0.01	0.02	0.01	0.00	0.04	0.05	0.05	0.00	0.03	0.03
Mg	0.00	0.00	0.00	0.00	0.00	0.00	0.00	0.00	0.08	0.10	0.10	0.14	0.00	0.00	0.00
Ca	0.00	0.00	0.00	0.00	0.00	0.15	0.00	0.00	0.00	0.00	0.00	0.00	0.03	0.09	0.05
Ba	0.00	0.01	0.00	0.00	0.00	0.00	0.01	0.00	0.02	0.02	0.00	0.00	0.00	0.00	0.00
Na	0.07	0.10	0.06	0.07	0.10	0.05	0.04	0.04	0.10	0.10	0.08	0.04	0.49	0.73	0.72
K	0.52	0.82	0.80	0.80	0.82	0.78	0.78	0.78	0.79	0.77	0.77	0.79	0.08	0.17	0.20
tot. cat.	5.00	5.00	5.00	5.00	5.00	5.00	5.00	5.00	5.00	5.00	5.00	5.00	5.00	5.00	5.00
tot. oxy.	8.11	8.11	8.12	8.23	8.17	8.23	8.28	8.31	8.33	8.09	8.07	8.08	8.85	8.04	8.06

Table 4.52 End Member Composition of Alkali Feldspars in Biotite Granite Gneiss

Sample no	b13														
End Member															
Analyses	1	2	3	4	5	6	7	8	9	10	11	12	13	14	15
An	5.41	0.00	0.00	0.00	0.00	0.00	0.00	0.00	0.00	0.00	0.00	0.00	4.49	9.20	5.37
Ab	23.10	7.87	11.25	6.95	7.58	10.91	6.37	4.74	4.72	11.63	11.04	8.98	81.46	73.90	73.93
Or	71.50	92.13	88.75	93.05	92.42	89.09	93.63	95.26	95.28	88.37	88.96	91.02	14.05	16.90	20.70

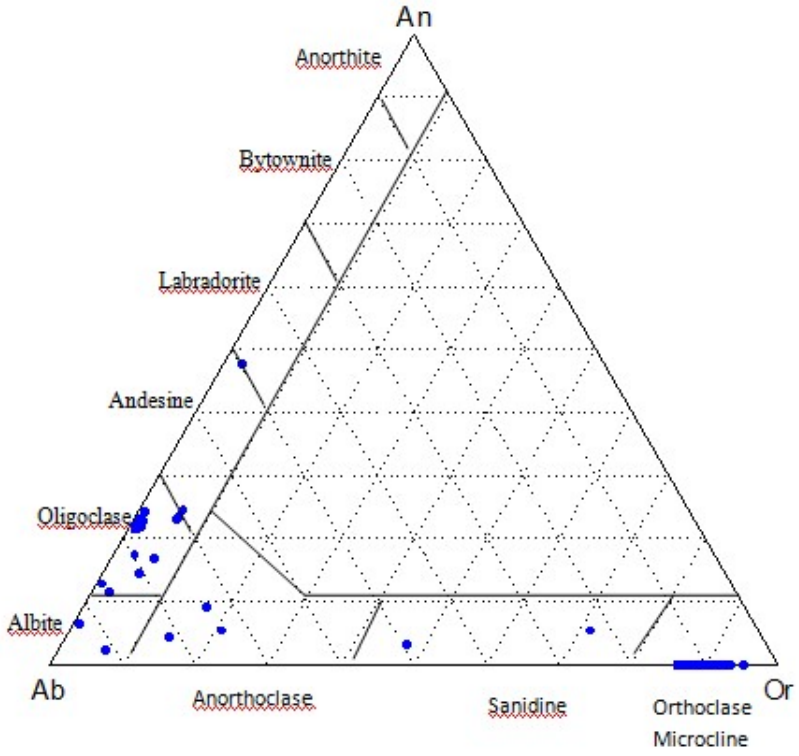

Fig.4.121 Plot of Ab-An-Or for Feldspars in the Biotite Granite Gneiss (After Deer *et. al.*, 1963).

Table 4.53 Representative Electron Microprobe Analyses of Feldspar in Biotite Hornblende Gneiss.

Sample no	bh4	K-feldspars							Plagioclase							
Analyses	1	2	3	4	5	6	7	8	9	10	11	12	13	14	15	16
SiO_2	64.18	64.19	64.62	64.26	64.27	64.33	64.26	64.43	64.88	65.15	64.78	64.69	64.92	64.88	64.71	65.18
TiO_2	0.00	0.00	0.00	0.00	0.00	0.00	0.00	0.00	0.00	0.00	0.00	0.00	0.00	0.00	0.00	0.00
Al_2O_3	17.96	18.04	18.13	17.99	18.20	18.03	17.98	18.27	21.24	21.30	21.26	21.29	21.20	21.18	21.40	21.11
Fe(O)t	0.27	0.00	0.00	0.00	0.00	0.00	0.00	0.14	0.00	0.00	0.00	0.00	0.00	0.00	0.00	0.00
CaO	0.00	0.00	0.12	0.00	0.00	0.00	0.00	0.00	2.53	2.47	2.56	2.62	2.55	2.65	2.59	2.44
BaO	0.00	0.00	0.00	0.00	0.00	0.00	0.00	0.23	0.00	0.00	0.00	0.00	0.00	0.00	0.00	0.00
Na_2O	0.91	0.90	2.91	1.20	0.93	1.08	0.95	1.29	11.06	10.59	10.76	10.99	10.83	10.85	10.96	10.60
K_2O	16.31	16.46	14.13	16.09	16.44	16.27	16.45	15.49	0.15	0.11	0.18	0.24	0.22	0.20	0.19	0.16
Total	99.62	99.59	99.92	99.54	99.83	99.72	99.64	99.85	99.86	99.62	99.55	99.84	99.71	99.75	99.85	99.48

Table 4.54 Structural Formulae of Feldspar in Biotite Hornblende Gneiss based on 32 O_2

Structural Formulae based on 32 O_2	K-feldspars								Plagioclase							
Sample no	bh4															
Analyses	1	2	3	4	5	6	7	8	9	10	11	12	13	14	15	16
Si	2.967	2.966	2.943	2.966	2.962	2.966	2.967	2.971	2.839	2.868	2.849	2.832	2.850	2.847	2.833	2.873
Ti	0.000	0.000	0.000	0.000	0.000	0.000	0.000	0.000	0.000	0.000	0.000	0.000	0.000	0.000	0.000	0.000
Al	0.979	0.983	0.973	0.979	0.988	0.980	0.979	0.993	1.096	1.105	1.102	1.098	1.097	1.095	1.104	1.097
Ca	0.000	0.000	0.006	0.000	0.000	0.000	0.000	0.000	0.119	0.117	0.121	0.123	0.120	0.124	0.122	0.115
Ba	0.000	0.000	0.000	0.000	0.000	0.000	0.000	0.004	0.000	0.000	0.000	0.000	0.000	0.000	0.000	0.000
Na	0.082	0.080	0.257	0.107	0.083	0.097	0.085	0.116	0.938	0.904	0.918	0.933	0.922	0.923	0.930	0.906
K	0.962	0.971	0.821	0.948	0.967	0.957	0.969	0.911	0.009	0.006	0.010	0.013	0.012	0.011	0.010	0.009
tot. cat.	5.000	5.000	5.000	5.000	5.000	5.000	5.000	5.000	5.000	5.000	5.000	5.000	5.000	5.000	5.000	5.000
tot. oxy.	7.940	7.932	7.890	7.928	7.932	7.929	7.930	7.957	7.914	7.965	7.936	7.908	7.931	7.927	7.915	7.965

Table 4.55 End Member Composition of Feldspars in Biotite Hornblende Gneiss

Sample no	bh4			K-Feldspars					Plagioclase							
End Member																
Analyses	1	2	3	4	5	6	7	8	9	10	11	12	13	14	15	16
An	0	0	0.52	0.00	0.00	0.00	0.00	0.00	11.15	11.35	11.49	11.50	11.38	11.75	11.45	11.18
Ab	7.85	7.65	23.72	10.17	7.88	9.18	8.03	11.26	88.04	88.05	87.52	87.26	87.48	87.19	87.56	87.96
Or	92.15	92.35	75.76	89.83	92.12	90.82	91.97	88.74	0.80	0.60	0.99	1.24	1.14	1.06	0.98	0.86

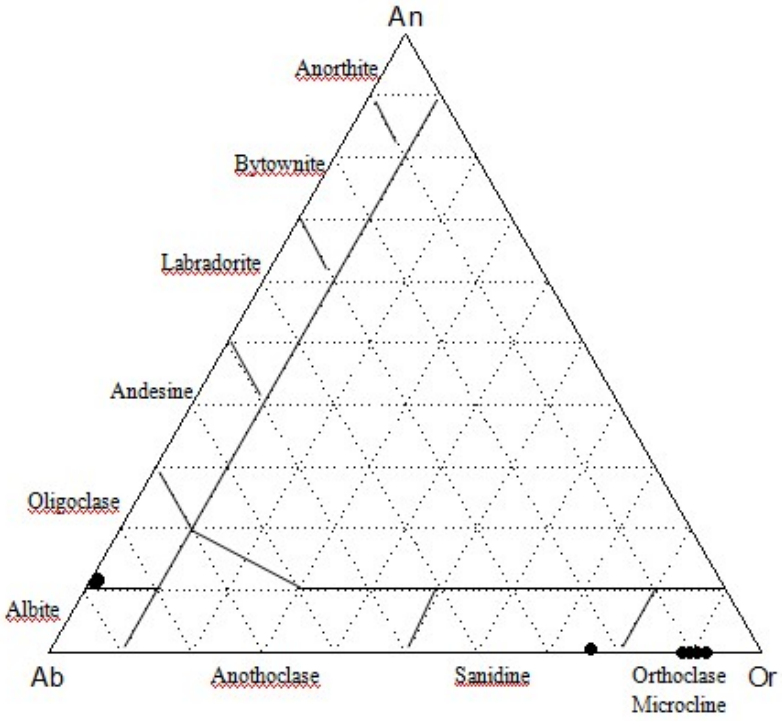

Fig.4.122 Plot of Ab-An-Or for Feldspars in the Biotite Hornblende Gneiss (after: Deer *et. al.*, 1963)

4.4.2 Biotite

Biotite composition in the granodioritic, biotite granite gneiss and biotite hornblende gneiss were normalized based on 24 O_2 atoms, with all Fe assumed to be Fe^{2+} and the formula calculated on anhydrous basis (Fig.4.123).

Biotites in the granodioritc gneiss samples presented (Table 4.56) showed variation in SiO_2 content from 36.23 to 52.58 wt. %, TiO_2 content ranged from 2.51 to 4.12 wt. %, Al_2O_3 content ranged from 15.03 to 16.66 wt. % and low values of MnO, CaO and Na_2O were revealed. There is a significant variation in the compositions of FeO (13.38 to 21.45), MgO (6.28 to 8.79) and K_2O (6.89 to 10.69) with X_{Fe} (Fe/Fe+Mg) varying from 0.51 to 0.59 in the granodioritic gneiss (Table 4.57).

The chemical analyses of biotites in the biotite granite gneiss samples (Tables 4.58 - 4.61) revealed SiO_2 content that ranged from 35.45 to 59.07%; Al_2O_3, 13.94 to 19.46 %; FeO, 22.80 to 24.83%; MgO, 6.28 to 15.03% and K_2O, 3.76 to 10.37%. The results also showed TiO_2 concentrations that ranged from 3.77 to 4.90% and as high as 11.37% in one of the spot of the sample. The concentrations of CaO, Na_2O and MnO were low. Ratio of X_{Fe} (Fe/Fe+Mg) ranged from 0.29 to 0.92 in the biotite granite gneiss.

Mineral chemistry of biotite in biotite hornblende gneiss rock (Table 4.62) yielded little variations; SiO_2 content ranged 33.03 to 35.70%; TiO_2, 2.28 to 3.17; Al_2O_3, 16.32 to 17.54%; FeO, 29.79 to 33.59% and K_2O, 9.74 to 10.11%. MgO (0.31 to 0.45%) content was low compare with granodioritic and biotite granite gneiss samples. Higher constant value of X_{Fe} (0.99) was recorded in the biotite hornblende gneiss (Table. 4.63).

Discriminate diagram of Nachit et.al. (2005) was used to differentiate the biotite into primary magmatic, reequilibrated primary biotite and neoformed biotite. The result revealed that the biotite composition of the granodioritic and biotite granite gneiss were mainly primary magmatic biotite, while the biotite hornblende gneiss and spots of biotite granite gneiss fell in the reequilibrated primary biotite (Fig.4.124).

Using the plot of Al^{iv} versus Fe/Fe+Mg (Deer *et. al*. 1992), composition of the biotite plotted in the phlogopite-biotite field, with the biotite hornblende gneiss occupying siderophyllite corner-Fe rich end member (Fig.4.125).

The plot of FeO-MgO-A_2O_3 (Abdel-Rahman, 1994) revealed that granodioritic and biotite granite gneiss plotted mainly in the peraluminous suite while the biotite hornblende gneiss falls in the anorogenic alkaline suite (Fig.4.126). The high constant value of X_{Fe} (0.99) for the biotite hornblende gneiss may be suggesting strongly evolved gneiss from alkaline granite (Nachit *et.al*. 2005). This can also be confirmed by the plot of MgO against FeO (Fig.4.127).

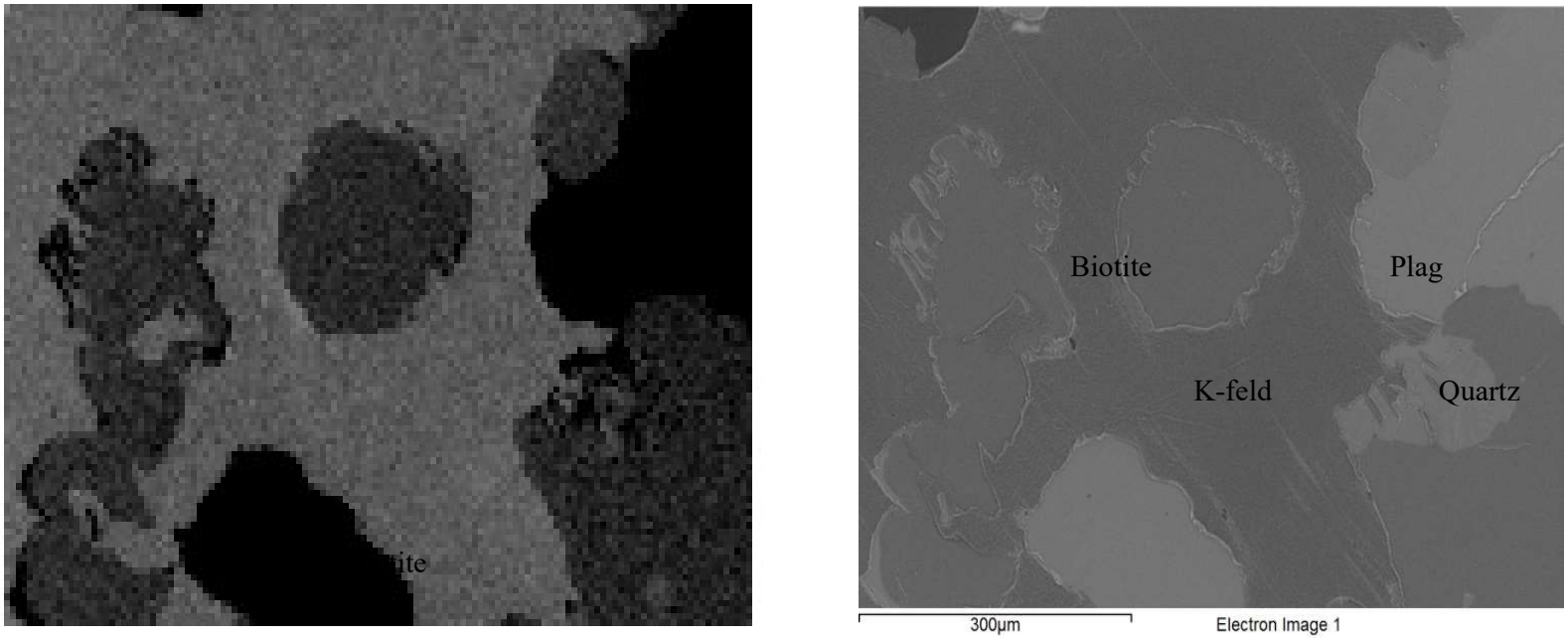

Fig.4.123 Micro-Probe Image of Biotite Flakes in the Biotite Granite Gneiss (coordinate: N07″ 43.541′, E 03″ 46.330′)

Table 4.56 Representative Elemental Composition (wt %) of Biotite in Granodioritic Gneiss.

Sample no	G11								G6							
Analyses	1	2	3	4	5	6	7	8	1	2	3	4	5	6	7	8
SiO_2	47.93	47.92	48.25	50.22	50.03	52.58	50.34	48.29	36.51	36.87	36.46	36.81	36.29	37.53	36.23	36.93
TiO_2	2.57	2.51	2.62	2.84	2.83	2.70	2.84	2.98	3.88	3.78	3.35	3.87	4.08	4.12	3.72	3.98
Al_2O_3	16.15	16.01	16.14	15.46	14.98	15.13	15.03	15.37	15.56	16.15	16.08	16.33	15.64	16.66	15.43	15.81
FeO	15.69	16.00	15.40	15.03	14.64	13.38	14.75	15.38	21.45	21.03	21.21	20.94	21.20	19.70	21.56	21.25
MnO	0.00	0.00	0.00	0.00	0.00	0.24	0.00	0.00	0.26	0.29	0.20	0.26	0.30	0.15	0.22	0.34
MgO	7.44	7.22	7.48	7.51	7.50	6.28	7.70	8.13	8.25	8.37	8.46	8.63	8.47	8.79	8.51	8.47
CaO	1.05	1.10	1.04	0.00	0.65	0.99	0.80	0.74	0.00	0.00	0.00	0.00	0.00	0.00	0.00	0.00
Na_2O	1.96	1.97	1.98	1.04	1.18	1.81	1.37	1.46	0.00	0.00	0.00	0.00	0.20	0.19	0.00	0.19
K_2O	7.23	7.29	7.09	7.88	8.19	6.89	7.17	7.65	10.39	10.46	10.69	10.47	10.41	10.33	10.42	10.21
H_2O*calc	4.36	4.35	4.38	4.41	4.40	4.47	4.42	4.37	3.91	3.95	3.92	3.97	3.92	4.01	3.89	3.96
O=F,Cl	0.00	0.00	0.00	0.00	0.00	0.00	0.00	0.00	0.00	0.00	0.00	0.00	0.00	0.00	0.00	0.00
Total	104.36	104.35	104.38	104.41	104.40	104.47	104.42	104.37	96.29	96.95	96.46	97.31	96.59	97.46	96.42	97.18

Table 4.57 Structural Formulae of Biotite in the Granodioritic Gneiss based on 24 O_2 atoms

Sample no	G11								G6							
Cations	1	2	3	4	5	6	7	8	1	2	3	4	5	6	7	8
Si	6.59	6.60	6.61	6.83	6.82	7.06	6.83	6.63	5.60	5.60	5.58	5.56	5.55	5.61	5.58	5.60
Al iv	1.41	1.40	1.39	1.17	1.18	0.94	1.17	1.37	2.40	2.40	2.42	2.44	2.45	2.39	2.42	2.40
Al vi	1.20	1.20	1.22	1.30	1.23	1.45	1.24	1.11	0.41	0.48	0.48	0.47	0.37	0.54	0.38	0.42
Ti	0.27	0.26	0.27	0.29	0.29	0.27	0.29	0.31	0.45	0.43	0.39	0.44	0.47	0.46	0.43	0.45
Fe	1.80	1.84	1.76	1.71	1.67	1.50	1.67	1.77	2.75	2.67	2.72	2.65	2.71	2.46	2.78	2.69
Mn	0.00	0.00	0.00	0.00	0.00	0.03	0.00	0.00	0.03	0.04	0.03	0.03	0.04	0.02	0.03	0.04
Mg	1.52	1.48	1.53	1.52	1.52	1.26	1.56	1.66	1.89	1.89	1.93	1.94	1.93	1.96	1.95	1.91
Ca	0.15	0.16	0.15	0.00	0.09	0.14	0.12	0.11	0.00	0.00	0.00	0.00	0.00	0.00	0.00	0.00
Na	0.52	0.52	0.53	0.28	0.31	0.47	0.36	0.39	0.00	0.00	0.00	0.00	0.06	0.06	0.00	0.05
K	1.27	1.28	1.24	1.37	1.43	1.18	1.24	1.34	2.03	2.03	2.09	2.02	2.03	1.97	2.05	1.97
OH*	4.00	4.00	4.00	4.00	4.00	4.00	4.00	4.00	4.00	4.00	4.00	4.00	4.00	4.00	4.00	4.00
TOTAL	18.74	18.75	18.70	18.47	18.55	18.30	18.48	18.69	19.56	19.54	19.63	19.55	19.61	19.47	19.61	19.55
Y total	4.79	4.78	4.78	4.82	4.72	4.51	4.76	4.85	5.53	5.52	5.54	5.53	5.52	5.45	5.57	5.52
X total	1.94	1.97	1.92	1.64	1.83	1.79	1.72	1.84	2.03	2.03	2.09	2.02	2.09	2.02	2.05	2.03
Al total	2.62	2.60	2.61	2.48	2.41	2.39	2.41	2.49	2.81	2.89	2.90	2.91	2.82	2.93	2.80	2.82
Fe/Fe+Mg	0.54	0.55	0.54	0.53	0.52	0.54	0.52	0.51	0.59	0.59	0.58	0.58	0.58	0.56	0.59	0.58
XFeO*	0.68	0.69	0.67	0.67	0.66	0.68	0.66	0.65	0.72	0.72	0.72	0.71	0.72	0.69	0.72	0.72

XFeO* = (FeO+MnO)/(FeO+MnO+MgO) (after: Nachit*et al.*, 2005)

Table 4.58 Representative Elemental Composition (wt %) of Biotite in Biotite Granite Gneiss.

Sample no	**b3**								**b4**							
Analyses	1	2	3	4	5	6	7	8	1	2	3	4	5	6	7	8
SiO_2	36.02	37.09	36.17	35.45	35.50	36.28	36.02	36.26	35.86	36.36	35.94	35.89	36.00	35.49	36.74	35.96
TiO_2	4.68	3.63	4.90	4.83	4.38	4.37	4.52	4.33	3.77	3.37	3.37	3.82	4.00	3.58	3.55	3.88
Al_2O_3	14.75	14.16	14.35	14.21	13.94	14.32	14.35	14.80	15.39	15.98	15.32	15.22	15.71	15.75	15.87	15.65
Fe(O)t	23.83	23.31	23.75	24.27	24.83	23.97	24.05	23.50	23.55	22.80	24.25	23.98	23.75	24.10	23.15	23.98
MnO	0.31	0.28	0.27	0.36	0.31	0.34	0.36	0.34	0.21	0.00	0.39	0.25	0.33	0.49	0.30	0.26
MgO	7.33	8.01	7.46	7.27	7.33	7.77	7.69	7.66	6.67	7.38	6.87	6.88	6.46	6.64	6.89	6.28
CaO	0.00	0.00	0.00	0.00	0.00	0.00	0.00	0.00	0.00	0.00	0.00	0.00	0.00	0.00	0.11	0.00
Na_2O	0.00	0.22	0.00	0.20	0.00	0.00	0.00	0.00	0.00	0.00	0.00	0.00	0.00	0.00	0.00	0.00
K_2O	9.36	9.58	9.38	9.30	9.57	9.42	9.38	9.41	10.29	10.29	10.12	10.37	10.30	10.37	10.26	10.21
H_2O*calc	3.88	3.89	3.88	3.84	3.82	3.88	3.87	3.89	3.84	3.89	3.85	3.86	3.87	3.85	3.91	3.86
O=F,Cl	0	0	0	0	0	0	0	0	0	0	0	0	0	0	0	0
Total	100.16	100.18	100.16	99.73	99.68	100.35	100.24	100.19	99.59	100.07	100.11	100.26	100.41	100.26	100.78	100.08

Table 4.59 Structural Formulae of Biotite in the Biotite Granite Gneiss based on 24 O_2 atoms

Sample no	b3								b4							
Cations	1	2	3	4	5	6	7	8	1	2	3	4	5	6	7	8
Si	5.57	5.72	5.59	5.54	5.57	5.61	5.58	5.60	5.60	5.61	5.59	5.58	5.57	5.53	5.64	5.59
Al iv	2.43	2.28	2.41	2.46	2.43	2.39	2.42	2.40	2.40	2.39	2.41	2.42	2.43	2.47	2.36	2.41
Al vi	0.26	0.29	0.21	0.15	0.14	0.22	0.20	0.29	0.43	0.51	0.40	0.37	0.44	0.42	0.50	0.45
Ti	0.54	0.42	0.57	0.57	0.52	0.51	0.53	0.50	0.44	0.39	0.39	0.45	0.47	0.42	0.41	0.45
Fe	3.08	3.01	3.07	3.17	3.26	3.10	3.11	3.03	3.07	2.94	3.16	3.12	3.07	3.14	2.97	3.12
Mn	0.04	0.04	0.04	0.05	0.04	0.04	0.05	0.04	0.03	0.00	0.05	0.03	0.04	0.06	0.04	0.03
Mg	1.69	1.84	1.72	1.69	1.71	1.79	1.77	1.76	1.55	1.70	1.59	1.59	1.49	1.54	1.58	1.45
Ca	0.00	0.00	0.00	0.00	0.00	0.00	0.00	0.00	0	0	0	0	0	0	0.02	0
Na	0.00	0.06	0.00	0.06	0.00	0.00	0.00	0.00	0	0	0	0	0	0	0	0
K	1.85	1.88	1.85	1.85	1.91	1.86	1.85	1.85	2.05	2.02	2.01	2.06	2.03	2.06	2.01	2.02
OH*	4.00	4.00	4.00	4.00	4.00	4.00	4.00	4.00	4	4	4	4	4	4	4	4
TOTAL	19.46	19.55	19.46	19.55	19.58	19.51	19.51	19.48	19.57	19.56	19.61	19.61	19.55	19.64	19.53	19.54
Y total	5.62	5.60	5.60	5.63	5.67	5.65	5.66	5.63	5.52	5.54	5.60	5.55	5.51	5.58	5.50	5.51
X total	1.85	1.95	1.85	1.92	1.91	1.86	1.85	1.85	2.05	2.02	2.01	2.06	2.03	2.06	2.03	2.02
Al total	2.69	2.57	2.62	2.62	2.58	2.61	2.62	2.69	2.83	2.90	2.81	2.79	2.87	2.89	2.87	2.87
Fe/Fe+Mg	0.65	0.62	0.64	0.65	0.66	0.63	0.64	0.63	0.66	0.63	0.66	0.66	0.67	0.67	0.65	0.68
XFeO*	0.77	0.75	0.76	0.77	0.77	0.76	0.76	0.76	0.78	0.76	0.78	0.78	0.79	0.79	0.77	0.79

XFeO* = (FeO+MnO)/(FeO+MnO+MgO) (after: Nachit*et al.*, 2005)

Table 4.60 Elemental Composition (wt %) of Biotite in Biotite Granite Granite Gneiss.

Sample no	b16						b13					
Analyses	1	2	3	4	5	6	1	2	3	4	5	6
SiO_2	59.07	43.75	43.46	44.00	44.25	41.27	44.62	46.20	46.43	45.89	48.75	46.98
TiO_2	0.00	3.35	3.37	3.38	3.33	11.37	1.54	1.13	1.16	1.29	1.05	1.06
Al_2O_3	12.48	19.03	19.27	19.46	19.11	12.67	14.35	14.34	14.24	14.13	15.22	14.74
Fe(O)t	20.75	18.61	18.77	18.02	18.11	23.10	10.88	10.97	11.13	10.74	11.20	11.22
MnO	0.00	0.00	0.00	0.00	0.00	0.00	0.35	0.37	0.31	0.37		
MgO	1.62	4.96	4.75	4.68	4.59	1.17	14.88	15.03	14.88	15.02	14.49	14.21
CaO	1.17	0.00	0.00	0.00	0.00	0.00	0.79	0.00	0.00	0.73	0.00	0.00
Na_2O	0.56	0.47	0.56	0.47	0.54	0.81	0.43	0.56	0.41	0.48	0.82	0.41
K_2O	3.76	9.82	9.82	9.98	10.08	9.62	9.30	8.65	9.25	8.82	8.47	9.14
F	0.00	0.00	0.00	0.00	0.00	0.00	2.63	2.54	2.00	2.30		2.04
H_2O*calc	4.47	4.25	4.24	4.26	4.26	4.09	3.00	3.09	3.35	3.20	4.45	3.35
Total	103.88	104.25	104.24	104.26	104.26	104.09	102.77	102.86	103.17	102.96	104.45	103.15

Table 4.61 Structural Formulae of Biotite in the Biotite Granite Gneiss based on 24 O_2 atoms

Sample no	b16						b13					
Cations	1	2	3	4	5	6	1	2	3	4	5	6
Si	7.92	6.17	6.14	6.19	6.23	6.05	6.30	6.46	6.47	6.42	6.57	6.52
Al iv	0.08	1.83	1.86	1.81	1.77	1.95	1.70	1.54	1.53	1.58	1.43	1.48
Al vi	1.89	1.34	1.35	1.42	1.40	0.24	0.69	0.82	0.81	0.75	0.99	0.94
Ti	0.00	0.36	0.36	0.36	0.35	1.25	0.16	0.12	0.12	0.14	0.11	0.11
Fe	2.33	2.20	2.22	2.12	2.13	2.83	1.29	1.28	1.30	1.26	1.26	1.30
Mn	0.00	0.00	0.00	0.00	0.00	0.00	0.04	0.04	0.04	0.04	0.00	0.00
Mg	0.32	1.04	1.00	0.98	0.96	0.26	3.14	3.13	3.09	3.13	2.91	2.94
Ca	0.17	0.00	0.00	0.00	0.00	0.00	0.12	0.00	0.00	0.11	0.00	0.00
Na	0.14	0.13	0.15	0.13	0.15	0.23	0.12	0.15	0.11	0.13	0.21	0.11
K	0.64	1.77	1.77	1.79	1.81	1.80	1.68	1.54	1.64	1.57	1.46	1.62
OH*	4.00	4.00	4.00	4.00	4.00	4.00	2.82	2.88	3.12	2.98	4.00	3.10
F	0.00	0.00	0.00	0.00	0.00	0.00	1.18	1.12	0.88	1.02	0.00	0.90
TOTAL	17.49	18.83	18.86	18.80	18.81	18.61	19.23	19.09	19.11	19.13	18.95	19.02
Y total	4.54	4.94	4.93	4.88	4.85	4.58	5.32	5.40	5.36	5.32	5.27	5.29
X total	0.95	1.90	1.92	1.92	1.96	2.03	1.91	1.69	1.76	1.81	1.67	1.73
Al total	1.97	3.17	3.21	3.23	3.17	2.19	2.39	2.36	2.34	2.33	2.42	2.41
Fe/Fe+Mg	0.88	0.68	0.69	0.68	0.69	0.92	0.29	0.29	0.30	0.29	0.30	0.31

Table 4.62 Elemental Composition (wt %) of Biotite in Biotite Hornblende Gneiss.

Sample no	bh4									
Analyses	1	2	3	4	5	6	7	8	9	10
SiO_2	33.74	33.50	33.90	33.78	34.66	34.58	35.70	33.96	33.03	34.24
TiO_2	2.52	3.17	2.37	2.28	2.92	2.90	2.81	2.75	2.83	2.79
Al_2O_3	16.32	16.39	16.52	16.18	16.93	16.73	17.54	17.02	16.33	16.71
Fe(O)t	33.59	32.59	33.50	33.44	31.11	31.29	29.79	32.33	33.18	32.51
MnO	0.24	0.32	0.16	0.47	0.22	0.23	0.25	0.30	0.30	0.28
MgO	0.45	0.37	0.35	0.35	0.42	0.42	0.31	0.36	0.37	0.39
CaO	0.00	0.00	0.00	0.00	0.00	0.00	0.00	0.00	0.00	0.00
Na_2O	0.00	0.22	0.00	0.28	0.00	0.21	0.23	0.20	0.28	0.00
K_2O	9.78	9.87	9.82	9.74	9.93	9.89	9.67	9.87	10.11	9.85
Cr_2O_3	0.00	0.00	0.00	0.00	0.00	0.00	0.00	0.00	0.00	0.00
H_2O*calc	3.69	3.69	3.69	3.68	3.73	3.72	3.78	3.72	3.66	3.72
Total	100.32	100.13	100.31	100.21	99.93	99.97	100.08	100.50	100.08	100.50

Table 4.63 Structural Formulae of Biotite in the Biotite Hornblende Gneiss based on 24 O_2 atoms

Sample no	bh4									
Cations	1	2	3	4	5	6	7	8	9	10
Si	5.49	5.45	5.50	5.51	5.57	5.57	5.67	5.48	5.40	5.52
Al iv	2.51	2.55	2.50	2.49	2.43	2.43	2.33	2.52	2.60	2.48
Al vi	0.61	0.59	0.67	0.61	0.78	0.74	0.95	0.71	0.55	0.69
Ti	0.31	0.39	0.29	0.28	0.35	0.35	0.34	0.33	0.35	0.34
Fe	4.57	4.43	4.55	4.56	4.18	4.21	3.95	4.36	4.54	4.38
Mn	0.03	0.04	0.02	0.07	0.03	0.03	0.03	0.04	0.04	0.04
Mg	0.11	0.09	0.08	0.09	0.10	0.10	0.07	0.09	0.09	0.09
Na	0	0.07	0.00	0.09	0.00	0.07	0.07	0.06	0.09	0.00
K	2.03	2.05	2.03	2.03	2.04	2.03	1.96	2.03	2.11	2.03
OH*	4	4	4	4	4	4	4	4	4	4
TOTAL	19.65	19.65	19.64	19.72	19.49	19.54	19.37	19.62	19.77	19.57
Y total	5.63	5.54	5.61	5.60	5.45	5.44	5.34	5.53	5.57	5.54
X total	2.03	2.12	2.03	2.12	2.04	2.10	2.03	2.09	2.20	2.03
Al total	3.13	3.14	3.16	3.11	3.21	3.18	3.28	3.23	3.15	3.18
Fe/Fe+Mg	0.98	0.98	0.98	0.98	0.98	0.98	0.98	0.98	0.98	0.98

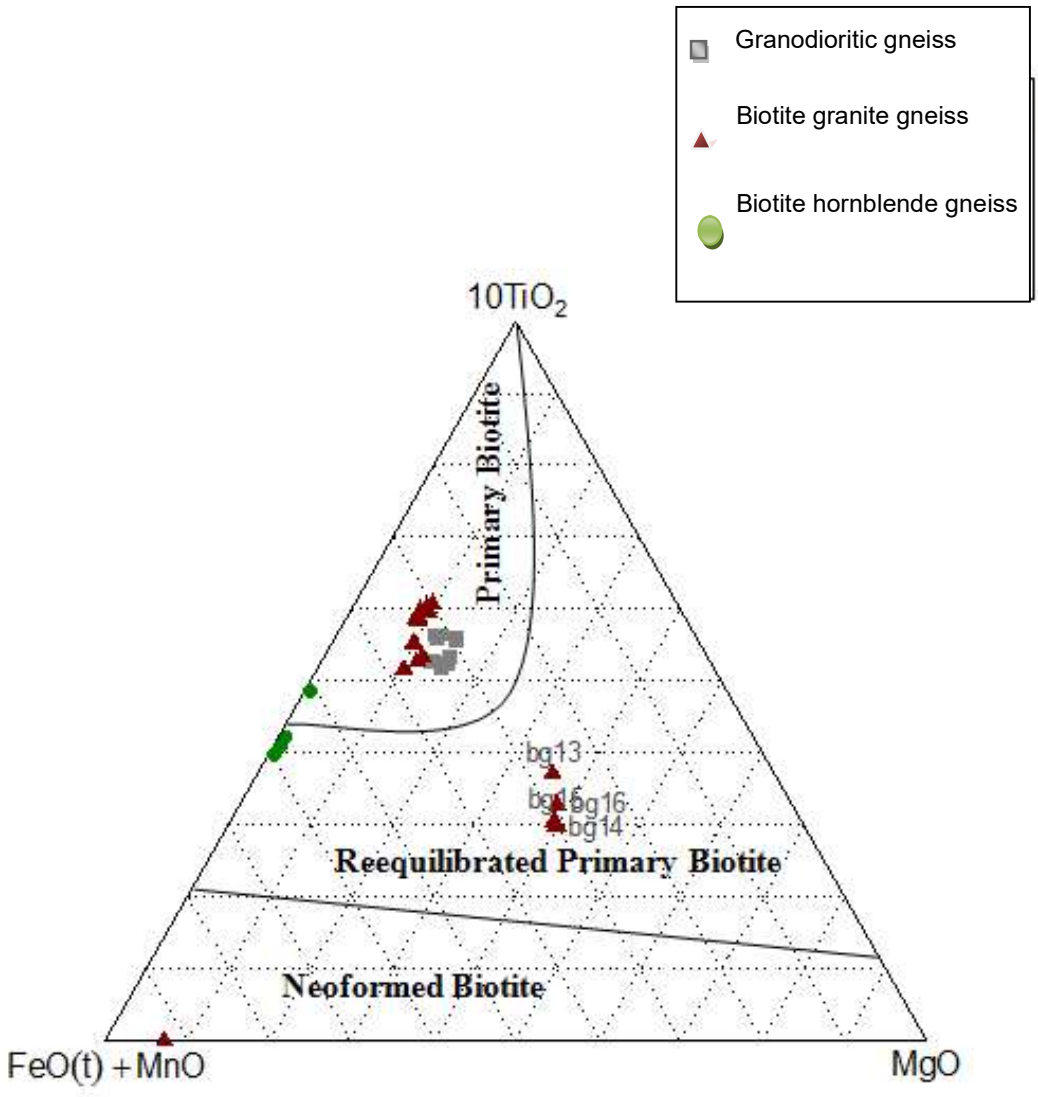

Fig.4.124 (FeO(t)+MnO)-10*TiO_2-MgO Plot for Biotites in Rock (After Nachit *et. al.*, 2005) .

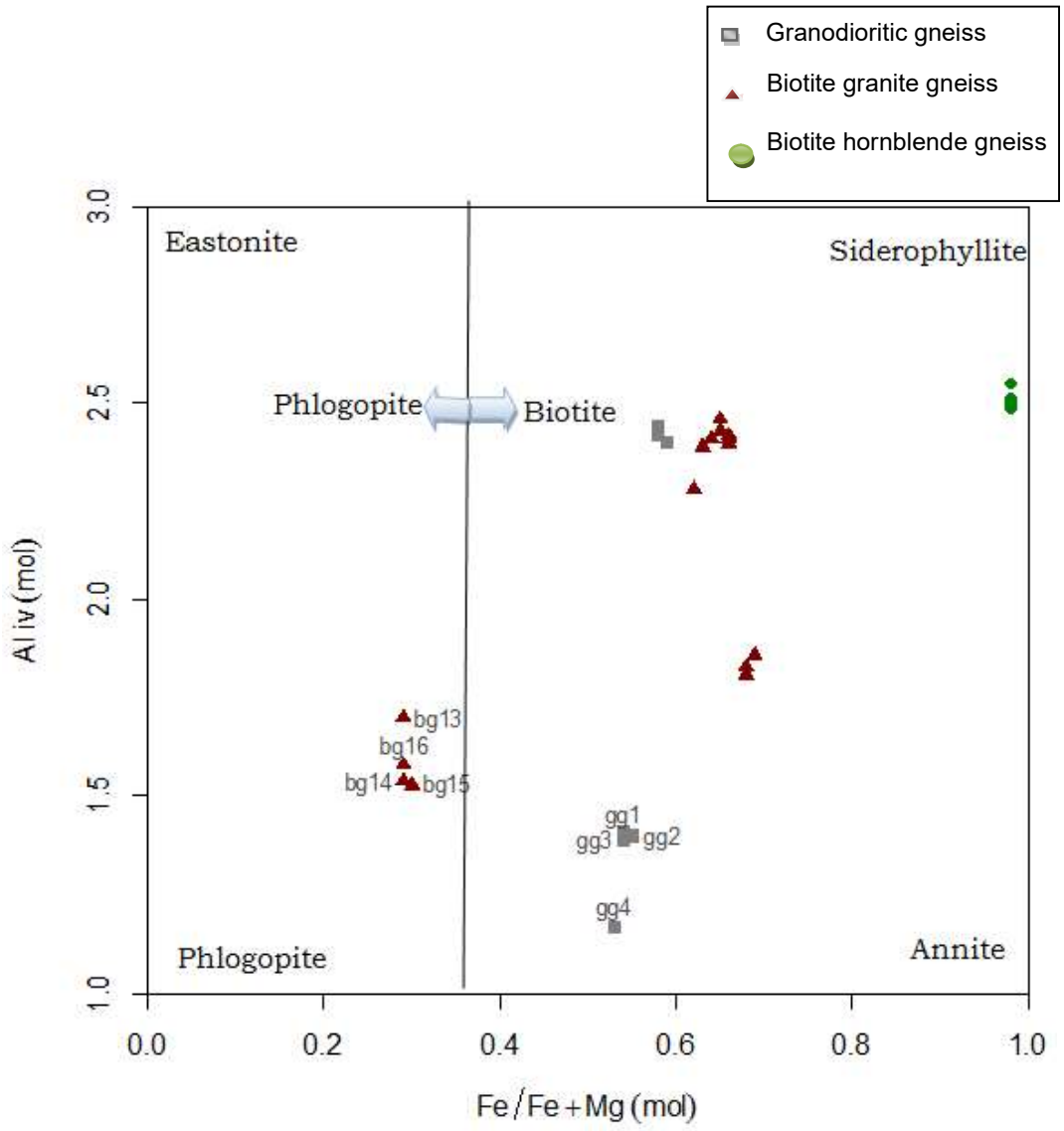

Fig.4.125 Plot of Al (iv) (apfu) vs Fe/(Fe+Mg) for Biotites in the Rocks. (After Deer, 1992).

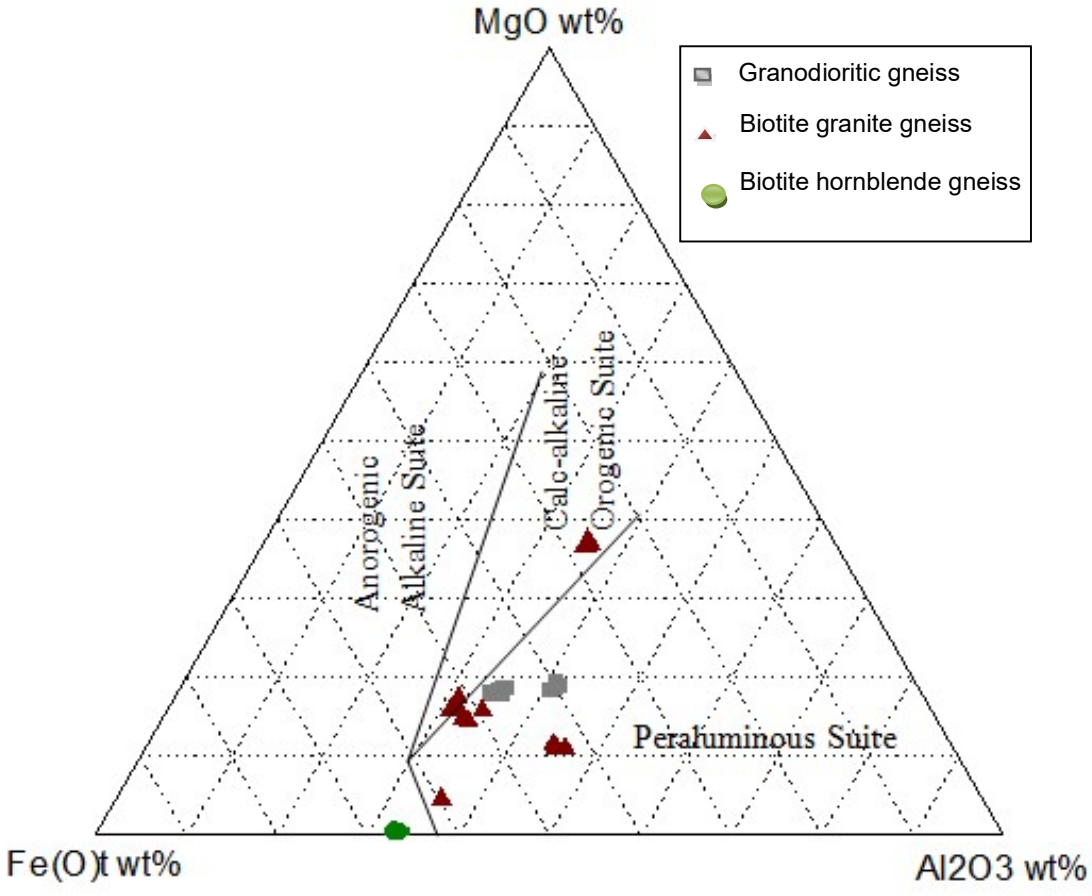

Fig.4.126 Plot of $FeO_{(t)}$-MgO-Al_2O_3 Showing the Peraluminous Nature of the Primary to Re-Equilibrated Biotites of Granodioritic and Biotite Granite Gneiss, while Biotite Hornblende Ggneiss Shows Alkaline Nature. (After Abdel-Rahman, 1994)

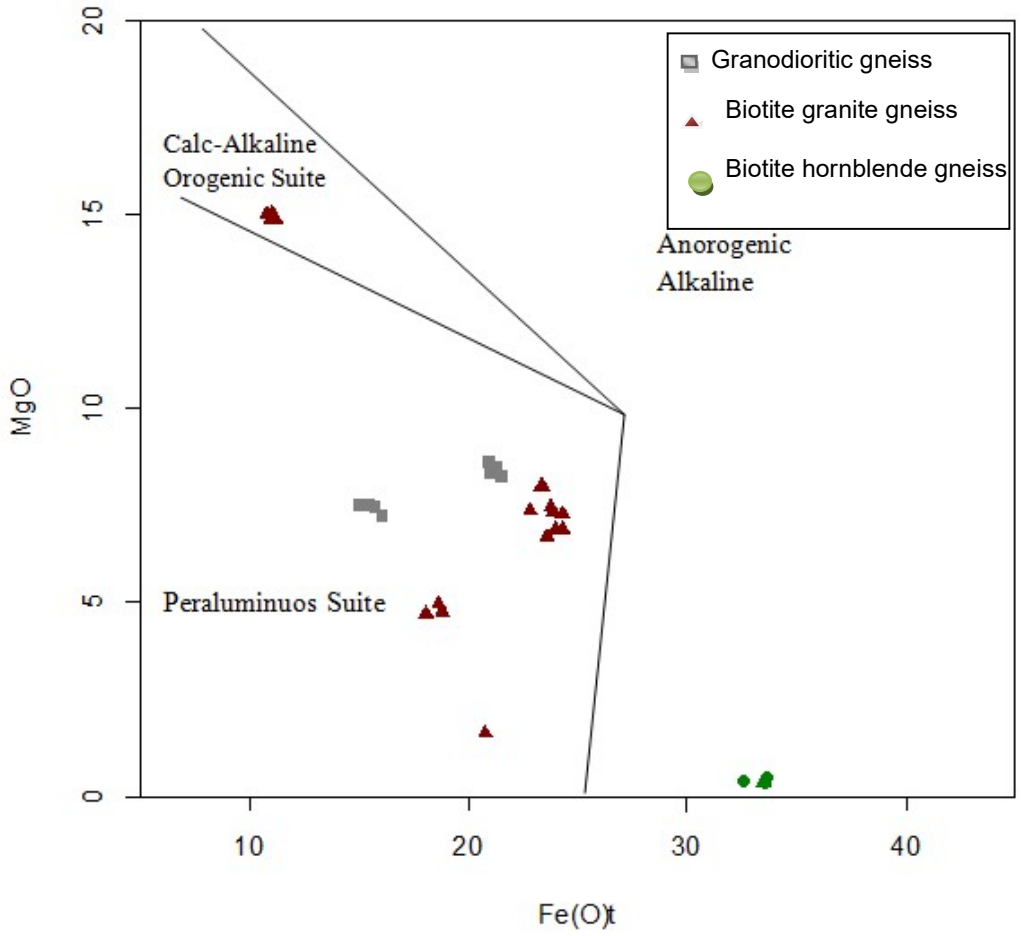

Fig.4.127 Plot of MgO against FeO(t) Showing the Peraluminous Nature of the Primary to Re-equilibrated Primary Biotites of Granodioritic and Biotite Granite Gneiss while Biotite Hornblende Gneiss Shows Alkaline Nature. (After Abdel-Rahman, 1994)

4.4.3 Amphiboles

Amphibole is common in the granodioritic gneiss but less in the biotite granite gneisses. Micro-probe image of tabular hornblende minerals (Fig.4.128) revealed the closed association with biotite, sphene, plagioclase and quartz mineral in the granodioritic gneiss. Representative reformatted oxide analyses of hornblende in each sample of granodioritic and biotite granite gneiss is presented in Table 4.64 and 4.65 on the basis of 23 O_2.

The result of the analysed amphibole revealed that SiO_2 varies from 38.24 to 48.87 wt.%, TiO_2 (0.33 to 1.81 wt.%), Al_2O_3 (7.79 to 9.64 wt.%), FeO (13.07 to 21.11 wt.%), MnO (<0.42), MgO (5.11 to 7.98 wt.%), CaO (9.55 to 21.82 wt.%). Na_2O (0.84 to 2.07 wt.%) and K_2O (1.31 to 4.01 wt.%). All the amphibole were mainly ferro-hornblende on the binary plot of $Mg/(Mg+Fe^{2+})$ versus Si (Leake*et. al,* 1997, Fig.4.129).

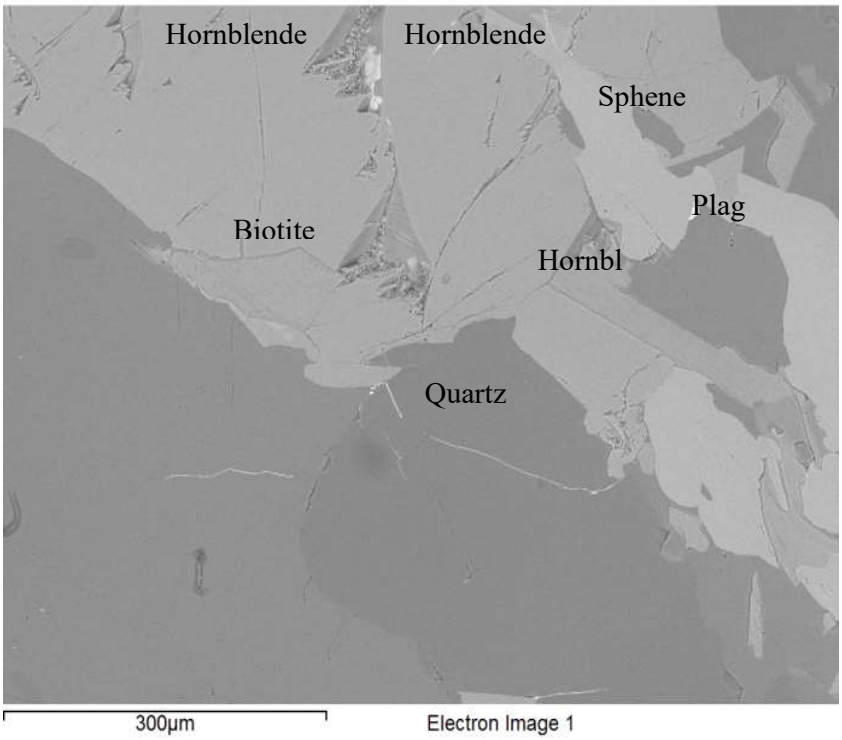

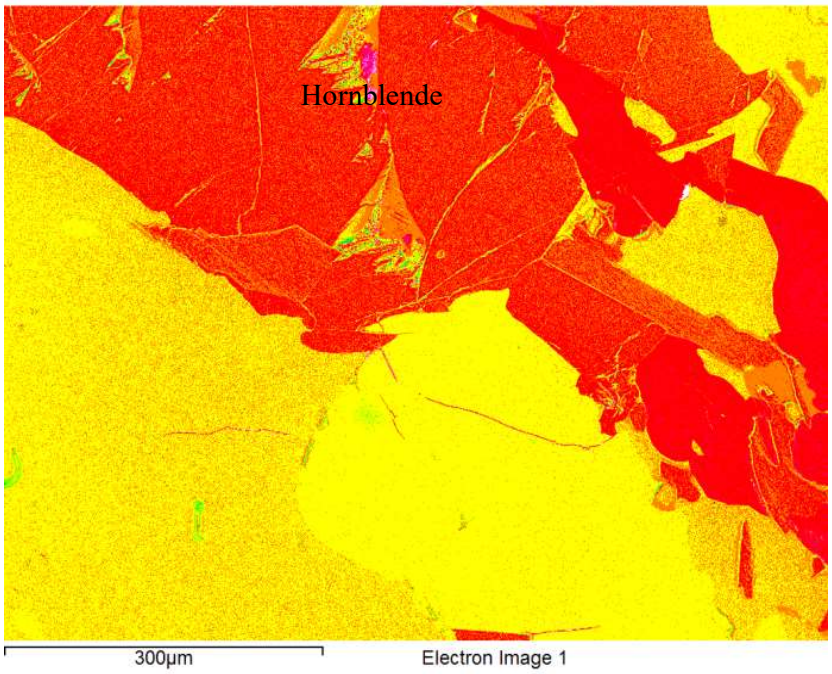

Fig.4.128 Micro-Probe Image of Hornblende Minerals in the Granodioritic Gneiss

Table 4.64 Reformatted Oxide Percentages of Amphiboles in the Granodioritic and Biotite Granite Gneiss

Sample no.	**G11**						**b16**
Analyses	1	2	3	4	5	6	1
SiO_2	38.24	46.28	47.11	47.01	47.29	48.87	42.98
TiO_2	1.81	1.38	1.52	1.29	1.42	1.59	0.33
Al_2O_3	9.64	11.97	11.45	11.64	11.44	11.38	7.79
FeO	21.11	18.25	17.59	17.94	17.62	16.80	13.07
MnO	0.00	0.33	0.40	0.34	0.39	0.42	0.00
MgO	5.11	7.67	7.94	7.98	7.92	7.46	5.59
CaO	9.55	10.92	10.62	10.52	10.55	10.19	21.82
Na_2O	2.07	1.70	1.90	1.89	1.91	1.80	0.84
K_2O	1.31	1.51	1.47	1.40	1.46	1.50	4.01
H_2O*calc	1.76	2.05	2.06	2.06	2.06	2.08	1.91
Total	90.67	102.05	102.06	102.06	102.06	102.08	96,42

Granodioritic gneiss- Sample no G11; Biotite granite gneiss-Sample no b16

Table 4.65 Structural Formulae and Classification of Amphibole based on 23 O_2.

Sample no.	**G11**						**b16**
Cations	1	2	3	4	5	6	1
Si	6.52	6.78	6.87	6.86	6.89	7.05	6.76
Al^{iv}	1.48	1.22	1.13	1.14	1.11	0.95	1.24
Al^{vi}	0.46	0.84	0.83	0.86	0.85	0.99	0.20
Ti	0.23	0.15	0.17	0.14	0.16	0.17	0.04
Fe^{3+}	0.10	0.00	0.00	0.00	0.00	0.00	0.00
Fe^{2+}	2.91	2.23	2.14	2.19	2.15	2.03	1.72
Mn	0.00	0.04	0.05	0.04	0.05	0.05	0.00
Mg	1.30	1.67	1.73	1.73	1.72	1.61	1.31
Ca	1.74	1.71	1.66	1.64	1.65	1.58	3.68
Na	0.68	0.48	0.54	0.53	0.54	0.50	0.26
K	0.28	0.28	0.27	0.26	0.27	0.28	0.81
OH*	2	2	2	2	2	2	2
Total	17.71	17.42	17.39	17.40	17.38	17.20	18.01
$Fe^2/(Fe^2+Fe^3)$	1.23	1.47	1.60	1.55	1.62	1.88	1.09
$Mg/(Mg+Fe^{2+})$	0.30	0.43	0.45	0.44	0.45	0.44	0.43
$Fe^{3+}/(Fe^{3+}+Al^{vi})$	0	0	0	0	0	0	0.00
Amphibole name	Ferro-edenite	Ferro hornblende	Ferro-hornblende	Ferro-hornblende	Ferro-hornblende		Ferro-edenite

Granodioritic gneiss- Sample no G11; Biotite granite gneiss-Sample no b16

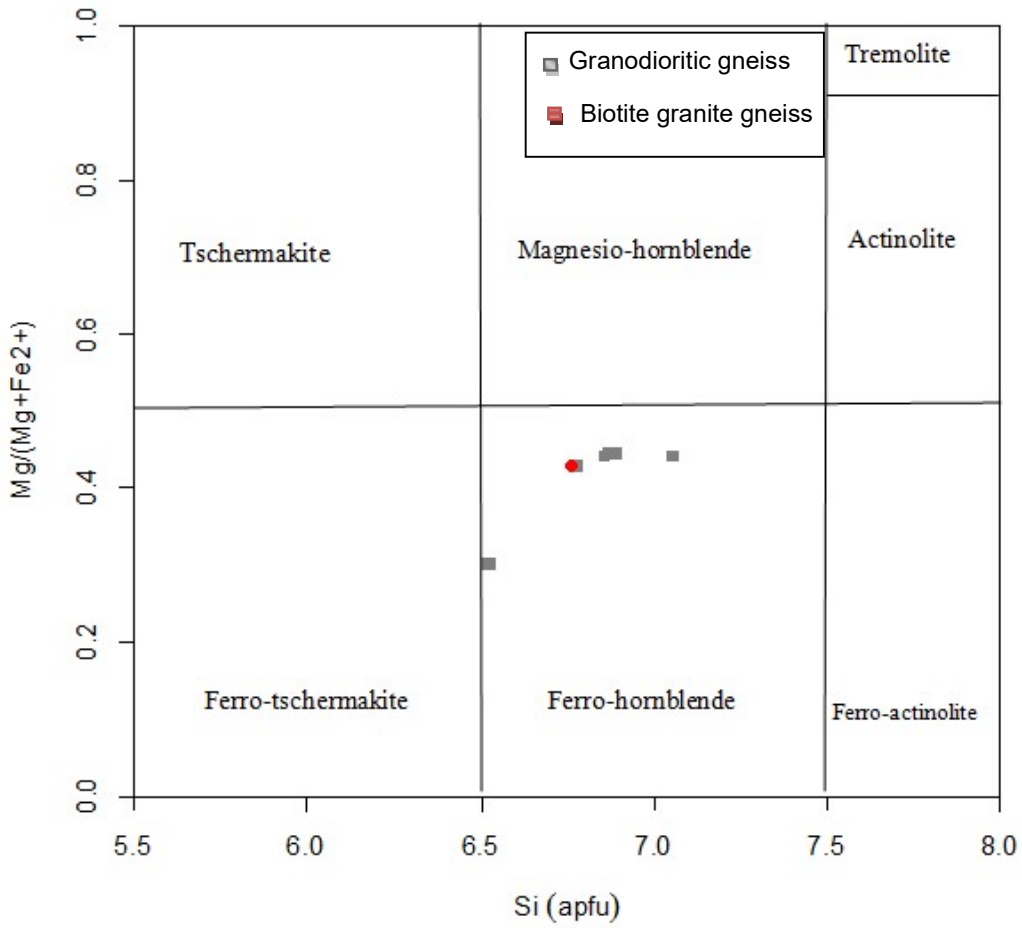

Fig.4.129 Binary Plot of Mg/(Mg+Fe^{2+}) against Si (apfu) of Amphiboles in Granodioritic and Biotite Granite Gneiss (After Leake *et. al.*, 1997).

4.4.4 Accessory Minerals

The chemical analyses of garnet in biotite granite gneiss (Table 4.66) were recalculated on the basis of $12O_2$ with the molecular proportion of their end member component. The garnet porphyroblast in petrographic section (Fig.4.73) as well as in the micro-probe image (Fig4.130) has variable chemical composition dominated by SiO_2 (34.12 to 47.33%), FeO (29.04 to 51.17%), Al_2O_3 (6.06 to 19.45%), with minor amounts of MnO (1.00 to 2.02%), MgO (0.81 to 2.17%), and CaO (0.90 to 2.44%). The garnet components are chiefly almandine variety (82.96 to 84.27mol %) with subsidiary amount of pyrope (3.54 to 10.44mol %), grossular (2.19 to 3.72mol %) and spessartine (2.87 to 4.95mol%) (Fig.4.131 and 4.132) and X_{Fe} ratio ranges from (0.89 to 0.97).

Chlorite flakes is another ferromagnesian mineral in the granodioritic gneiss. The major elements compositional variations with their structural formula are presented in Table 4.67 on the basis of $28O_2$ equivalents. The chlorite displayed different component variations with SiO_2 ranged 26.11 to 34.43 wt%; Al_2O_3, 16.37 to 16.98wt%; FeO, 21.03 to 33.64wt%; MgO, 8.20 to 14.92wt% and Fe_2O_3, 0.40 to 2.59wt% (Fig. 4.133 and 4.134). The ratio of Fe/(Fe+Mg) ranged from 0.49 to 0.70, while Si (apfu) content was from 5.64 to 6.11. This led to the classification of the chlorite as brunsvigite variety (Fig.4.135).

Apatite was found in both granodioritic and biotite granite gneiss (Fig4.136). Analyses of apatite were recalculated on the basis of $26(O_2, OH, F)$ (Table 4.68). The result of apatite analyses in the rock samples revealed significant amount of CaO (34.80 to 54.28 wt%) and P_2O_5 (31.13 to 42.59wt%) with lesser amount of SiO_2 (<20.80wt%) and FeO (<3.84wt%). The presence of appreciable amount of Florine (3.13 to 4.25 wt %), hence the apatite fall in fluoro-apatite end member (Deer *et. al*, 1992).

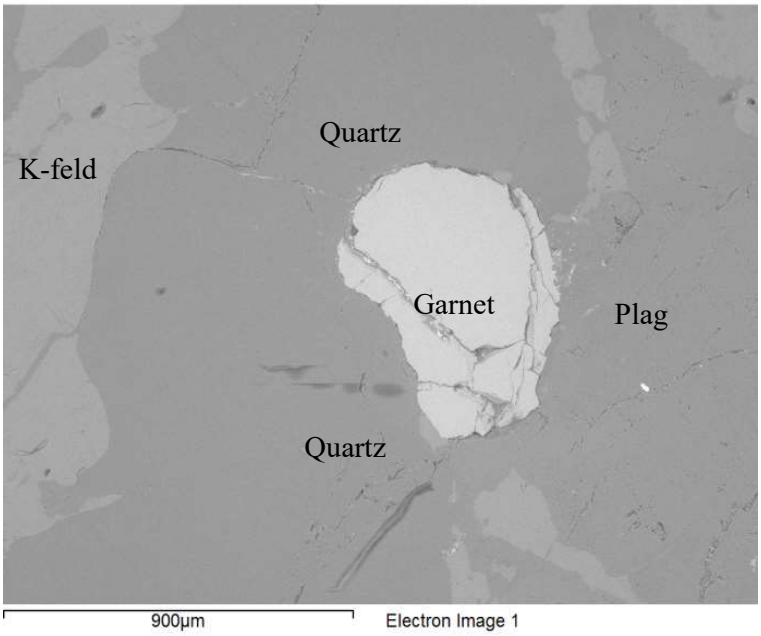

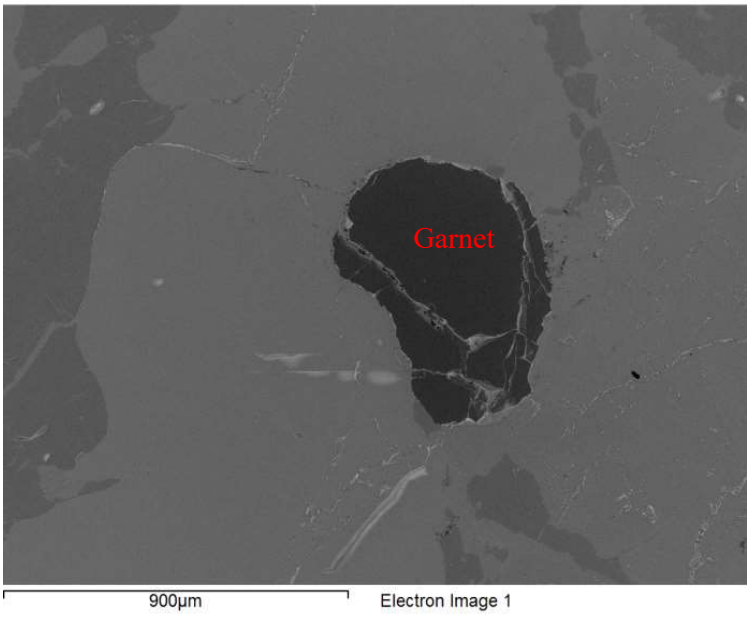

Fig4.130 Micro-Probe Image of Porphyroblastic Garnet in the Biotite Granite Gneiss

Table 4.66 Microprobe Analyses and Structural Formulae of Garnets in the Biotite Granite Gneiss.

Sample no	**b16**						
Oxide	1	2	3	4	5	6	7
SiO_2	47.33	44.74	46.34	45.24	47.02	34.34	34.12
TiO_2	0.00	0.00	0.00	0.00	0.00	0.00	0.00
Al_2O_3	18.32	19.45	19.14	19.28	19.02	6.06	6.56
Fe_2O_3	0.00	0.00	0.00	0.00	0.00	0.00	0.00
FeO	29.66	30.71	29.51	30.69	29.04	50.27	51.17
MnO	1.05	1.05	1.03	1.17	1.00	2.01	1.83
MgO	2.09	2.17	2.08	1.99	1.94	1.25	0.81
CaO	0.90	1.08	0.99	0.91	0.97	2.02	2.44
Total	99.35	99.18	99.09	99.28	98.98	95.94	96.93
cations	**Structural Formulae (based on 12 O_2)**						
Si	3.84	3.63	3.76	3.67	3.82	3.08	3.03
Ti	0.00	0.00	0.00	0.00	0.00	0.00	0.00
Al	1.75	1.86	1.83	1.84	1.82	0.64	0.69
Fe^{3+}	0.00	0.00	0.00	0.00	0.00	1.20	1.25
Fe^{2+}	2.01	2.08	2.00	2.08	1.97	2.56	2.56
Mn	0.07	0.07	0.07	0.08	0.07	0.15	0.14
Mg	0.25	0.26	0.25	0.24	0.23	0.17	0.11
Ca	0.08	0.09	0.09	0.08	0.08	0.19	0.23
tot. cat.	8	8	8	8	8	8	8
tot. oxy.	12.7	12.6	12.7	12.6	12.7	12	12
X(Fe)							
Fe_T/Fe_T+Mg	0.89	0.89	0.89	0.90	0.89	0.96	0.97
$Fe^{2+}/Fe^{2+}+Mg$	0.89	0.89	0.89	0.90	0.89	0.94	0.96

Table 4.66 (continue) Micro-Probe Analyses and Structural Formulae of Garnets in the Biotite Granite Gneiss.

End member mol%	**b16** 1	2	3	4	5	6	**7**
Almandine	83.33	82.96	83.07	83.89	83.58	83.33	84.27
Pyrope	10.44	10.44	10.42	9.70	9.94	5.42	3.54
Grossular	3.22	3.72	3.58	3.18	3.58	2.19	2.72
spessartine	3.00	2.87	2.94	3.23	2.90	4.95	4.54
Uvarovite	0.00	0.00	0.00	0.00	0.00	0.00	0.00
Andradite	0.00	0.00	0.00	0.00	0.00	4.11	4.93
Ca-Ti Gt	0.00	0.00	0.00	0.00	0.00	0.00	0.00
Total	100	100	100	100	100	100.00	100.00

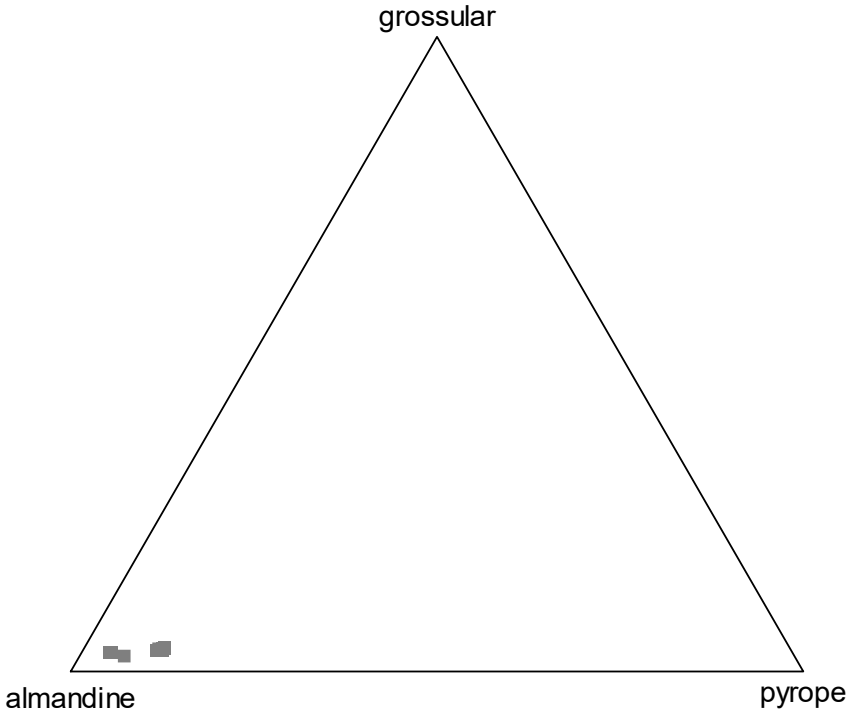

Fig.4.131 Plot of Alm-Gro-Pyr showing Almandine, Grossular and Pyrope Composition of Garnets in Biotite Granite Gneiss.

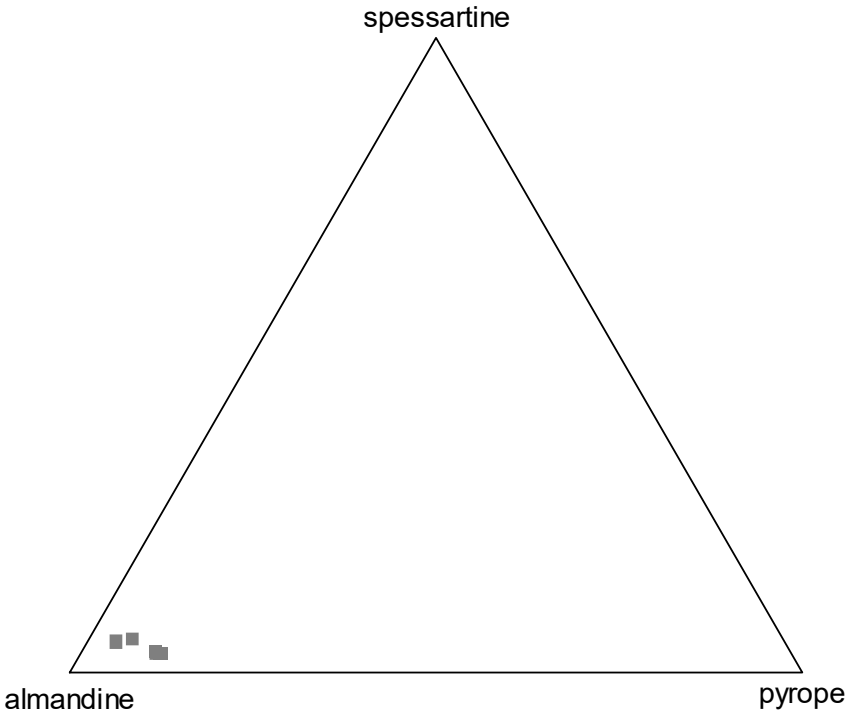

Fig.4.132 Plot of Alm-Sps-Pyr showing Almandine, Spessartine and Pyrope Composition of Garnets in Biotite Granite Gneiss.

Table 4.67 Reformatted Oxide Percentages of Chlorites in Granodioritic Gneiss in the Study Area.

Sample no	**G6**					
Oxide	1	2	3	4	5	6
SiO_2	26.22	26.11	27.32	28.05	28.22	34.43
TiO_2	0.00	0.00	0.33	0.37	0.26	2.87
Al_2O_3	16.37	18.98	16.42	16.53	16.59	16.89
Cr_2O_3	0.00	0.00	0.00	0.00	0.00	0.00
Fe_2O_3	1.01	0.40	1.19	1.56	1.81	2.59
FeO	33.64	25.05	27.81	26.43	26.15	21.03
MnO	0.20	0.23	0.51	0.37	0.61	0.30
MgO	8.26	14.92	11.91	12.16	12.35	10.84
CaO	0.10	0.00	0.38	0.19	0.13	1.23
K_2O	0.00	0.00	0.11	0.46	0.15	5.49
H_2O*calc	10.53	11.09	10.88	10.97	11.01	12.32
Total	96.33	96.78	96.86	97.10	97.28	107.99

Table 4.67 (continue) Reformatted Oxide Percentages of Chlorites in Granodioritic Gneiss in the Study Area.

Reformatted oxide percentages based on 28 oxygen (with $Fe^{2+/}Fe^{3+}$ and OH calculated assuming full site occupancy)						
Sample no	G6					
	1	2	3	4	5	6
Si	5.96	5.64	6.00	6.09	6.11	6.50
Al^{iv}	2.04	2.36	2.00	1.91	1.89	1.50
Al^{vi}	2.35	2.48	2.27	2.35	2.37	2.38
Ti	0.00	0.00	0.05	0.06	0.04	0.41
Cr	0.00	0.00	0.00	0.00	0.00	0.00
Fe^{3+}	0.17	0.07	0.20	0.25	0.30	0.37
Fe^{2+}	6.39	4.53	5.11	4.80	4.73	3.32
Mn	0.04	0.04	0.09	0.07	0.11	0.05
Mg	2.80	4.80	3.90	3.93	3.99	3.05
Ni	0.00	0.00	0.00	0.00	0.00	0.00
Zn	0.00	0.00	0.00	0.00	0.00	0.00
Ca	0.03	0.00	0.09	0.04	0.03	0.25
K	0.00	0.00	0.06	0.26	0.08	2.64
OH*	16	16	16	16	16	16
Total	35.78	35.92	35.77	35.77	35.65	36.47
Fe/Fe+Mg	0.70	0.49	0.58	0.56	0.56	0.55

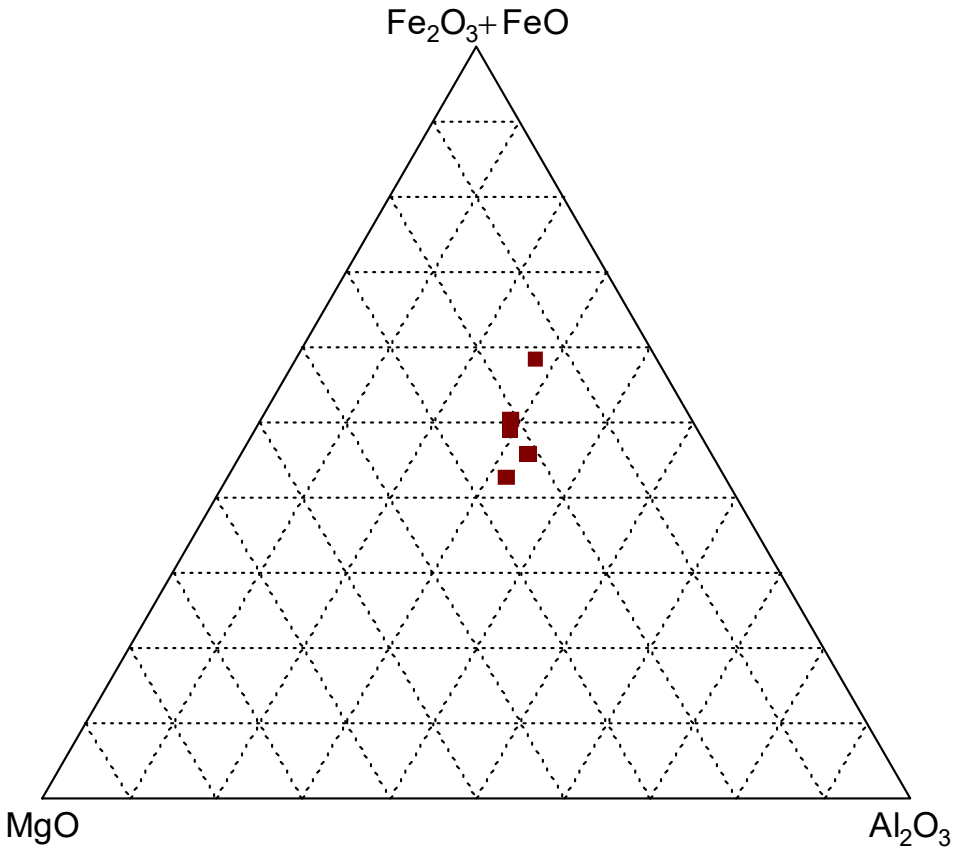

Fig.4.133 Ternary Plot of MgO-Fe_2O_3+FeO-Al_2O_3 Showing Compositional Variations in Chlorite from Granodioritic Gneiss.

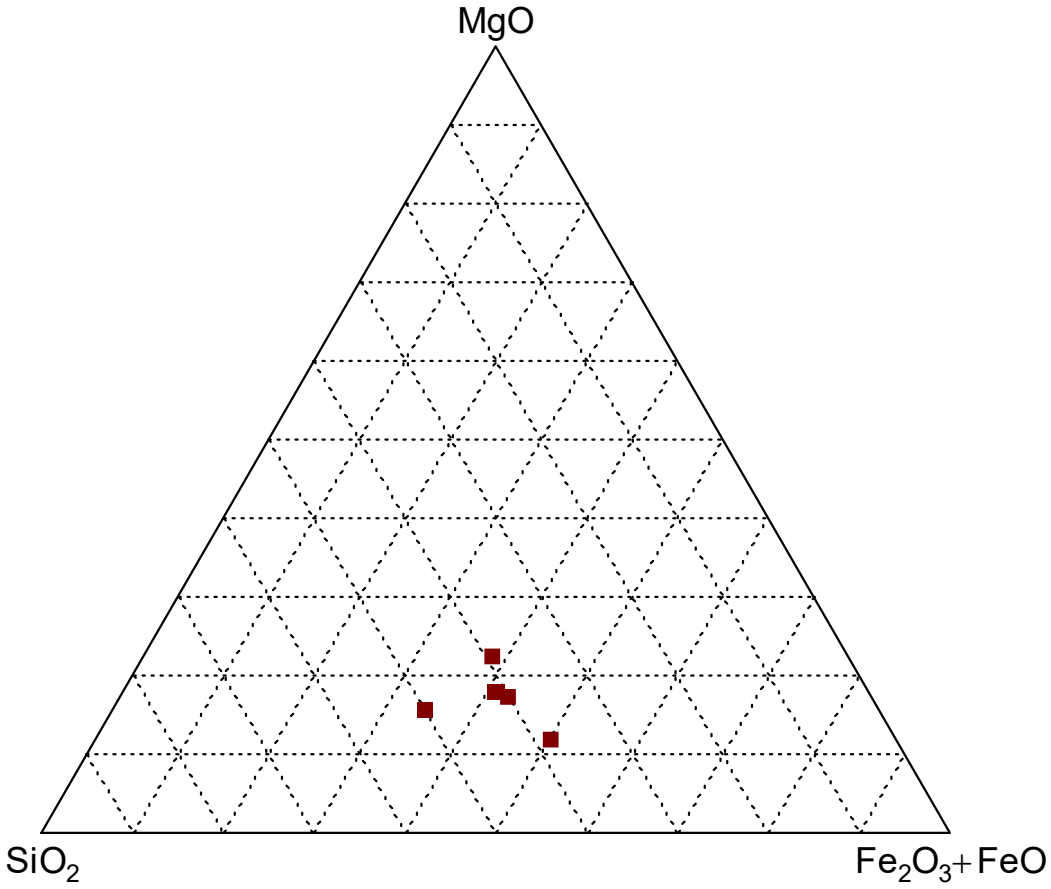

Fig.4.134 Ternary Plot of SiO_2-MgO-Fe_2O_3+FeO Showing Compositional Variation in Chlorite from Granodioritic Gneiss.

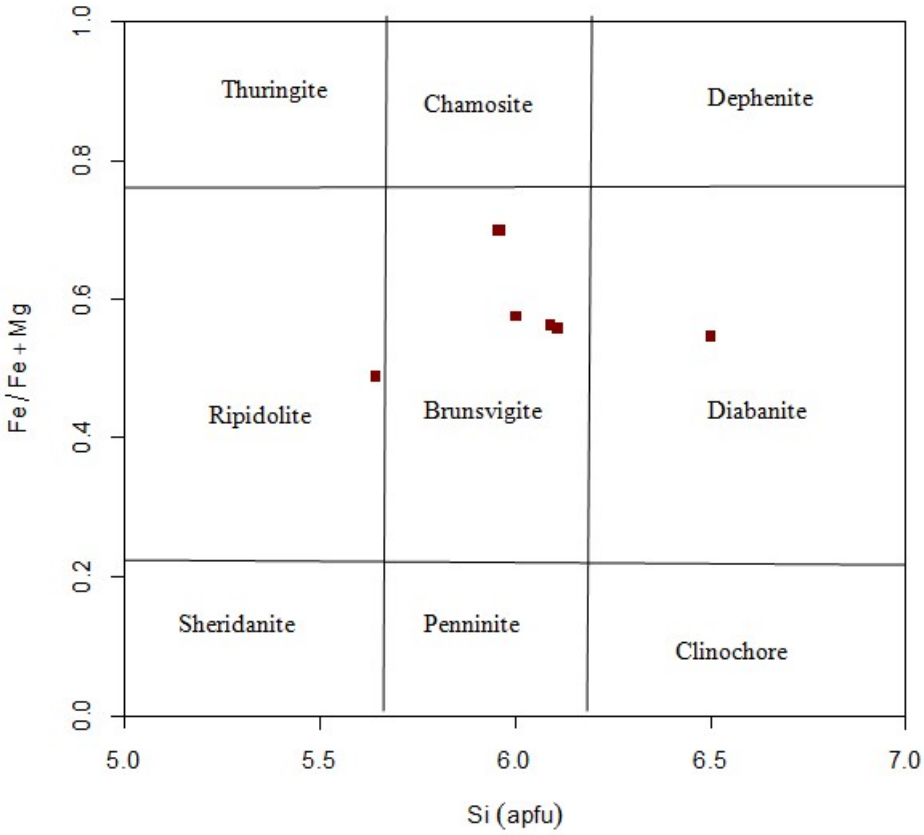

Fig.4.135 Compositional Variations of Chlorites in Terms of Fe/(Fe+Mg) versus Si in the Granodioritic Gneiss. (After Hey,1954).

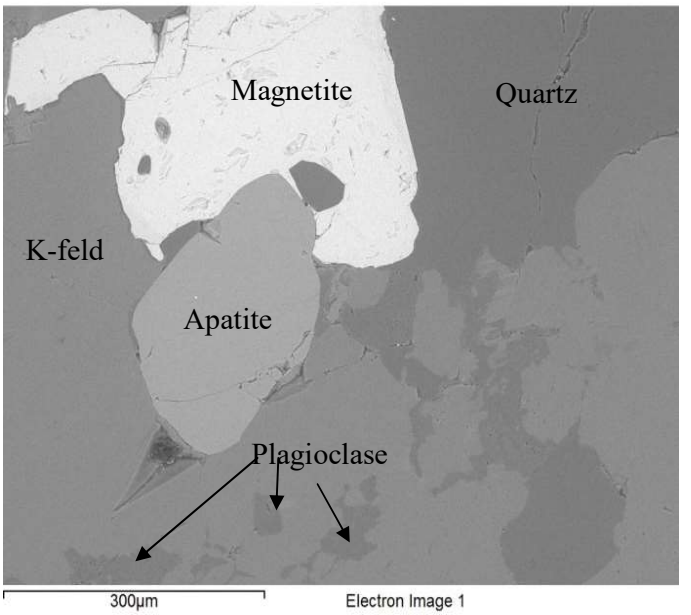

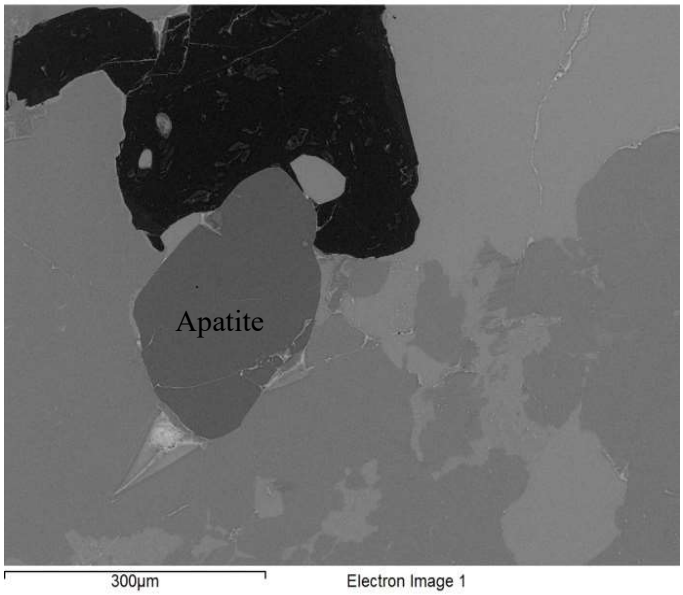

Fig.4.136 Micro-Probe Image of Apatite in the Biotite Granite Gneiss.

Table 4.68 Microprobe Analyses of Apatite on the Basis of $26O_2$ in the Granodioritic and Biotite Granite Gneiss.

Sample no.	**G11**						**b13**		
Analyses	1	2	3	4	5	6	1	2	3
SiO_2	0.00	0.00	0.00	0.00	0.00	12.76	10.69	9.83	20.80
FeO	0.00	0.00	0.00	0.00	0.00	0.30	2.04	3.84	0.55
CaO	54.28	54.01	54.05	54.03	54.02	41.49	41.68	41.67	34.80
Na_2O	0.00	0.00	0.00	0.00	0.00	0.97	0.00	0.26	0.35
P_2O_5	42.40	42.56	42.59	42.49	42.48	37.80	37.04	36.47	31.13
Cl	0.00	0.00	0.00	0.00	0.00	0.00	0.00	0.00	0.00
F	3.34	3.46	3.37	3.45	3.49	3.62	4.25	4.11	3.13
Total	100.02	100.02	100.02	99.96	99.99	96.94	95.70	96.18	90.77
Cation									
Si	0.00	0.00	0.00	0.00	0.00	2.03	1.75	1.62	3.46
Fe	0.00	0.00	0.00	0.00	0.00	0.04	0.28	0.53	0.08
Ca	9.49	9.43	9.44	9.44	9.44	7.08	7.30	7.37	6.19
Na	0.00	0.00	0.00	0.00	0.00	0.30	0.00	0.08	0.11
P	5.86	5.87	5.88	5.87	5.86	5.10	5.13	5.10	4.38
Cl	0.00	0.00	0.00	0.00	0.00	0.00	0.00	0.00	0.00
F	1.72	1.78	1.74	1.78	1.80	1.82	2.20	2.15	1.64
OH	-0.72	-0.78	-0.74	-0.78	-0.80	-0.82	-1.20	-1.15	-0.64
Total	16.35	16.30	16.32	16.31	16.30	15.56	15.46	15.70	15.21

Results of chemical analyses of titanite were recalculated on the basis of 1Si ions in the unit cell and the structural formulae for each sample of granodioritic gneiss and biotite granite gneiss (Table 4.69). The oxide composition revealed significant amount of SiO_2 (38.53 to 48.61 wt%), TiO_2 (22.90 to 26.27 wt%), CaO (20.99 to 21.88wt%), and F (<2.48wt%) with minor amount of Al_2O_3 (3.17 to 5.93wt%), FeO_{total} (1.53 to 3.75wt%) and Na_2O (<1.30wt%). The results indicate chemical substitution of Ti by Al and excess of Si, while substitution of Ca contents was by Fe^{2+}, Mg, Na and K ions.

Zircon occurs as inclusions in the quartz and k-feldspars in the biotite granite gneiss (Fig.4.137). The composition of zircon contain substantial amount of ZrO_2 (49.04 to 49.74 wt%), SiO_2 (39.65 to 47.53wt%) and Al_2O_3(1.56 to 4.67wt%) with HfO_2 (1.36wt%) (Table 4.70).

The oxide composition with the structural formulae of rutile needle in the biotite gneiss contained appreciable amount of TiO_2 (64.50 to 70.32 wt%) with minor amount of FeO (1.29 to 1.86wt%) (Table 4.71) and it occurs as inclusions in K-feldspars mineral. Exsolution blebs of magnetite occur in association with titanite in the sample (Fig.4.138). Table 4.72 present the analyses of oxide composition and the structural formulae of magmatite in the granodioritic gneiss and biotite granite gneiss samples.

Table 4.69 Microprobe Analyses of Titanite (sphene) on the Basis of 1Si in the Granodioritic and Biotite Granite Gneiss.

Sample no	G6				b13			
Analyses	1	2	3	4	1	2	3	4
SiO_2	42.40	42.72	42.48	41.51	46.85	46.20	48.61	38.53
TiO_2	24.82	23.95	26.27	26.22	23.72	22.90	23.50	24.39
Al_2O_3	5.44	5.43	4.98	5.70	3.69	4.42	3.17	5.93
FeO_{Total}	3.16	3.75	2.32	2.21	1.54	1.72	1.53	3.15
MgO	1.05	1.30	0.67	0.61	0.00	0.00	0.00	1.80
CaO	21.55	21.29	21.81	21.88	21.38	21.43	20.99	22.31
Na_2O	1.16	1.10	0.99	1.38	0.00	0.00	0.00	0.31
K_2O	0.41	0.46	0.48	0.50	0.44	0.50	0.43	1.03
F	0.00	0.00	0.00	0.00	2.08	2.48	1.52	2.24
Total	100.00	100.00	100.00	100.00	99.69	99.65	99.76	99.69
Cation	Structural formulae on the basis of 1Si							
Si	1.32	1.33	1.32	1.29	1.46	1.45	1.50	1.25
Ti	0.58	0.56	0.61	0.61	0.56	0.54	0.54	0.59
Al	0.20	0.20	0.18	0.21	0.14	0.16	0.12	0.23
Fe^{2+}	0.08	0.10	0.06	0.06	0.04	0.05	0.04	0.09
Mg	0.05	0.06	0.03	0.03	0.00	0.00	0.00	0.09
Ca	0.72	0.71	0.73	0.73	0.71	0.72	0.69	0.77
Na	0.07	0.07	0.06	0.08	0.00	0.00	0.00	0.02
K	0.02	0.02	0.02	0.02	0.02	0.02	0.02	0.04
F	0.00	0.00	0.00	0.00	0.21	0.25	0.15	0.23
Total	3.04	3.05	3.01	3.04	3.13	3.18	3.06	3.31

G6-Granodioritic gneiss, b13- Biotite granite gneiss

Table 4.70 Microprobe Analyses of Accessory Zircon on the Basis $16O_2$ in the Biotite Granite Gneiss.

Sample no	**b16**	**b13**
SiO_2	39.65	47.53
ZrO_2	49.74	49.04
Hf O_2	1.36	0.00
Al_2O_3	4.67	1.56
FeO	0.59	0.77
Total	100.00	100.00
Cation on $16O_2$	Structural formulaebasis	
Si	6.68	5.20
Zr	0.30	2.62
Hf	0.07	0.00
Al	0.93	0.20
Fe_{total}	0.08	0.07
Total	8.05	8.09

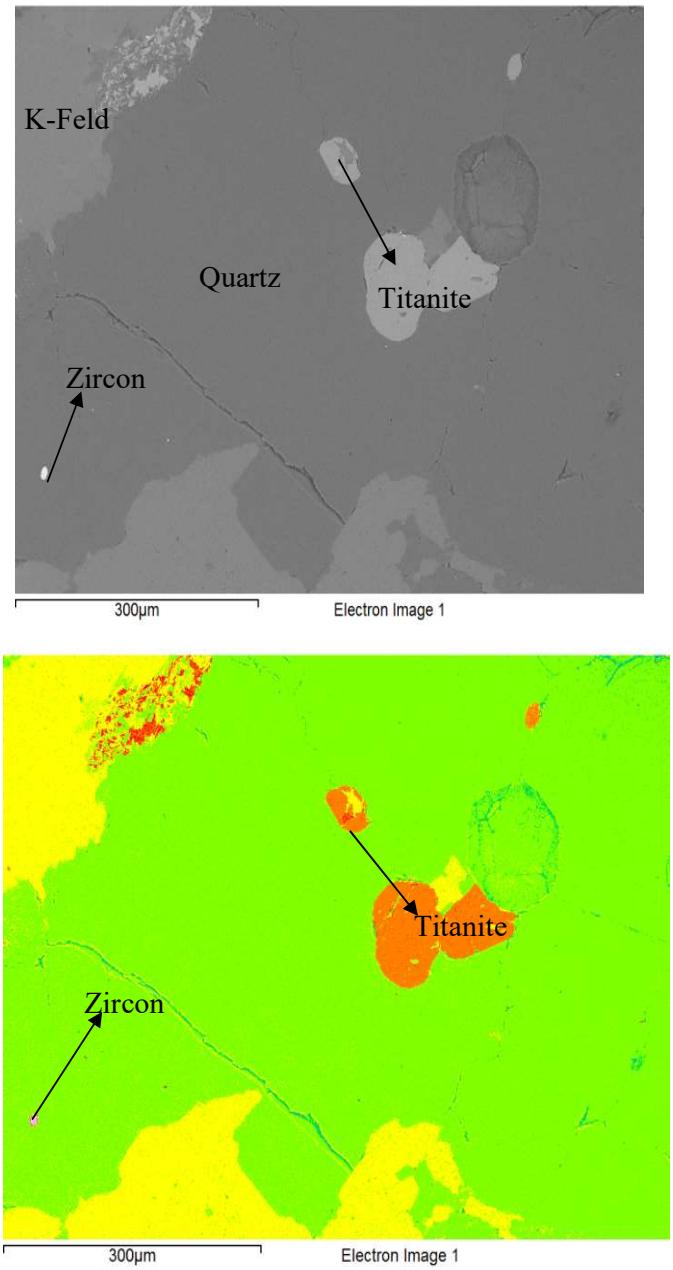

Fig4.137 Micro-Probe Image of Titanite and Zircon Inclusion in Quartz in the Biotite Granite Gneiss.

Table 4.71 Microprobe Analyses of Accessory Rutile on the Basis $2O_2$ in the Biotite Granite Gneiss.

Sample no	**b13**	
Analyses	1	2
TiO_2	70.32	64.50
Cr_2O_3	0.00	0.00
Al_2O_3	4.63	5.28
Nb_2O_5	0.00	0.00
FeO	1.29	1.86
MnO	0.00	0.00
MgO	0.00	0.00
CaO	1.38	0.38
SiO_2	18.25	21.81
Total	95.87	93.84
Cation on the basis of $2O_2$		
Ti	0.69	0.64
Cr	0.00	0.00
Al	0.07	0.08
Nb	0.00	0.00
Fe	0.01	0.02
Mn	0.00	0.00
Mg	0.00	0.00
Ca	0.02	0.01
Si	0.24	0.29
TOTAL	1.03	1.03

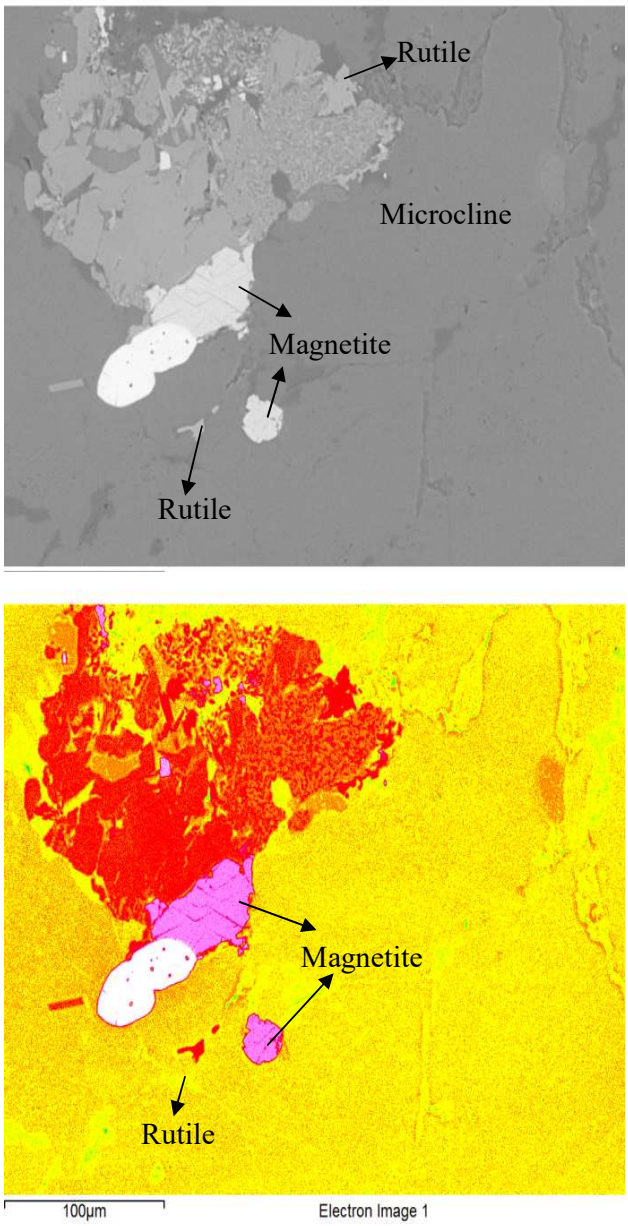

Fig.4.138 Micro-Probe Image of Magnetite and Inclusion of Rutile Needle in Microcline in the Biotite Granite Gneiss.

Table 4.72 Microprobe Analyses of Magnetite on the Basis $4O_2$ in the Granodioritic and Biotite Granite Gneiss.

Sample no	**G6**	**b16**		**b13**										
Analyses	1	1	2	1	2	3	4	5	6	7	8	9	10	11
SiO_2	20.26	34.34	34.12	14.07	16.91	20.54	20.80	23.79	23.60	23.28	24.11	23.75	24.59	21.53
TiO_2	3.45	0.00	0.00	0.00	0.00	9.32	8.90	6.80	6.98	11.29	7.49	7.39	3.98	4.38
Al_2O_3	6.09	6.06	6.56	2.81	2.12	4.76	4.85	5.52	5.55	5.85	5.99	5.87	6.12	4.50
FeO	62.36	50.27	51.17	80.75	79.61	61.46	61.52	60.59	60.64	55.79	58.42	58.99	61.25	63.05
MnO	0.00	2.01	1.83	0.00	0.00	0.00	0.00	0.00	0.00	0.00	0.00	0.00	0.00	0.00
MgO	1.07	1.25	0.81	0.00	0.00	0.00	0.00	0.00	0.00	0.00	0.00	0.00	0.00	0.00
CaO	4.16	2.02	2.44	0.60	0.63	1.33	1.16	0.00	0.00	0.33	0.48	0.45	0.45	4.10
Na_2O	2.16	0.47	0.45	0.00	0.00	0.50	0.57	0.45	0.45	0.55	0.48	0.60	0.57	0.45
K_2O	0.45	1.50	1.61	1.19	0.73	2.08	2.21	2.86	2.78	2.91	3.03	2.95	3.04	1.99
TOTAL	100.00	97.91	99.00	9.42	100.00	100.00	100.00	100.00	100.00	100.00	100.00	100.00	100.00	100.00

Table 4.72 (continue) Microprobe Analyses of Magnetite on the Basis $4O_2$ in the Granodioritic and Biotite Granite Gneiss.

Sample no	**G6**	**b16**		**b13**										
Analyses	1	1	2	1	2	3	4	5	6	7	8	9	10	11
Si	0.69	1.07	1.05	0.55	0.64	0.70	0.70	0.79	0.78	0.76	0.79	0.78	0.82	0.74
Al	0.25	0.22	0.24	0.13	0.09	0.19	0.19	0.22	0.22	0.22	0.23	0.23	0.24	0.18
Ti	0.09	0.00	0.00	0.00	0.00	0.24	0.23	0.17	0.17	0.28	0.18	0.18	0.10	0.11
Fe	1.78	1.31	1.32	2.65	2.53	1.74	1.74	1.68	1.68	1.51	1.60	1.63	1.70	1.81
Mn	0.00	0.05	0.05	0.00	0.00	0.00	0.00	0.00	0.00	0.00	0.00	0.00	0.00	0.00
Mg	0.05	0.06	0.04	0.00	0.00	0.00	0.00	0.00	0.00	0.00	0.00	0.00	0.00	0.00
Ca	0.15	0.07	0.08	0.03	0.03	0.05	0.04	0.00	0.00	0.01	0.02	0.02	0.02	0.15
Na	0.14	0.03	0.03	0.00	0.00	0.03	0.04	0.03	0.03	0.03	0.03	0.04	0.04	0.03
K	0.02	0.06	0.06	0.06	0.04	0.09	0.10	0.12	0.12	0.12	0.13	0.12	0.13	0.09
Total	3.18	2.86	2.87	3.41	3.33	3.03	3.04	3.01	3.01	2.93	2.99	3.00	3.04	3.11

G6- Granodioritic gneiss, b13 and b16 are Biotite Granite Gneiss

4.5 Metallic Mineralisation Potentials of Sheet 241, Oyo SE

A summary of some metallic elements in the lithologic units of Sheet 241, Oyo SE revealed the anomalous concentrations of Copper (Cu), Lead (Pb), Zinc (Zn), Nickel (Ni) and Gold (Au) (Table 4.73). Result of Whole Rock analysis revealed that Cu values ranged from 8.5 to 43.3ppm; 7.0 to 26.8ppm and 7.9 to 64.2ppm in the pelitic schist, biotite hornblende and biotite granite gneisses respectively, while 10.4ppm and 32ppm were recorded in the leucogranite and pegmatite respectively.

Lead (Pb) concentration in schists, biotite hornblende and biotite granite gneisses ranged from 3.4 to 31.7ppm, 3.0 to 30.8ppm and 3.0 to 39.5ppm respectively. The leucogranite and pegmatite both have Pb cconcentration of 2.9ppm and 6.0ppm.

Zinc (Zn) composition varies between broad limit with the schists (31.0-128ppm); biotite hornblende gneiss (34.0-132.0ppm); biotite granite gneiss (32.0-16.0ppm); leucogranite (46ppm) and pegmatite (21ppm).

Nickel (Ni) values contained in the schists ranged from 4.9 to 12.9ppm, while biotite hornblende and biotite granite gneiss ranged from 4.8 to 13.4ppm and 7.0 to 14.6ppm respectively. Leucogranite contained 7.6ppm concentration of Nickel, while 2.4ppm was recorded in the pegmatite.

The Whole Rock analyses revealed anomalous concentrations of Gold (Au) in the schists (0.6-30.8ppb) and pegmatite (15.5ppb) which are in close association with the quartz schist. Gold contents in the biotite hornblende and biotite granite gneisses ranged from <0.5 to 12.8ppb and <0.5 to 7.7ppb respectively.

The concentrations of the Cu, Pb, Zn, Ni and Au were superimposed on the geology of the area (Fig.4.139 to Fig.4.143), while the histogram was also used to indicate the minimum and maximum values of these metallic minerals in the different lithologic units (Fig.4.144) in order to show their mineralisation potentials.

Table 4.73 Summary of Selected Metallic Mineralisation Potentials in Lithologic Units.

RockUnits →	**Pelitic Schist**		**Biotite Hornblende Gneiss**		**Biotite Granite Gneiss**		**Leuco-granite**	**Pegmatite**
Metals ↓	Range	Mean	Range	Mean	Range	Mean		
Cu	8.5-43.3	22.3	7.0-26.8	16.3	7.9-64.2	19.0	10.4	32.0
Pb	3.4-31.7	15.3	3.0-30.8	14.8	3.0-39.5	11.8	2.9	6.0
Zn	31.0-128.0	65.0	34.0-132.0	72.1	32.0-136.0	62.9	46.0	21.0
Ni	4.9-12.9	8.3	4.8-13.4	9.6	7.0-14.6	8.6	7.6	2.4
Au(ppb)	0.6-30.8	9.7	<0.5-12.8	4.7	<0.5-7.7	2.9	<0.5	15.3

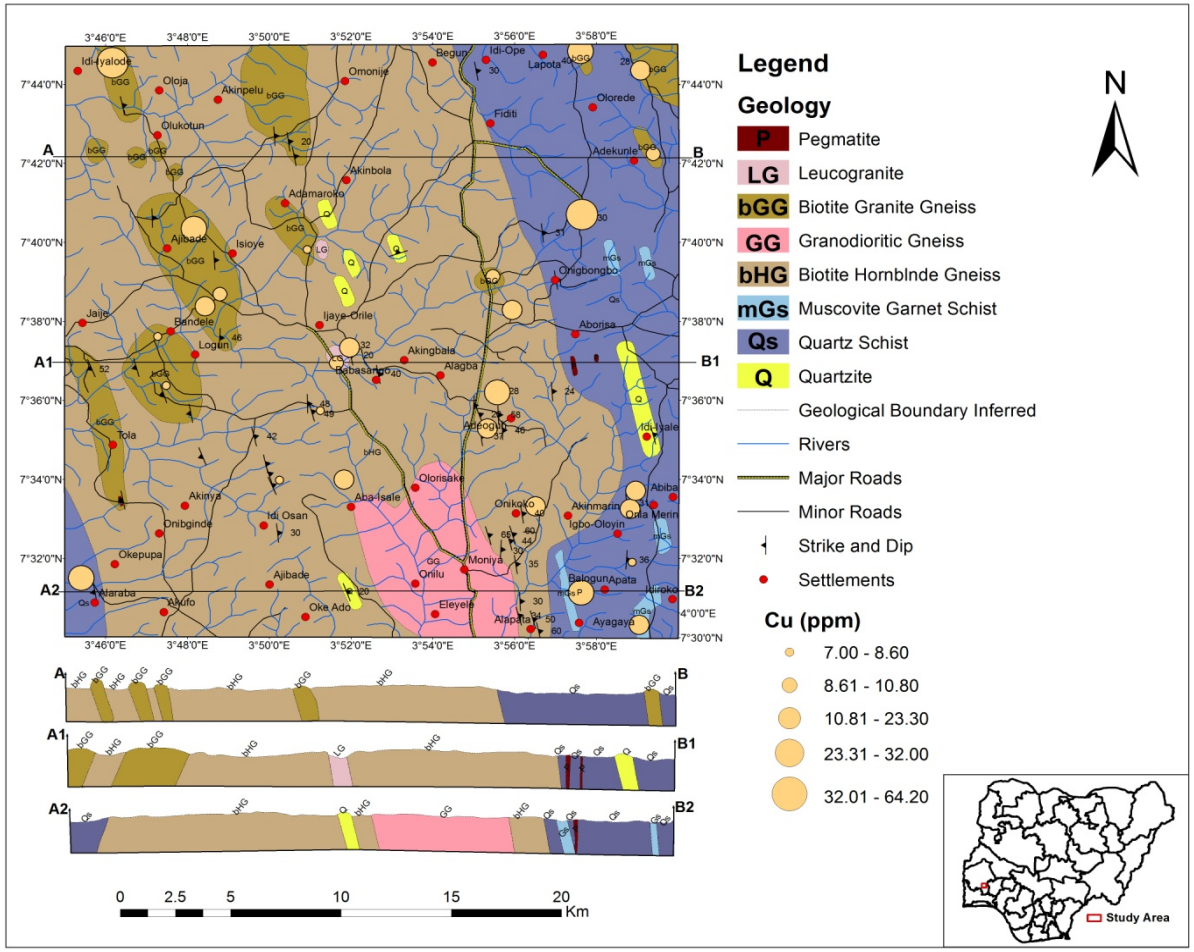

Fig.4.139 Copper (Cu) Metal Mineralisation in the Lithologic Units.

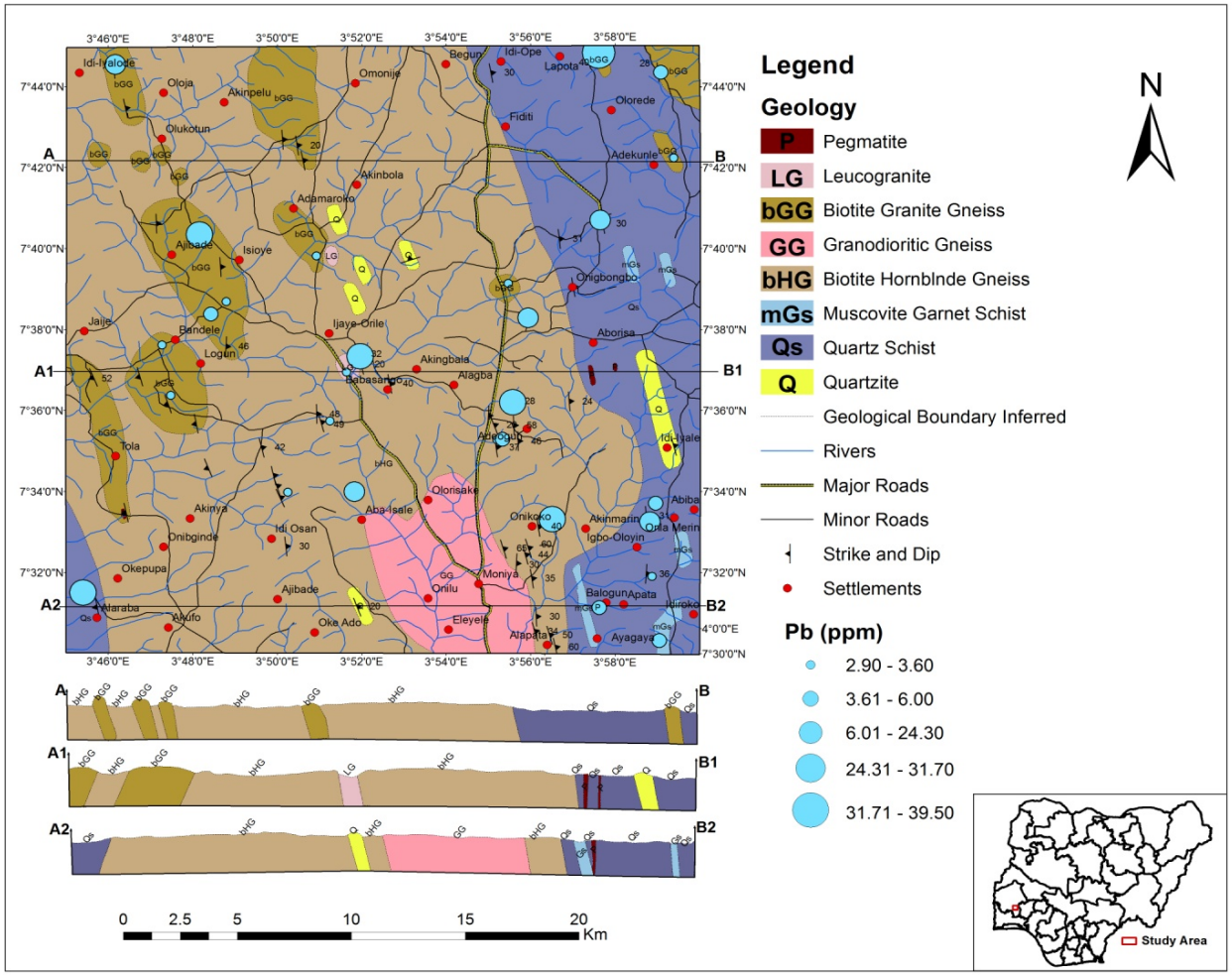

Fig.4.140 Lead (Pb) Metal Mineralisation in the Lithologic Units.

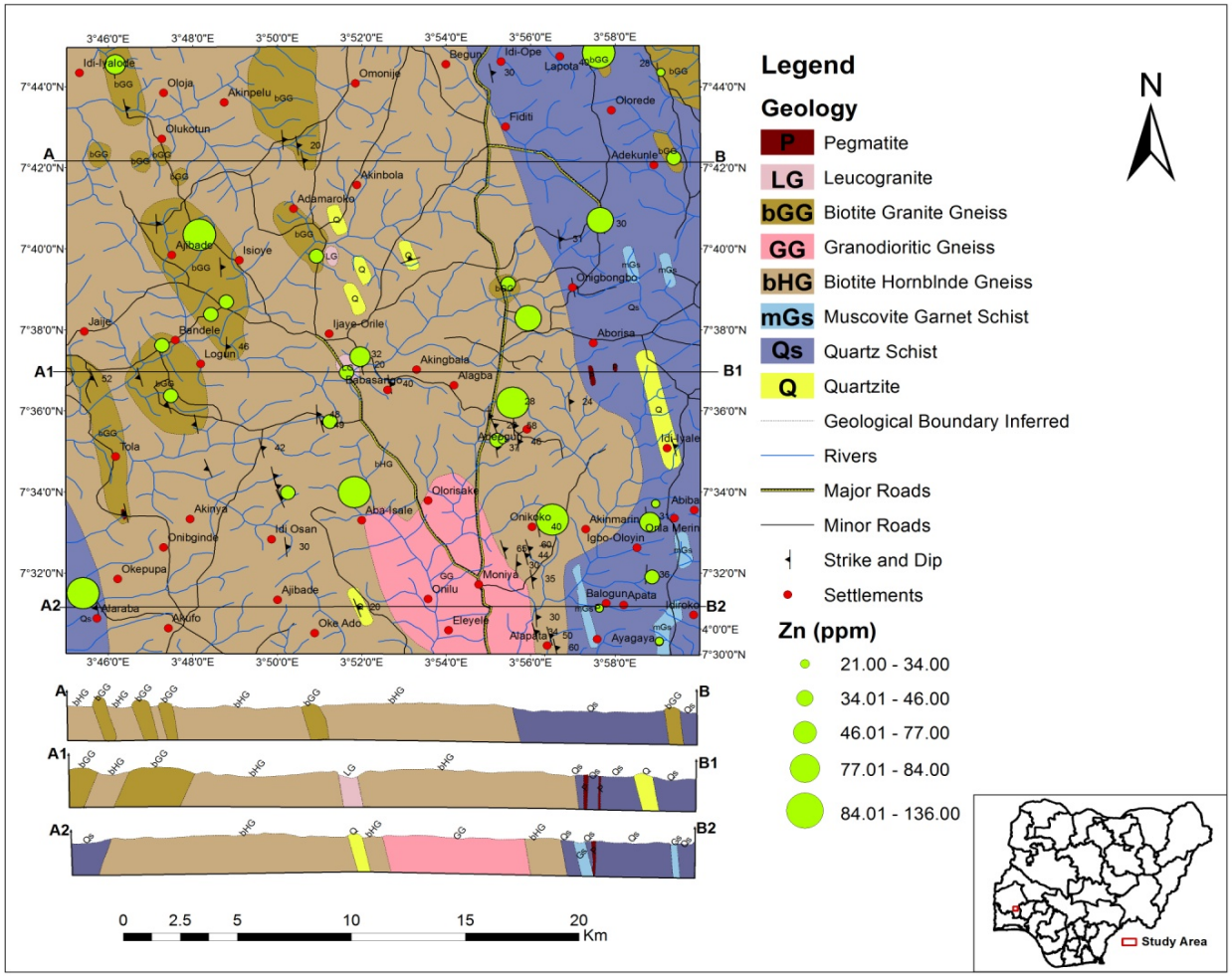

Fig.4.141 Zinc (Zn) Metal Mineralisation in the Lithologic Units.

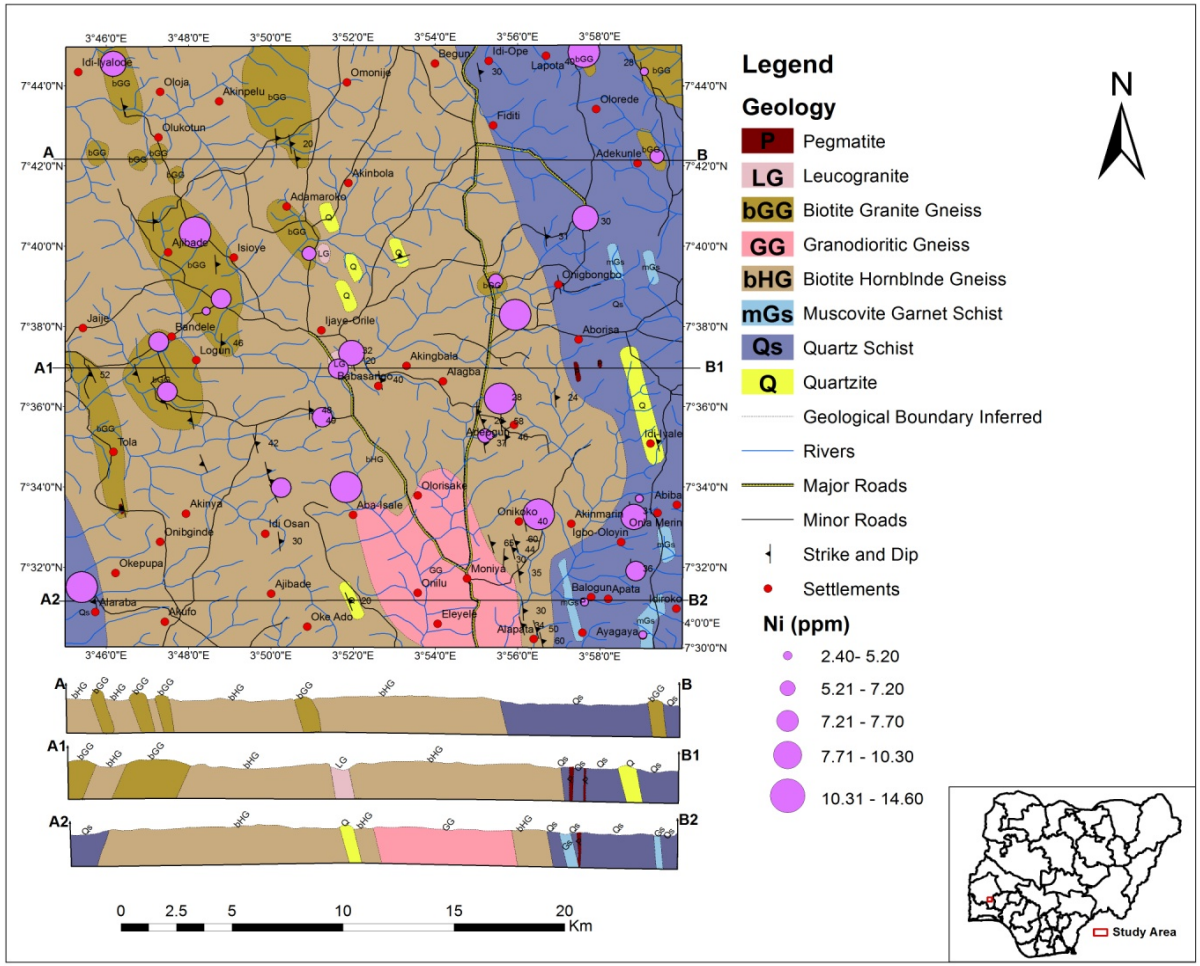

Fig.4.142 Nickel (Ni) Metal Mineralisation in the Lithologic Units.

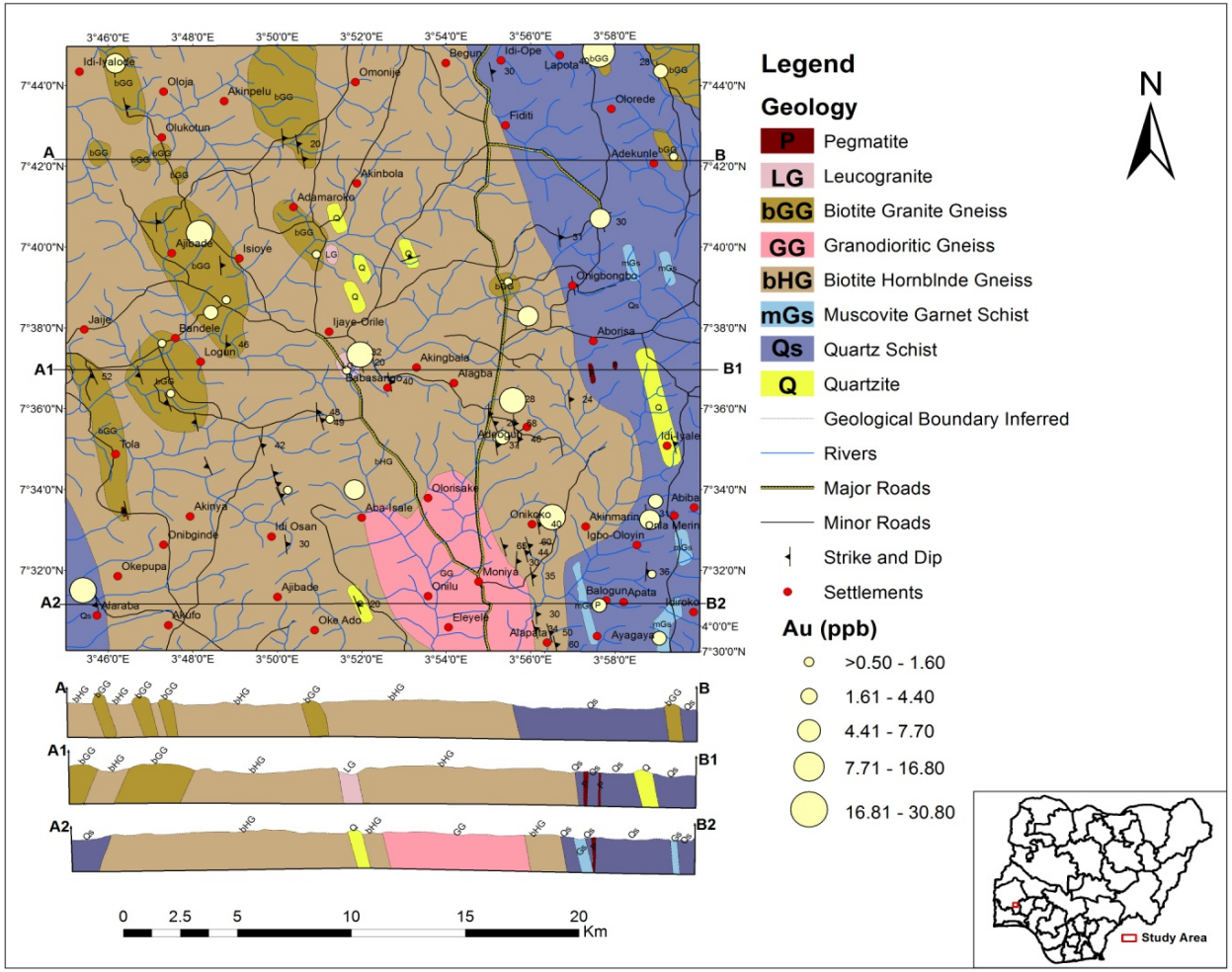

Fig.4.143 Gold (Au) Mineralisation in the Lithologic Units.

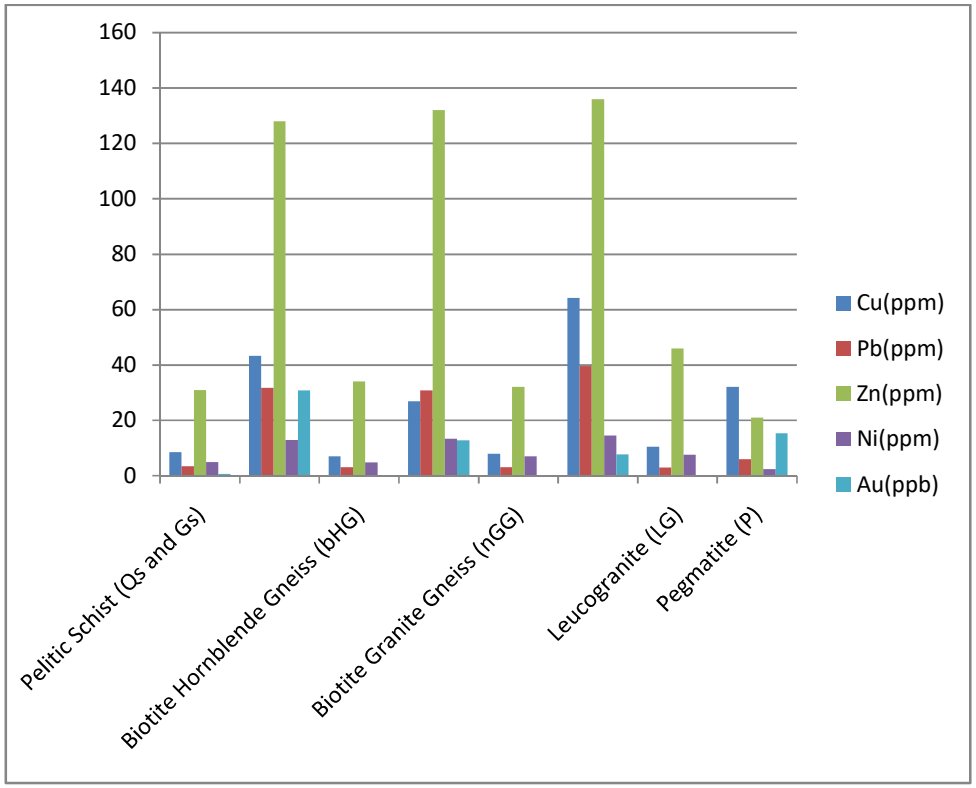

Fig.4.144 Minimum and Maximum Concentrations of the Metallic Minerals in the Different Lithologic Units

CHAPTER FIVE

SUMMARY AND CONCLUSION

5.1 Summary

Field characteristics, petrography and geochemical study of the rocks in the study area of sheet 241, Oyo SE, indicate the occurrence of quartzite, quartz-schist, Muscovite garnet schist, biotite hornblende gneiss, granodioritic gneiss, biotite granite gneiss, leucogranite, pegmatite, dolerite dyke and quartz veins.

Quartzite exhibited granoblastic texture with quartz mineral having very high percentage. The anhedral quartz displayed irregular grain boundary, grain fractures and undulose extinction in response to recrystallization.

The textural features of the quartz schist showed numerous platy muscovite and biotite minerals displaying spaced crenulation cleavages (S_2) on earlier fabric in the matrix of quartz and plagioclase feldspars. The muscovite garnet schist exhibited similar mineralogical assemblages with the quartz schist in addition to the presence of garnet indicating metamorphism from greenschist facies to amphibolites facies. The protolith of the pelitic schist were dominantly of sedimentary origin plotting in the wacke-arkose field which occurred in the passive tectonic margin field.The schists were observed to have undergone low degree of weathering, enriched Large ion lithophile (LIL) element and LREE.

The biotite hornblende and granodioritic gneisses were metamorphosed at Mid-Amphibolite facies condition of 5-10kbar at temperature between 600-670^{o}C (Baker, 1998). Xenoblastic, myrmeckitic, granoblastic and porphyroblastic textures characterize the gneisses. The gneisses conformed to the mixed origin protoliths of both igneous and sedimentary rock, which are calc-alkaline and mildly peraluminous in nature indicating corundum normative. The geotectonic environment of biotite hornblende gneiss fell within the continental arc field of syn-collision volcanic arc granite field settings.

The biotite granite gneiss has undergone partial melting resulting in the formation of abundance leucosome and augens structure- characteristics of migmatitic and tectonized terrains of upper Amphibolite facies. The granitic gneiss has igneous origin with I-type granite character and mildly peraluminous in nature. The gneiss can be suggested to be emplaced within thick Pan-African crust setting of >30km in pre-plate to syn-post collision orogeny setting.

A separate unit of leucogranite exhibits mymerkitic texture, high calc-alkaline and peraluminous in nature and fell within syn-collision region. Field observations indicate that the leucogranite were the leucocratic component of the biotite-hornblende gneiss that outcropped at the central part of the study area which were emplaced within a fairly thickened Pan-African crustal setting (<30km).

The pegmatite rocks were typically coarse, displayed porphyritic texture with microcline phenocryst as well as graphic intergrowth. It belongs to non-mineralized muscovite class. Quartz veins occurred as lenses and veins which cross-cut most of the gneisses and the granite rocks. Dolerite dykes observed were seen cutting across most of the biotite hornblende gneiss, showing varying thickness and length.

Folds, joints and shear zones were recognized during the transverse mapping exercise. Foliation trends in NW-SE with moderate dipping were observed. Mineral lineations as defined by the preferred dimensional orientation of in-equant grains.

The mineral chemistry of the gneissic samples revealed predominant of plagioclase feldspars of oligoclase ($An_{10.43}$-$An_{27.82}$) to low andesine ($An_{31.42}$-$An_{31.81}$) composition in the granodioritic gneiss and low oligoclase ($An_{11.15}$-$An_{11.75}$) in the biotite hornblende gneiss. The presences of orthoclase and microcline feldspars ($Or_{75.76}$-$Or_{92.35}$) were much more observed in the biotite granite gneiss unit than in the other gneissic units. Biotite composition in the granodioritic and biotite granite gneiss were mainly of primary magmatic biotite and plotted in phlogopite-biotite field while the biotite hornblende gneiss fell in the reequilibrated primary biotite and plotted in siderophyllite corner. The amphibole in the granodioritic gneiss were mainly ferro- hornblende on the binary plot of $Mg/(Mg+Fe^{2+})$ versus Si (Leake *et. al* 1997). Garnet porphyroblast in the biotite granite gneiss are chiefly of almandine composition while chlorite mineral found in the granodioritic gneiss occurred as brunsvigite variety. Apatite fell in flouro-

apatite end member, and exsolution blebs of magnetite in association with titanite minerals were observed in the samples of granodioritic and biotite granite gneiss units.

Rutile needles and zircon inclusions in quartz and k-feldspars were observed in the biotite granite gneiss unit. Some metallic elements in the lithologic units of Sheet 241, Oyo SE revealed the anomalous concentrations of Copper (Cu), Lead (Pb), Zinc (Zn), Nickel (Ni) and Gold (Au)

5.2 Conclusion

The study area falls within the Precambrian basement complex of Southwestern Nigeria. Different lithologies were observed within the basement which displayed different petrographic characteristics as well as chemical and mineral composition. Geological map of Sheet 241, Oyo SE on a scale of 1:50,000 was produced and anomalous metal concentrations of Cu, Pb, Zn, Ni and Au were found in the schist, gneisses and pegmatite from the study area.

5.3 Contribution to knowledge

The research work has contributed to knowledge in the aspects of conducting detailed characterisation of the rock units on bases the their petrological and geochemical compositions, investigation of the mineralisation potentials as well as in the production of geological map of Sheet 241, Oyo SE on a scale of 1:50,000

References

Abdel-Karim, A.M. 2012. Younger gabbro from south Sinai: petrology, geochemistry and petrogenetic aspects. *International Research Journal of Geology and Mining* 2:41- 53.

Abdel-Rahman, A.M. 1994. Nature of biotites from alkaline, calcalkaline and peraluminous magmas. *Journal of Petrology* 35: 525-541.

Adedoyin, A.D., Adekeye, J.I.D. and Ojo, O.J. 2014. Geochemical composition and petrogenesis of schist and amphibolites of part of sheet 203 (Lafiagi) SW and 224 (Osi) NW, southwest Nigeria. *Ilorin Journal of science* 1.1:1-17.

Afolabi, O.A. 2018. Geological mapping and geochemical characterisation of lithologic units in part of Sheet 243, Ilesha, Southwestern Nigeria. Ph.D. Thesis. Dept. of Geology. University of Ibadan. 469pp.

Agbi, I and Ekwueme, B.N. 2018. Preliminary review of the geology of the hornblende biotite gneiss of theObudu Plateau southeastern Nigeria.*Global Journal of Geology Science*17: 75-83.

Ajibade, A.C, Fitches, W.R. and Wright, J.B. 1979. The Zungerumylonites, Nigeria: recognition of a major unit. *Rev de GeolGeog Phys* 21:359–363.

Ajayi, T.R. and Suh, C.E., 1999. Partially extractable metals in the amphibolites of Ife-Ilesha area: alithogeochemical approach for gold exploration. *Jounal of Mineral Geology*35.2: 103-116.

Akinola, O.O, Bolarinwa, A.T and Ademilua, O.L. 2014. Lithologic features and petrochemical characteristics of metasedimentary rocks of Igbetti area, southwestern Nigeria. *Indian Journal Science Resources and Technology* 2.4: 82-89.

Bafor, B.E. 1981. The occurrence of sulphide mineralization in the Egbe area of southwestern Nigeria. *Journal of Mineral Geology*18.1: 175-179.

Barker, A.J. 1998. *Introduction to metamorphic texture and microstructures*. 2nd Ed. Stanley Thomes Pub. Ltd.

Batchelor, R.A. and Bowden, P. 1985. Petrogenetic interpretation of granitoid rocks series using multicationicparameters.*Chemical Geology* 48:43-55.

Best, M.G. 2003. *Igneous and Metamorphic Petrology*. 2nded. Blackwell science. 1-717.

Bhatia, M.R. and Crook, K.A.W. 1986. Trace element characteristics of graywackes and tectonic setting discrimination of sedimentary basins. *Contributions to Mineralogy and Petrology* 92: 181–193.

Black, R., Latouche, L., Lie´geois, J.P., Caby, R. and Bertrand, J.M. 1994. Pan-African displaced terranes in the Tuareg shield central Sahara. *Geology* 22: 641–644.

Boesse, T.N. and Ocan, O.O. 1988. Geology and evolution of the Ife-Ilesha schist belt southwestern Nigeria. *Symposium on Benin-Nigeria geo-traverse of Proterozoic geology and tectonics of high grade terains*. 87-107.

Boynton, W.V. 1984. Cosmochemistry of the rare earth elements: meteorite studies.

Breemen, O.V., Hutchinson, J. and Bowden, P. 1975. Age and Origin of the Nigeria Mesozoic granites: a Rb/Sr isotopic study. *Contribution to Mineral Petrology* 50: 157-172.

Bruguier, O., Dada, S. and Lancelot, J.R. 1994. Early Archaean component (≥3.56 Ga)within a 3.05 Ga orthogneiss from northern Nigeria: U-Pb zircon evidence. *Earth Planet Science Letter*125: 89-103.

Caby, R. 1989. Precambrian terranes of Benin–Nigeria and Northeast Brazil and the Late Proterozoic South Atlantic fit. *Geological Society America Special Paper* 230: 145–158.

Chappel, B.W. and White, A.J.R. 1974. Two constrasting granite types. *Pacific Geoloy* 8:173-174.

Cerny, P. and Burt, M. 1984. Paragenesis, crystallochemical characteristics and geochemical evolution of micas in granitic pegmatites. In: Bailly, S.W. Ed. *Micas Reviews in Mineralogy* 13: 257-297.

Condie, K.C.1973 Arheaen magmatism and crustal thinkening, *Geological Society of America Bulletin* 84: 2981-2992.

Cox, K.G., Bell, J.D. and Pankhurst, R.J. 1979. *The interpretation of igneous rocks*. George Allen and Unwin.

Dada, S.S., Tubosun, I.A., Lancelot, J.R. and Lar, A.U. 1993. Late Archaean U-Pb age for the reactivated basement of northeastern Nigeria. *Journal of African Earth Science* 16.4, 405-412.

Dada, S.S. 1999. Geochemistry and petrogenesis of the reworked Archaean gneiss complex of North central Nigeria: major and trace element studies on Kaduna amphibolites and migmatite gneisses. *Global Journal of pure and applied sciences* 5.4: 535-543.

Dada, S.S. 1999. Geochemistry, U-Pb, Rb-Sr and accessory mineralogy characteristics of the SarkinPawa migmatite gneiss, North central Nigeria. *Global Journal of pure and applied science* 6.1&2: 126-136.

Deer, W.A., Howie, R.A. and Zussman, J. 1963. *Rock forming silicates*. New York: John Wiley and Sons Inc.

Deer, W.A., Howie, R.A. and Zussman, J. 1992. *An introduction to the rock- forming Minerals*. 2nd Ed. Prentice Hall. 358.

De La Roche, H., Leterrier, J., Grandclaude, P. and Marchal, M. 1980. A classification of volcanic and plutonic rocks using R1R2- diagram and major element analyses—its relationships with current nomenclature. *Chemical Geology* 29:183–210.

Egbuniwe, I.G. 1982. Geotectonic evolution of Maru Belt, northwestern Nigeria, *unpublished Ph.D thesis of the University of Wales, U.K.*

Ekwueme, B.N. 2003. *The Precambrian geology and evolution of the southeastern basement complex.* University of Calabar press Nigeria. 135.

Elueze, A.A. 1981.Goechemistry and petrotectonic setting of meta sedimentary rocks of the schist belt of Ilesha area S.W Nigeria. *Precambrian Research*19.167-177.

Elueze, A.A. 1982. Petrochemistry of Precambrian gneisses and migmatites ln the Western part of Nigeria. *RevistaBrasileira de Geociencias* 12.1-3: 301-306.

Elueze, A.A. and Okunlola, O.A. 2003. Petrochemical and petrogenetic characteristics of metasedimentary rocks of Lokoja-Jakuraschist belt, Central Nigeria in:Elueze A. A ed.*Journal of Mining and Geology* 39.1: 21-27.

Elueze, A.A. and Bolarinwa, A.T. 2004. Petrochemistry and petrogenesis of granitic gneiss in Abeokuta area, SW Nigeria. *Journal of Mining and Geology* 40.1: 1-8.

Elueze, A.A.. and Kehinde-Phillip, O.O. 2008. Geochemical and petrogenetic trends of syenite and charnockitic rocks of Oke-Iho and Osuntedo areas southwestern Nigeria. *Journal of Mining and Geology* 44.1: 21-36.

Emofurieta, W.O. and Ekuajemi, V.O. 1995. Lime products and economic aspects of Igbetti, Ososo and Jakuramarble deposits in S. W Nigeria. *Journal of Mining and Geology*, 31.1: 89-97.

Falconer, J.D. 1911. *The Geology and Geography of Northern Nigeria.* MacMillan, London.

Garrels, R.M. and Mackenzie, F.T. 1971. Evolution of sedimentary rocks. W.W. Norton and Co. Inc. New York. 394.

Grant N.K. 1970. Geochronology of Precambrian basement rocks from Ibadan, south western Nigeria. *Earth planetary Sci*ence 10.1:29 – 38.

Grant, N.K. 1978. Structural distinction between a metasedimentary cover and underlying basement in the 600m.y. old Pan-African domain of northwestern Nigeria.*West Africa. Geology Society 89: 50-58.*

Gubanov, A. P. and Mooney, W. D. 2009. New global geological maps of crustal basement age. Eos transactions, AGU, 90, Fall Meet. Supplementary Abstract T53B-1583.

Harris, N.B.W., Pearce, J.A. and Tindle, A.G. 1986. Geochemical characteristics of collision-zone magmatism.In: Coward, M.P. and Reis, A.C Eds.*Collision Tectonics Special Pub. Geology Society* 19:67-81.

Herron, M.M. 1988. Geochemical classification of terreginous sands and shales from core log data. *Sedimentary Petrology* 58: 820-829.

Hey, M.H. 1954. A new review of chlorites. *The Mineralogy Magazine and Journal of the Mineralogical Society* 30.224: 278-292.

Hobbs, B.E., Winthrop, D.M. and Williams, P.F. 1976. *An outline of structural geology*. John Wiley & Sons, New York. *100-400*.

Holt, R.W. 1982. The geotectonicevolution of the Ankabelt in the Precambrian basement complex of N.W. Nigeria. *Unpublished Ph.D. Thesis, The Open University.*

Irvine, T.N. and Baragar, W.R.A., 1971. A guide to the chemical classification of the common volcanic rocks. *Canadian Journal of Earth Sciences* 8:523-548.

Janousek, V., Farrow, C.M. and Erban, V. 2006. Interpretation of whole rock geochemistry data in Igneous Geochemistry: introducing geochemical data toolkit (GCDKit). *Journal of Petrology* 47: 1255-1259.

Jones H.A and Hockey R.D. 1964. The geology of part of southwestern Nigeria. *Geological Survey of Nigeria.* 31:1 – 101.

Kearey, P. 2001. *The New Penguin Dictionary of Geology*. 243.

Kennedy, W.G. 1964. The structural differentiation of African in the Pan-African (+500 MA) tectonic episode. *Resource Institute of African Geology. Leeds 8th Annual Rpt. Science Results* 48.

Kolawole, M.S, Onimisi, M. and Olobaniyi, S.B. 2017. Field occurrence and structural characteristics of basement rocks around Kabba-Bunu area in part of Kabba-Lokoja-Igarra schist belt, southwestern Nigeria. *Global Journal of pure and applied sciences* 23: 263-274

Kleemann, G.J.and Twist, D. 1989. The compositionally zoned sheet-like granite pluton of the Bushveld complex: evidence bearing on the nature of A-type magmatism. *Journal of Petrology*30.6: 1383-1414.

Leake, B.E., Woolley, A.R., Arps, C.E.S., Birch, W.D., Gilbert, M.C., Grice, J.D., Hawthorne, F.C., Kato, A., Kisch, H.J. andKrivovichev, V.G. 1997. Nomenclature of amphiboles: report of the subcommittee on amphiboles of the international mineralogical association commission on new minerals and mineral names. *Canadian Mineralogist* 35: 219-246.

Luth, W.C., Jahnas, R.H. and Tuttle, F. 1964. The granitic system at pressure of 4 to 10kilo bars. *Journal of Geophysical research* 694: 759-773.

McCurry, P. 1976. The geology of the Precambrian to Lower Palaeozoic rocks of Northern Nigeria. In: *A review of geology of Nigeria*. Kogbe, C.A. ed. Elizabethan Publ., Nig. 15-39.

McDonough, W. F. and Sun, S.-S. 1995. Composition of the earth. *Chemical Geology* 120: 223–253.

McLennan S.M., Nance W. B., and Taylor S. R. 1980. Rare earth element-thorium correlations in sedimentary rocks, and the composition of the continental crust. *Geochimica etCosmochimica Acta* 44: 1833–1839.

McLennan S.M., Hemming, S.R., Taylor, S.R., and Erickson, K.A., 1985. Early Proterozoic crustal evolution*:* geochemical and Nd, Pb isotopic evidence from metasedimentary rocks*,* Southnorthern America. *Geochimica et Cocmochimica, Acta* 59: 1153-1127.

McLennan S.M. 1989a. Rare earth elements in sedimentary rocks: influence of provenance and sedimentary processes. In: Lipin, B.R. and McKay, G.A. Eds.*Geochemistry and Mineralogy of Rare Earth Elements: Reviews in Mineralogy*.

McLennan S.M., Hemming, S., McDaniel, D.K. and Hanson, G.N. 1993. Geochemical approaches to sedimentation, provenance, and tectonics. In: Johnsson, M.J. and Basu, A. Eds. Processes controlling the composition of clastic sediments.*Geological Society of America. Special Paper 284, Colorado*.

Middlemost, E.A.K. 1985.Magmas and magnetic rocks. Longman Group Limited. 266.

Miyashiro, A. 1974. Volcanic rock series in island arcs and active continental margins. *American Journal Science* 274: 321-355.

Nachit, H., Ibhi, A., Abia, E.H. and Ohoud, M.B. 2005. Discrimination between primary magmatic biotites, re-equilibrated biotites and neoformed biotites. *CR Geosciences* 337: 1415-1420.

Nakamura, N. 1974. Determination of REE, Ba, Fe, Mg, Na and K in carbonaceous and ordinary chondrites. *Geochimical et Cosmochimical Acta* 38: 757-775.

Nesbitt, H.W. and Young G.M. 1982. Early Proterozoic climates and plate motions inferred from major element chemistry of Lutites. *Nature* 199:715-717.

Obaje, N.J., 2009. Geology and mineral resources of Nigeria. Lecture Notes in Earth Sciences. In: S. Bhattacharji, S., Neugebauer, B.H.J.,Reitner, B.J., Stuwe, K.G.and Graz Eds. 1-31.

O'Connor, J.J. 1965. A classification of quartz-rich igneous rocks based on feldspars ratio. *U.S. Geological survey, professional pappers* 525:79-84.

Odunyemi, A and Adeyeye, O 2011. Geochemistry of the granitic gneiss of Arigidi Area, SW Nigeria. *Nature and Science* 9:5.

Okeke, P. O. and Meju, M.A. 1985. Chemical evidence for the sedimentary origin of supracrustal rocks, Southwest Nigeria. *Journal of Mining and Geology* 22.1 and 2: 97-104.

Okonkwo, C.T. and Winchester, J.A. 2004. Geochemistry of Granitic rocks in Jebba area South-Western Nigeria. *Journal of Mining Geology 40.*2: 95-100.

Okonkwo, C.T. 2005 Geochemistry of quartzites and quartz mica schists in Jebba Area, southwestern Nigeria. *Journal of Mining and Geology* 41.2: 163-173.

Okonkwo, C.T. and Gavev, V.Y. 2012. U-Pb geochronology of the Jebba granitic gneiss and its implications for the Paleooroterooic evolution of Jebbaarea,southwestern Nigeria. *International journal of Geoscience* 3: 1065-1073.

Okunlola, O.A. and Solomon, J. 2006. Compositional trends in relation to Ta-Nb mineralization in Precambrian pegmatites of Aramoko, Ara-Ijero area, SW Nigeria. *Journal of Mining Geology*42.2: 113-126.

Okunlola, O.A., Adeigbe, O.C. and Oluwatoke, O.O. 2009. Compositional and petrogenetic features of Ibadan area, southwestern Nigeria. *Earth Science Resource Journal* 13.2: 119-133.

Okunlola, O.A. and Okoroafor, R.E. 2009. Geochemical and petrogenetic features of schistose rock of the Okemesi fold belt, southwestern Nigeria. *Material and Geoenvironment* 56. 2:148-162.

Olanrewaju, V.O and Ajayi, T.R. 1993. Microprobe studies of main ferromagnesian minerals in the amphibolites of Ife-Ilesha schist belt, south west Nigeria. *Journal of Mining and Geology* 29.2: 59-69.

Olobaniyi, S.B and Mücke, A 2011. Chemical composition of chromite and intergrown chlorite in metamorphosed ultramafic rocks (serpentinite and talc schist) of the Egbe-Isanlu schist belt, southwest Nigeria: genetic implications. *Journal of Mining and Geology.* 47.2: 115-134.

Oyawoye, M.O. 1972**.** Basement complex of Nigeria in: *African Geology. Ibadan*: University Press. 62-98.

Oyinloye, A.O. 1992. Genesis of the Iperindo gold deposit, Ilesha schist belt, southwestern Nigeria. Unpublished thesis of the University of Wales, Cardiff, U.K. 1-267.

Oyinloye, A.O. 2011. Geology and geotectonic setting of the basement complex rocks in the southwestern Nigeria: implication on provenance and evolution. *Earth and Environment Science*

Oyawoye, M.O., 1964. Geology of Nigeria Basement Complex. *Journal of mining Geology.*1,2: 87-102.

Pearce, J.A. 1983. Role of the sub-continental lithosphere in magma genesis at active continental margin. In: Hawkesworth, C.J. and Norry, M.J. Eds. *Continental basalts and mantle xenoliths*. Shiva Nantwich. 230-209.

Pearce, J.A. Harris, N.B. and Tindle, A.G. 1984 Trace elements discrimination diagrams for the tectonic interpretation of granitic rocks. *Journal of Petrology* 25.4: 956-983.

Peccerillo, A and Taylor, S.R. 1976. Geochemistry of Eocene calc-alkaline volcanic rocks from the Kastamonu Area, Northern Turkey," *Contributions to Mineralogy and Pe-trology* 58.1: 63-81.

Rahaman, M.A. 1971. Classification of rocks in the Nigerian Precambrian basement complex. *Paper read at Annual Conference of Nigerian mining, geological and mutallurgical Society.*

Rahaman, M.A. 1973. The geology of the distinct around Iseyin Western State, Nigeria. Ph.D. Thesis University of Ibadan. unpub. 268.

Rahaman, M.A. 1976. Review of the basement geology of the south-western Nigeria. In: C.A. Kogbe ed. *Geology of Nigeria*. Elizabethan publ.

Rahaman, M.A. 1981**.** Petrology andGeochemistry of older Granites from some parts of Northern Nigeria, *Journal of Min*ing Geology 17: 2.

Rahaman, M.A. 1988. Recent advances in the study of the basement complex of Nigeria. *Symposium on the Geology of Nigeria, Obafemi Awolowo University, Nigeria*.

Roser, B. P., and Korsch , R. J. 1988. Provenanacesignatures of sandstone mudstone suites determined using discriminant function analysis of major element data. *Chemical Geology* 67: 119–139.

Rollinson, H.R. 1993. Using geochemical data, evaluation, presentation, interpretation. Longman scientific and technical.

Russ, W.1957. The Geology of part of Niger, Zaria and Sokoto provinces with special reference to the occurrence of gold. *Nigeria Geology Survey* 27: 42.

Shand, S.J.1943 .Eruptive rocks, their genesis, composition, classification and their relation to ore-deposits with a chapter on meteorite. New York: John Wiley & Sons.

Taylor, S. R. and McLenan, S.M. 1985. The continental crust: Its composition and evolution. Blackwell, Oxford University Press. 312.

Thompson, R.N. 1982. British Tertiary province. *Scottish Journal of Geology* 18:49-107.

Tilley, C.E. 1925. Metamorphic zones in the southern highlands of Scotland. *Journal of the Geological Society of London* 81: 100–112.

Tubosun, I.A., Lancelot, J.R., Rahaman, M.A. and Ocan, O. 1984. U-Pb Pan-African ages of two charnockite-granite associations from SW Nigeria, *Contribution Mineralogy and Petrology* 88: 18:8-195.

Turner D.C. 1983**.** Upper Proterozoic schist belts in the Nigerian sector of the Pan-African Province of West Africa. *Precambrian Research* 4: 307- 319.

Trustwell, J.F. and Cope R.N. 1963. The geology of parts of Niger and Zaria provinces, Northern Nigeria. *Nigeria Geol.ogical Survery Bull*ettin 29: 52.

Weaver, B.L. and Tarney, J. 1984. Empirical approach to estimating the composition of the continental crust. Nature (London). 310: 575-577.

Wedepohl. K.H. 1995. The composition of the continental crust. *Geochimical Cosmochimical Acta* 59:1217–1232.

Werner, C.D. 1987. Saxoniagranulites igneous or lithoigneous - A contributions to the geochemical diagnosis of the original rocks in the high grade metamorphic complexes. In: Contributions of the geology of the Saxonian granulite massif (Sochisishes Granulite birge), Gerstenberger, H Ed .Zeitschrift Mitteillung. 133: 221-250.

Wilson, M. 1989. *Igneous Petrogenesis*. Unwin Hyman, London. 461.

Woakes, M., Ajibade C.A. and Rahaman, M.A. 1987. Some metallogenic features of the Nigerian Basement *Journal of Africa Science.* 5: 655-664.

Wright, E.P. 1971. Basement Complex. In: *The Geology of the Jos Plateau*. Ed. MacLeod, N.,

Wu, G., Chen, Y.C., Chen, Y.J., Zeng, Q.T., 2012. Zircon U–Pb ages of the metamorphic supracrustal rocks of the Xinghuadukou Group and granitic complexes in the Argun massif of the northern Great Hinggan Range, NE China, and their tectonic implications. *Journal of Asian Earth Sciences* 49: 214–233.

Xiao-Fa Yang, Deng-Fa He, Qing-Chen Wang, Yong Tang, Hui-Fei Tao, Di LiXiao-Fa Yang, Deng-Fa He, Qing-Chen Wang, Yong Tang, and Hui-Fei Tao, Di Li. 2012. Provenance and tectonic setting of the Carboniferous sedimentary rocks of the East Junggar Basin, China: Evidence from geochemistry and U–Pb zircon geochronology. Elsever pub. Gondwana Research 22: 567–584

Appendix
Enclosed map